Epitranscriptomic regulation of DNA repair genes

Karen Kristjánsdóttir

December 2024

School of Health Sciences

FACULTY OF MEDICINE

UNIVERSITY OF ICELAND

Epitranscriptomic regulation of DNA repair genes

Karen Kristjánsdóttir

Thesis for the degree of Philosophiae Doctor

Supervisor(s)

Stefán Þórarinn Sigurðsson

Þorkell Guðjónsson

Doctoral committee

Hans Tómas Björnsson, PhD

Anindya Roy, PhD

December 2024

School of Health Sciences

FACULTY OF MEDICINE

UNIVERSITY OF ICELAND

Áhrif RNA sviperfða á tjáningu DNA viðgerðargena

Karen Kristjánsdóttir

Ritgerð til doktorsgráðu

Leiðbeinandi/leiðbeinendur

Stefán Þórarinn Sigurðsson

Þorkell Guðjónsson

Doktorsnefnd

Hans Tómas Björnsson, PhD

Anindya Roy, PhD

Desember 2024

Heilbrigðisvísindasvið

LÆKNADEILD

HÁSKÓLI ÍSLANDS

ISBN 978-9935-9732-9-0

ORCID: 0000000252917449

Reykjavik, Iceland 2024

Ágrip

RNA sviperfðir vísa til stjórnunar á genatjáningu eftir umritun með breytingum á RNA sem geta haft áhrif á virkni og uppbyggingu RNA sameindarinnar án þessa að valda breytingum í ríbósakjarnsýru röðinni. RNA breytingar finnast á öllum gerðum RNA þar á meðal mRNA þar sem metýleringar eru eitt algengasta form breytinga. Tvær af þekktustu mRNA metýleringunum eru N^6-metýladenósín (m^6A) og N^1-metýladenósín (m^1A) en báðar breytingarnar eru afturkræfar. Rannsóknir hafa sýnt fram á að mRNA metýleringar taka þátt í og hafa áhrif á marga líffræðilega ferla, þar á meðal DNA skemmdarviðbragði í frumum. Viðbrögð frumna við DNA skemmdum eru mikilvæg fyrir lífvænleika þeirra og til að viðhalda stöðugleika erfðamengisins. DNA tvíþáttabrot (DTB) eru talin alvarlegasta gerð af DNA skemmdum þar sem galli í viðgerðum á DTB getur leitt til frumudauða og stuðlað að krabbameinsmyndun. Hæfni frumna að greina og gera við DNA DTB á réttan hátt er nauðsynleg til að frumur haldi erfðafræðilegum stöðugleika og til að flytja réttar erfðaupplýsingar frá einni kynslóð til annarrar.

ALKBH3 og FTO (ALKBH9) eru díoxýgenasr sem tilheyra AlkB prótínfjölskyldunni. ALKBH3 hefur vel skilgreint hlutverk í viðgerðum á alkýlerandi DNA skemmdum en er einnig þekkt fyrir að starfa sem mRNA demtýlasi ásamt örðum meðlimum í AlkB prótín fjölskylunni. Nánar tekið, þá fjarlægir ALKBH3 m^1A af mRNA og FTO er þekktast fyrir að fjarlægja m^6A af mRNA. Fyrri rannsóknir frá Rannsóknarstofu í krabbameinsfræðum hafa sýnt að stýrilsvæði ALKBH3 er metýlerað í ~20% af brjóstakrabbameinum. Þessi sviperfðastjórnun leiðir til minni ALKBH3 tjáningar og verri lifunar hjá brjóstakrabbameins sjúklingum. Frekari rannsóknir á ALKBH3 og öðrum AlkB prótín meðlimum leiddu í ljóst að þöggun á ALKBH3 og FTO (ALKBH9), leiddi til taps á prótíntjáningu RNF168, lykilpróteini sem tekur þátt í viðgerð á DTB.

Fyrsta markmið þessa verkefnis var að skilgreina stjórnunarhlutverk ALKBH3 og FTO á prótíntjáningu RNF168. Í ljós kom að tap á ALKBH3 og FTO leiddi til aukinna m^1A og m^6A metýleringarmerkja á umriti *RNF168* sem leiðir til skerts mRNA útflutnings og tapi á prótíntjáningu. Bentu þessar niðurstöður til þess að ALKBH3 og FTO gætu stjórnað RNF168 í gengum RNA sviperfðir, ný leið í stjórnun á RNF168 prótín tjáningu.

Seinna markmið verkefnisins fólst í að kanna möguleg áhrif ALKBH3 og FTO á DNA skemmdarviðbragð frumna, sem rekja má til stjórnunar þeirra á RNF168. Genaþöggun á ALKBH3 og FTO leiddi í ljós að frumur sem skortir ALKBH3 eða FTO sýndu sterk merki um truflun á starfsemi RNF168, þar á meðal að 53BP1 prótínið kom ekki lengur að DNA DTB. Frekari rannsóknir sýndu fram á að frumur með skerta ALKBH3 og FTO virkni höfðu skerta getu til að gera við DTB. Einnig kom í ljós aukinn erfðafræðilegur óstöðugleiki og aukið varnarleysi fyrir lyfjum sem valda DNA skemmdum við tap á ALKBH3 og FTO.

Þessar niðurstöður benda til nýrrar gerðar stjórnunar á RNF168 og sýna þátttöku mRNA breytinga í að hafa áhrif á DNA DTB viðgerðarsvörun. Enn fremur, gefa niðurstöðurnar úr þessu verkefni vísbendingar um samspil alkýleringarviðgerðar og DNA DTB viðgerðar. Það að fjarlæga mRNA metýleringar hafi áhrif á DNA skemmdarviðbragðið er ný viðbót við ört stækkandi heim RNA sviperfða og mun einnig hafa þýðingu fyrir rannsóknir á DNA viðgerðum. Einnig að demetýlasar hafi hlutverk í að viðhalda stöðugleika erfðamengisins og svörun frumna við krabbameinslyfjum gæti reynst mikilvæg fyrir þróun krabbameins. Tap á ALKBH3 og FTO gæti verið notað sem hugsanleg vísbending fyrir svörun við krabbameinsmeðferð, bæði vegna skorts á alkýlerunarviðgerð og hugsanlega vegna skorts á DNA tvíþáttabrotum sem undirstrikar mögulegan klíníska ávinning af þessu verkefni.

Lykilorð:

RNA sviperfðir, DNA viðgerðir, mRNA metýleringar, DNA tvíþáttabrot, RNF168.

Abstract

Epitranscriptomics refers to post-transcriptional regulation of gene expression via RNA modifications, which can affect the function and structure of RNAs but do not entail any changes to the ribonucleotide sequence. RNA modifications are found on all forms of RNA including messenger RNA (mRNA) with methylations being the most common forms of mRNA modifications. Two such mRNA methylations are N^6-methyladenosine (m^6A) and N^1-methyladenosine (m^1A) which are known to be reversible. Studies have demonstrated that mRNA methylations are involved in and influence numerous biological processes including the DNA damage response. The DNA damage response is vital for the maintenance of genomic integrity and cell survival. DNA double strand breaks (DSB) are thought the most cytotoxic form of DNA damage as unrepaired or incorrectly repaired DSBs can result in cell death or lead to increased genomic instability and increase risk of cancer development. The ability to detect and correctly repair DNA DSB is vital for cells to maintain genome stability and to transfer correct genetic information from one generation to the next.

ALKBH3 and FTO (ALKBH9) are dioxygenases belonging to the AlkB protein family. ALKBH3 has a well-established role in DNA alkylation repair but can also act as an mRNA demethylase, a function shared with other members of the AlkB family. Specifically, ALKBH3 removes m^1A from mRNA, whereas FTO is primarily recognized for demethylating m^6A from mRNA. In a previously published article, the Sigurdsson laboratory revealed that ALKBH3 is promoter hyper-methylated in ~20% of breast cancers. This form of epigenetic regulation reduced ALKBH3 expression and was correlated with reduced survival. Exploring the function of silencing ALKBH3 and other members of the AlkB family revealed that knockdown of ALKBH3 and FTO caused protein downregulation of RNF168, a pivotal protein in DNA DSB repair.

The first aim of this project involved elucidating the regulatory role ALKBH3 and FTO have on RNF168. Further exploration into silencing ALKBH3 and FTO revealed that loss of ALKBH3 and FTO lead to increased m^1A and m^6A methylation marks on the *RNF168* transcript, resulting in impaired mRNA export and decreased protein expression. These results point towards a novel form of epitranscriptomic regulation of RNF168.

The secondary aim of this project was to explore the potential influence of ALKBH3 and FTO on the DNA DSB response, attributed to their regulation of RNF168. Cells depleted of ALKBH3 and FTO demonstrate strong signs of RNF168 dysfunction, including impaired 53BP1 recruitment to DNA DSB and altered DNA DSB repair dynamics. Subsequent investigations revealed heightened genome instability and increased sensitivity to genotoxic agents upon the loss of ALKBH3 and FTO.

The findings presented in this thesis present a novel regulatory mechanism for RNF168 and unveil the involvement of mRNA modification in DNA DSB repair signaling. Furthermore, providing evidence of interplay between alkylation repair and DNA DSB repair. The removal of mRNA modification from the DNA repair factor RNF168, presents a new regulatory mechanism into the DNA DSB repair signaling, making it a unique addition to the rapidly evolving field of epitranscriptomics. The fact that demethylases play a part in genomic maintenance and cell survival in response to genotoxic agents is likely to have impact on the DNA repair field and could prove to be a vital factor to cancer development. Lack of ALKBH3 and FTO might be used as a potential marker for cancer treatment response due to both lack of alkylation repair and possibly because of DNA double strand repair deficiency, highlighting the possible clinical benefits of this project.

Keywords:

Epitranscriptomic, DNA repair, mRNA methylations DNA Double strand breaks, RNF168.

Acknowledgements

First and foremost, I would like to express my gratitude to my supervisor, Stefán Sigurðsson, for giving me the opportunity to be a part of this exciting project and for providing valuable guidance and support throughout the years of my PhD. His availability for discussions, patience, and support over the past five years have been greatly appreciated. It has been a great privilege to study under his mentorship.

Furthermore, I wish to express my sincere appreciation to my co-supervisor, Þorkell Guðjónsson, whose expertise and guidance have been invaluable to the advancement of this project. His insightful instructions and constructive feedback have contributed significantly to my professional development. Additionally, his precision and attention to detail have elevated this project to a level I could not have achieved on my own.

I would like to thank my PhD committee members, Hans Tómas Björnsson and Anindya Roy, for their invaluable input and advice during the years of this project. Thanks to my research group team members, current and previous, for their help and input towards this project. Special thanks to Drífa Hrund Guðmundsdóttir for all the supportive talks, help troubleshooting experiments, and advice. Thanks to Birta Dröfn Jónsdóttir, an M.Sc. student who entered the project at a crucial time and provided a much-needed gust of energy. I would also like to mention all the wonderful people at Sturlugata 8 and all the brilliant scientists at the BioMedical Center, whom I have had the privilege of working with and learning from. Thank you all for your scientific input, assistance, and friendship.

Finally, my heartfelt gratitude goes to my family. My mother, for her consistent encouragement to keep going, and to my wonderful husband, Zenel, for his unwavering love, support, and encouragement. Thank you for always believing in me; your support means the world to me.

The work presented in this thesis was carried out at the Biomedical Center at the University of Iceland and the Department of Biochemistry and Molecular Biology, Faculty of Medicine, School of Health Science. This project was funded by a project grant (grant nr: 185242), a doctoral student grant (grant no: 228323-051) from the Icelandic Research Fund, and a grant from the Blue Nail, a community organization that supports primary cancer research in Iceland.

Contents

List of Abbreviations

AA: Amino acid

ALKBH3: Alpha-Ketoglutarate Dependent Dioxygenase 3

AlkB: The Alpha -ketoglutarate-dependent dioxygenase family

Alt-NHEJ: Alternative non-homologous end joining.

ATM: Ataxia Telangiectasia Mutated

ATR: ATM and Rad3-Related

BARD1: BRCA1 associated ring domain 1.

BER: Base excision repair

BLM: bloom syndrome helicase

BRCA1: Breast Cancer gene 1

BRCA2: Breast Cancer gene 2

BURD domain: BRCT-domain-associated ubiquitin-dep

cDNA: Complementary DNA

CLF: XRCC4-like factor

CDKs: Cyclin-dependent kinase

Chk: Checkpoint kinase

co-IP: Co-immunoprecipitation

CRISPR: Clustered Regularly Interspaced Short Palindromic Repeats

c-NHEJ: Classical non-homologous end joining.

CtIP: C-terminal interacting protein.

DDR: DNA Damage Response

DNA-2: DNA replication helicase 2

DNA-PK: DNA-dependent protein kinase

DSB: Double Strand Breaks

DTT: Dithiothreitol

DUB: Deubiquitinating enzymes

eIF3: Eukaryotic Initiation Factor 3

ERCC1: Excision Repair Endonuclease Non-Catalytic Subunit

EXO1: Exonuclease 1

FACS: Fluorescence activated cell sorting

FTO: Fat Mass and Obesity-Associated Protein

GO: Gene Ontology

GSEA: Gene Set Enrichment Analysis

H2AX: H2A histone family member X

HJ: Holliday Junction

HNRNP: Heterogeneous ribonucleoprotein family

HR: Homologous Recombination

ICL: Interstrand Crosslink Repair

IF: immunofluoresence

IN: Input

IP: Immunoprecipitation

IR: Ionizing Radiation

KD: Knockdown

KO: Knockout

LB: Lysogeny broth

L3MBTL2: Lethal (3) Malignant Brain Tumor-Like Protein 2

Lig: DNA ligase

MeRIP: Methylations specific immunoprecipitation

MDC1: Mediator of DNA Damage and Checkpoint 1

METTL: Methyltransferase Like protein

MMC: Mitomycin C

MMR: Mismatch Repair

MMS: Methyl methane-sulphonate

MRN: MRE11-RAD5-NBS1

MS: Mass Spectrometry

m^1A: N^1-methyladenosine

m^3C: N^3-methylcytocyne

m^3T: 3-Methylthymine

m^6A: N^6-Methyladenosine

m^6A_m: N^6,2′ -O-dimethyladenosine

NA: not applicable

NK: not known.

NC: Negative Control

NCS: Neocarzinostatin

NER: Nucleotide Excision Repair

NERF: Nerve Growth Factor Enhancer

PARP1: Poly(ADP-ribose) polymerase1

PARPi: PARP inhibitors

PALB2: Partner and Localizer of BRCA2

PAXX: paralog of XRCC4 and CLF

Polθ: DNA polymerase theta

PC: Positive Control

PTM: Post-transcriptional modification

PTIP: PAXIP1 Associated Protein 1

qPCR: Quantitative polymer chain reaction

RIDDLE: Radiosensitivity, immunodeficiency, dysmorphic features, and learning difficulties

RIF1: Rap1 Interacting Factor 1

RNF8: Ring Finger Protein 8

RNF168: Ring Finger Protein 168

RPA: Replication Protein A

RT: Room Temperature

SD: Standard deviation

SDS: Sodium Dodecyl Sulfate

SDSA: synthesis-dependent strand annealing

sgRNA: single-guide RNAs

siRNA: Small Interfering RNA

SNP: Single Nucleotide Polymorphism

SR: Serine-arginine rich

SSA: Single Strand Annealing

SSB: Single Strand Break

ssDNA: single stranded DNA

TPM: Transcripts Per Million

UTR: Untranslated Region

WB: Western blot

XPF: Excision Repair Cross-Complementation Group 4

XRCC: X-ray repair cross-complement protein

List of Figures

List of Tables

List of Original Papers

This thesis is based on the following original publications, which are referred to in the text by their Roman numerals I):

I. **The oxidative demethylases ALKBH3 and FTO contribute to efficient RNF168 dependent DNA double-strand break signaling.**

   Thorkell Guðjónsson ¶, Karen Kristjánsdóttir ¶, Stefan Thor Hermanowicz, Kritika Kirty, Birta Dröfn Jónsdóttir, Arnar Ingi Vilhjálmsson, Snædís Ragnarsdóttir, Drífa Hrund Guðmundsdóttir, Erla Sveinbjörnsdóttir and Stefán Sigurðsson. Submitted for publication.

   ¶ Authors contributed equally to this work

In addition, a considerable amount of unpublished data is presented.

Declaration of Contribution

I performed the experimental work presented in this thesis, with some exceptions. Þorkell Guðjónsson assisted in the generation of some of the confocal data and western blot data included in this thesis. Two knockout cell lines used in this thesis were generated with the aid of M.Sc. student Arnar I. Viðarsson. Kritika Kirty and Stefán Hermanowicz optimized and performed the RNA Scope experiments. PhD student Drífa H. Guðmundsdóttir and M.Sc. student Birta D. Jónsdóttir contributed to DNA repair assay experiments and, María Rose Bustos performed analysis of RNA sequencing data. Mass spectrometry experiments were conducted in professor Rolfsson's laboratory, and research scientist Christian Christensen helped in the mass spectrometry analysis. Erla Sveinbjörnsdóttir, a biomedical scientist at the Department of Genetics and Molecular Medicine at the University Hospital, provided her expert opinion on metaphase spread analysis.

Aside from the experimental work, I contributed to experimental design with help from supervisors Stefán Sigurðsson and Þorkell Guðjónsson. I also contributed to planning and devising methodologies, and data analysis.

The original paper is currently in progress and was written by me together with project supervisors, Þorkell Guðjónsson and Stefán Sigurðsson.

1 Introduction

1.1 Genomic stability and the DNA damage response

Genomic stability is essential for maintaining the health and proper function of cells, preventing diseases, ensuring accurate genetic inheritance, and supporting the sustained survival and evolution of species. It is essential for safeguarding cellular integrity by preventing errors in DNA replication and protecting against internal and external genotoxic stressors. Internal genotoxic stressors include reactive oxygen species produced during cellular metabolism while external factors comprise ultraviolet (UV) light, ionizing radiation (IR), or DNA-damaging chemicals. Genome instability is a key characteristic of most cancers, believed to arise due to the impaired capacity to address damaged DNA (Hanahan et al., 2011). Extensive research efforts have been focused on genomic instability, aiming to comprehend and impede the progression of tumors, with the ultimate goal of conquering cancer, a leading global cause of mortality.

In order to prevent genome instability, cells have developed a sophisticated signaling system termed the DNA damage-response (DDR) that detects the damage, signals their presence, and promotes repair (Harper et al., 2007; Harrison et al., 2006; Rouse et al., 2002) (Figure 1). The DDR comprises cell-cycle checkpoints, cell death pathways as well as various DNA repair mechanisms including nucleotide excision repair (NER), base excision repair (BER), interstrand crosslink repair (ICL), mismatch repair (MMR), and double-stranded break (DSB) repair (Giglia-Mari et al., 2011; Jackson et al., 2009). The biological importance of functional DRR for human health is made evident by the severe outcomes of inherited defects in DDR factors resulting in various diseases such as neurological degeneration, premature aging, immune deficiency, and severe cancer susceptibility (Hoeijmakers, 2001, 2009). The primary cause of genome instability is DNA damage, and the human genome suffers from thousands of various DNA lesions every day arising from both endogenous and environmental causes (Kass et al., 2010; Lindahl, 1993). Certain forms of damage, like oxidative damage to DNA bases, occur and undergo repair as frequently as 10^5 lesions per cell on a daily basis while more serious damage such as DNA double strands breaks happen less frequently (Hoeijmakers, 2009).

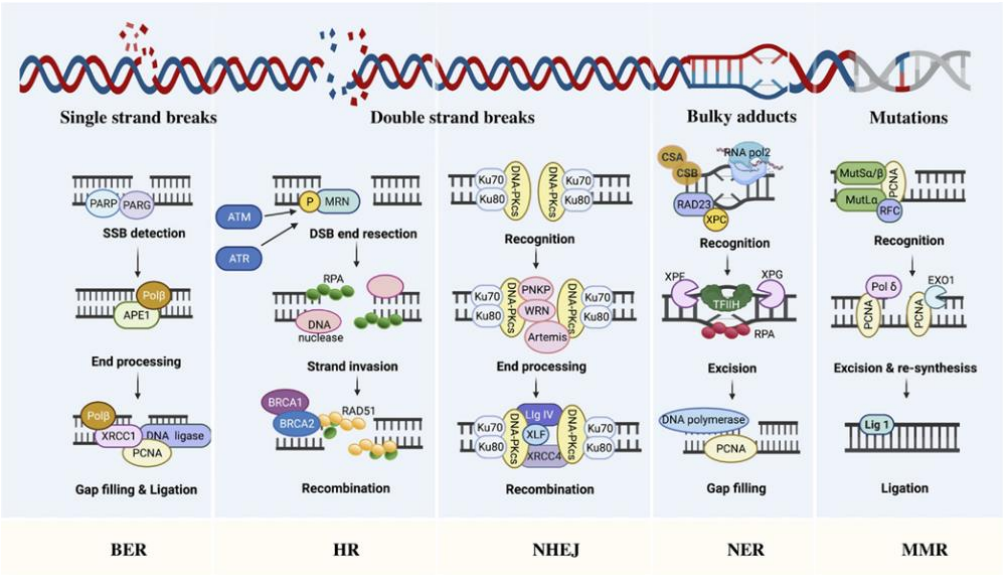

Figure 1. Summary of the major DNA repair pathways for mending distinct DNA lesions.

Single-strand breaks (SSBs) undergo restoration through both direct and indirect base excision repair (BER), while double-strand breaks (DSBs) are rectified through homologous recombination (HR) and non-homologous end joining (NHEJ). Mismatch repair (MMR) addresses replication errors, and nucleotide excision repair (NER) tackles DNA adducts (M. Wang et al., 2021).

1.2 DNA Double Strand Breaks

Chromosome breaks or DNA double strand breaks (DSB) are the most serious type of DNA damage caused by exposure to exogenous agents such as ionizing radiation, environmental mutagens, UV light or chemotherapeutic drugs (Lieber, 2010) (Thompson, 2012). DSBs can also occur from endogenous processes including replication stress, stalled replication fork and reactive oxygen species (Alexander et al., 2016; Cannan et al., 2016). Failure to repair DSBs can result in cell death as persistent DSBs can initiate apoptosis. Improperly repaired DSBs can result in chromosomal rearrangements such as translocations, insertions, and deletions, these genetic alterations can cause significant genomic instability and can contribute to carcinogenesis (Mills et al., 2003). In the event of DSB formation, cells trigger a cascade of protein recruitment to the break site, prompting local changes to the chromatin structure, enabling DNA repair proteins to reach the site of damage. Eukaryotic cells have two major conserved pathways to deal with DNA DSBs: Homologous Recombination (HR) and Non-homologous end joining, also known as classical non-homologous end joining (c-NHEJ). In addition to these highly efficient pathways, two other more error prone repair pathways exist called single-strand annealing (SSA) and alternative NHEJ (alt-NHEJ) (Ochs et al., 2016; Pannunzio et al., 2014).

1.2.1 DNA DSB damage recognition

Mammalian cells are equipped with highly efficient mechanisms for detecting DSBs and signaling their presence to the DNA repair and replication machinery (Figure 2). The MRE11-RAD50-NBS1 (MRN) complex is considered the main DSB sensor, which detects the break, binds them, and activates the transducers of the cellular response to the DSB. Other models have been proposed for the initial protein response DSB. This includes speculation that Poly (ADP-ribose) polymerase 1 (PARP1) initiates the repair response to recruit MRE11 and NBS1, or that Ku70/80 heterodimer binds immediately to the broken DNA ends to stabilize them (Haince McDonald Rodrigue Déry et al., 2008; Walker et al., 2001). The established consensus is however in agreement that the recruitment of the MRN complex is central for the DNA damage response signaling process. The nuclease activity of the MRN complex is recognized for facilitating DNA end resection, directing DNA repair toward HR in the presence of sister chromatin. Moreover, the MRN complex is implicated in c-NHEJ as knockdown (KD) of MRE11 in mammalian cells has been shown to diminish the efficiency of end-joining in c-NHEJ (Rass et al., 2009), although it's full function within c-NHEJ is not as well understood and require further research.

Once bound to DSBs, the MRN complex can recruit and activate various DDR proteins, including ATM (Qiu et al., 2021). The ATM (Ataxia Telangiectasia Mutated), ATR (ATM and Rad3-Related) and DNA-PK (DNA-dependent protein) kinases are the key DSB transducers and are responsible for phosphorylating numerous DDR substrates and by that activate the DDR cascade. While ATM is predominantly activated by DSBs, ATR responds to a wide range of DNA damage, including DSBs but is most commonly associated with stalled or collapsed replication forks during S-phase (Liu et al., 2007). ATM resides within cells as an inactive dimer but when a DSB occurs ATM undergoes auto-phosphorylation and separation, transitioning into an active, single-molecule ATM kinase that attaches to the DSB. At the site of the break, ATM phosphorylates and activates numerous mediators and effectors responsible for DSB responses, including Chk1, Chk2, MDC1 and BRCA1 (Ayoub et al., 2009; Bartek et al., 2007; Harper et al., 2007; Marechal et al., 2013; Pardo et al., 2009; Riches et al., 2008; Shibata et al., 2021). One of ATMs key actions involves phosphorylating the C-terminal tail of the histone variant H2A histone family member X (H2AX) on Serine 139, a crucial step that serves as a focal point for recruiting MDC1 (Mediator of DNA Damage Checkpoint 1) and subsequently initiating ubiquitination cascades by Ring Finger Protein 8 and 168 (RNF8 and RNF168) (Burma et al., 2001). The RNF8-RNF168 ubiquitination cascade recruits main regulators of DNA DSB repair pathway choice, 53BP1 (p53 binding protein) and breast cancer gene 1 (BRCA1).

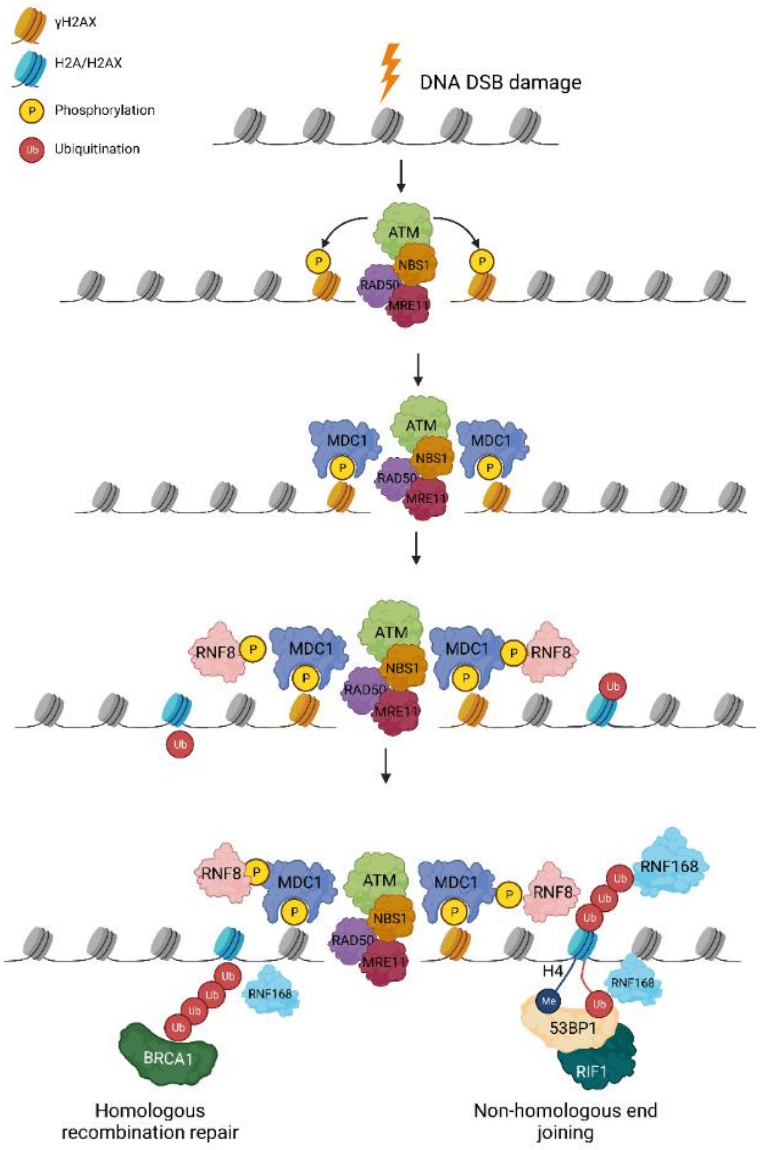

Figure 2. Simplified overview of the detection of DNA Double strand breaks.

Upon DSB forming the MRN complex (NBS1, RAD50 and MRE11) recognizes and binds to the break triggering the DDR response. ATM is recruited by NBS1 and phosphorylates H2AX into γH2AX along with multiple other proteins inducing MDC1. MDC1 phosphorylation induces an ubiquitin cascade performed by RNF8 and RNF168, which ubiquitinate several histones including H2A/H2AX. Histones ubiquitination is recognized by 53BP1 which promotes c-NHEJ repair or by BRCA1 and its associated proteins to promote HR repair. The figure was created using BioRender (biorender.com).

1.2.2 Classical non-homologous end joining

Classical non-homologous end joining is the predominant repair pathway in human cells, repairing the majority of all DSBs (Karanam et al., 2012). C-NHEJ is a relatively fast process that repairs DSB throughout the cell cycle though a set of mechanistically distinct steps to join DNA ends by direct ligation (Hefferin et al., 2005). The c-NHEJ pathway employs proteins capable of recognizing, trimming, polymerizing, and joining DNA ends in a versatile manner (Figure 3). The onset of c-NHEJ begins with the attachment of the Ku70/80 heterodimer to the end of the DSB. Binding of Ku heterodimer to DSB servers as a scaffold to recruit various c-NHEJ repair components, which include the DNA-dependent protein kinase catalytic subunit (DNA-PKcs), DNA ligase IV (LIG4), and accompanying scaffold proteins like XRCC4 (X-Ray Repair Cross Complementing 4), XRCC4-like factor (CLF), and the paralog of XRCC4 and CLF (PAXX) (Ahnesorg et al., 2006; Buck et al., 2006; Gottlieb et al., 1993; Nick McElhinny et al., 2000; Ochi et al., 2015). The Ku70/Ku80 heterodimer forms a complex with DNA-PKcs, which acts as the kinase catalytic subunit of the DNA-PK complex. The formed DNA-PK complex is activated at DSBs, resulting in the phosphorylation of members of the c-NHEJ machinery. Next the ARTEMIS nuclease is recruited to processes the DSBs, followed by DNA synthesis by DNA polymerase μ or λ and finally the last step is ligation, performed by the XLF-XRCC4-DNA Ligase IV complex (Lieber, 2010; Ruis et al., 2008; Scully et al., 2019).

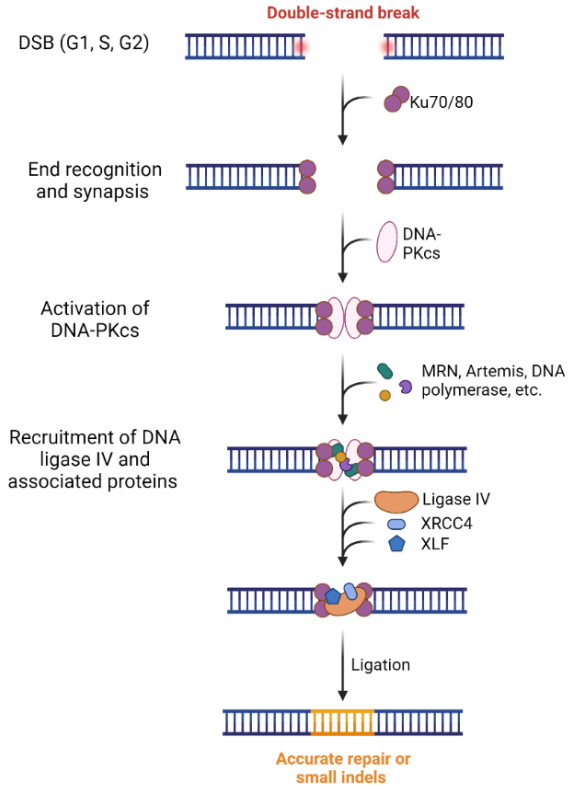

Figure 3. Schematic overview of classical non homologous end joining repair.

c-NHEJ remains active throughout the cell cycle, resulting in precise repair or the generation of small insertions or deletions (indels) (Mirman et al., 2020). Figure created using BioRender.

1.2.3 Homologous recombination

Homologous recombination is a multi-step process that is considered the more precise and complex method for repairing DNA DSBs (Figure 4). HR takes place exclusively in late S and G2 part of the cell cycle and uses homologous DNA template for the repair, most often the sister chromatid (Takata et al., 1998). A major step in directing DSB repair towards HR is end resection which involves the removal of nucleotides in a 5′ – 3′ direction from the DNA end, resulting in the creation of a 3′ single-stranded DNA (ssDNA) overhang. The resection process involves several key proteins, including the MRN complex, BRCA1, BARD1 (BRCA1 Associated Ring Domain 1), EXO1 (exonuclease 1), DNA2 (DNA replication helicase 2), and the bloom syndrome (BLM) helicase. MRE11 along with CtIP (c-terminal interacting protein), initiates the process by making an incision in one DNA strand near the site of the break, utilizing its 5′ –3′ endonuclease activity. Following this, it proceeds to degrade the same strand with its continuous 3′ –5′ exonuclease activity. This action leads to the displacement of Ku70/Ku80 from the break site as a result of MRE11's end-processing activity,

effectively and provides entry point for DNA2, BLM and EXO1 which mediate further end resection (Nimonkar et al., 2011). Other DNA repair proteins have been implicated in the end resection process, such as BRCA1 which forms a complex with BARD1 and interacts with CtIP and MRN to aid in end resection (Tarsounas et al., 2020). However, the precise mechanisms governing the coordinated regulation of these resection factors remain elusive and require further investigation.

Following end resection, the replication protein A (RPA) rapidly binds to the ssDNA overhang preventing formation of any secondary structure and degradation (Sugiyama et al., 1997). RPA is later replaced by the DNA recombinase RAD51 which forms nucleoprotein filament to initiate the homology search for complementary sequences. RAD51 loading onto DNA is regulated by BRCA2 and PALB2 (Partner and Localizer of BRCA2) (Lin et al., 1984) along with RAD51 paralogues, such as RAD51B, RAD51C, RAD51D, XRCC2, and XRCC3 (Jensen et al., 2013; Thacker, 2005). Nevertheless, the full extent of the functions performed by the RAD51 paralogues remains incompletely understood.
RAD51 filaments, along with RAD54, participate in the search for and invasion of the homologous DNA sequence. Subsequently, RAD51 dissociates from the ssDNA, allowing for base-pairing between the invading and complementary donor strands. Once homology is established, a displacement loop (D-loop) is generated, forming a primer-template junction that facilitates DNA repair synthesis. The 3′ end of the D-loop, which has invaded the structure, can undergo extension by a DNA polymerase. This polymerase utilizes the homologous strand as a template for DNA synthesis.

After repair synthesis is finished, HR can progress through two pathways: synthesis-dependent strand annealing (SDSA) or Holliday junction (HJ) formation (Heyer et al., 2010). In SDSA, the extended break end is displaced from the D-loop and subsequently anneals to the complementary sequence at the non-invading end and ends in non-crossover product. HJs can be formed through the annealing of the non-invading end to the displaced strand of the D-loop in a second-end capture step, or possibly by the simultaneous invasion of the two resected ends into the donor and their subsequent extension (Matos et al., 2014). To ensure proper chromosome segregation, the intertwined strands must be separated, which can occur through two distinct mechanisms. Double HJs, which are common HR intermediates, can be processed via migration by the BTR (BLM, TOP3A-RMI) complex which can separate the sister chromatin without genetic exchanges. Alternatively, HJ can be resolved later in the cell cycle by SLX1-SLX4-MUS81-EME1 complex resulting in crossover or non-crossover products (Stephen C West 2015).

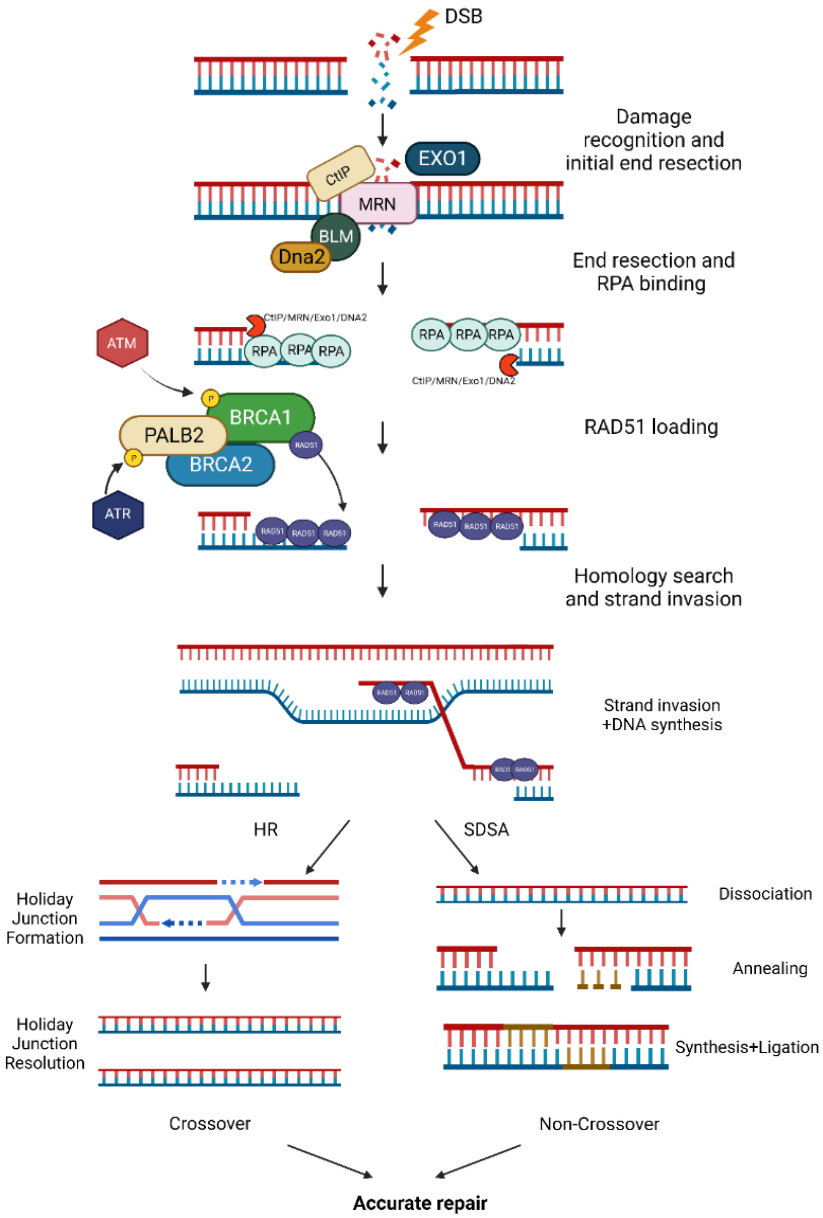

Figure 4. Schematic overview of homologous recombination repair.

HR repair involves the creation of 3′ overhangs suitable for Rad51 loading. Precise repair occurs through synthesis-dependent strand annealing (SDSA), or complete homologous recombination (HR) followed by the dissolution or resolution of the double Holliday junction (Mirman et al., 2020). Figure created using BioRender.

1.2.4 Alternative non-homologous end joining

Alternative end joining (Alt-NHEJ), also known as microhomology-mediated end joining is defined as an error prone repair pathway, which functions without the use of c-NHEJ factors and operates on 3'-ssDNA ends (Figure 5) (Yan et al., 2007). Alt-NHEJ repair of DSBs is most active during the S and G2 phases of the cell cycle (Xiong et al., 2015) and requires a Pol θ (DNA polymerase theta) (Koole et al., 2014; Mateos-Gomez et al., 2015; Wood et al., 2016), with the potential involvement of PARP1, CtIP and the MRN complex (Han et al., 2008; Masani et al., 2016; Sfeir et al., 2015).

The first step of alt-NHEJ requires end resection performed by endonuclease activity of MRN which is activated by phosphorylated CtIP. MRN trims the DNA ends and creating 3'-overhangs spanning 15 to 100 nucleotides (Xie et al., 2009). The MRN/CtIP complex is recruited to the DSB by PARP1 which serves as a detector for breaks in the DNA structure (G. Yang et al., 2018). The next step is the alignment and linking of the DNA ends by the short microhomologies performed by MRN, Polθ and PARP1 (Haince McDonald Rodrigue Dery et al., 2008). Next the nucleases ERCC1\XPF digest the 3' tail, thereby generating gaps within the DNA strand which are filled by Polθ-mediated DNA synthesis (Kent et al., 2015). Finally, the DNA ligase 3 (LIG3)/XRCC1 complex repairs the DNA, specifically XRCC1, a scaffolding protein, facilitates the proximity of LIG3 to DNA breaks through a physical interaction with both PARP-1 and the MRN complex, ultimately resulting in DSB repair.

Alt-NHEJ is considered an error prone repair pathway due to several reasons, including imprecise end joining mechanisms and delayed repair kinetics (Wang et al., 2003). The exonuclease and endonuclease machinery within this pathway generate substantial deletions, revealing microhomology regions (Zhuang et al., 2009). Polθ, with its low-fidelity gap-filling capability, plays a role in introducing significant sequence irregularities, especially insertions, at repair sites. This is a result of Polθ's terminal transferase activity and the repetitive synthesis of ssDNA (Arana et al., 2008; Wood et al., 2016). Alt-NHEJ has been suggested to have a role as a backup repair mechanism when HR and c-NHEJ are defective (Iliakis et al., 2015). Several hypotheses have been proposed that once c-NHEJ and HR machinery have attempted repair and by some means DNA end processing has failed, alt-NHEJ takes over the DNA DSB repair. Alt-NHEJ therefore presents a hopeful avenue for therapy in cases of cancer with deficiencies in HR or c-NHEJ. Impeding alt-NHEJ has the potential to selectively eradicate cancer cells reliant on this pathway for DNA repair, thereby preserving the integrity of healthy cells. Alt-NHEJ has exhibited heightened activity in various cancers, including breast (Tobin et al., 2012), leukemia (Hahnel et al., 2014) and neuroblastoma (Newman et al., 2015). Specifically, in neuroblastomas, alt-NHEJ has been shown to play a crucial role in both cell survival and genomic instability. Consequently, inhibition of key alt-NHEJ factors lead to accumulation of DSB and cells death (Newman et al., 2015).

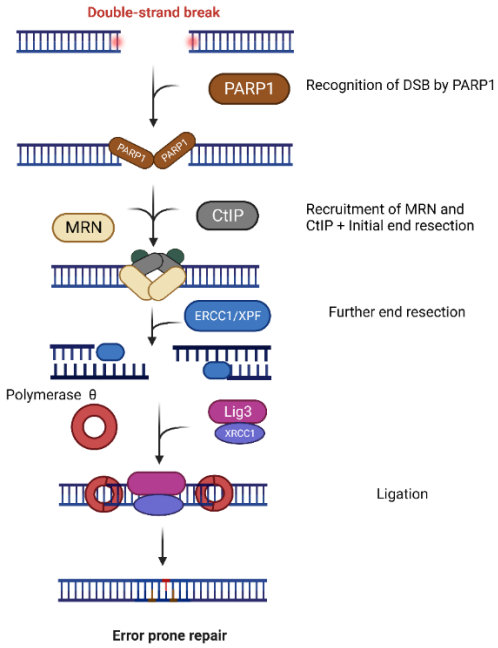

Figure 5. Schematic overview of alternative non-homologous end joining repair.

Alternative non-homologous end joining (alt-NHEJ) depends on PARP1 for the recognition of the DSB and recruit MRN complex and CtIP to the break where MRN initiates end resection. The ERCC1 nuclease performs additional end resection, creating a gap in the DNA strand that is filled in by the error prone Polθ. Finally, the Lig3/XRCC1 complex ligates the strands together. Alt-NHEJ is considered an error-prone pathway, leading to significant sequence irregularities, particularly insertions (highlighted in red), at repair sites. Figure created using BioRender.

1.2.5 Single strand annealing

Single strand annealing (SSA) is a DSB repair pathway that is independent of RAD51 that joins two homologous 3′-ssDNA via annealing, at the cost of deletion of the intervening sequence between the repeats (Paques et al., 1999). SSA has been observed in mammalian cells as well as in various model organisms, including *S. cerevisiae*, *A. thaliana*, *D. melanogaster*, and *C. elegans* (Do et al., 2014; Ivanov et al., 1996; Orel et al., 2003; Pontier et al., 2009). In mammalian cells SSA is dependent on RAD52 (Benitez et al., 2018). DNA end resection that takes place during SSA repair is extensive, leading to a large overhang and pairing of a long homology which result in loss of genetic material, making SSA an error prone repair pathway (Ceccaldi et al., 2016). Unlike HR repair, SSA does not need a homologous donor sequence. Similar to alt-NHEJ, SSA requires extensive 5′-end resection of DSB end to reveal complementary homologous sequences, however, when compared to alt-NHEJ, the end resection in SSA is more extensive. SSA end resection is generated by the MRN complex and CtIP to form 15-100 nucleotide 3′ ssDNA tail, at this point SSA and alt-NHEJ diverge. While the microhomology annealing of alt-NHEJ is enough for Polθ to extend one DNA

strand, generating a stable structure for ligation, SSA calls for more sequence homology and a further extension reliant on the action of EXO1, BLM or DNA2 in order to generate longer 3′-ssDNA tails (Mimitou et al., 2008; Symington et al., 2011).

Following the end resection, secondary structures of the long 3′-ssDNA tails are prevented by coating the tail with RPA. The subsequent phases of SSA encompass the alignment of the adjacent repeats and the ensuing removal of non-homologous 3′ ssDNA tails. These processes are facilitated by RAD52 and ERCC1 with RAD52 mediates the pairing of ssDNA substrates (Rothenberg et al., 2008) and displaces the RPA molecules coating the ssDNA. Simultaneously, ERCC1 (Excision Repair Endonuclease Non-Catalytic Subunit 1) forms a complex with XPF (excision repair cross-complementation group 4), which proficiently cleaves the 3′ ssDNA tail through nucleolytic activity (Motycka et al., 2004). DNA polymerases, with support from DNA ligases, fill any gaps. The non-homologous region of the 3′ssDNA tail which must be processed and removed before ligation by XPF-ERCC1 means that the intervening sequences between the complementary regions are lost, making SSA a mutagenic repair pathway (Figure 6). It is important to note that not all the ligases or polymerases participating in SSA have been identified (Bhargava et al., 2016).

Research has confirmed that the process of DSB end resection, which results in the creation of 3′-ssDNA, represents a crucial stage in SSA repair. For instance, the success of SSA is reliant on CtIP, (Ceppi et al., 2020), a key factor responsible for end resection. On the other hand, factors that inhibit end resection have been observed to suppress SSA. This includes elements of the DNA damage response pathway, such as H2AX, RNF168, 53BP1, and Rap1 interacting factor 1 (RIF1) (Escribano-Diaz et al., 2013; Munoz et al., 2012). Like alt-NHEJ, SSA has been suggested as an alternative repair of DSB in HR compromised cells (Deniz et al., 2017), in particular BRCA deficient cells (van de Kooij et al., 2023) leading to the possibility of SSA related proteins as targets in BRCA deficient cancer.

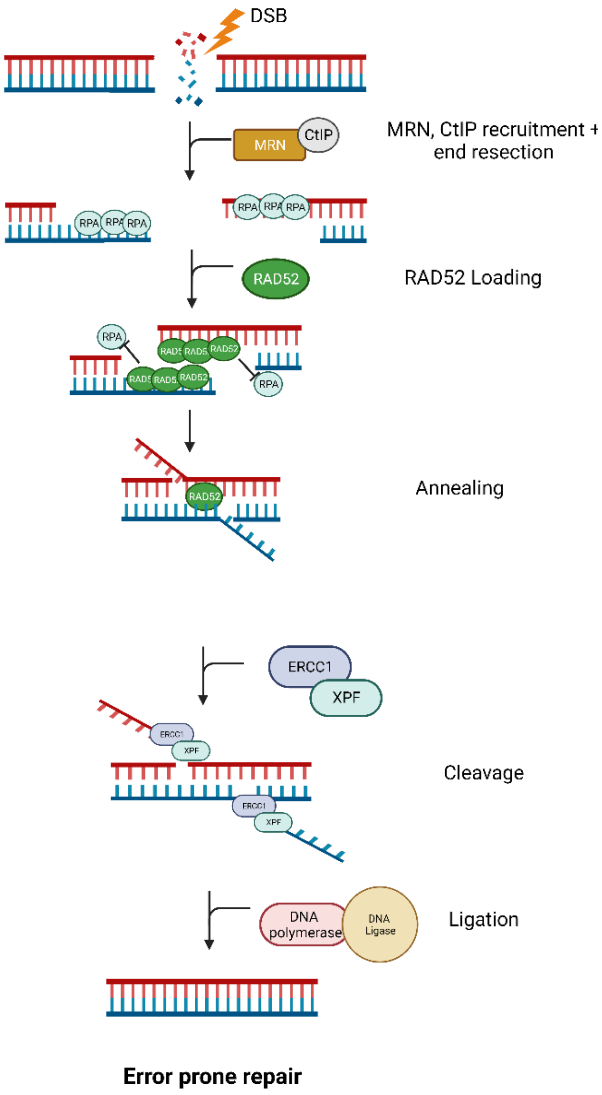

Figure 6. Schematic overview of Single strand annealing repair.

Single-strand annealing (SSA) repair is facilitated by RAD52 and requires extensive end resection by the MRN complex and CtIP, followed by the loading of RPA to prevent the formation of secondary structures. RAD52 interacts with RPA-coated single strands and facilitates the annealing of complementary regions, aligning the DNA ends and exposing nonhomologous 3′ single-strand tails. ERCC1/XPF removes the 3′ tails, and any gaps are filled in by DNA ligase and polymerase. Figure created using BioRender.

1.2.6 DNA repair defects

Genetic disruption of any of the DSB repair pathways or the DDR cause genomic instability in mammalian cells and inherited deficiencies in genes in theses pathways play a role in numerous human disorders, such as heightened vulnerability to cancer, neurological impairment, and immunodeficiency. These disorders include Ataxia-telangiectasia, Riddle Syndrome, Bloom syndrome, Nijmegen syndrome, DNA ligase 4 syndrome and Artemis deficiency (Altmann et al., 2016; Moshous et al., 2001; Taylor et al., 2019).

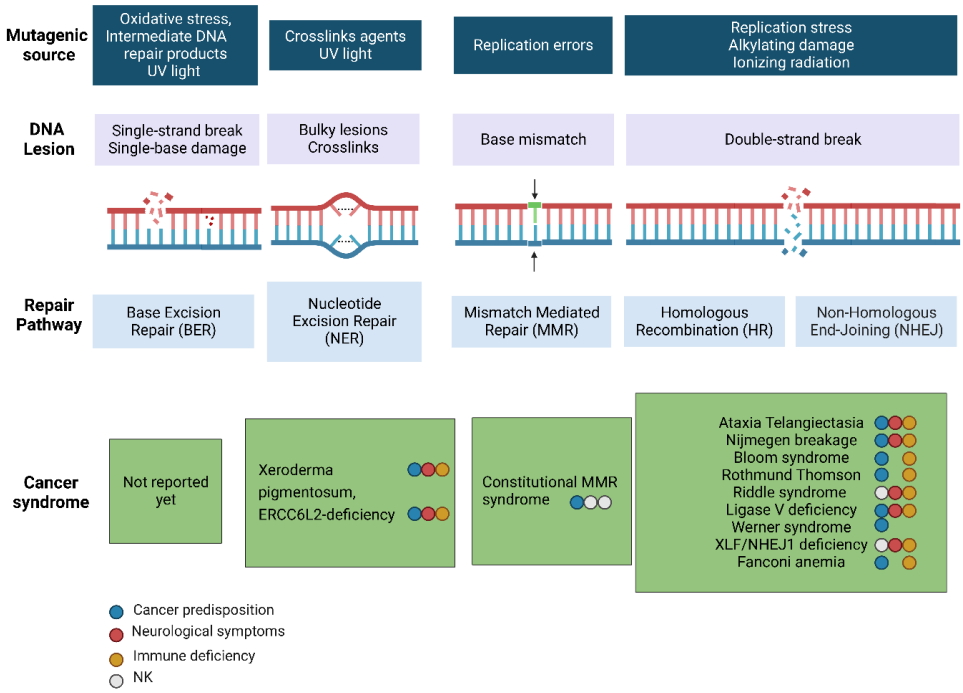

Figure 7. DNA repair disorders associated with cancer predisposition.

Schematic overview of human diseases associated with deficient mechanisms of DNA damage repair. Syndromes caused by mutations in genes involved in DNA damage repair categorized by syndrome, DDR pathways affected, and presenting symptoms (Sharma et al., 2020). Not known (NK). Figure created using BioRender.

In cancer cells, DNA repair pathways are often impaired due to mutations in DNA repair or DNA signaling proteins. In certain cases, these mutations may be classified as passenger events with no functional impact, while in others, they can impair DDR pathways leading to increased genomic instability (Figure 7). One of the best-known example is the tumor suppressor genes *BRCA1* and *BRCA2* which are frequently found mutated in cancers, specifically breast and ovarian cancer (Venkitaraman, 2002). As

previously mentioned, both BRCA1 and BRCA2 are vital for HR repair of DSBs but are also important for the resolution of R loops (Crossley et al., 2019) and protecting against stalled replication forks as BRCA1/BRCA2 deficient cells cannot properly repair collapsed replication forks (Schlacher et al., 2011). Mutations in other HR genes, such as *PALB2*, *BRIP1*, *RAD51C*, and *RAD51D* are also found cancer (Antoniou et al., 2014; Suszynska et al., 2020). HR genes are not the only DNA repair genes found mutated in cancer as defects in the c-NHEJ pathway have also been associated with cancer, with mutations in *KU70*, *KU80* and *DNA ligase 4* found in number of cancers including lung and breast cancer (Lee et al., 2007; Willems et al., 2008; Yin et al., 2012). Furthermore, mutations have also been found in DNA damage checkpoint genes in cancer for example *CHK1*, *CHK2*, *ATM* and *ATR* (Bartek et al., 2003; Weber et al., 2015).

While genomic instability can drive tumorigenesis, compromised DDR pathways can also make cancer cells more vulnerable to further defects in the DDR and to DNA damage. Targeting particular DDR proteins in cancer cells with DDR defects or elevated genomic instability can induce synthetic lethality, offering a promising approach for cancer therapy (O'Connor, 2015). One of the best-known examples of synthetic lethality in cancer is PARP inhibitors (PARPi) which are used to target HR-deficient cells (Bryant et al., 2005). PARPi inhibits PARP1 and PARP2, consequently impeding the BER pathway. This inhibition results in an elevated accumulation of ssDNA breaks in the genome, which during DNA replication are converted into DSB. HR deficient cells are sensitive to PARPi as they are unable to repair the replication induced DSB. Other DDR inhibitors exist and have shown efficacy in cancer cells with increased genomic instability or DDR defects, these including ATR and ATM inhibitors (Yap et al., 2020) (Shu et al., 2023). Although DDR inhibitors show great efficacy in cancer treatment, long-term usage often leads to the development of drug resistance. Several mechanisms contributing to PARPi resistance have been identified, prompting extensive research efforts to overcome this challenge (H. Li et al., 2020). Even with extensive studies of DNA repair and DNA damage signaling pathways in cancer there is still a lack of complete understanding of how these pathways function in different oncogenic contexts. The reasons behind the loss of specific DDR pathways in certain cancer types and whether different tissue and cell types respond differently to the loss of DDR pathways remain unclear. Comprehending the diverse origins of genomic instability in cancer cells and the implications of defects in DDR within various oncogenic contexts is essential for devising targeted strategies to induce synthetic lethality and to overcome challenges such as DDR inhibitor resistance.

1.2.7 Choice of DNA DSB repair pathway

Maintaining genomic integrity relies on the delicate balance between DSB repair pathways. Each pathway is suited to specific circumstances and choosing the wrong one can result in ineffective repair, potentially increasing genomic instability (Ceccaldi

et al., 2016). The choice of repair pathway is influenced by factors including end resection, chromatin context, cell cycle phase, and the DNA lesion itself. The current working model of DNA DSB repair dictates that c-NHEJ is the predominant repair pathway of DSB in humans since it can operate throughout the cell cycle (Davis et al., 2013; Lieber, 2010). The three other available repair pathways (HR, SSA and alt-NHEJ) are constrained to S and G2 stage of the cell cycle due to their dependence on 3′ ssDNA overhang caused by DNA end resection (Ceccaldi et al., 2016; T. Liu et al., 2016). End resection catalyzes the nucleotide degradation of the broken end in the 5′-3′ direction therefore plays a substantial role in regulating pathway choice (Figure 8).

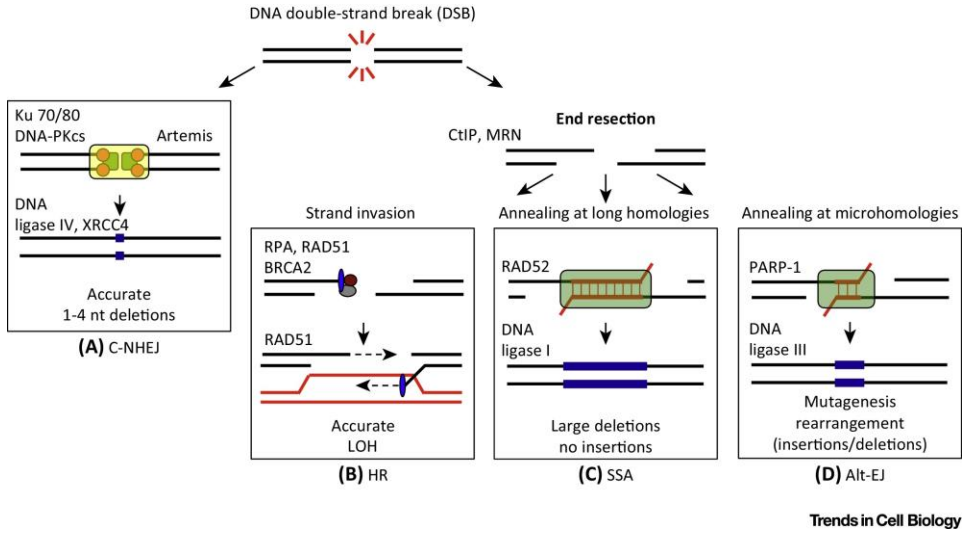

Figure 8. DNA end resection and the four approaches to repair DNA DSB.

DNA end resection can influence the choice of DSB repair pathway. When end resection is blocked, c-NHEJ repair (A) is favored. When end resection occurs, HR (B), SSA(C) and alt-NHEJ (D) can compete to repair the DSB (Ceccaldi et al., 2016).

DNA end resection only takes place in S/G2 phase of the cell cycle (Longhese et al., 2010) and is a two strep process. The first step relies on the MRN complex and associated CtIP protein to start end processing which displaces the Ku70/Ku80 complex from DSB ends in human cells (Chanut et al., 2016; Langerak et al., 2011; Mimitou et al., 2010). In the second step DNA ends are processed further by DNA2-BLM and EXO1 to generate long stretches of ssDNA (Nimonkar et al., 2011; Takata et al., 1998). The 3′ overhang created by DNA end resection not only inhibits c-NHEJ, as it prefers blunt DNA ends but also dictates the choice among the other three pathways (HR, SSA and alt-NHEJ) (Hauer et al., 2017; Nick McElhinny et al., 2000). The two key proteins when it comes to regulate DNA DSB repair pathway choice are 53BP1 and BRCA1.

ATM, MDC1, MRN complex, and the RING finger E3 ubiquitin ligases RNF8 and RNF168 are some of the initial components observed in DNA damage foci (Bekker-Jensen et al., 2010). The recruitment of 53BP1 and BRCA1 occurs subsequently, relying on the previously mentioned upstream factors (Mailand et al., 2007). 53BP1 is quickly localized to DSB as it recognizes histone methylation (H4 Lys20) and ubiquitination on histone H2A at Lys15, which is performed by RNF168 (Botuyan et al., 2006). ATM phosphorylates 53BP1 N-terminal region which leads to recruitment of Pax2 transactivation interaction protein (PTIP) and RIF1 to limit DNA end resection during G1 phase of the cell cycle (Callen et al., 2013; Chapman et al., 2013; Escribano-Diaz & Durocher, 2013; Escribano-Diaz Orthwein et al., 2013; Feng et al., 2013). PTIP's role in blocking end resection involves recruiting a downstream protein, Artemis, which induces c-NHJE by trimming DNA ends (J. Wang et al., 2014). RIF1 recruits a fairly newly discovered proteins complex, the Shieldin complex, which protects DSB from BRCA1-dependent end resection (Arnoult et al., 2017; Noordermeer et al., 2018).

Cyclin-dependent kinase (CDKs) activity which increases as cells enter S phase, is an important step for the activation of the end resection machinery and for repair proteins important for HR repair (Aylon et al., 2004; Ferretti et al., 2013; Hustedt et al., 2016; Ira et al., 2004; Symington et al., 2011). Phosphorylation of CtIP by CDKs promotes CtIP-BRCA1 interaction in S/G2 phase of the cell cycle (Reczek et al., 2013; Yu et al., 2004) allowing BRCA1 to antagonizes c-NHEJ by impairing RIF1 retention in a CtIP dependent manner, thereby enabling DNA end resection (Bunting et al., 2010; Daley et al., 2014) (Chapman et al., 2013; Escribano-Diaz et al., 2013; Feng et al., 2013). HR is suppressed during G1 by a variety of mechanisms including destabilization of CtIP by proteasome-mediated degradation (Germani et al., 2003). In G1 phase, 53BP1 and RIF1 prevent BRCA1 recruitment to DSB sites (Callen et al., 2013; Chapman et al., 2013; Feng et al., 2013), leading to a battle between 53BP1-RIF1-PTIP and BRCA1 to determine end protection or resection.

DSB end structure is another factor that can influence repair pathway choice (Chapman et al., 2012; Liu et al., 2014; Shibata, 2017). In general, DSB can be categorized into one-and two ended DSBs (Shibata, 2017). One ended breaks are the result of replication forks encountering a single stranded break (SSB) and are preferably repaired by HR due to the lack of another DNA end for end joining (Bunting et al., 2010; Wang et al., 2013). Two ended DSBs are generated by ionizing radiation or DNA topoisomerases II inhibitor like etoposide. Normal healthy cells utilize c-NHEJ to fix the majority of two-ended breaks but in G2 HR can repair ~30% of two-ended DSBs (Beucher et al., 2009).

1.3 RNF168

Ring finger protein 168 (RNF168) is a 571-amino acid nuclear protein with E3 ubiquitin protein ligase activity. It is a key protein in the regulation of DDR pathway and is important to maintain genome stability (Bohgaki et al., 2011; Doil et al., 2009; Stewart

et al., 2009). Initially discovered due to its association with radiosensitivity, immunodeficiency, dysmorphic features, and learning difficulties (RIDDLE) syndrome, first reported in 2007 (Stewart et al., 2007). RIDDLE syndrome is a rare genetic disorder in humans caused by a mutation in RNF168 and is linked to impaired DSB repair due to loss of 53BP1 recruitment to the site of DSBs (Devgan et al., 2011; Stewart et al., 2009). Individuals diagnosed with RIDDLE syndrome display a broad clinical spectrum, featuring symptoms like ataxia, learning challenges, respiratory issues, microcephaly, heightened radiosensitivity, and diminished immunoglobulin levels. In mice RNF168 knockout (KO) results in faulty recruitment of key DNA DSB repair factors to the site of DNA damage and the mice suffer from radiosensitivity, immune-defect and decreased spermatogenesis (Bohgaki et al., 2011). Collectively, RNF168 is considered a multifaceted regulator of the intricately orchestrated DDR pathway at damaged chromatin and a guardian of genome stability.

1.3.1 The role of RNF168 in the DNA damage response

The chromatin, consisting of DNA and associated histone and non-histone proteins, plays a critical role in shaping the structure and functionality of the genome. To effectively repair DNA damage, the DDR signaling network orchestrates the assembly of multi-protein complexes at the damaged chromatin. The spatiotemporal dynamics of these protein complexes at damage sites are primarily regulated by post-transcriptional modifications (PTMs) (Huen et al., 2008). One such PTM is ubiquitination which is known to play a significant role in coordinating the cellular response to DSBs to ensure accurate and efficient repair (Popovic et al., 2014). Ubiquitination not only facilitates recruitment of key DDR factors to DSB but also has a vital role in determining the appropriate repair pathway for DSB repair. RNF168 has been identified as a crucial component in orchestrating ubiquitin signaling within the DDR and together with another E3 ligase, RNF8, promotes histone ubiquitination of H2A/H2AX in response to DNA DSBs (Doyle et al., 2010).

RNF168 is recruited to the damaged chromatin via the MRN complex and ATM kinase (Lee et al., 2004; Uziel et al., 2003). ATM phosphorylates H2AX at serine 139, creating γH2AX, which acts as a docking station for the binding of MDC1, which in returns recruits RNF8 via protein-protein interactions (Bekker-Jensen et al., 2010; Scully et al., 2019). RNF168 recruitment to DSB is further dependent on the activities of RNF8 and Lethal(3)malignant brain tumor-like protein 2 (L3MBTL2) (Nowsheen et al., 2018). ATM-dependent phosphorylation of L3MBTL2 relocates it to the proximity of the DNA lesion. RNF8 then acts on this phosphorylated L3MBTL2, producing K63-linked polyubiquitin chains which is subsequently identified by RNF168 via its ubiquitin binding domain, anchoring RNF168 to the DNA lesion (Doil et al., 2009; Nowsheen et al., 2018).

Once RNF168 is recruited to the damaged chromatin it ubiquitinates site-specific H2A mono-ubiquitination at K13 (H2A/H2AXK13ub) and K15 (H2A/H2AXK15ub) while also collaborating with RNF8 to generate K63-linked ubiquitin chains (Gatti et al., 2012; Mattiroli et al., 2012; Pinato et al., 2009). The H2A/H2AXK13/15ub acts as a recruitment scaffold for recruiting DNA repair proteins that bind to ubiquitin at the damaged chromatin, such as 53BP1 through its ubiquitin-dependent recruitment motif (Fradet-Turcotte et al., 2013). The RNF8/RNF168-catalyzed K63-linked ubiquitin chain is also responsible for the recruitment of the BRCA1-Abraxas-RAP80-MERIT40 (BRCA1-A) complex (Sobhian et al., 2007). The BRCA1-A complex is composed of seven proteins, including BRCA1 and RAP80 is thought to fine-tune the repair function of BRCA1 by influencing DNA end resection (Coleman et al., 2011). In addition to the conventional K63-linked ubiquitin chains, RNF168 is also responsible for generating non-canonical K27-linked ubiquitin chains on chromatin. K27 ubiquitination is essential for the appropriate initiation of the DDR and the assembly of DSB repair proteins (Gatti et al., 2015), further highlighting the importance of RNF168 for DDR signaling.

Including its involvement in repairing DNA DSBs, the process of chromatin ubiquitination also plays a crucial role in various other pathways responsible for maintaining genomic integrity. This includes DNA crosslinks repair (Katsuki et al., 2021), telomeres maintenance (Rai et al., 2011), facilitating DNA replication (Schmid et al., 2018), resolving R-loops (Patel et al., 2021), and preventing the transcription machinery from accessing damaged DNA sites (Shanbhag et al., 2010). While it generally contributes positively to genome maintenance, excessive activation of the RNF8/RNF168-dependent chromatin signaling pathway can have detrimental effects on cellular function (Altmeyer et al., 2013; Gudjonsson et al., 2012), occasionally leading to tumorigenesis (Patel et al., 2021).

Changes in the abundance of RNF168 within the cell nucleus can lead to significant alterations in the dynamics of DNA DSB repair, increasing the utilization of error-prone repair methods (Zong et al., 2015) and promoting non-homologous end joining at exposed telomere ends (Peuscher et al., 2011), thus elevating the risk of introducing mutations and chromosome end fusions. Consequently, cells have developed a set of mechanisms to counteract the actions of RNF168 on damaged chromatin. Negative regulators, including deubiquitinating enzymes (DUBs) counteract RNF168-mediated ubiquitination at damaged chromatin, preventing excessive signal spreading, (Lancini et al., 2014; Mosbech et al., 2013) and competitive binding of RNF169 to H2A ubiquitination mediated by RNF168 resulting in displacement of 53BP1 and RAP80 from DSBs (Chen et al., 2012; Poulsen et al., 2012). A more precise form of RNF168 control is exerted by two ubiquitin E3 ligases, TRIP12 and UBR5. TRIP12 and UBR5 are upstream regulators of RNF168 which strictly regulate RNF168 nuclear pool by degrading RNF168 thereby preventing unwarranted ubiquitin signal amplification and to suppress excessive spread of ubiquitination to undamaged chromosomes in the vicinity of DNA lesions (Gudjonsson et al., 2012). Additionally, recent investigations

have revealed that UBA80 and UBA52, unique ubiquitin-ribosomal fusion proteins, serve as additional regulatory factors of RNF168. Their function involves limiting RNF168 engagement to damaged chromatin to fine-tune the ubiquitin DDR signaling (Lee et al., 2023).

1.3.1.1 *RNF168 Ubiquitination and choice of DNA repair pathway*

As previously mentioned, DSB can be repaired by two major pathways: c-NHEJ and HR. The decision between HR and NHEJ is controlled by a signaling pathway that entails the stepwise modification of chromatin surrounding DSBs (Polo et al., 2011). This pathway involves the combined action of both RNF8 and RNF168 which promote the ubiquitin-dependent recruitment of the BRCA1 and 53BP1 to DSB (Doil et al., 2009; Escribano-Diaz et al., 2013; Huen et al., 2007; Mailand et al., 2007; Stewart et al., 2009; Wang et al., 2007).

In general, c-NHEJ is reliant on 53BP1 binding to H2A/H2AX K13/15 ubiquitination which is mediated by RNF168. 53BP1 recruits RIF1 which inhibit DNA end-resection and subsequently HR (Chapman et al., 2012; Escribano-Diaz et al., 2013; Munoz et al., 2012; Schwertman et al., 2016). The current consensus underscores the pivotal role of end resection in determining the choice of DNA DSB pathway. Following the formation of DSB a competition between 53BP1 and BRCA1 takes place to guide the cell towards c-NHEJ or HR (Daley et al., 2014). Interestingly, the ubiquitination actions of RNF168 do not seem to be intrinsically inhibitory to HR as the end resection inhibition takes place downstream of RNF168-53BP1 via RIF1 recruitment. With the inhibitory impact of RIF1 relieved, RNF168 is still capable of ubiquitinating the chromatin in S/G2 phase (Doil et al., 2009). Furthermore, other repair proteins besides 53BP1 have shown binding affinity to the RNF168 mediated H2A/H2AX-K15 ubiquitination including RAD18 via its UB2 domain and BARD1 via its BRCT domain (Figure 9) (Becker et al., 2021; Hu et al., 2017; Mustofa et al., 2021).

A 2021 study conducted by Becker et al., provided insights into the mechanisms by which RNF168 facilitates the recruitment of BRCA1 via the H2AX-K15 ubiquitination modification. Their research demonstrated that BARD1 is recruited to DNA damage via a dual mechanism involving both interactions with H2AK15ub through a BRCT-domain-associated ubiquitin-dependent recruitment motif (BUDR) and through interactions with histone H4 unmethylated at K20 via BARD ANK domain, subsequently recruiting BRCA1 to DSB. Disruption of the BUDR motif compromised HR repair and induced PARPi sensitivity (Becker et al., 2021). The findings from Becker et al., were later corroborated by Krais et al., which likewise found that mutating the BUDR motif of BARD1 or hindering RNF168 ubiquitination activity, reduced BRCA1 recruitment to DSB. More specifically, Krais et al., established essential molecular interactions between RNF168 ubiquitination and the PALB2-BRCA2-mediated HR repair pathway by demonstrating that the BARD1 recruitment via the BURD motif is vital for subsequent recruitment of BRCA1-P complex (BRCA1-PALB2-BRCA2-RAD51) to DNA DSB.

Furthermore, their research suggested that RNF168 recruits BRCA1-P complex independently of the BRCA1-A complex, with RNF8-RAD80-BRCA1 signaling providing a backup route in RNF168$^{-/-}$ and BARD1$^{-/-}$ cells (Krais et al., 2021).

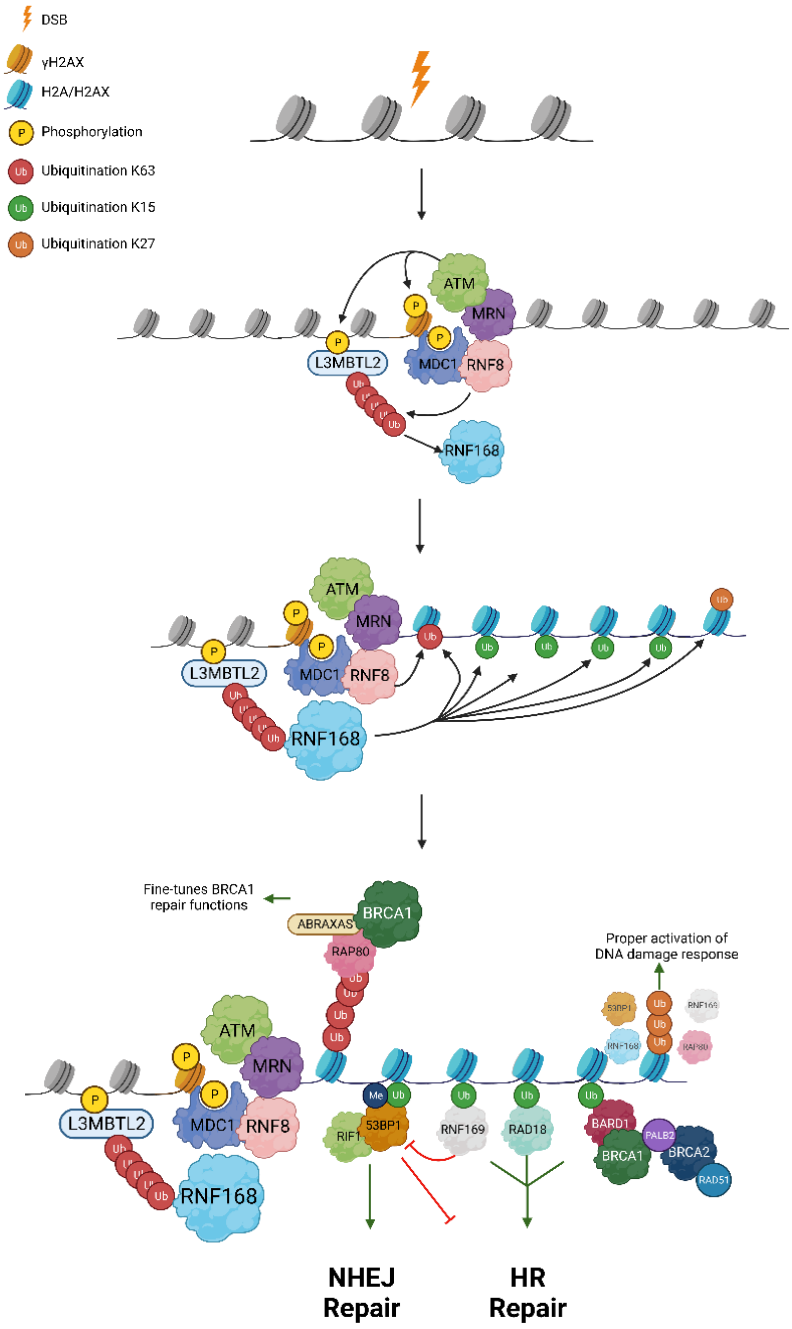

Figure 9. A simplified overview of RNF8-RNF168 chromatin ubiquitination in response to DSBs.

Induction of DSB leads to phosphorylation of H2AX to γH2AX by ATM, which is recruited to DSB via the MRN complex. ATM recruits MDC1 which in turn recruits RNF8. RNF8-mediated K63-ubiquitination of L3MBTL2 has been proposed to recruit RNF168. The concerted efforts of RNF8 and RNF168 result in K63-linked ubiquitin chains (red), responsible for recruiting the RAP80 and BRCA1-A complex. RNF168 mono-ubiquitinates H2A/H2AX on K15 (green), which acts as a recruitment scaffold for DNA DSB repair proteins such as 53BP1 (driving NHEJ repair), RAD18, RNF169, and BARD1 (driving HR repair). RNF168 further mediates non-canonical K27-linked ubiquitin chains (orange), recognized by repair factors including 53BP1, RNF169, and RAP80. K27 ubiquitination is thought to be vital for the proper activation of the DDR response (Gatti et al., 2015). Figure created using BioRender.

In 2017, Luijsterburg et al., unveiled an unexpected role for RNF168, demonstrating its involvement in coupling the HR machinery to the ubiquitination of H2A/H2AX in S/G2 cells. The study revealed that RNF168 plays a role in recruiting PALB2 to DSB in an H2A-K13/K15 ubiquitin-dependent manner. RNF168 and PALB2 interacted in a direct protein-protein manner via a newly identified PALB2-inteacting-domoain (PID) on RNF168 and WD domain of PALB2 to facilitated PALB2 chromatin interaction. PALB2 recruitment, in turn, facilitates the assembly of BRCA2 and RAD51 at DSBs, key components in the HR repair pathway. RNF168 mediated recruitment of PALB2 to DSB was found to be independently of the BRCA1-A complex as it took place downstream of BRCA1. Luijsterburg et al., further revealed that loss of RNF168 lead to defective HR repair in S/G2, along with impaired RAD51 and PALB2 recruitment to DSB. Furthermore, cellular depletion of RNF168 was shown to increase sensitivity to PARP inhibitors, a characteristic hallmark of defective HR repair (Luijsterburg et al., 2017).

In a 2019 study, Zong et al., confirmed the ubiquitin dependent RNF168 recruitment of PALB2 and provided nuanced insights into the physiological significance of RNF168-mediated PALB2-chromatin loading. Their research demonstrated that cells activate a RNF168-dependent pathway as a backup mechanism to recruit PALB2 and RAD51, promoting HR when BRCA1 protein expression or its interaction with PALB2 falls below the 50% threshold. Furthermore, Zong and colleagues showed that RNF168 activity was essential to restore HR and cell viability in *BRCA1/53BP1* deficient cells and in order to maintain genomic stability and prevent tumorigenesis in *BRCA1* heterozygous mice (D. L. Zong et al., 2019). In the absence of BRCA1, research has demonstrated that downregulation of RNF168 provides BRCA1 null cancers cells with lingering level of HR via recruitment of PALB2 which is essential for the BRCA1 null cells to retain tumorigenicity and vitality. Reintroducing RNF168 expression resulted in BRCA1 null cell death and delayed tumor formation (Krais et al., 2020). From this, it is evident that RNF168-mediated ubiquitination plays a more substantial role in HR repair beyond opposing the initial end resection step. Collectively the current research points toward RNF168 as a versatile regulator of the intricate orchestrated DDR pathway at damaged chromatin.

1.4 Alkylating damage

Alkylating lesions, a prevalent form of DNA damage, arise from both environmental factors and endogenous processes (Rydberg et al., 1982). These lesions result from alkylating agents, compounds capable of transferring alkyl groups onto nucleophilic nitrogen or oxygen atoms found in DNA base molecule (Shrivastav et al., 2010). Alkylating agents induce nucleophilic substitution reactions, operating via monomolecular (S_N1) or bimolecular (S_N2) mechanisms. S_N2 agents primarily target ring nitrogen atoms in bases, while S_N1 agents can interact with both nitrogen and external oxygen atoms. Alkylating agents also create adducts with RNA and protein and this is likely to play a role in their cytotoxic effects. Repair of alkylating damage is critical as most alkylating lesions are mutagenic and cytotoxic. Cells have therefore developed several DNA repair mechanisms in order to protect against alkylating damage. Depending on the type of damage, cells rely on three major repair pathways to repair alkylating damage: direct repair by the AlkB family of enzymes, direct demethylation by O6-methylguanine DNA methyltransferase and the removal of the modified base by base excision repair. This thesis will focus on the AlkB protein family.

1.4.1 The Alpha -ketoglutarate-dependent dioxygenase family

The Alpha-ketoglutarate-dependent dioxygenase (AlkB) family is Fe (II) and alpha-ketoglutarate- dependent enzymes. They are a part of the DNA damage response network (Fedeles et al., 2015) and remove alkylating damage from nucleic acid bases via oxidative dealkylation using cofactors Fe (II) and α-ketoglutarate. This process removes the methyl group by converting alpha-ketoglutarate to succinate, releasing carbon dioxide and formaldehyde (Sedgwick et al., 2007). The initial identification of the AlkB protein occurred in *Escherichia coli* (*E. coli*) in 1977 (Samson et al., 1977). AlkB exhibits a broad spectrum of substrates, encompassing N^1-methyladenine (m^1A) and N^3-methylcytosine (m^3C) lesions in ssDNA (Falnes et al., 2002; Trewick et al., 2002). Mammalian cells have 9 AlkB homologs, ALKBH1-8, and the Fat mass and obesity-associated protein (FTO), also known as ALKBH9 (Figure 10) (Aas et al., 2003; Duncan et al., 2002). Only a subset of these proteins function as DNA repair enzymes. The remaining homologs lack any documented activity on DNA substrates; instead, they perform demethylation on RNA or proteins. Out of the nine members only ALKBH2 and ALKBH3 are known to have DNA repair activity, being the only homologs that complement the function of *E. coli* AlkB *in vivo* (Aas et al., 2003; Duncan et al., 2002). Other members of AlkB family include ALKBH5 and FTO which have a well-defined role as mRNA m^6A demethylases (Fu et al., 2013; Jia et al., 2011; Linder et al., 2015). ALKBH1 mainly acts as a tRNA demethylase by removing m^1A from various tRNAs (F. Liu et al., 2016) and ALKBH8 has a tRNA preference and demethylases 5-carboxy methyl uridine (Fu et al., 2010; Songe-Moller et al., 2010). ALKBH4, ALKBH6, and ALKBH7 have less well-defined roles; however, studies have indicated that ALKBH4 has demethylating activity towards proteins (Bjornstad et al., 2011), ALKBH7 towards

mitochondrial tRNA (Zhang et al., 2021) and ALKBH6 has been shown to contribute to the maintenance of genome stability during S_N2 alkylating agent-mediated DNA damage (Zhao et al., 2021).

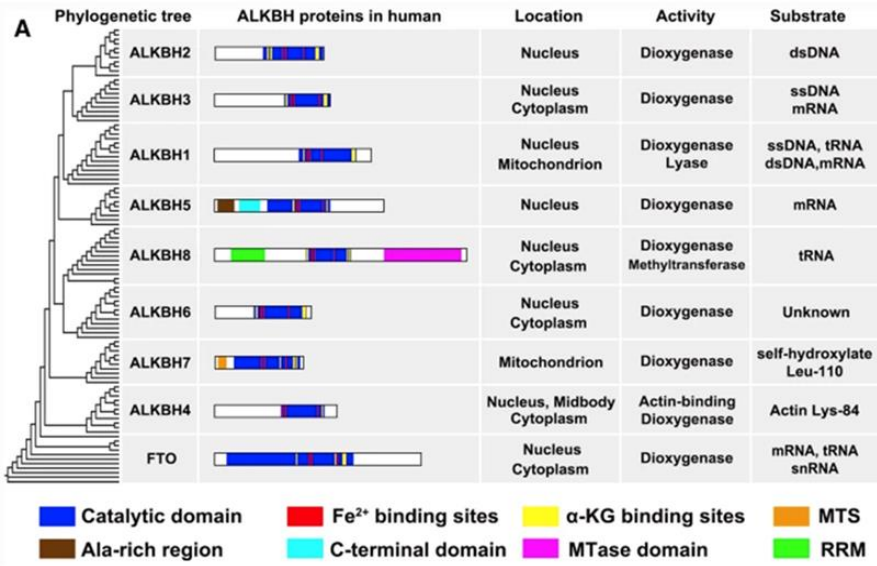

Figure 10. Overview of the AlkB family of proteins.

The phylogenetic tree of the AlkB family. Showing locations, key elements, activity, and substrate of the nine different AlkB proteins. Distinct color boxes represent different elements of the AlkB proteins (Xu et al., 2021).

1.4.2 ALKBH3

Alpha-Ketoglutarate Dependent Dioxygenase 3 (ALKBH3) is responsible for removing m^3C from ssDNA. ALKBH3 demethylation activity is dependent on the presence of ASCC3 helicase which is important for unwinding the DNA in order to access the single-stranded substrate needed for ALKBH3-mediated DNA repair (Falnes et al., 2004; Ougland et al., 2015). The lack of ALKBH3 leads to elevated levels of m^3C damage in human cells, which are believed to hamper cell growth and result in spontaneous DSBs in a cell-type-specific manner (Dango et al., 2011). As an alkylating damage repair enzyme ALKBH3 plays a role in maintaining genomic stability as alkylated DNA bases are known to inhibit DNA replication and if left unrepaired can result in DSB. In cancer cell lines reliant on ALKBH3 to repair alkylating damage, depletion of ALKBH3 leads to decreased survival, both in cell culture and increased hypersensitivity to methyl methane-sulphonate (MMS) (Dango et al., 2011).

In addition to DNA alkylation repair, ALKBH3 has also proven to be capable of acting as RNA demethylase, in particular ALKBH3 has been found to remove m^1A from mRNA

in vitro (Aas et al., 2003; Li et al., 2016) and removing m^6A, m^1A and m^3C from tRNAs (Alemu. et al., 2016; Falnes et al., 2007; Ueda et al., 2017). In 2016, Li et al utilized a combination of m^1A immunoprecipitation and RNA sequencing to highlight the prevalence of m^1A as an internal mRNA modification in HEK293T cells. Furthermore, they illustrated the reversibility of m^1A methylation, identifying it as a substrate of ALKBH3 by pinpointing thousands of reversible m^1A sites in ALKBH3 knockout HEK239T cells (Li et al., 2016). Similarly, in 2016, Dominissini et al employed liquid chromatography-tandem mass spectrometry to reveal increased m^1A methylation levels on mRNA in HEK293T cells with a mutated form of the ALKBH3 protein compared to the wild-type. Providing further evidence for ALKBH3's role in reversing the m^1A modification on mRNA (Dominissini et al., 2016). However, it is important to point out that the prevalence of m^1A modification on mRNA has been subjected to scrutiny as different studies (Safra et al., 2017; Schwartz, 2018) have reported that m^1A is less abundant on mRNA than previously reported by Dominissini and Li (Dominissini et al., 2016; Li et al., 2016).. For further information on the controversy of the m^1A modification on mRNA see chapter 1.5.1.2.

1.4.2.1 *ALKBH3 and cancer*

ALKBH3 has been found to be aberrantly expressed in numerous cancers and is known to be overexpressed in pancreatic cancer (Yamato et al., 2012), hepatocellular carcinoma (Q. Wang et al., 2018), renal cell carcinoma (Hotta et al., 2015), urothelial carcinoma (Shimada et al., 2012) and lung cancer (Tasaki et al., 2011). In all these cancers, upregulation of ALKBH3 expression was observed in tumor tissues, as opposed to normal tissues, and was correlated with reduced overall patient survival. Furthermore, ALKBH3 was found to contribute to cancer cell survival, and targeting ALKBH3 suppressed cell survival both *in vivo* and *in vitro*. Besides suppressing cell survival, ALKBH3 silencing has been shown to hinder tumor growth and migration, with involvement in signaling pathways like VEGF (in pancreatic cancer), NOX-2-ROS, and Tweak/Fn12-VEGF (in urothelial carcinoma) (Shimada et al., 2012; Yamato et al., 2012). In non-small-lung cancer and hepatocellular carcinoma KD of ALKBH3 resulted in induced expression of the cell cycle inhibitors p21 and p27, ultimately leading to cell cycle arrest, senescence, and suppressed cancer cell growth (Tasaki et al., 2011; Q. Wang et al., 2018). Collectively, the research suggests that ALKBH3 contributes to various aspects of cancer cell survival and development, potentially making it an intriguing therapeutic target for cancer therapy. These findings warrant further investigation into inhibiting ALKBH3 expression as a potential treatment strategy for certain cancers.

Conversely, ALKBH3 expression has also been found to be downregulated in a number of cancers, including breast cancer and Hodgkin lymphoma. Stefansson et al., demonstrated the epigenetic silencing of ALKBH3 in breast cancer via GpC promoter methylation. Utilizing data from both the TCGA and samples from an Icelandic breast

cancer cohort, the study revealed that ALKBH3 underwent GpC promoter methylation, resulting in transcriptional silencing in breast cancer. Notably, increased ALKBH3 promoter methylation (>20%) was associated with reduced survival (Stefansson et al., 2017). In a 2018 Pan-Cancer analysis conducted by Knijnenburg et al., it was revealed that ALKBH3 downregulation primarily resulted from epigenetic alterations. Using data from TCGA and employing integrative molecular and genomic analyses to assess DDR alterations in cancer, the study identified ALKBH3 as the second most frequently epigenetically silenced DDR gene. Specifically, 8% of all tested cancer samples (n=9125, spanning 33 cancer types) exhibited downregulation of ALKBH3 through epigenetic silencing events. (Knijnenburg et al., 2018). ALKBH3 has additionally been found to be epigenetically silenced by promoter methylation in Hodgkin lymphoma (Esteve-Puig et al., 2021). ALKBH3 promoter methylation led to transcriptional inactivation of ALKBH3 and a change in the m^1A methylation patterns in Hodgkin lymphoma cells, where increased m^1A sites were noted in cells depleted of ALKBH3. Specifically, inactivation of ALKBH3 led to increased m^1A peaks on collagen type 1 and 2 (COL1A2 and COL1A1), along with increased protein expression of both COL1A2 and COL1A1, a vital acellular components of the microenvironment of Hodgkins lymphoma. Hypermethylation of the ALKBH3 promoter was also detected in 18% (14 out of 18) of human primary Hodgkin lymphomas tested, correlating with shorter overall patient survival (Esteve-Puig et al., 2021). Epigenetic silencing of ALKBH3 in cancers may potentially serve as a novel prognostic biomarker, particularly in breast cancer and Hodgkin's lymphoma.

ALKBH3 has also been shown to affect other cancer due to its role as and RNA demethylase (Z. Chen et al., 2019). Recent research has provided evidence demonstrating that ALKBH3 contributes to cell invasion in breast and ovarian cancer by increasing the stability of *CSF-1* mRNA by demethylating m^1A from its transcript (Woo et al., 2019). The colony-stimulating factor (CSF-1) has been documented to play crucial roles in regulating tumor-associated macrophages within the tumor microenvironment and contributing to the onset and progression of numerous cancers (Ao et al., 2017; Wu Chen et al., 2022)

1.4.3 FTO

The fat mass and obesity associated protein (FTO), has been strongly linked with obesity and increased body mass index as mutations in FTO correlate with increased risk of obesity (Chu et al., 2008; Liu et al., 2013). FTO was first discovered in 2007 where it was reported to demethylate 3-methylthymine (m^3T) in ssDNA (Gerken et al., 2007). Despite showing some affinity for ssDNA FTO is best known for demethylating RNA and in 2011 FTO was first reported to catalyze the demethylation of N^6-methyladenosine (m^6A) on mRNA both *in vivo* and *in vitro* (Fu et al., 2013; Jia et al., 2011) thereby providing the first evidence of reversible post-transcriptional modifications on mRNA. Subsequent studies have demonstrated that FTO has

demethylating activity towards N^6,2′-O-dimethyladenosine (m^6A_m) located in the 5′end of mRNA (Mauer et al., 2017b), on snRNA (Mauer et al., 2019) and m^1A on tRNA (J. Li et al., 2021). It is noteworthy to mention that, despite its primary recognition for catalyzing m^6A demethylation on mRNA, FTO exhibits a higher affinity for m^6A_m as opposed to m^6A (Mauer et al., 2017a). Interestingly, it has been revealed that FTOs mRNA substrate specificity is influenced by its intracellular localization. In the nucleus, FTO predominantly targets m^6A methylated mRNA, whereas m^6A_m methylated mRNA is the primary target of FTO in the cytoplasm (Wei et al., 2018). The m^6A modification is the most abundant and prevalent internal modification found in eukaryotic mRNA, playing diverse and crucial roles in normal biological processes. As an m^6A demethylase, FTO has been shown to influence numerous physiological functions in humans. These functions encompass eukaryotic metabolism (Frayling et al., 2007), circadian rhythms (Mathiyalagan et al., 2019; C. Y. Wang et al., 2015), spermiogenesis (Wu et al., 2023) and autophagy (Yang et al., 2022).

Inactivation of the FTO gene in humans gives rise to an autosomal-recessive lethal syndrome. Cultured cells derived from individuals afflicted by this syndrome exhibited compromised proliferation and expedited senescence (Boissel et al., 2009). In mice the loss of FTO results in delayed growth after birth and a notable decrease in both adipose tissue and lean body mass (Fischer et al., 2009). More recently loss of FTO has been linked to regulation of cell cycle and mitosis checkpoint in spermatogonia in mice (Huang et al., 2018).

1.4.3.1 *FTO in cancer*

Gene variations in FTO have been correlated with increased cancer risk and in numerous scenarios where the escalated cancer risk can be directly attributed to obesity (Lan et al., 2020). However, there are certain cases where no apparent connection to obesity is observed, such as increased melanoma risk (Iles et al., 2013) and HER2-negative breast cancer (Montazeri et al., 2022). FTO has also been linked to cancer though its role as an m^6A demethylase. Research has demonstrated that m^6A levels disrupted in multiple cancer types due to overexpression of FTO, including breast cancer (Niu et al., 2019), acute myelogenous leukemia, non-small cell lung cancer (J. Li Y. Han et al., 2019; Liu et al., 2018; H. Shi et al., 2020), gastric cancer (Y. Li et al., 2019), pancreatic cancer (Garg et al., 2022), cervical cancer (Zou et al., 2019), ovarian cancer (L. Zhao et al., 2020), bladder cancer (Tao et al., 2021) and glioblastoma (Cui et al., 2017; Kaklamani et al., 2011; Z. Li et al., 2017; Niu et al., 2019). Elevated FTO expression has, in certain cancers, exhibited a positive correlation with shorter overall survival, increased migration, and invasion (Gao et al., 2023; Zou et al., 2019). FTO has been observed to promote cancer stem cell self-renewal and reshape cancer immunity in leukemia. This is achieved by suppressing the expression of immune checkpoint genes through the removal of m^6A from mRNA, thereby decreasing mRNA stability (Garg et al., 2022).

FTO downregulation has also been reported in numerous cancers including colorectal cancer (Ruan et al., 2021) where FTO downregulation correlates with worse survival. In epithelial cancer reduced FTO expression is associated with increased invasion, metastasis, and worse clinical outcome (Jeschke et al., 2021). Comparable downregulation patters of FTO are evident in breast cancer (Wu et al., 2019), pancreatic cancer (Zeng et al., 2021) and more. For a comprehensive overview of aberrant FTO expression in several types of cancers, please refer to Figure 11.

In addition to its role in cancer, FTO is recognized as a significant contributor to the onset of age-related and metabolic conditions, including type 2 diabetes mellitus, cardiovascular disease, and dementia (Li et al., 2018; Sabarneh et al., 2018). Loss of FTO has also been shown to lead to enhancements in metabolic syndrome, glucose tolerance, and a decrease in ectopic fat accumulation in the liver, suggesting that FTO could be a valuable target for the regulation of metabolic disorders (Ikels et al., 2014).

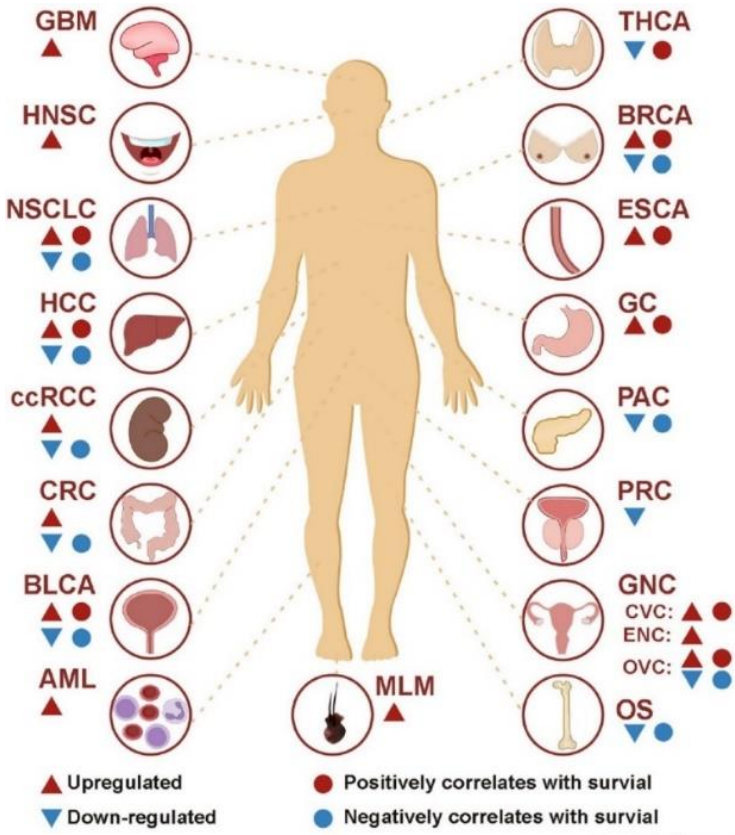

Figure 11. The aberrant expression and prognostic significance of FTO in different cancers.

A red triangle denotes upregulated FTO, while a blue triangle indicates downregulation. A red circle represents a high FTO expression correlating with poorer survival, and a blue circle signifies a high FTO expression associated with better survival. Abbreviations: AML, acute myeloid leukemia; BLCA, bladder cancer; BRCA, breast cancer; ccRCC, clear cell renal cell carcinoma; CRC, colorectal cancer; CVC, cervical cancer; ENC, endometrial cancer; ESCA, esophageal carcinoma; GBM, glioblastoma; GC, gastric cancer; GNC, gynecological cancer; HCC, hepatocellular carcinoma; HNSCC, head and neck squamous cell carcinoma; MLM, melanoma; NSCLC, non-small cell lung cancer; OS, osteosarcoma; OVC, ovarian cancer; PAC, pancreatic cancer; PRC, prostate cancer; THCA, thyroid cancer (Li et al., 2022).

FTO exhibits dual functions in cancer, acting as both an inhibitor and promoter. Its significant involvement at the onset, advancement, and progression of diverse cancers is primarily attributed to its m^6A demethylase activity. Given its crucial role in numerous diseases, FTO holds potential as a promising target for the diagnosis and treatment of various conditions, with a particular focus on cancer. Given growing comprehension of the role FTO has in many diverse types of cancers along with the elucidation of the FTO crystal structure has led to the development of small-molecule inhibitors targeting FTO for cancer therapy. Several FTO inhibitors, evaluated for their therapeutic effects in various tumor models, both *in vitro* and *in vivo,* show promising efficacy, suggesting potential translation into clinical applications for cancer therapy (S. Gao et al., 2021; Huff et al., 2021; Zhou et al., 2021).

1.5 Epitranscriptomics – RNA modifications

RNA modifications are post-transcriptional changes made to the chemical composition of RNAs that can change the function, structure, and catalytic activity of RNAs that do not involve any changes to the RNA sequence, thereby forming a new layer of post-transcriptional regulation, collectively referred to as epitranscriptomic or RNA epigenetics. Post-transcriptional regulation plays a pivotal role in governing gene expression programs that determine a wide array of cellular functions and decisions regarding cell fate.

The emerging field of epitranscriptomics started with the discovery of pseudouridine (Ψ) in the 1950s (Davis et al., 1957) and currently there are around 170 known RNA modifications found on all forms of RNA (Cappannini et al., 2023). Previous research has demonstrated that RNA modifications are common in transfer RNA (tRNA), ribosomal RNA (rRNA), small nuclear RNA (snRNA), mRNA and small nucleolar RNA (snoRNA) along with other types or RNAs (Saletore et al., 2012). Despite the longstanding awareness of RNA modifications spanning more than six decades, the recognition of modifications within the coding sequences of mRNAs as potential regulators of gene expression has only materialized in the past two decades. This delayed recognition can be attributed to technological limitations along with the focus of earlier studies being on the more abundant and heavily modified RNAs (tRNA and rRNA). The technological limitations have in recent years been gradually addressed and

mitigated, facilitating a more comprehensive understanding of the intricate role RNA modifications play in gene regulation. In the last ~15 years technical advances have made mRNA studies more widespread (Grosjean et al., 1997; Janin et al., 2020; Roundtree Evans et al., 2017).

1.5.1 mRNA methylations

One of the most common forms of RNA modification are methylations which play a role in many important mRNA processes e.g. alternative splicing, stability, mRNA export and translational efficiency (Mauer et al., 2017b; Slobodin et al., 2017; X. Wang et al., 2014; Wickramasinghe et al., 2015; Yang et al., 2017; Zhao et al., 2014). Other than the 5'cap and 3'polyadenyation, mRNA contains several modified nucleosides, including base isomerization to produce pseudouridine (Ψ); methylation of the ribose sugar to produce 2'O-methylation (Nm) and methylation of the bases to produce N^6-methyladenosine , N^1-methyladenosine and 5-methylcytosine (m^5C) (48). Transcriptome-wide mapping of RNA modifications revealed widespread distribution of m^6A, Nm and Ψ while the prevalence of other such as m^5C and m^1A are thought to be less common (Carlile et al., 2014; Dai et al., 2017; Mauer et al., 2017b; Meyer et al., 2012). Over the past few years, as researchers have uncovered methylation associated proteins and harnessed advanced high-throughput sequencing technology, the enigma surrounding mRNA methylation has slowly unraveled, shedding light on its biological significance and practical applications of these mRNA modifications.

Methylation associated proteins, as the name implies, are proteins that regulate or interact with mRNA methylations on RNA. These proteins fall into three categories: methyltransferases or "writers" which place the methylations on mRNA, methylation recognition proteins or "readers" that bind to the methylation and then affect a downstream process of the mRNA and finally demethylases or "erasers" that remove the methylation from mRNA. The discovery of methylation associated proteins and advances in transcriptome-wide sequencing have demonstrated that mRNA modifications are dynamic and reversible, thereby presenting a new post-transcriptional gene regulation in eukaryotes.

1.5.1.1 *N^6-Methyladenosine*

When a methylation occurs at the sixth nitrogen atom of the adenylated RNA, it is known as **N^6-methyladenosie (m^6A)** (Figure 12, methyl group displayed in red). The presence of m^6A on mRNA was first discovered in the 1970s (Desrosiers et al., 1974; Schibler et al., 1977) and it is the most prevalent internal mRNA modification with roughly 25% of all eukaryotic mRNA harboring at least one m^6A modification (Dominissini et al., 2012; Meyer et al., 2012). In addition to mRNA, m^6A modification has been discovered in various RNA types, including tRNAs, rRNAs, circular RNAs (circRNAs), micro RNAs (miRNAs), and long non-coding (lncRNAs) transcripts (N. Liu et al., 2016).

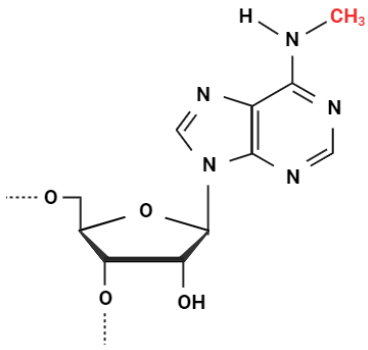

Figure 12. Schematic view of N^6-methyladeonsine.

Methylation of m^{6}A is orchestrated by a multicomponent methyltransferase complex of which Methyltransferase Like 3 and 14 (METTL3; METTL14) and Wilms Tumor 1 Associated protein (WTAP) are the most widely studied (Figure 13) (Y. Yang et al., 2018). Other proteins that are a part of this complex include RBM15/15B (RNA Binding Motif Protein 15), CBLL1 (Cbl Proto-Oncogene Like 1, HAKAI), VIRMA (Vir Like m^{6}A Methyltransferase Associated), KIAA1429 (Vir Like m^{6}A Methyltransferase Associated) and ZC3H13 (Zinc Finger CCCH-Type Containing 13). The METTL3/METTL4 complex recognizes and places m^{6}A within the RRACH consensus motif (R=A or G, H=A, C or U) (Dominissini et al., 2012; P. Wang et al., 2016) which are usually enrich in the 3' untranslated region (UTR), in long internal exons or near the stop codon (Dominissini et al., 2012; Meyer et al., 2012).

The effects of m^{6}A modification are determined by RNA binding proteins that can recognize m^{6}A on the RNA. These proteins, as previously mentioned, are called m^{6}A readers. To date several m^{6}A reader proteins have been identified in mammalian cells, of which YTH domain family of proteins: YTHDF1-3 and YTHDC1-2 are the most studied (Berlivet et al., 2019). Initial studies regarding the YTDHF proteins suggested that the YTHDF paralogs have unique physiological roles once bound to m^{6}A methylated mRNA due to their different RNA binding sites. YTHDF1 was primarily thought to function to enhance the translation of m^{6}A-methylated mRNA by facilitating ribosome assembly on m^{6}A mRNA and regulating the translation kinetics by interacting with the translation initiator factor such as Eukaryotic initiation factor 3 (eIF3) (X. Wang et al., 2015). YTHDF2 was found to affect mRNA stability by mediating mRNA degradation via recruitment of RNA-degrading enzymes or adaptor proteins to trigger rapid degradation of the m^{6}A-containing mRNA (Du et al., 2016; Park et al., 2019; X. Wang et al., 2014). YTHDF3 has been suggested to facilitate both degradation and translation of m^{6}A methylated mRNA. YTHDF3 interact with the ribosome, aiding in translation initiation (A. Li et al., 2017) and promotes mRNA degradation in a similar approach to YTHDF2 (Shi et al., 2017).

However, it is important to note that recent research has challenged the unique mRNA binding properties of the YTHDF proteins and their distinct regulatory effects on mRNA. In 2020, two publications proposed an alternative model for the function of the YTHDF proteins, suggesting that their primary role is to promote mRNA degradation (Lasman et al., 2020; Zaccara et al., 2020). Subsequent studies have supported these findings, providing further evidence for this revised functional concept (Arribas-Hernandez et al., 2021; Kontur et al., 2020; Y. Li et al., 2020; Niu et al., 2022).

In their 2020 study, Zaccara et al. showed that the YTHDF proteins shared an almost identical RNA-binding surface and were able to bind to the same mRNAs. Furthermore, they demonstrated that the YTHDF proteins shared subcellular localization and that YTHDF1 did not induce translation but instead promoted mRNA degradation, along with YTHDF2 and YTHDF3. Through a series of siRNA-mediated KD experiments in HeLa cells and leukemia cells, Zaccara and colleagues provided evidence that the YTHDF proteins may be functionally redundant, as double or triple KD of the YTHDF proteins had a more significant impact on mRNA expression compared to KD of a single YTHDF paralog (Zaccara et al., 2020). These findings were later supported by Lasman et al., who demonstrated that KO of a single YTHDF paralog had little to no effect on degradation rates in mouse embryonic stem cells, whereas depletion of all three YTHDF proteins resulted in a significant reduction in degradation rates. Lasman et al. also showed that the YTHDF paralogs exhibit different expression levels in various tissues, meaning that KD of a single paralog in certain cell types may have minimal effects, as the other paralogs might compensate and promote m^{6}A-mediated mRNA degradation (Lasman et al., 2020). Whether the YTHDF proteins are fully redundant or capable of performing unique regulatory functions on mRNA remains to be determined, and further research is needed for a more definitive conclusion.

YTHDC1 is the only m^{6}A reader found located in the nucleus of cells, while the previously mentioned YTH-family members along with YTHDC2 are found in the cytoplasm. YTHDC1 regulates alternative splicing of m^{6}A methylated mRNA by interacting with mRNA splicing factors SRSF10 and SRSF3 (Xiao et al., 2016). In addition, YTHDC1 has been shown to play a significant role in mRNA export of m^{6}A methylated mRNA, also via interaction with SRSF3 (Roundtree Luo et al., 2017). Finally, YTHDC2, distinguished by its structural variance from other YTH family members due to the presence of a helicase domain, is recognized for its crucial role in facilitating the progression of the meiotic program in the germline by binding and promoting degradation of m^{6}A-containing mRNA (Wojtas et al., 2017).

Other known m^{6}A readers include IGF2 mRNA-binding proteins (IGF2BPs) which are a well-preserved family of single-stranded RNA-binding proteins (RBPs) that exhibit specific recognition of m^{6}A-modified RNA and have a notable impact on the fate of the associated transcripts (Korn et al., 2021). Members of the Heterogeneous ribonucleoprotein family (hnRNPs), best known for their role in alternative splicing and

mRNA processes, have also been recognized as m⁶A readers. This includes hnRNPC, hnRNPA1 and hnRNPA2B1 (Alarcon et al., 2015). Additional RNA-binding proteins involved in translation have been recognized as potential m⁶A readers, e.g. eIF3 (Meyer et al., 2015), fragile X-messenger ribonucleoprotein 1 (FMR1) and staphylococcal nuclease-like (SN-like) domain-containing protein 1 (SND1) (Petri et al., 2023). To date the m⁶A modification has two known demethylation proteins, ALKBH5 and FTO which are known for specifically removing m⁶A from mRNA (Jia et al., 2011; Zheng et al., 2013).

The m⁶A modification is present in a variety of organisms and linked to diverse biological functions such as: meiosis in yeast (Schwartz et al., 2013), plant development (Zhong et al., 2008), mouse spermatogenesis (Lin et al., 2017) and mouse embryogenesis (Y. Wang et al., 2018). In addition, m⁶A has been shown to influence almost all stages of the mRNA life cycle including mRNA stability, translation control, cellular differentiation, and alternative splicing (Alarcon et al., 2015; Batista et al., 2014; Meyer et al., 2012; Tang et al., 2018; Xiao et al., 2016; J. Zhou et al., 2018). Consequently, it is not surprising that misregulation of m⁶A has been implicated in numerous physiological defects including cancer, obesity, brain development abnormalities and other diseases (Barbieri et al., 2017; Cheng et al., 2019; Choe et al., 2018; D. Dai et al., 2018; Z. Li et al., 2017; Roost et al., 2015).

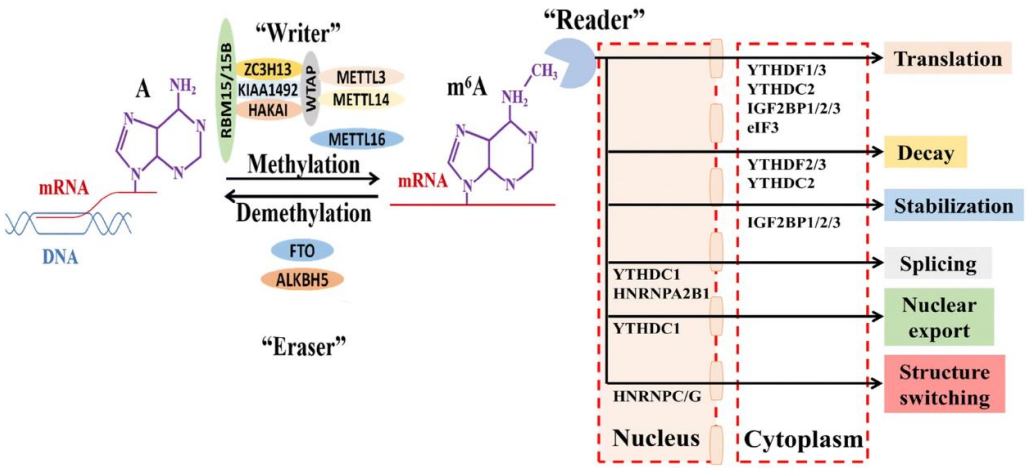

Figure 13. Overview of m⁶A mRNA associated proteins.

Methylation writer complex composed of METTL3, 14, WTAP, RM15/15B and more, places m⁶A onto mRNA. Methylation readers bind to the m⁶A modification and affect a downstream process indicated in colored boxes. Reader proteins can be found in both the nucleus and cytoplasm. FTO and ALKBH5 are the only known m⁶A erasers that remove the m⁶A methylation from mRNA (J. Li X. Yang et al., 2019).

Accumulating evidence shows that m^{6}A plays a dual role in cancer by both regulating expression of oncogenes and tumor suppressors, thus affecting cancer progression(L. He et al., 2018; S. Wang et al., 2018). In addition, research has demonstrated that dysregulation of the m^{6}A machinery i.e., writer, erasers and reader proteins are frequently found to be aberrantly expressed in various types of cancers, contributing to cancer initiation and progression (Barbieri et al., 2017; Y. Chen et al., 2019; Huang et al., 2020; Q. Li et al., 2021; Z. Li et al., 2017; Shen et al., 2020; Zheng et al., 2013). The existing body of scholarly work regarding m^{6}A and its associated proteins in cancer is too broad to cover within the scope of this thesis. For an overview, please refer to Figure 14 and Table 1 (He et al., 2019).

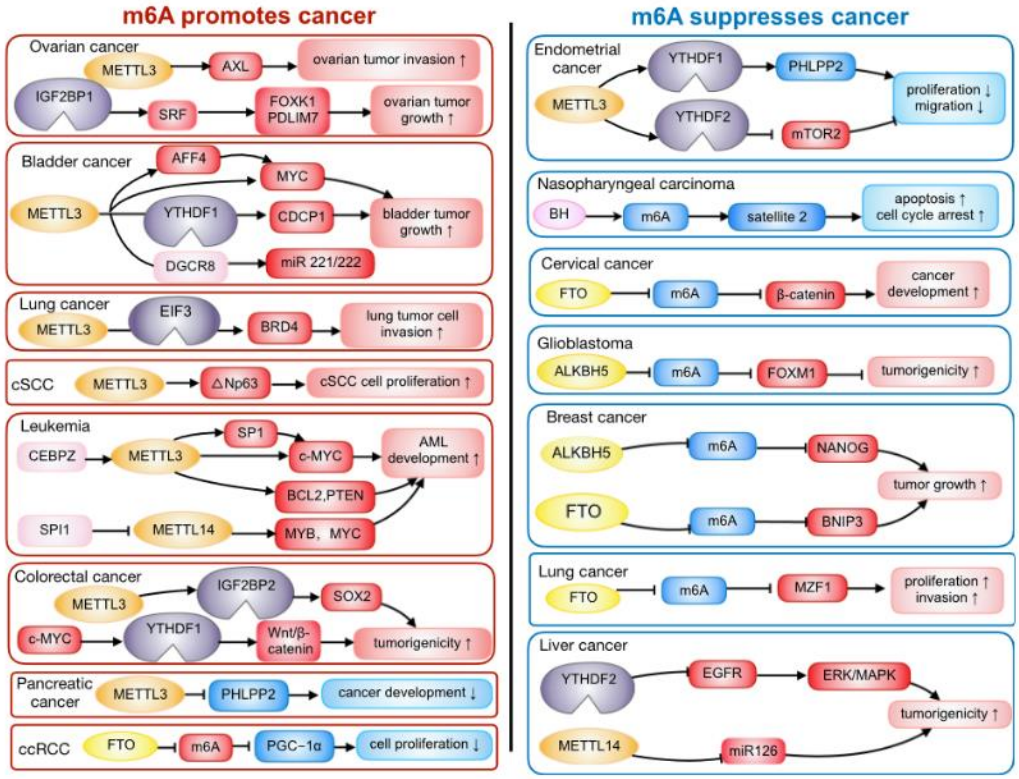

Figure 14. Overview of the involvement of m^{6}A and its associated proteins in cancer.

The m^{6}A modification plays a dual role in cancer, as it can either promote or hinder cancer progression and pathogenesis. It achieves this by enhancing the expression of oncogenes and inhibiting the expression of tumor suppressor genes, or conversely, by inhibiting oncogene expression and enhancing tumor suppressor gene expression. Pathways on the left (red) are examples of where m^{6}A promotes cancer and pathways on the right (blue) demonstrated examples of when m^{6}A suppresses cancer. The m^{6}A associated proteins are labelled in yellow (writers and erasers) and in grey (readers) (He et al., 2019).

Table 1. N^6-methyladenosine function and role in cancer.

Cancer Type	m⁶A protein	RNA Target	Effect on target RNA	m⁶A influence in cancer	Reference
AML	METTL3	c-MYC, BCL2, PTEN	Translation	Inhibits cell apoptosis & differentiation.	(Vu et al., 2017)
	METTL3	SP1	Translation	Reduces cell differentiation & induces cell proliferation.	(Barbieri et al., 2017)
Breast cancer	ALKBH5	NANOG	Stabilization	Reduces tumor formation & inhibits breast cancer stem cell population.	(Zhang et al., 2016)
	FTO	BNIP3	Degradation	Inhibits metastasis, cell proliferation & colony formation	(Niu et al., 2019)
	METTL3	HBXIP	Expression	Inhibits apoptosis & induces invasion, proliferation, metastasis.	(Cai et al., 2018)
CSCC	FTO	β-catenin	Expression	Enhances resistance to chemo-radiotherapy.	(S. Zhou et al., 2018)
GSC	ALKBH5	FOXM1	Expression	Impairs tumorigenicity & proliferation.	(Zhang et al., 2017)
	METTL3	SOX2	Stability	Enhances the formation of neurosphere.	(Visvanathan et al., 2018)
HCC	METTL14	miRNA 126	Splicing	Limits tumor metastasis & reduces invasiveness & migration of HepG2 cells.	(Ma et al., 2017)
LUSC	FTO	MZF1	Stability	Induces apoptosis & inhibits invasion & proliferation.	(Liu et al., 2018)
Ovarian cancer	METTL3	AXL	Translation	Promotes ovarian tumor invasion & growth.	(Hua et al., 2018)
Pancreatic cancer	ALKBH5	KCNK15-AS1	Expression	Induces invasion & migration.	(Y. He et al., 2018)
Renal cell carcinoma	FTO	PGC-1α	Stability	Increases cell growth & enables apoptosis.	(Zhuang et al., 2019)

1.5.1.1.1.1 m^{6}A in DNA repair and genomic stability

A recent body of research has unveiled the potential role of m^{6}A in orchestrating DNA repair and maintaining genome stability in response to DNA damage. Firstly, in a publication from 2017 Xiang and colleagues revealed that poly(A)$^+$ RNA is rapidly m^{6}A methylated and transiently induced at DNA damage site in response to UV irradiation. The m^{6}A methylation was found on numerous poly(A)$^+$ transcripts and is regulated by FTO and METTL3. In the absence of METTL3 methylation activity, cells demonstrated increased sensitivity and delayed repair to UV damage. DNA polymerase κ, a crucial component of nucleotide excision repair (NER) and trans-lesion synthesis pathways responsible for repairing UV-induced lesions (Ogi et al., 2006; Yoon et al., 2009), was recruited to UV damage sites simultaneously with m^{6}A RNA. This recruitment was contingent upon the catalytic activity of METTL3, thereby contributing to the facilitation of DNA repair (Xiang et al., 2017). In this publication both METTL3 and FTO were found to localize to the site of UV-damage site however, METTL3 localization preceded that of FTO possibly allowing for a brief window of m^{6}A RNA accumulation in order to respond to UV damage before being demethylated by FTO. In a more recent study, FTO expression emerged as a pivotal protective factor against genotoxic stress in mouse osteoblasts. FTO KO conferred cellular sensitivity to UV and H_2O_2, thereby promoting cell death. FTO was found to remove m^{6}A methylation from a number of DNA repair transcripts, resulting in increased mRNA stability and ultimately increasing protection in osteoblasts from DNA damage (Q. Zhang et al., 2019).

Secondly, m^{6}A has also been found to mediate the repair of DSBs. DSB induced activation of METTL3 by ATM phosphorylation leads to METTL3 localization to sites of DNA damage, where it adds m^{6}A to RNAs associated with DNA damage. This modification serves to attract the m^{6}A reader protein YTHDC1 for protective functions. Consequently, the METTL3-m^{6}A-YTHDC1 axis regulates the presence of DNA-RNA hybrids at DSB sites, which then attract RAD51 and BRCA1 to facilitate HR-mediated repair. Cells lacking METTL3 exhibit impaired HR, accumulation of unrepaired DSBs, and genomic instability (Zhang et al., 2020). Finally, m^{6}A has also been implicated in the regulation of R-loop formation (Abakir et al., 2020; Yang et al., 2019), in direct DNA repair by stimulating translation of the repair enzyme O^6-methylguanine DNA methyltransferase in mice (Ozkurede et al., 2019) and the regulation of telomere length and genomic integrity in human cancer (Lee et al., 2021). Despite these examples, our current understanding of the multifaceted role of m^{6}A in regulating genome stability and DNA repair is still in its early stages and further research is necessary.

1.5.1.2 *N1-Methyladenosine*

When a methylation occurs at the first nitrogen atom of the adenylated RNA, it is known as **N^1-methyladenosine (m^{1}A)** (Figure 15, methyl group displayed in red) and was first reported in 1961 (Dunn, 1961). m^{1}A is not as well defined as m^{6}A but is found on tRNA (Cozen et al., 2015), rRNA (Peifer et al., 2013), mRNA (Dominissini et al., 2016; Li et al., 2016; X. Li X. Xiong et al., 2017; Safra et al., 2017; Zhou et al., 2019) and lncRNAs (Shi et al., 2021), with tRNAs being the most heavily modified with m^{1}A.

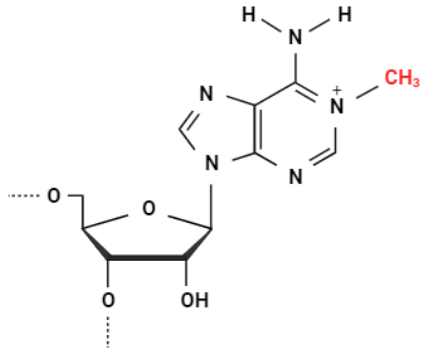

Figure 15. Schematic overview of N^1-Methyladenosine.

In mRNA, m^1A has been discovered in every mRNA segment, including the coding sequence (CDS), 5'UTR and 3'UTR. It has mostly been found in the highly structured 5'UTR and near start codons and has been found to be correlate with enhancement in translation (Dominissini et al., 2016; Li et al., 2016). Dominissini et al found m^1A to be enriched din GC rich areas while Li et al found m^1A to be associated with purine-rich motives. These prior studies indicated that, on average, the m^1A/A ratio in mRNA stands at roughly 0,015% to 0,054% in mammalian cells. This ratio is relatively low when compared to the m^6A/A ratio in mRNA as the occurrence of m^1A is around 6-fold less than that of m^6A (Dominissini et al., 2016; Li et al., 2016; Yang et al., 2020). The earlier transcriptome-wide mapping studies conducted by Dominissini and Li demonstrated the presence of m^1A across thousands of distinct gene transcripts. However, these studies have faced criticism due to their lack of single-nucleotide resolution in detecting m^1A and for not identifying the enzyme responsible for catalyzing m^1A on mRNA.

The development of m^1A sequencing techniques and new single-base resolution methods have greatly aided in uncovering the presence of m^1A in nuclear, cytosolic, and mitochondrial-encoded transcripts (X. Li X. Xiong et al., 2017; Safra et al., 2017). These studies utilize the fact that during revers transcription m^1A causes misincorporation or termination, allowing for the identification of m^1A at single-base resolution. In 2017 Li et al reported 740 m^1A site in the HEK293T transcriptome using such single-base resolution method where 473 m^1A sites were found in mRNA and lncRNAs transcripts in HEK293T cells. The majority of these m^1A sites were situated within the 5' UTR which aligns with earlier findings (Dominissini et al., 2016; Li et al., 2016). Li et al., shed further light on m^1A and its location within the mRNA and demonstrated that m^1A modifications located in the CDS have a slight preference for codon types with arginine (CGA) and at the first nucleotide (Cap+1) at the 5' end of the mRNA which was linked with increased translation efficiency. Li and colleagues further demonstrated that m^1A is prevalent in mitochondrially encoded transcripts, where it disrupts the process of mitochondrial translation (X. Li X. Xiong et al., 2017).

The development of single-base resolution methods has also prompted criticism regarding the reported prevalence of m^1A, particularly in cytosolic mRNA (Safra et al., 2017; Schwartz, 2018). As mentioned earlier (1.4.2), the prevalence of m^1A on mRNA has been contested by Safra et al., who reported the m^1A modification to be less abundant than previously revealed by Li and Dominissini with only 10 m^1A sites identified in human mRNA (Safra et al., 2017). However, other studies have suggested that the sequencing technique used by Safra et al. has limited sensitivity and does not provide an accurate picture of the prevalence of m^1A on mRNA (Xiong et al., 2018; L. Y. Zhao et al., 2020). Moreover, independent studies have reported m^1A/A ratios comparable to those observed by Dominissini and Li, providing additional validation for the number of m^1A sites in mRNA (Xu et al., 2017). Finally, a more recent study using an evolved reverse transcriptase that reads through m^1A more efficiently reported hundreds of m^1A sites in human mRNA (Zhou et al., 2019). Collectively, the research indicates that the m^1A modification is present on human mRNA; however, its precise abundance remains uncertain and warrants further investigation. Advancements in sequencing methods and optimization of technologies are necessary to achieve transcriptome-wide and single-base resolution detection of m^1A.

As with other mRNA methylations, m^1A has methylation associated proteins that interact with m^1A on RNA (Figure 16). TRMT61 and TRMT6 are m^1A methyltransferases that form a heterotetrametric complex to methylated tRNA (Anderson et al., 2000; M. Wang et al., 2016) and in some nuclear mRNAs within a GUUCRA (R=A or G) tRNA-like motif with T-loop-like structure (X. Li X. Xiong et al., 2017; Safra et al., 2017). TRMT61A serves as the catalytic subunit and contains a binding pocket for the methyl donor, S-adenosyl-L-methionine (SAM). Other m^1A methyltransferase include TRMT61B, best known to methylate mitochondrial 16S rRNA (Bar-Yaacov et al., 2016), TRMT10C that methylases mitochondrial (mt)-tRNA coupled with SDR5C1 (Vilardo et al., 2012) and mt-mRNA (Safra et al., 2017).

m^1A has several known demethylases, all members of the AlkB protein family. ALKBH1 was first discovered to mediate demethylation of m^1A on tRNA in 2016 (F. Liu et al., 2016) and on mt-RNA (Kawarada et al., 2017). ALKBH3 is known to demethylase both m^1A and m^3C in tRNA, along with demethylating m^1A on mRNA (Z. Chen et al., 2019; Dominissini et al., 2016; X. Li J. Peng et al., 2017; Woo et al., 2019). To date, ALKBH3 is the only known m^1A mRNA demethylase and has been shown to specifically recognize m^1A site in HEK293T cell, possibly hinting at ALKBH3 role in transcriptional regulation (Li et al., 2016). ALKBH3's role in transcriptional regulation has previously been contested by Liefke et al., which demonstrates that ALKBH3 does not directly influence the transcription of its target genes (Liefke et al., 2015). It is however worth considering that Liefke et al., approached ALKBH3 and its influence on transcription from a DNA standpoint. Using ChIP-Seq to analyze the binding sites of ALKBH3 in the DNA and examining the expression of those genes following ALKBH3 depletion. Whether ALKBH3 is able to influence transcription via m^1A-mRNA demethylation is still

an area of active research and requires further investigation. In addition to ALKBH3 both ALKBH7 and FTO have demonstrated m^1A demethylase activity. FTO has proven able to remove m^1A from tRNA (Wei et al., 2018) while ALKBH7, which is localized in the mitochondria, is known to eliminate m^1A modification mitochondrial RNA (Zhang et al., 2021).

Four members of the YTH-domain containing family have been shown to be able to interact with m^1A *in vitro*, YTHDC1, YTHDF1-3 (X. Dai et al., 2018; Safra et al., 2017). YTHDF2 has been shown to bind to m^1A mRNA and accelerate their degradation while YTHDF1 and YTHDF3 help promote translation (Seo et al., 2020; Q. Zheng et al., 2020). Less information is available on whether these readers bind to m^1A *in vivo* and what cellular and molecular events are influenced by this. Conflicting evidence exists regarding YTHDC1's role as a m^1A reader. While research by Seo et al., have demonstrated that YTHDC1 has no affinity for m^1A (Seo et al., 2020) other studies have associated YTHDC1 to mRNA regulation via m^1A interaction *in vitro* (X. Dai et al., 2018). As previously mentioned, these same four proteins have been reported as m^6A readers and their binding affinity for m^1A is weaker than m^6A.

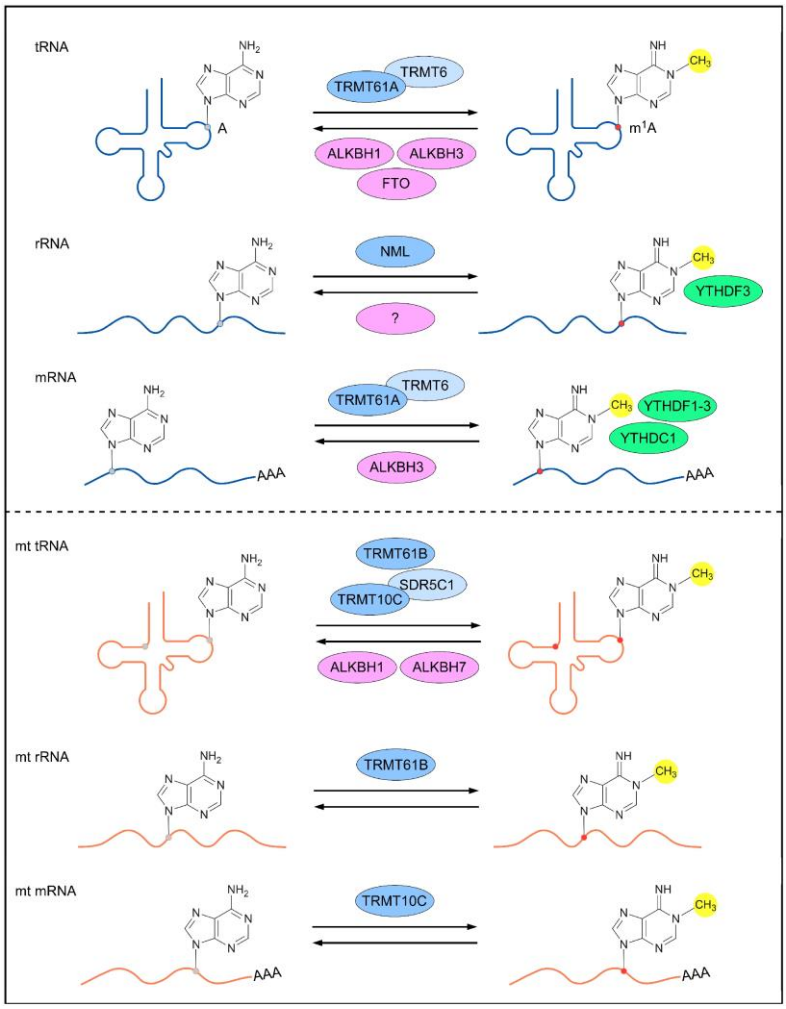

Figure 16. m^{1}A associated proteins on tRNA, rRNA and mRNA.

Top panel denotes nuclear RNAs (mRNA, tRNA and rRNA) and their associated proteins. The bottom panel displays mitochondrial RNAs. Methyltransferases are labelled in blue (dark blue: catalytic core of the methyltransferase complex), methyl erases in purple and m^{1}A-binding proteins (readers) in green (Jin et al., 2022).

The regulatory influence of m^{1}A varies across different types of RNA and since its discovery extensive efforts have been dedicated to unravelling its dynamic role in RNA metabolism and gene expression regulation. In mRNA the m^{1}A modification has been shown to block Watson-Crick base pairing thereby affecting protein translation and reverse transcription (Aas et al., 2003). Recent research performed by Qi et al., using transcriptome wide sequencing in primary mouse neuron cells demonstrated that m^{1}A peaks in different regions have different effects on gene expression. They reveal that m^{1}A peaks situated in the stop codons promoted gene expression, while those located in the CDS and 3′ UTR inhibit gene expression (Qi et al., 2023). Prior to this Li et al.,

demonstrated that m^1A modification positioned at the initial and secondary positions of the 5′ UTR within the transcript can enhance protein translation (X. Li X. Xiong et al., 2017), this promotion it thought to be even higher for m^1A at the cap+1 position (X. Li X. Xiong et al., 2017). Collectively, m^1A peaks located at various positions within the transcript exert distinct effects on both transcription and translation processes. Despite this, the physiological function of m^1A modification remains unclear.

The limited exploration of m^1A RNA modification as a pathological feature has predominantly centered on its contribution to tumor progression. However, it is noteworthy that dysregulation of m^1A and its associated proteins has been linked to a spectrum of diseases, encompassing cancer, Alzheimer's disease (Shafik et al., 2022), and cardiovascular conditions (Wu Jiang et al., 2022). Like m^6A, m^1A has demonstrated a dual role in cancer, exhibiting both suppressive and promotional roles in cancer (Figure 17). The m^1A regulators ALKBH3, TRMT6 and TRMT61A have been shown to promote proliferation via tRNA regulation in in gastrointestinal cancer (J. Li et al., 2021; Zhao et al., 2019), colorectal cancer (Y. Gao et al., 2021), hepatocellular carcinoma (Q. M. Shi et al., 2020) prostate cancer (Konishi et al., 2005; Ueda et al., 2017), bladder cancer (Shi et al., 2015), liver cancer (Y. Wang et al., 2021) and glioma (Macari et al., 2016).

In breast and ovarian cancer ALKBH3 has been shown to enhances the translation *CSF-1* mRNA by demethylating a m^1A resulting in increased cancer cell invasion (Woo et al., 2019). Additionally, the m^1A reader YTHDF3 has been identified as an inhibitor of trophoblast invasion and migration by enhancing the degradation of IGF1R mRNA (Esteve-Puig et al., 2021; Q. Zheng et al., 2020). The intricate regulatory network involving m^1A methylation is active in various cancer types and offers potential for further exploration. Moreover, the potential for developing targeted cancer therapies associated with m^1A is a promising area for research.

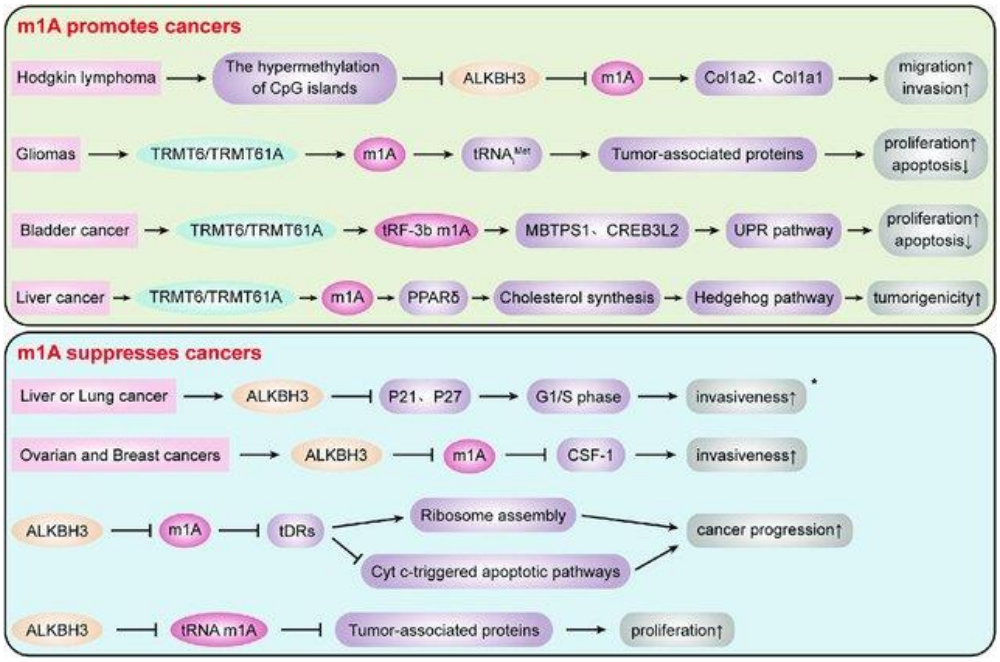

Figure 17. The potential roles of m^{1}A in cancer progression.

The m^{1}A modifications play a crucial role in numerous cancers, often involving the addition or removal of m^{1}A modifications in the mRNA of oncogenes or tumor suppressor genes. This process regulates the expression of oncogenes or tumor suppressor genes by interacting with m^{1}A through reader proteins or hindering the recognition of m^{1}A markers by readers. Upper panel demonstrates when the m^{1}A modification has a promotional role in cancer and lower panel shows when m^{1}A has a suppressive role in cancer (Weidong Xiong, 2023)

1.5.1.3 *N^6,2′-O-dimethyladenosine*

N^6,2′-O-dimethyladenosine (m^{6}A$_m$) refers to when methylations are located on the sixth nitrogen atom of the adenylated RNA and the adenosine hydroxyl group at position 2′ is replaced by a methoxy group (Figure 18, methyl group displayed in red). m^{6}A$_m$ is situated at the initial transcribed nucleotide position near the cap in numerous mRNAs and snRNAs in mammals, and it is also found as an internal modification in the snRNA U2 (Ramanathan et al., 2016).

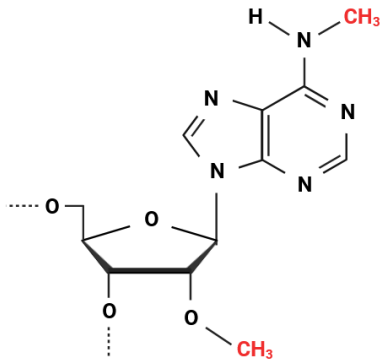

Figure 18. Schematic overview of N^6,2′-O-dimethyladenosine.

In contrast to m^{6}A which is placed on mRNA by a complex of proteins, m^{6}A$_m$ is added by a one protein: PCIF1 (Phosphorylated CTD Interacting Factor 1) (Sendinc et al., 2019). PCIF1 has been shown to add m^{6}A$_m$ to the first nucleotide after the 5′ N^7-methylguanosine (m^{7}G) cap by several independent studies (Akichika et al., 2019; Boulias et al., 2019; Sun et al., 2019). Mice lacking PCIF1 have been found to display significant growth defects but are viable (Pandey et al., 2020). FTO is the only known demethylase capable of removing m^{6}A$_m$ on mRNA and snRNA (X. Zhang et al., 2019). Studies have reported that FTO-mediates the removal of m^{6}A$_m$ and that m^{6}A$_m$ function is related to mRNA metabolism (Mauer et al., 2017a; Wei et al., 2018). As of current writing, there are no known methylation readers for m^{6}A$_m$.

Due to its location on the 5′cap, m^{6}A$_m$ was initially thought to promote RNA stability via resisting the de-capping enzyme Dcp2 (Mauer et al., 2017b). This was later validated in transcriptomic data from mouse tissue (Pandey et al., 2020) though m^{6}A$_m$ showed negligible effect on Dcp2 *in vitro* (Sikorski et al., 2020). Further studies on m^{6}A$_m$ and mRNA stability have demonstrated that PCIF1 KD caused significantly decrease in the stability of a subgroup of m^{6}A$_m$ containing mRNAs in both HEK293 and HELA cells (Boulias et al., 2019). Conversely, other research has raised skepticism about the role of m^{6}A$_m$ in mRNA stability, indicating that m^{6}A$_m$ has the opposite or no effect on mRNA stability (Akichika et al., 2019; Sendinc et al., 2019). Further research is needed on m^{6}A$_m$ to clarify its role in mRNA stability and on mRNA function in general.

2 Aims

Both ALKBH3 and FTO have a role in repairing alkylated DNA and RNA by oxidative demethylation in addition to having important implications for cancer progression. Previous publication from the Sigurdsson laboratory (Stefansson et al., 2017) demonstrated that the ALKBH3's promoter region is hypermethylated in more than 20% of breast cancer leading to a significant reduction of ALKBH3 mRNA and protein expression. This reduced ALKBH3 expression correlated with worse patient outcomes and decreased survival. Subsequent investigations unveiled that loss of both ALKBH3 and FTO resulted in decreased protein expression of RNF168, a key protein in DSB signaling and repair pathway choice.

The aim of this thesis was to study the impact of ALKBH3 and FTO on the response to DNA double strand breaks via their epitranscriptomic regulation of RNF168.

2.1 Specific aims

Specific aims were as follows:

Aim 1: To elucidate the regulatory role ALKBH3 and FTO play in normal function of RNF168.

Hypothesis: ALKBH3 and FTO regulate RNF168 epitranscriptomically i.e., by removing methylation marks from the *RNF168* transcript thereby allowing for normal protein expression of RNF168.

Aim 2: To characterize the impact ALKBH3 and FTO have on the DNA DSB repair response via regulation of RNF168.

Hypothesis: As ALKBH3 and FTO are important for efficient RNF168 expression and due to RNF168 crucial role in efficient repair of DSB, loss of either of these two proteins will affect the cell's ability to correctly repair DSB and maintain genomic integrity.

3 Materials and Methods

3.1 Materials

3.1.1 Antibodies

Table 2. Antibodies and their dilution used in western blot (WB), immunofluorescence (IF) and RNA immunoprecipitation (IP).

Target	Source	Identifier	WB dilution	IF dilution	RNA IP
53BP1	Santa Cruz	sc-22760	1:2000	1:100	-
Actin	AMD Millipore	MAB1501R	1:10000	-	-
Alexa Fluor 488 Anti-mouse IgG1	Life Technologies	A21121	-	1:1000	-
Alexa Fluor 488 Anti-Rabbit IgG	Life Technologies	A32731	-	1:1000	-
Alexa Fluor 555 Anti rabbit IgG	Life Technologies	A21434	-	1:1000	-
Alexa Fluor 647 Anti rabbit IgG	Life Technologies	A27040	-	1:1000	-
ALKBH3	Millipore	09-882	1:500	1:250	-
ASCC3	Bethyl	A304-014A-M	1:1000	1:1000	-
ATM	Santa Cruz	sc-23921	1:500	-	-
ATR	Santa Cruz	sc-1887	1:500	-	-
BRCA1	Calbiochem	OP92	1:1000	-	-
FLAG	Cell Signaling	14793	1:1000	1:1000	-
Flag M2	Sigma Aldrich	F1804	1:1000	1:1000	-
FTO	Abcam	ab126605	-	1:1000	-
gamma-H2AX	Cell Signaling	9718S	1:1000	1:500	-
gamma-H2AX	Abcam	ab22551	1:1000	1:1000	-
HRP Secondary Anti mouse	Santa Cruz	sc-2096	1:10000	-	-
HRP Secondary Anti rabbit	Santa Cruz	sc-2357	1:10000	-	-
MDC1	Abcam	ab11171	-	1:2000	-
N^1-methyladenosine	Medical and Biological Laboratories	D345-3		-	5µg

N^6-metyladenosine	NEB	E1610S	-	-	5µg
N^6-metyladenosine	Merk Millipore	ABE572	-	-	5µg
RIF1	Bethyl	A300-569A	1:500	1:500	-
RNF168	Millipore	ABE367	1:500	1:250	-
RNF8	Santa Cruz	sc-133971	-	1:500	-
SMC1	Abcam	ab9262	1:1000	-	-
Vinculin	Santa Cruz	sc-5573	1:1000	-	-

3.1.2 Small interfering RNAs

Table 3. List of small linterfering RNAs.

siRNA	Sequence 5'-3-	Identifier	Source
siRNA Control	*NA*	4390843	Thermo Fisher
siALKBH3 #1	*GGACCUUGUUAAUCAUGGAtt*	s47967	Thermo Fisher
siALKBH3 #2	*CAUGGGACCUUGUUAAUCAtt*	s47968	Thermo Fisher
siALKBH3 #3	*GCAACUCAUFUUGGUAAUAtt*	122027	Thermo Fisher
siALKBH3 #4	*UAGUGAGGGUUCAUCAUCACUGUGC*	10620318	Thermo Fisher
siFTO #1	*CCAAGGAGACUGCUAUUUCtt*	278910	Thermo Fisher
siFTO #2	*CAUUACCUGCUGAUCAGAAtt*	s35511	Thermo Fisher
siFTO #3	*GAGAAGAAAUUCAUAAUGAtt*	s35512	Thermo Fisher
siFTO #4	*GCCUAACCUACUUUCCUCUtt*	272126	Thermo Fisher
siFTO #5	*GGCACCAGUCCUAAGGUGAtt*	272127	Thermo Fisher
siFTO #6	*CAUCCUCAUUGGUAAUCCAtt*	278910	Thermo Fisher
siALKBH2	*GAATCTGACTTTTCGTAAA*	s42494	Thermo Fisher
siALKBH5	*GGCUCAUCCUUACGUAGUUtt*	s29688	Thermo Fisher
siRNF168	*GGCGAAGAGCGAUGGAAGAtt*	126171	Thermo Fisher
siBRCA2	*GGAUUAUACAUAUUUCGCAtt*	s2085	Thermo Fisher
siASCC3	*CAAGCAAGAUAAUUAUAAUtt*	s21605	Thermo Fisher

Table 4. List of single guide RNA.

sgRNA	Sequence 5′-3-	Source
ALKBH3-1	*CCCAGGGUCUGUUUGUAUCC*	Synthego
ALKBH3-2	*CAGAGGACUGGCAUCAGAGA*	Synthego
ALKBH3-3	*UACUAGGAAACAUUCCAGAG*	Synthego
FTO-1	*GCUUCUCGGAGAAUUAGUUU*	Synthego
FTO-2	*UGGCUGCUUAUUUCGGGACC*	Synthego
FTO-3	*CCGGUAUCUCGCAUCCUCAU*	Synthego
Positive Control-1	*CUCUCAGCUGGUACACGGCA*	Synthego
Positive Control-2	*GAGAAUCAAAAUCGGUGAAU*	Synthego
Positive Control-3	*ACAAAACUGUGCUAGACAUG*	Synthego

3.1.3 Primers

Table 5. List of primers used in qPCR assay.

Primer Name	Sequence 5′-3-
RNF168 forward	*TCCAGTTACACCCAAGTCTGAA*
RNF168 reverse	*GAGGCTGACCCAAACTGAGA*
Beta actin forward	*AGGCACCAGGGCGTGAT*
Beta actin reverse	*GCCCACATAGGAATCCTTCTGAC*
GADPH forward	*GGCCTCCAAGGAGTAAGACC*
GADPH reverse	*AGGGGTCTACATGGCAACTG*
ALKBH3 forward primer	*AGCCACCAGTGATTGACAGAG*
ALKBH3 reverse primer	*ACAAACAGACCCTAGATACACCT*
FTO forward primer	*TGTTTTGGCCGGTTCACAAC*
FTO reverse primer	*ACATTCTGCAGAGCCAACTG*
HPRT1 qPCR reverse	*CTTCGTGGGGTCCTTTTCACC*
HPRT1 qPCR forward	*ACCAGTCAACAGGGGACATAA*

3.1.4 Plasmids

Table 6. List of plasmids.

Plasmid name	Catalog Number	Vendor
ALKBH3/ABH3 Gene ORF cDNA clone expression plasmid, N-Flag tag	HG15639-NF	Nordic Bio-Site
FTO gene ORF cDNA clone expression plasmid, N-Flag tag	HG12125-NF	Nordic Bio-Site
pCMV3-N-FLAG Negative Control	158-CV016	Nordic Bio-Site
pDRGFP plasmid	26475	Addgene
primEJ5GFP	44026	Addgene
hprtSAGFP	41594	Addgene
pAc-GFP-N1 vector	632469	Addgene

3.1.5 Drugs

Table 7. List of drugs and their usage.

Drug name	Catalog Number	Vendor	Use
Neocarzinostatin (NCS)	N9162	*Sigma-Aldrich*	Induce DSB. Clonogenic assay
Mitomycin C (MMC)	3258/2	*Bio-Techne*	Clonogenic assay
Colcemid	15212-012	*Invitrogen*	Metaphase arrest

3.2 Methods

3.2.1 Cell culture

All cells were grown using DMEM (Dulbecco's Modified Eagle Medium) with GlutaMAX and pyruvate (Thermo Fisher, LT-31966-021) supplemented fetal bovine serum (FBS, 10% Thermo Scientific, 10500064) penicillin (20 U/mL) and streptomycin (20 µg/mL) (Thermo Scientific, 15070-063) and cultured in 95% air with 5% CO2 at 37°C.

3.2.2 RNA isolation

RNA was extracted from cells using Tri-Reagent (Thermo Fisher Scientific, AM9738) according to manufacturer's instruction or using Monarch ® Total RNA Miniprep Kit (NEB, T2010S) according to manufacturer's instruction. The concentration of total RNA was measured using Nanodrop One.

3.2.3 siRNA transfection

All siRNA transfections were performed using Lipofectamine RNAiMAX transfection reagent (Thermo Fisher, 13778075) according to manufacturer's instructions. Cells were transfected with 10nM siRNA (Thermo Fisher) for 48-72h.

3.2.4 Plasmid transfection

Human osteosarcoma U2OS cells were transfected using GenJet™ *In Vitro* DNA Transfection reagent (Signagen, SL100488) according to manufacturer's instructions. All plasmid transfections were performed for 48h.

3.2.5 Plasmid mutagenesis

Site-directed mutagenesis was performed on ALKBH3-FLAG (HG15639-NF) and FTO-FLAG (HG12125-NF) tagged plasmids using Q5 Site-Direct Mutagenesis kit (NEB, E0554S) and Q5 High-Fidelity DNA polymerase (NEB, M0491) to create a catalytically inactive version of each plasmid (Jia et al., 2011; Sundheim et al., 2006). Primers were designed to mutate the Fe^{2+} binding site of each plasmid (Table 8) by altering Histidine (H0191) aspartic acid (D193) to Alanine for ALKBH3 plasmid and Histidine (H231) and aspartic acid (D233) changed to Alanine for FTO plasmid. Altering the Fe^{2+} binding site renders each plasmid catalytically inactive as ALKBH3 and FTO are dioxygenases that rely on Fe^{2+} as a cofactor for enzymatic activity (Fedeles et al., 2015). PCR reaction was carried out in a thermocycler as described in Table 10. Following PCR reaction, plasmids were subjected to plasmid transformation, midi-prep plasmid preparation and sequencing to confirm that mutagenesis worked.

Table 8. Primers used for FLAG-plasmid mutagenesis

Primer name	Sequence
ALKBH3_Mut_Fw	TGCTGATGAACCCTCACTAGGGAG
ALKBH3_Mut_Rev	CTAGCCCAGTCCACGCTGTCCTT
FTO_Mut_Fw	TGCTGAAAATCTGGTGGACAGG
FTO_Mut_Rev	TGAGCCCAGCTCACTGCCATTTTC

Table 9. Thermocycler conditions for Q5 High-fidelity DNA polymerase

PCR thermocycler Program				
Step	**Temp**	**Time**	**ALKBH3**	**FTO**
Initial denature	98°C	30 sec		
Denature	98°C	10 sec		
Annealing	-	30 sec	65°C	60°C
Extension	72°C	2 min		

3.2.6 Plasmid transformation

The plasmid mutagenesis PCR products were transformed using NEB 5-alpha Competent E. coli cells. 60µL of complemented cells were incubated with 5µL of PCR product, mixed by gentile flicking, incubated on ice for 30min followed by heat shock at 30 sec at 42°C and lastly 5 min incubation on ice. 300 µL of Super Optimal broth with Catabolite repression (SOC) media was added to the transformation mix and the tube incubated in a shaking incubator at 37C, 250 RPM for 45 min. Following incubation, 100µL of culture was spread on Lysogeny broth (LB) agar plates with 50µg/mL Kanamycin (Thermo Fisher, 15160054) at 37°C overnight (ON) followed by Midiprep Plasmid preparation.

3.2.7 Midiprep plasmid preparation

Using previously transformed bacterial culture plates, one colony was placed into Erlenmeyer flask containing 200mL LB media with 50µg/mL Kanamycin and left to grow at 37°C, 250 RPM for 10-18h. For isolation of copious quantities of plasmid from bacterial culture using NucleoBond Xtra Midi kit (Macherey Nagel, 740410.50) was used according to manufacturer's instructions. DNA concentration was measured using Nanodrop 1000 spectrophotometer (Thermo Fisher) and plasmids sent for DNA sequencing at deCODE Genetics to confirm the introduction of mutation in Fe^{2+} binding site. For more information on ALKBH3 and FTO plasmids see Appendix A.

3.2.8 Complementary DNA synthesis

Complementary DNA (cDNA) synthesis was performed using 1µg of total RNA isolated using previously described methods, Oligo(dT)12-18 primers (Thermo Fisher, SO132) and SuperScript ™ II Reverse Transcriptase (Thermo Fisher, 18064014) according to manufacturer's instructions.

3.2.9 Quantitative polymer chain reaction (qPCR)

Following cDNA synthesis, a qPCR assay was carried out utilizing SYBR Green master mix (Thermo Fisher, A25742) in the Bio-Rad CFX384 system (Table 10). For each reaction 2,5µL of SYBR Green master mix was combined with 2µL of diluted cDNA, 0,15 µL of 10µM reverse and forward primer and 0,2 µL of nuclease free water for a total of 5µL reaction. Subsequent analysis was conducted using Bio-Rad CFX Manager version 3.0. The threshold cycle number (Cq) was determined for each sample in triplicate. Gene expression levels for the genes of interest were then normalized to housekeeping genes (HPRT, Beta Actin, or GAPDH) and calculated using the $2^{-\Delta\Delta CT}$ method for relative quantification as previously described by Livak er al., (Livak et al., 2001).

Table 10. Thermocycler conditions for qPCR.

qPCR thermocycler Program			
Step	Cycles	Temperature (°C)	Time (min)
1. Uracil-DNA glycosylases activation	1	50	02:00
2. Polymerase activation	1	95	02:00
3.Denature	40	95	00:15
4. Annealing/Extension		58-60	01:00
5-7. Melting curve	1	95	00:15
	1	60	00:30
	1	95	00:15

3.2.10 Methylations specific immunoprecipitation (MeRIP)

MeRIP was performed following previously documented m^6A-sequencing protocol (Zeng et al., 2018, Dominissini et al., 2013) with a few adjustments. 30µL of both protein A and protein G magnetic beads (Thermo Fisher, 10002D, 10004D,) were incubated with 300µg of total RNA, along with 5µg of m^6A or m^1A antibody, 10% of total RNA was saved as input sample. IP-RNA was eluted with 300µL of elution buffer (100mM KCl, 5mM $MgCl_2$, 10mM HEPES, 0.5% Tween-20, 1mM DTT, 0.1% SDS, RNAse inhibitor 100U and 15 µg/mL proteinase K) for 2 min at RT followed by 30 min at 50°C. RNA was separated from beads using magnetic rack, supernatant was collected into a new tubes and phenol-chloroform (Sigma Aldrich, P3803) extraction

used to isolated IP-RNA. IP-RNA was precipitated using 100% ethanol, 3M sodium acetate pH 5,2 and 20µg glycogen (Thermo Fisher, R0561T).

3.2.11 MeRIP-qPCR

MeRIP real-time qPCR involved evaluating the relative expression of gene of interest in both IP-RNA and input RNA samples. cDNA was synthesized as previously described, using Oligo(dT)12-18 primers and Superscript II, followed by quantitative analysis of using SYBR Green master mix. The pulldown efficiency was determined as a percentage of input by calculating the difference in Ct values using the formula: 2^-(Ct[IP]-Ct[Input-logDF]) * 10, where DF represents the input dilution factor, 10%. GAPDH expression was utilized as a reference to normalize the target gene expression in the IP sample.

3.2.12 Cellular fractionation

After subjecting cells to siRNA treatment for 48h, cellular fractionation was carried out to isolate cytoplasmic and nuclear RNA. This isolation process was conducted using the RNA Subcellular Isolation Kit from Active Motif (25501), following the manufacturer's instructions. Subsequently, qPCR assay was performed as previously detailed. Gene expression levels for the genes of interest were then normalized to housekeeping genes (HPRT or GAPDH) and control sample, calculated using the $2^{-\Delta\Delta CT}$ method. The nuclear-to-cytoplasmic ratio was determined as the ratio of mRNA expression in the nucleus compared to mRNA expression in the cytoplasm using the following formula:

$$Nuclear\ to\ Cytoplasmic\ ratio = \frac{Nuclear\ expression\ gene\ 1\ (2^{-\Delta\Delta CT})}{Cytoplasmic\ expression\ gene\ 1(2^{-\Delta\Delta CT})}$$

Ratio greater than 1 denotes more expression in the nucleus while ratio lower than 1 corresponds to more expression in the cytoplasm.

3.2.13 FLAG-tagged protein co-Immunoprecipitation.

U2OS cells were harvested 48 h following previously described plasmid transfection using GenJet™ In Vitro DNA Transfection reagent. The cells were lysed with 1 mL of FLAG lysis buffer (150 mM NaCl, 50 mM Tris HCl pH 7.4, 1% TRITON X-100and 1 mM EDTA) supplemented with a protease inhibitor cocktail at a 1:100 ratio. Cells were incubated with the lysis buffer for 30 min on a shaker at 4°C, followed by centrifugation at 14.000 rpm for 10 min to remove cell debris. The resulting supernatant was transferred to a chilled 1.5 mL tube, with 100 µL (10%) preserved as an input control.

The remaining lysate was mixed with Anti-FLAG-conjugated agarose beads (Sigma-Aldrich, 2220) and rotated ON at 4°C. Following ON incubation, agarose beads were

washed three times with ice-cold TBS buffer (50 mM Tris HCl pH 7.4, 150 mM NaCl), with a 1-minute centrifugation step between each wash. For elution, 100 µL of 300 ng/µL 3xFLAG peptide (Sigma, F4799) was added to the sample, followed by an ON incubation at 4°C with gentle shaking. After ON elution, samples were centrifuged at 7.000g for 1 minute, and the resulting supernatant was collected as the immunoprecipitation sample. Immunoprecipitation and input samples were subjected to downstream analysis either by immunoblotting or mass spectrometry.

3.2.14 SDS-polyacrylamide gel electrophoresis (PAGE)

Proteins were extracted from cells at 80-100% confluency, utilizing 2x Laemmli sample buffer (Santa Cruz, sc-286963), and subsequently treatment with Benzonase nuclease (Sigma Aldrich, E1014) for 30 min at 37°C. Following Benzonase treatment, samples were subjected to electrophoresis at 90V for 1h-1h 30 min using 6, 8, or 10% SDS-acrylamide gels (Table 11). SDS-gels were assembled using Mini-PROTEAN® Tetra Vertical electrophoresis system (Bio-Rad, 1658004) and filled with running buffer (190mM Glycine, Sigma Aldrich, G8898, 25mM Tris, Sigma Aldrich, T1378 and 0.1% SDS, Sigma Aldrich, D6750). For size comparison, PageRuler™ Pre-stained Protein Ladder, 10 to 180 kDa (Thermo Fisher, 26616) or Spectra™ Multicolor High Range Protein Ladder (Thermo Fisher, LC5699) were used.

Table 11. SDS acrylamide gels.

Running gel			
Reagent	Volume (mL) to 10 mL 6% gel	Volume (mL) to 10 mL 8% gel	Volume (mL) to 10 mL 10 % gel
MilliQ H_2O	5,3	4,6	4
30% Acrylamide (Bio-Rad, 161-0148)	2	2,7	3,3
1.5M Tris (pH 8,8)	2,5	2,5	2,5
10%SDS	0,1	0,1	0,1
10% Ammonium persulfate (Thermo Fisher, A3678-25G)	0,1	0,1	0,1
TEMED (Sigma Aldrich, T7024)	0,008	0,006	0,004

Stacking Gel	
Reagent	Volume (mL) to 4 mL stacking gel
MilliQ H_2O	2,7
30% Acrylamide (Bio-Rad, 161-0148)	0,67
1.0M Tris (pH 6,8)	0,5
10%SDS	0,04
10% Ammonium persulfate (Thermo Fisher, A3678-25G)	0,04
TEMED (Sigma Aldrich, T7024)	0,004

3.2.15 Immunoblotting (Western Blot)

Following SDS PAGE proteins were transferred onto nitrocellulose membranes (Santa Cruz, sc-3724) at 90V for a 90 min using the Mini Trans-Blot® Cell electrophoresis system (Bio-Rad, 170390) and transfer buffer (190mM Glycine, Sigma Aldrich, G8898, 25mM Tris, Sigma Aldrich, T1378 and 20% Methanol, Sigma Aldrich, 34860). Membranes were blocked for 30 min at RT using blocking buffer (1xPBS, Thermo Fisher, 18912014 and 5% milk Carl Roth, T145.2). For primary antibody incubation, membranes were kept at 4°C ON with primary antibody diluted in blocking buffer (For antibody dilution see Table 2). Membranes were washed 3x using wash buffer (1xPBS and 0.1% Tween-20) for 5 min. Subsequently, secondary antibodies (diluted at 1:10.000 in blocking buffer) were incubated with the membrane for 1 hour at RT. After secondary antibody incubation, membranes were washed with wash buffer 3x for 5 min, followed by a final 5min wash using MilliQ water. The membrane was developed using Luminol Reagent (Santa Cruz, sc-2048) and visualized using a ChemiDoc XRS+ system from Bio-Rad.

3.2.16 BCA Assay

To analyze total protein concentration of protein samples a Bicinchoninic acid (BCA) protein assay kit (Sigma Aldrich, 71285) was used according to manufacturer's instructions. The BCA assay relies on a highly sensitive and selective colorimetric method for detecting the presence of the cuprous cation (Cu^+), achieved using bicinchoninic acid. This method enables the quantification of protein concentration by observing a color change in the sample solution, shifting from green to purple in direct proportion to the protein concentration. BCA interacts with the reduced Cu+ ions, leading to the formation of a purple-colored complex that is soluble in water and demonstrates a strong, linear increase in absorbance at 562 nm as the protein concentration rises. To determine the concentration of an unknown sample an established standard curve is necessary. In this study, a known concentration of bovine serum albumin (BSA) was utilized to construct this standard curve, employing three replicates for each BSA sample.

3.2.17 UPLC- Mass spectrometry

Prior to mass spectrometry analysis protein concentration was established using a previously described BSA assay. 20µg of proteins were precipitated using cold (-20°C) isopropanol (1:4 ratio protein: isopropanol) and left ON at -20°C. Following precipitation samples were centrifuged at 14.000g for 10 min, supernatant removed and protein pellet airdried at RT for 60 min. Samples were reconstituted in 20µL of digestion buffer (1M DTT, 8% Rapi-Gest and 1M ammonium bicarbonate), followed by 10 sec sonication and finally incubation at 60°C for 60 min. Next samples were alkylated by 200 mM iodoacetamide at RT in the dark for 30 min. The excess iodoacetamide was then neutralized by the addition of 1 M DTT, and this quenching

step occurred for 20 min at RT, also in the dark. Subsequently, the samples were subjected to an overnight digestion using 1.5 µg of trypsin at 37 °C. After ON digestion, 6µL of 10% trifluoracetic acid was added to the samples, followed by centrifugation at 14000g for 10 min at 4°C and supernatant removed to a new tube. Samples were cleaned using an Oasis HLB 96-well plate as previously described (Gilar et al., 2001). Finally, samples were resuspended in 5% acetonitrile with 0,1% formic acid to a final concentration of 400 ng/µL and 12,5µL of sample used for MS/MS analysis. Peptides were analyzed on a Waters Synapt XS mass spectrometer using Ultra definition MS^E acquisition mode. Mobile Phase A consisted of water with 0.1% (v/v) formic acid and Mobile Phase B consisted of Acetonitrile with 0.1% (v/v) formic acid using a gradient of 5-40% mobile phase B and a flow rate of 300 nL/min over 90 min.

3.2.17.1 *Mass Spectrometry analysis*

Raw data was imported into Progenesis QI for Proteomics (Version 4.2, Waters) and runs were automatically aligned using the most suitable run for alignment reference. Peak picking was performed using automatic sensitivity method, maximum allowable ion charge of 20 and retention time limits before 12 min and after 110 min. Peptide identification was performed using the following search criteria:

Table 12. Mass Spectrometry analysis criteria

Mass spectrometry analysis	
Proteome	Homo sapiens (Human) ID: UP000005640
Enzyme	Trypsin
Max missed cleavages	3
Fixed modifications	Carbamidomethyl C
Variable modifications	Acetyl N-term; Deamidation N; Deamidation Q; Oxidation M

Protein measurements were subsequently exported to a .csv file for further analysis in Microsoft Excel.

3.2.18 Metaphase spread.

Following 48h incubation period with siRNA at a concentration of 10nM, U2OS cells were exposed to 500ng/µL of Colcemid (Invitrogen, 15212-012) to induce metaphase arrest. Cells were then trypsinized, followed by 20 min incubation at 37°C in a 75mM KCl solution to induce cell swelling. Subsequently, samples were centrifuged at 1000 rpm, supernatant was removed, and the cell pellet was resuspended in a fixing solution consisting of a 3:1 mixture of methanol and acetic acid. Fixing step was repeated three times ending with chromosomes suspended in 200µL of the fixing solution.

Microscope slides were prepared by placing the chromosome suspension on slides using the HANABI metaphase spreader from ADS Biotech. The slides were then stained with Giemsa staining, scanned and images were automatically captured using the DUET-3 automated imaging system from BioView. The analysis of these images, including counting aberrations, was performed using Solo software from BioView.

3.2.19 Clonogenic assay

Following a 48-hour incubation period with siRNA at a concentration of 10nM, cells were counted and then seeded in triplicate into six-well plates, with 500 cells per well (or 2500 cells for the siFTO condition). Following this, cells were subjected to 24-hour treatment with Mitomycin C (Bio-Techne, 3258/2) or a 1-hour treatment with NCS (Sigma-Aldrich, N9162). The cells were subsequently given fresh media and cultured for an additional 11 to 14 days, during which time colonies formed. Colonies were stained with crystal violet and counted. The survival fraction was calculated according to previously described method (Franken et al., 2006). CRISPR-Cas9 KO cells were seeded out in low density (500 cells) in six well plates and treated as described for siRNA samples.

3.2.20 Micronuclei assay

U2OS cells cultured on coverslips were subjected to siRNA (10nM) treatment for 48h. Following siRNA treatment cells were fixed with 4% paraformaldehyde for 15 min, followed by permeabilization using 0.2% Triton-X for 5 min, and 1h of blocking with DMEM containing 10% FBS. Subsequently, cells were stained using Nuclear DAPI stain (Sigma-Aldrich, D9542) diluted 1:5000 for 1 hour at RT. Coverslips were mounted on glass slides using Fluoroshield mounting medium (Sigma Aldrich- F6182). CRISPR clones were cultured, fixed, and stained using the same methods. Images were captured using an FV1200 Olympus inverted confocal microscope, with nuclear DAPI staining visualized using excitation by a 405 nm laser. For each condition, 5-10 images were randomly acquired using a 20x objective and imported into ImageJ and Cell Profiler for subsequent image analysis. Approximately 200-300 cells were analyzed for each condition.

3.2.21 RNA sequencing

RNA was isolated using Monarch ® Total RNA Miniprep Kit (NEB, T2010S) according to manufacturer's instruction from cells previously treated with siRNA (10nM) for 48h. The RNA samples were analyzed using a bioanalyzer, all samples were found to have RNA integrity of 9.8 and higher and siRNA mediated gene silencing confirmed by previously described qPRC analysis.

3.2.21.1 *Library preparation and sequencing*

Downstream sample preparation was conducted by deCODE genetics. cDNA libraries were produced from RNA samples using the Illumina TruSeq RNA v2 Prep Kit (Illumina, RS-122-2001). Fragmentation of RNA samples was performed at 94°C with divalent cations followed by first strand cDNA synthesis using SuperScript IV reverse transcriptase (Invitrogen, 18090200) along with random hexamers, following manufacturer's instructions. Next, second-strand cDNA synthesis performed along with end repair, addition of a single A nucleotide, unique dual-indexed adaptor ligation, AMPure bead purification, and PCR amplification of the resultant products. The cDNA sequencing libraries obtained were assessed using LabChip GX (Perkin Elmer), diluted to 3nM, and stored at -20°C. For Illumina sequencing, the samples were combined and clustered on NovaSeq S4 v 1.0 flow cells through on-board clustering. The XP workflow was employed to conduct paired-end sequencing on NovaSeq6000 instruments, involving 2x125 cycles for incorporation and imaging, along with 2x8 cycles for the dual indexes. Real-time basecalling was executed using real time analysis v3.4.4, and the demultiplexing of Binary Base Call files and generation of FASTQ files were carried out using bcl2fastq2.20.

3.2.21.2 *RNA sequencing data analysis*

Kallisto was utilized to perform pseudo-alignment and transcript abundance estimation on Fastq files (Bray et al., 2016). Sleuth R-package version 0.30.0 (Pimentel et al., 2017) was used to normalize counts obtained from Kallisto and to perform statistical analysis. Principle component analysis plots and sample heatmaps were created using Sleuth to evaluate sample quality. Distribution plots of expressed genes in the samples were generated through Jupyter Notebooks (Kluyver et al., 2016) for additional quality assessment. Differentially expressed transcripts were visually represented using Volcano plots generated with Sleuth. Gene set enrichment analysis (Wu et al., 2021) was performed using the R package clusterProfiler. Graph modification was carried out using R packages ggplot2, RcolorBrewer, gridR, ggrepel, grid, and cowplot. Statistical analyses were conducted using the R package rstatix.

3.2.22 CRISPR-Cas9 generated knockout models.

To induce knockout of either the FTO or ALKBH3 gene, U2OS cells were transfected with three single-guide RNAs (sgRNAs) using the RNAiMAX transfection reagent along with the CRISPR/Cas9 system. 72h post transfection, cells were seeded at a low density, allowing individual clones to form. Individual clones were subsequently harvested, DNA isolated and Synthego Inc provided "Inference of CRISPR Edits" analysis tool was employed to assess specific fragment deletions or indels and to determine the overall knockout score for each sample. To confirm the knockout, validation was performed through western blot analysis and Sanger sequencing.

3.2.23 Immunofluorescence

Cells were cultured on coverslips, fixed with 4% paraformaldehyde for 15 min and permeabilized with 0.2% Triton-X for 5 min. Subsequently, they were subjected to a 1-hour blocking step with DMEM containing 10% FBS. Primary antibodies were applied at RT for 1½h, with varying dilutions (1:250, 1:500, or 1:1000). Following primary antibody incubation cells were washed 3x using 1xPBS. Next secondary antibodies (1:1000 dilution) and nuclear DNA stain DAPI (1:5000) were incubated for at RT for 1h. Subsequently cells were washed 3x using 1xPBS along with a single wash in MilliQ water and coverslips were placed onto glass slides using Fluoroshield mounting medium (Sigma Aldrich, F6182). An Olympus FV1200 inverted confocal microscope was utilized for image acquisition. Dual-color confocal images were captured with standard settings using laser lines at 488 nm, 546 nm, and 635 nm to excite Alexa Fluor 488, Alexa Fluor 555, and Alexa Fluor 647 dyes, separately. Excitation by 405 nm laser was used to capture images of DAPI nuclear staining. Each experimental condition was imaged randomly 5-10 times using a 20X objective and then imported into ImageJ and Cell Profiler for subsequent image analysis. A minimum of 200 cells were analyzed for each data point.

3.2.24 DNA damage induction

Neocarzinostatin (NCS) (Sigma Aldrich, N9162-100UG) is an effective DNA-damaging, radiomimetic anti-tumor antibiotic (Jadav et al., 2013) from *Streptomyces carzinostaticus* a gram-positive bacteria. NCS is made up of a complex consisting of a small molecule called an enediyne chromophore attached to a single-chain protein composed of 113 amino acids. When a thiol is introduced, the chromophore transforms into a highly reactive biradical species, which can selectively cause breaks in DNA strands by removing hydrogen from the deoxyribose of DNA thereby causing DNA to be cleaved (Edo et al., 1997). NCS impedes DNA synthesis, proliferation by prompting cell cycle arrest in G2 and demonstrates antitumor effects against a range of human tumors.

Mitomycin C (MMC) (Bio-Techne, 3258/2) is an alkylating chemotherapy drug derived from *Streptomyces caespitosus* a gram-positive actinobacteria (Tomasz, 1995). MMC is a potent cross-linking reagent that induces DNA crosslinking leading to replication and transcriptional stress and eventually apoptosis. This is accomplished by reductive activation of Mitomycin to form a mitosene, which reacts via N-alkylation with 7-N-guanine nucleotide residues in the minor groove of DNA at the location of 5′ -CpG-3′ sequence that causes DNA crosslinking. MMC induced DSBs are the results of collapse of inter-strand cross-link-stalled replication forks (Al-Minawi et al., 2009). DNA crosslink induced by MMC can be repaired by different DNA repair pathways including DNA DSB repair (Lee et al., 2006; McHugh et al., 2001).

3.2.25 DNA DSB repair reporter assays

DNA DSB repair efficiency assay was performed in U2OS cells containing single pathway reporter systems: HR (Addgene, Plasmid #26475), NHEJ (Addgene, Plasmid #44026) or SSA (Addgene, Plasmid #41594) (see Appendix B for additional information on reporter systems). Each reporter system consists of construct that contains disrupted GFP gene separated by a rare restriction site, which is recognized by the endonuclease I-Sce1 (Gunn et al., 2012). U2OS cells were treated with siRNAs for 24h followed by co-transfected with plasmids expressing the endonuclease I-Sce1. I-Sce1 cuts the I-Sce1 sites flanking the GFP gene, creating a DSB. Repairing the DSB restores the GFP gene and enables detection of corresponding DSB repair via GFP signal emission. 48h post plasmid transfection HR, NHEJ or SSA rates are defined by quantifying GFP^+ cells by flow cytometry, fluorescence activated cell sorting (FACS) SH800 and FlowJo single cell analysis software V10 program.

pDRGFP and hprtSAGFP reporter system plasmids were a gift from Maria Jasin (Stark et al., 2004) and pimEJ5GFP was a gift from Jeremy Stark (Bennardo et al., 2008).

3.2.26 RNA Scope

RNA scope assay was performed using RNAScope® Multiplex Fluorescent Reagent Kit (ACD Bio, 323100), following manufacturers instruction. In short, after 48h incubation with siRNAs U2OS cells were fixed with 4% paraformaldehyde for 30 min followed by protease digestion using Pretreat protease III (ACD Bio 322340) for 10 min at RT. Cells were incubated with target probes (ACD Bio 300031/320861) for 2h at 40°C and washed two times with 1xRNAScope wash buffer (ACD Bio, 310091). Subsequently, primary, secondary, tertiary, and fluorescent probes (ACD bio, 320850) were applied successively for durations of 30, 15, 30, and 15 min, each followed by two 5 min washes in the wash buffer (ACD bio, 310091). Following this, cells were subjected to DAPI nuclear staining for 1 min, and the samples were promptly mounted on glass slides with mounting medium. Imaging was conducted with confocal microscopy using Olympus FLV1200, employing the 60X oil immersion objective in an unbiased manner, based on DAPI staining rather than RNAScope foci. Image analysis was performed using Image J and Cell Profiler 3.0, with approximately 200-300 cells counted for each treatment.

3.2.27 Statistical analysis

All data generated were taken from distinct samples and presented as mean ± SD. All statistical analysis was performed from experiments performed in a minimal three biological replicates. The statistical significance of experimental data was assessed using One-Way ANOVAT-test or two-tailed T-test using Graph Pad Prism 6 for windows, except for RNA sequencing data which was analyzed as described above in RNA sequencing data analysis chapter. P-values are as follows: ****$p<0.0001$, ***$p<0.001$, **$p<0.01$, *$p<0.05$.

4 Results

4.1 Deciphering the regulatory role of ALKBH3 and FTO in RNF168 function

4.1.1 ALKBH3 and DNA Double Strand Breaks

The initial interest in ALKBH3 arose from a previous publication by Stefansson et al., conducted by the Sigurdsson research group, where the primary focus was to investigate DNA repair genes subjected to epigenetic silencing in breast cancer through promoter methylations (Stefansson et al., 2017). A list of repair genes (n=178) (Kauffmann et al., 2008) were cross-referenced to genes undergoing CpG promoter methylation (n=456) identified using the Cancer Genome Atlas (TCGA). ALKBH3 emerged as one of the eight identified DNA repair genes undergoing promoter methylation with approximately 20% of the breast cancer samples within the TCGA dataset displaying ALKBH3 promoter methylations. This was validated in an Icelandic cohort (n=265), where roughly 27% of the samples in the Icelandic cohort (72 out of 265 cases) showed ALKBH3 promoter methylation. ALKBH3 promoter methylation correlated with reduced gene expression of ALKBH3 in breast cancer, observed across the TCGA dataset, Icelandic cohort and in breast cancer cell lines. Notably, promoter methylation of ALKBH3 was specific to cancer tissues and absent in normal breast tissue. This epigenetic alteration correlated with poor disease outcomes for patients, as a higher degree of ALKBH3 promoter methylation (>20%) was associated with reduced breast cancer-specific survival. Collectively these findings prompted the question: why did loss of ALKBH3 result in worse patient survival and is it only due to lack of DNA alkylation repair?

Prior to the study by Stefansson et al, Dango et al (Dango et al., 2011) had provided indication of a possible connection between ALKBH3 and DNA DSB repair. Their proteomics studies demonstrated that ALKBH3 interacts with proteins involved in DSB repair, namely RIF1 and CHD4, proteins both implicated in the regulation of DSB repair via the ubiquitin signaling pathway (Daley et al., 2013; Larsen et al., 2010). Further potential links between ALKBH3 and DNA DSB repair came from the interaction observed in the *E. coli* homolog of ALKBH3, AlkB, with RecA, the human homolog of RAD51 (Shivange et al., 2016).

In an effort to enhance our understanding of ALKBH3 and its potential involvement in DSB repair, we started by looking into the functional interaction between ALKBH3 and RIF1 and its recruitment partner 53BP1 following ALKBH3 KD in human osteosarcoma

cells (U2OS). This thesis predominantly employed U2OS cells as they are extensively employed in the examination of DNA repair and signaling, owing to their robust DNA damage response when compared to various other cancer cell lines. 53BP1 foci formation signifies the activation of the DSB-induced signaling pathway, and the absence of either RIF1 or 53BP1 can result in impairments in DNA DSB repair.

To determine if ALKBH3 was influencing the cellular response to DSB, ALKBH3 was silenced in U2OS cells using small interfering RNAs (siRNAs), followed by western blot analysis to examine 53BP1 and RIF1 protein expression (Figure 19 A). Recruitment of 53BP1 and RIF1 to sites of DSB was likewise examined in U2OS cells depleted of ALKBH3 and treated with Neocarzinostatin (NCS) to induce DNA DSB damage. Cells were immunostained for 53BP1, RIF1 and phosphorylated histone H2AX (γH2AX), a commonly used marker for DSB (Valdiglesias et al., 2013) (Figure 19B-E).

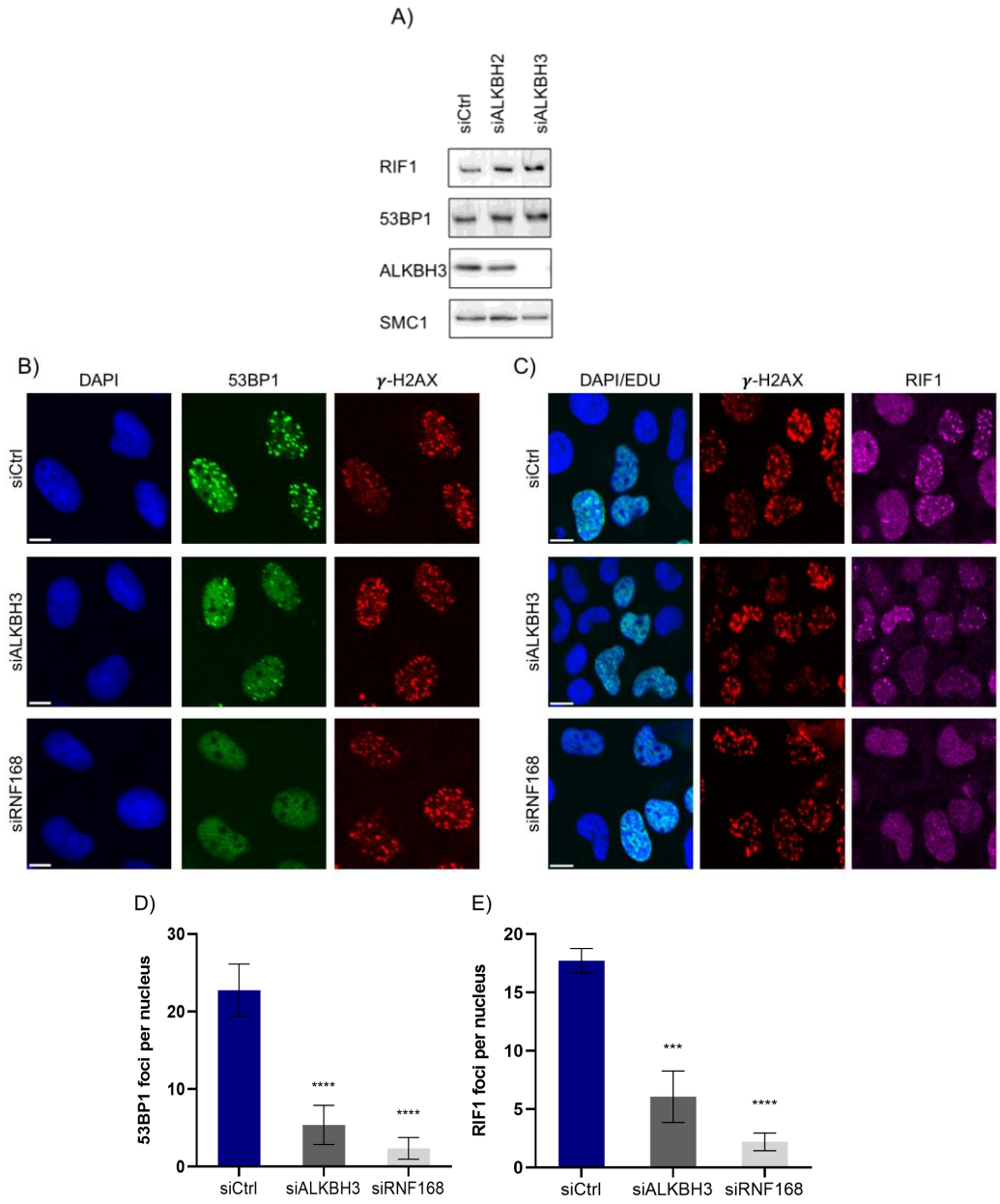

Figure 19. ALKBH3 knockdown results in reduced 53BP1 and RIF1 recruitment to DSBs.

A) U2Os cells treated with the above-mentioned siRNAs for 48h followed by western blot analysis of RIF1, 53BP1, ALKBH3 and SMC1 used as loading control. B-C) Representative images U2OS cells transfected with indicated siRNAs, 48h post transfection cells were treated with 50ng/mL of NCS for 15 min to induce DSBs and cells fixed 1h later. Cells were immunostained with 53BP1 (Green), RIF1 (purple) and γH2AX (red). Nuclear DNA was visualized by DAPI (blue), scale bar: 10μm. RNF168 was used as a positive control (PC). D- E) Quantification of 53BP1 and RIF1 foci from B, D, One-way ANOVA, n=3 mean±SD.

Cells depleted of ALKBH3 did not exhibit any discernible effect on the protein expression of RIF1 or 53BP1 (Figure 19A) when compared to cells treated with control and ALKBH2 siRNA. As previously mentioned, ALKBH2 along with ALKBH3 is the true functional homolog of the AlkB enzyme in *E. coli*. However, the depletion of ALKBH3 did lead to the decrease of recruitment of both RIF1 and 53BP1 to the site of DSB, without affecting γH2AX formation (Figure 19 B-E), suggesting that ALKBH3 could be impacting DNA DSB signaling.

To develop a clearer picture of how ALKBH3 influences the recruitment of 53BP1 and RIF1, we turned our attention upstream in the DNA DSB signaling pathway to the E3 ubiquitin ligases RNF8 and RNF168 which play a significant role in the recruitment of 53BP1 and RIF1. U2OS cells along with MCF7 breast cancer cells were depleted of ALKBH3, using two different siRNAs and protein expression of RNF8 and RNF168 examined (Figure 20). MCF7 cells were included in the analysis to eliminate the possibility of cell line-specific effects observed in U2OS cells. In addition, the PC-3 pancreatic cancer cell line, known for its relatively higher expression of ALKBH3 (Dango et al., 2011) and the non-cancerous HEK293T human embryonic kidney were employed to assess RNF168 expression in the absence of ALKBH3.

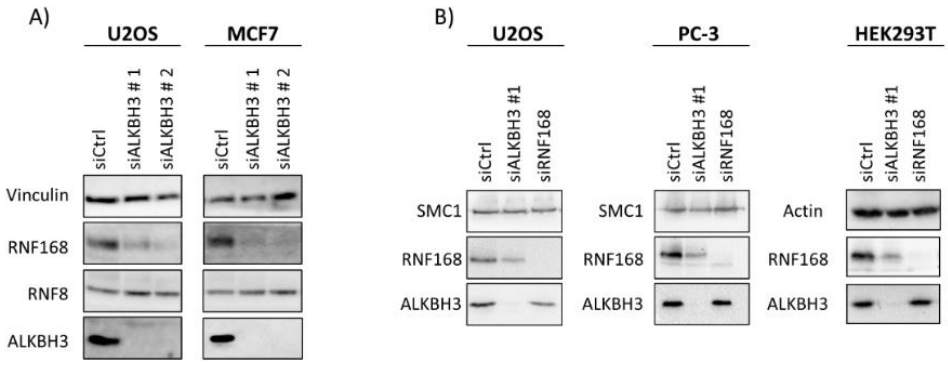

Figure 20. ALKBH3 knockdown results in reduced RNF168 protein expression.

A) U2OS and MCF7 cells treated with the above-mentioned siRNAs for 48h followed by western blot analysis of RNF8, RNF168 and ALKBH3, Vinculin used as a loading control. B) RNF168 and ALKBH3 protein expression analyzed by immunoblotting in U2O2, PC-3 and HEK293T cells 48h post siRNA transfection with the indicated siRNAs, SMC1 or Actin used as loading control.

Reduced expression of ALKBH3 led to decreased protein expression of RNF168 in all four tested cell lines but did not affect RNF8 in either U2OS or MCF7 cells (Figure 20). This suggests that the loss of RIF1 and 53BP1 recruitment to the site of DSB can likely be attributed to the decreased RNF168 expression. The observation that RNF8, 53BP1, and RIF1 protein levels were unaffected by ALKBH3 KD also indicates that the depletion of ALKBH3 is not causing a global reduction in gene expression.

Previous studies on ALKBH3 have suggested a potential role in influencing cell cycle progression as the loss of ALKBH3 has been shown to contribute to cell cycle arrest in the G1 phase (Kuang et al., 2022; Shimada et al., 2012; Tasaki et al., 2011). To eliminate the possibility that our observed RNF168 phenotype being dependent on the cell cycle, U2OS cells were depleted of ALKBH3 and were immunostained using cyclin A as a marker for the S/G2 phase of the cell cycle. This was performed to ascertain whether the downregulation of RNF168 was specific to G1 cells or if it occurred independently of the cell cycle.

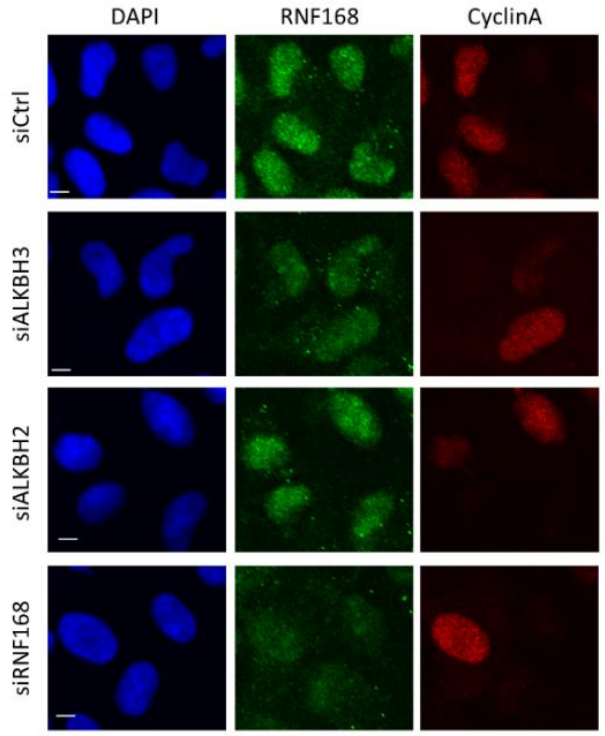

Figure 21. RNF168 downregulation is cell cycle independent.

Representative images of U2OS cells transfected with ALKBH3, ALKBH2, RNF168 and control siRNA for 48h and immunostained with DAPI (blue), RNF168 (green) and Cyclin A (red). Scale bar: 10μM.

The reduction in RNF168 protein expression resulting from ALKBH3 KD appeared to occur independently of the cell cycle phase (Figure 21), as evidenced by observed decrease in RNF168 expression in cells both outside of the S/G2 phase (cyclin A-negative cells) and cells in S/G2 phase (cyclin A positive cells).

4.1.2 Novel regulatory role of ALKBH3 on RNF168 function

ALKBH3 is primarily recognized for its pivotal role in repairing alkylating damage on ssDNA, a process facilitated by the DNA helicase ASCC3. ASCC3 unwinds the DNA thereby creating the necessary ssDNA for ALKBH3's alkylation repair activity (Dango et al., 2011). To explore if loss of RNF168 protein expression in the absence of ALKBH3 was occurring in relation to ALKBH3 role in alkylation damage repair we depleted U2OS cells of ASCC3 and ALKBH2 and examined RNF168 protein expression along with 53BP1 recruitment to DSBs (Figure 22). Should loss of ASCC3 result in a similar effect on RNF168 protein expression as loss of ALKBH3 it could indicate that ALKBH3 influence over RNF168 might be connected to its role in alkylation repair.

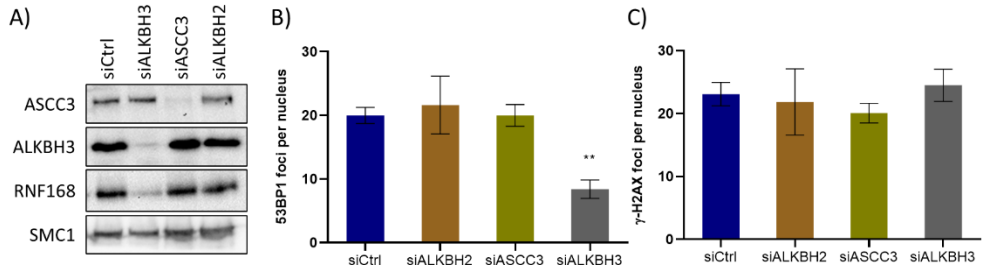

Figure 22. Depletion of ASCC3 and ALKBH2 had no discernible impact on RNF168 expression or 53BP1 recruitment.

A) U2OS cells treated with indicated siRNAs for 48h prior to protein analysis of ASCC3, ALKBH3 and RNF168 using western blot. SMC1 was used as loading control. B-C) Quantification of 53BP1 and γH2AX foci formation in U2OS cells treated with the indicated siRNAs for 48h followed by 50ng/mL NCS treatment to induce DSB for 15 min. 1h later cells were fixed and immunostained with antibodies for 53BP1 and γH2AX. One-way ANOVA, n=3 mean±SD.

Neither ALKBH2 nor ASCC3 exhibited any noticeable effect on RNF168 expression nor did depleting U2OS cells of ALKBH2 or ASCC3 have any impact on the recruitment of 53BP1 to DSB when DNA damage was induced (Figure 22). These findings suggest that ALKBH3 regulates RNF168 independently of ASCC3, pointing towards a distinct role for ALKBH3 beyond its canonical function in alkylating damage repair.

4.1.3 Elucidating ALKBH3's role in RNF168 regulation.

Having demonstrated that ALKBH3 influences protein expression of RNF168 in a number of cell lines, the focus turned towards clarifying how ALKBH3 influences RNF168 protein expression. Given that RNF168 plays a crucial role as a rate-limiting factor in the response to DSB, maintaining proper expression levels of RNF168 is essential for normal cellular function (Gudjonsson et al., 2012). One well-documented mechanism for regulating RNF168 involves protein turnover, a process that encompasses a series of factors within the ubiquitin-proteasome pathway of protein

degradation (Gudjonsson et al., 2012; Sharma et al., 2018; Zhu et al., 2015). To determine if the loss of ALKBH3 affected RNF168 protein turnover, U2OS cells were treated with control and ALKBH3 siRNA along with MG-132. MG-132 is a widely used proteasome inhibitor that binds to the active site of the β subunits of the 20S proteasome, thereby blocking its activity. To assess whether the lack of ALKBH3, in combination with MG-132 treatment, could rescue the RNF168 protein expression, the RNF168 expression was analyzed using western blot (Figure 23).

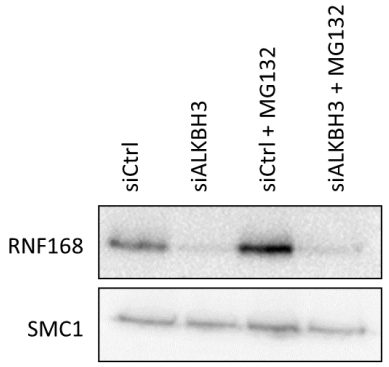

Figure 23. Depletion of ALKBH3 does not affect RNF168 protein turnover.

U2OS cells were treated with control siRNA and ALKBH3 siRNA for 48h followed by 3h treatment with 10μM MG-132. RNF168 expression was analyzed using western blot. SMC1 was used as loading control.

Knocking down ALKBH3 along with MG-132 treatment did not restore RNF168 protein expression demonstrating ALKBH3 was not influencing RNF168 protein turnover, this however did not rule out other forms of regulation. In light of the absence of known epigenetic or post-translational regulatory roles for ALKBH3, focus shifted towards exploring alternative forms of regulatory mechanisms. Initially, attention was directed to the synthesis of *RNF168* mRNA in the presence and absence of ALKBH3 (Figure 24 A) to assess if ALKBH3 exerted transcriptional influence on RNF168. Simultaneously, potential protein-protein interactions between ALKBH3 and RNF168 were investigated through co-immunoprecipitation (co-IP) followed by western blot analysis (Figure 24 B). Lastly, to test if ALKBH3 was influencing RNF168 at the site of DSBs, ALKBH3 recruitment to the site of DSB in response to DNA damage was evaluated (Figure 24 C).

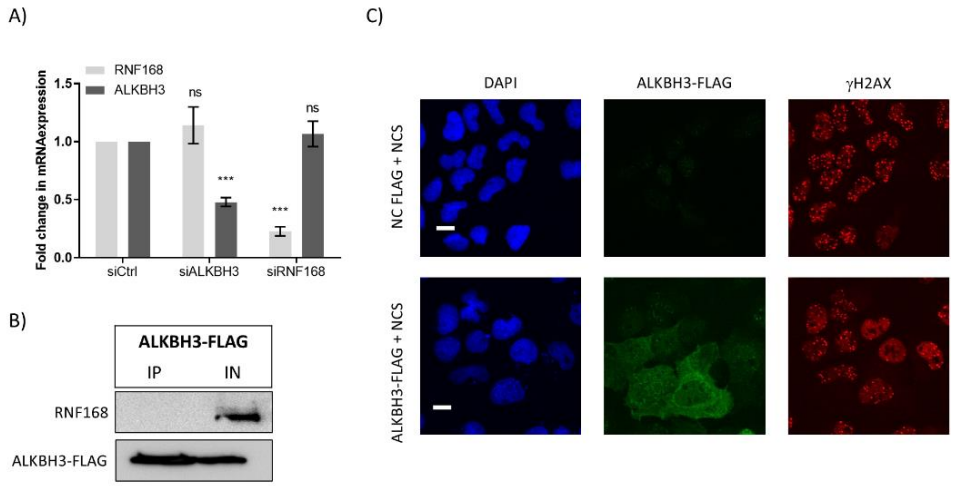

Figure 24. Deciphering ALKBH3's Regulatory Impact on RNF168.

A) Total *ALKBH3* and *RNF168* mRNA levels in U2OS cells treated with control, ALKBH3 and RNF168 siRNA followed by qPCR analysis, normalized to GAPDH housekeeping gene. One-way ANOVA, n=3 mean±SD. B) Western blot analysis of protein-protein co-immunoprecipitation in U2OS cells transfected with ALKBH3-FLAG tagged expression vector. Cell lysate was subjected to FLAG M2-pull down followed by immunoblotting using RNF168 and FLAG antibody. Input sample (IN), immunoprecipitation sample (IP). C) U2OS cells were transfected with ALKBH3-FLAG tagged expression vector or empty FLAG vector (NC FLAG). 48h post transfection cells were treated with 50ng/mL NCS for 15 min to induce DSBs, 1h later cells were fixed and stained with nuclear stain DAPI (blue), γH2AX (red) and FLAG-tagged ALKBH3 (green). Scale bar: 10μm.

Depleting U2OS cells of ALKBH3 did not have any discernible impact on the total mRNA levels of *RNF168*, and vice versa (Figure 24 A). This observation suggests that the reduced transcription is not the contributing factor to the decline in RNF168 protein expression. Furthermore, there was no evident protein-protein interaction between ALKBH3 and RNF168 (Figure 24 B), suggesting that the regulation of RNF168 by ALKBH3 may not involve direct physical interactions between these two proteins. Lastly, ALKBH3 was not being recruited to the site of DSB in response to DNA damage (Figure 24 C) and therefore likely not influencing RNF168 at the break site. From this we argued that further exploration into post-transcriptional regulatory mechanisms was necessary to provide deeper insights into ALKBH3's regulation of RNF168.

4.1.4 The epitranscriptomic influence on RNF168 by ALKBH3

Apart from its involvement in repairing DNA alkylation damage, ALKBH3 has been shown to influence gene expression by acting as an m^1A mRNA demethylase. In fact, transcriptome-wide mapping of m^1A modification in human cells (HEPG2, HEK293 and HELA) identified *RNF168*, along with thousands of transcripts, to contain the m^1A modification (Dominissini et al., 2016). It is important to point out that there has been

some discrepancy regarding the precise prevalence of m^{1}A modification on *RNF168*, as a second round of transcriptome-wide studies did not observe any modification of *RNF168* with m^{1}A (X. Li J. Peng et al., 2017; X. Li X. Xiong et al., 2017). The next step was to address the question of whether ALKBH3 regulates *RNF168* by removing a methylation mark from its transcript.

An m^{1}A methylation specific RNA immunoprecipitation followed by a qPCR (m^{1}A MeRIP-qPCR) was performed in cells depleted of ALKBH3 and compared to control cells (Figure 25). The hypothesis of this experiment is that the depletion of the m^{1}A demethylase, ALKBH3, results in increased m^{1}A methylation on the *RNF168* transcript. This increase in m^{1}A methylation leads to elevated amount of RNA that is immunoprecipitated, consequently yielding enrichment of *RFN168* levels in the subsequent qPCR analysis.

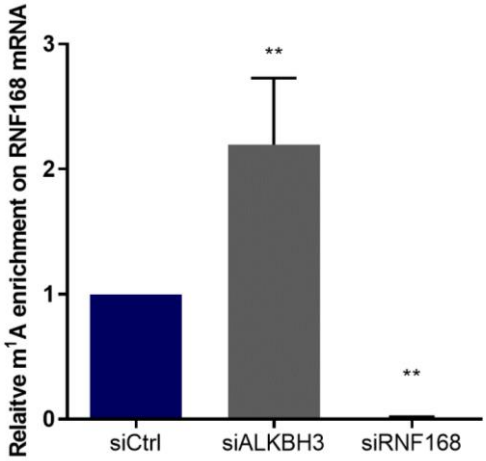

Figure 25. ALKBH3 depletion results in increased m^{1}A methylation marks on the *RNF168* transcript.

U2OS cells treated with control, ALKBH3 and RNF168 siRNA for 48h followed by m^{1}A MeRIP-qPCR. Graph shows relative quantification of *RNF168* mRNA levels from m^{1}A pulldown, expression normalized to GAPDH. One-way ANOVA, n=3 mean±SD.

RNF168 mRNA was found in both the control and ALKBH3 KD RNA immunoprecipitation samples. The ALKBH3-depleted sample exhibited approximately a 2.2-fold increase in *RNF168* mRNA levels compared to the control, suggesting the presence of the m^{1}A modification on the *RNF168* transcript.

As mRNA modifications are known to play crucial roles in various stages of the mRNA life cycle, encompassing translation, splicing, export, and stabilization, our next aim was to unveil the significance of ALKBH3-mediated removal of m^{1}A from *RNF168* transcripts. In recent years, research has illuminated the impact of mRNA modifications

on translation efficiency and mRNA stability. Given that qPCR analysis (Figure 24) had already revealed no discernible effect of ALKBH3 KD on *RNF168* mRNA levels, our focus shifted to exploring mRNA stability as it represents one of the most extensively researched ways in which methylation influences mRNA dynamics. RNA stability post ALKBH3 KD was tested in U2OS cells depleted of ALKBH3 and treated with Actinomycin D. Actinomycin D is a transcription inhibitor, commonly used in mRNA stability assays to block new mRNA synthesis and allowing for the assessment of mRNA decay by measuring mRNA abundance following transcription inhibition (Figure 26).

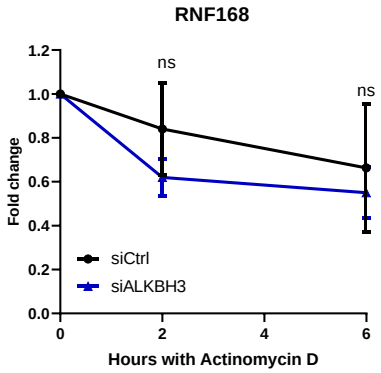

Figure 26. ALKBH3 knockdown had no effect on *RNF168* mRNA stability

RNF168 mRNA stability in U2OS cells treated with control and ALKBH3 siRNA for 48h followed by Actinomycin D treatment (8 µg/ml) followed by qPCR, normalized to HPRT housekeeping gene. N=3, mean±SD, two-tailed T-tes.

Knocking down ALKBH3 using siRNA had no statistically significant effect on *RNF168* mRNA stability compared to control siRNA, therefore we next moved towards mRNA export. To evaluate if *RNF168* mRNA export was affected by ALKBH3 m^1A demethylation an RNA cellular fractionation assay was performed. Cellular fractionation assay enables the isolation of cytoplasmic and nuclear RNA. Subsequently a qPCR assay was performed to compare *RNF168* mRNA expression in nucleus and cytoplasm in cells depleted of ALKBH3 (Figure 27).

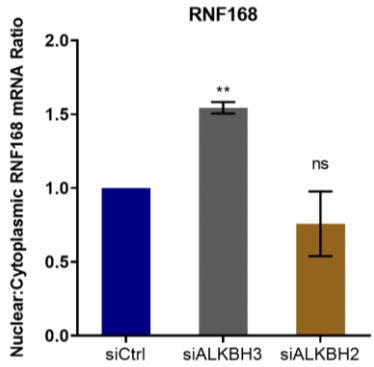

Figure 27. ALKBH3 knockdown results in increased nuclear retention of *RNF168* mRNA.

RNA fractionation assay. Ratio between nuclear and cytoplasmic *RNF168* mRNA expression in U2OS cells treated with control, ALKBH3 and ALKBH2 (NC) siRNAs for 48h followed by qPCR, expression normalized to housekeeping gene HPRT. Ratio>1 indicates more mRNA expression in nucleus, ratio<1 demonstrates more mRNA expression in cytoplasm. N=3, mean±SD, One-way ANOVA

Interestingly, loss of ALKBH3 resulted in higher mRNA expression of *RNF168* in the nucleus compared to both the control sample and cells depleted of ALKBH2 (Figure 27), suggesting a malfunction in *RNF168* mRNA export in the absence of ALKBH3. To further validate the mRNA export defects RNA Scope assay was performed in U2OS cells treated with control, RNF168 and ALKBH3 siRNA (Figure 28). RNA Scope is an *in-situ* hybridization technique that enables both quantification and visualization of the mRNA of interest.

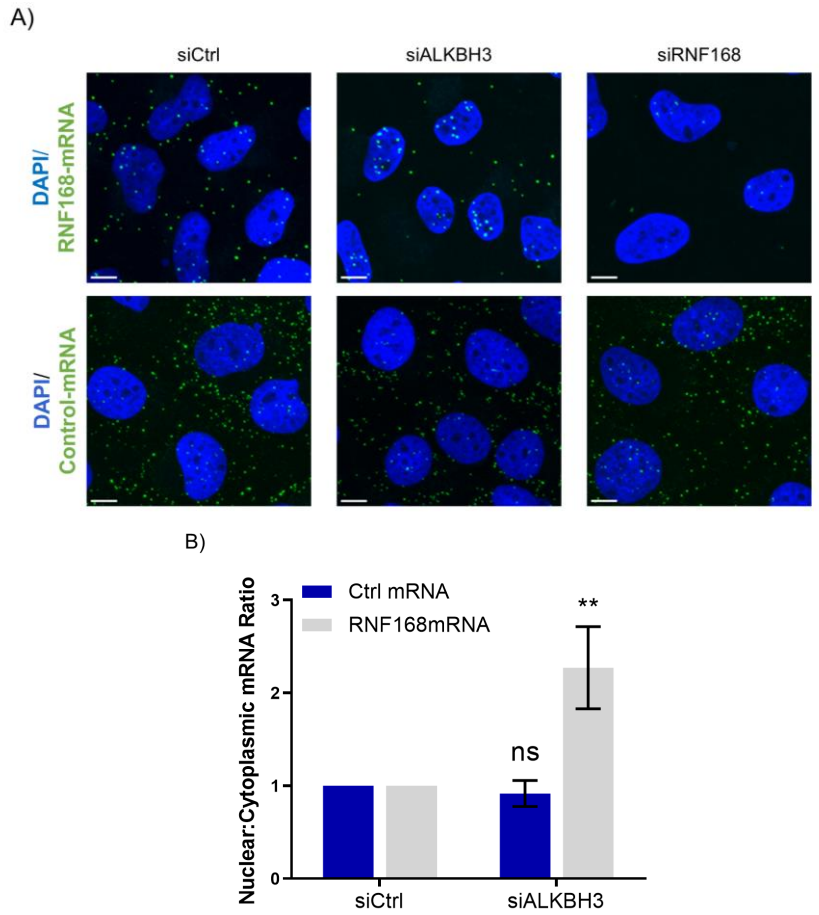

Figure 28. ALKBH3 promotes nuclear export of *RNF168* mRNA.

A) Representative pictures and B) quantification of RNA scope assay performed in U2OS cells treated with control and ALKBH3 siRNA for 48h followed by incubation with *RNF168* specific probes, control probes (green) and nucleus stain (DAPI). *PPIB* was used as control mRNA. Graph illustrates *RNF168* mRNA nuclear: cytoplasmic ratio where ratio>1 indicates more mRNA expression in nucleus, ratio<1 demonstrates more mRNA expression in cytoplasm. N=3, mean±SD, two-tailed T-test. Scale bar: 10μm

Cells depleted of ALKBH3 exhibited a notable elevation in the *RNF168* mRNA levels within the nucleus compared to the cytoplasm, approximately a 2.2-fold increase in contrast to the control sample. This observed shift supports the notion that the absence of ALKBH3 affects the nuclear export of *RNF168* mRNA. Importantly, the loss of ALKBH3 did not exert any discernible influence on the mRNA export of the control gene (peptidyl-propyl isomerase B: *PPIB*) (Figure 28).

The results obtained thus far indicate that ALKBH3 may play an epitranscriptomic regulatory role in relation to RNF168. These findings suggest that ALKBH3 may be involved in the removal of a distinct methylation mark from the *RNF168* transcript,

thereby facilitating the unimpeded export of *RNF168* mRNA and contributing to the maintenance of normal RNF168 protein expression.

4.1.5 Exploring the impact of other AlkB members on RNF168 function

ALKBH3 is one of nine members of the AlkB protein family where other members are known to have mRNA demethylase activity. These include ALKBH5 and FTO which have demonstrated demethylase activity towards mRNA and ALKBH1 which has been shown to remove RNA modifications from tRNA but has also displayed some affinity for mRNA. To explore the potential impact of other AlkB family members on RNF168, we knocked down members exhibiting demethylase activity (ALKBH1, ALKBH3, ALKBH5, and FTO) in U2OS cells, alongside ALKBH2 as a negative control (NC), and assessed RNF168 protein expression through a western blot assay (Figure 29). Among the examined AlkB members, only the depletion of FTO led to a reduction in RNF168 protein expression compared to the control sample. ALKBH1 KD and ALKBH5 KD showed no impact on RNF168, consistent with the findings for ALKBH2, as previously observed (Figure 19A and Figure 22A). To further confirm FTOs influence on RNF168 protein expression, FTO was depleted in HEK293T, and PC-3 cells followed by western blot assay to evaluate RNF168 protein expression (Figure 22 B-C).

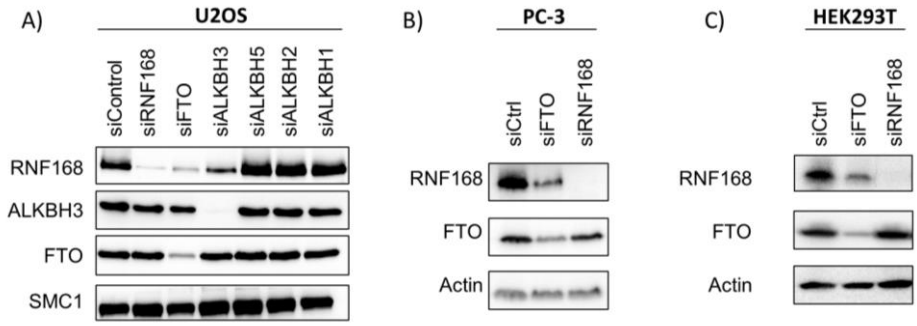

Figure 29. The effect of knocking down AlkB family members on RNF168 protein expression.

Western blot of protein expression in A) U2OS, B) PC-3 and C) HEK293T cells treated with the above-mentioned siRNAs for 48h and protein expression of RNF168, ALKBH3 and FTO examined. SMC1 and Actin were used as loading controls.

4.1.6 FTO depletion demonstrates similar RNF168 phenotype to ALKBH3 depletion

Considering the phenotypical similarities between the loss of FTO and ALKBH3 on RNF168 protein expression (Figure 29) we became interested in exploring if FTO was influencing RNF168 in a similar manner as ALKBH3. To start with we set out to examine the recruitment of 53BP1 in U2OS depleted of FTO. As our previous data had demonstrated that the depletion of ALKBH3 leads to a decrease in 53BP1 recruitment in cells (Figure 19), we hypothesized that the absence of FTO would similarly result in diminished 53BP1 recruitment in U2OS cells when DNA DSBs are induced. To test this hypothesis U2OS cells were treated with control, FTO and RNF168 siRNA, DNA damage induced using NCS and recruitment of 53BP1 to the site of DSB examined using confocal microscopy (Figure 30).

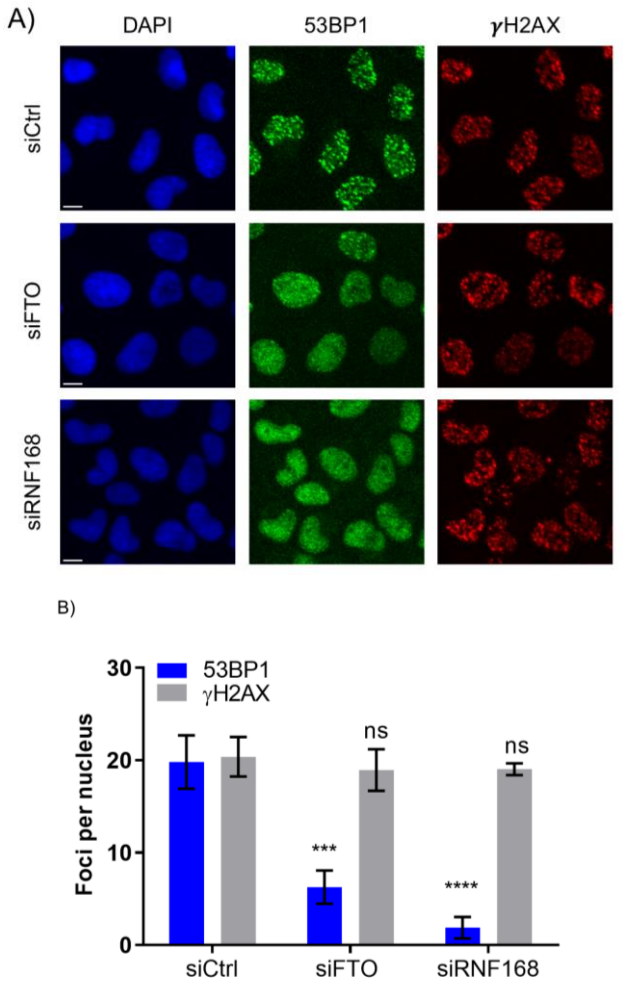

Figure 30. FTO depletion results in reduced 53BP1 recruitment to DSBs.

A) Representative images and B) quantification of U2OS cells transfected with indicated siRNAs, 48h post transfection cells were treated with NCS (50 ng/mL) for 15 min to induce DSB and cells fixed 1h later. Cells were immunostained with 53BP1 (Green) and γH2AX (red). Nuclear DNA was visualized by DAPI (blue). N=3 mean±SD, One-way ANOVA. Scale bar: 10μm

FTO-depleted cells exhibited a reduced recruitment of 53BP1 when DSBs were induced while the expression of γH2AX, an upstream DSB marker independent of RNF168's ubiquitin ligase function, remained unaffected. Based on this observation, we reasoned that just as ALKBH3, FTO is likely influencing the DSB signaling pathway via its effect on RNF168.

Next, to eliminate the possibility that FTO was recruited to the site of DNA DSBs and affecting the recruitment of 53BP1 or RNF168 at the DSB site, U2OS cells were treated with both control and FTO siRNA. Subsequently, DNA damage was induced using NCS, and the recruitment of FTO to DSBs was assessed using confocal microscopy (Figure 31).

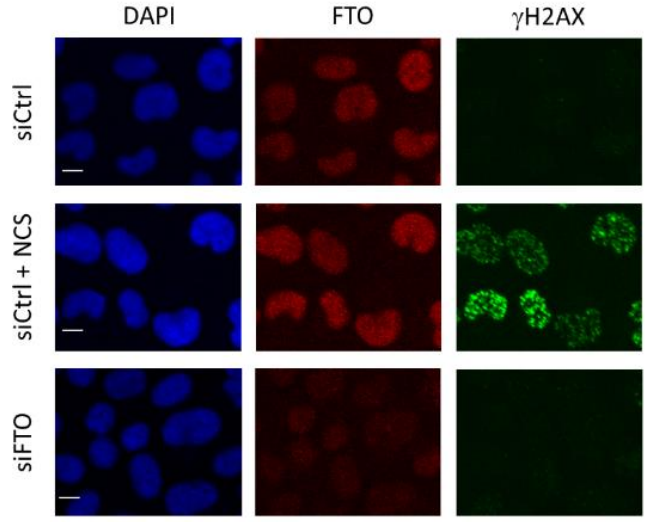

Figure 31. FTO is not recruited to the site of DSBs.

U2OS cells were treated with control and FTO siRNA for 48h, followed by NCS (50 ng/mL) treatment on control siRNA cells for 15 min and cells fixed 1h later. Cells were immunostained with FTO (red) and γH2AX (green). Nuclear DNA was visualized by DAPI (blue). Scale bar: 10μm. Treatment with FTO siRNA was performed to confirm the specificity of FTO antibody.

Upon induction of DNA DSB damage in U2OS cells, there was no observable recruitment of FTO to the site of DSB, as there was no overlap between FTO and the formation of γH2AX foci (DSB marker). This observation suggests that FTO does not exert a direct influence on RNF168 or the recruitment of 53BP1 at the site of DNA DSB.

4.1.7 The epitranscriptomic influence on RNF168 by FTO

After demonstrating that ALKBH3 and FTO KD results in similar RNF168 phenotype, affecting both RNF168 protein expression and resulting in loss of 53BP1 recruitment to DSB we next turned our attention to the question if FTO was influencing RNF168 epitranscriptomically, paralleling the role observed for ALKBH3. Given FTO's established role as an m^{6}A mRNA demethylase, we hypothesized that FTO might be responsible for removing an m^{6}A methylation mark from the *RNF168* transcript and regulating *RNF168* in a comparable manner as ALKBH3. To investigate this possibility a m^{6}A MeRIP-qPCR was performed (Figure 32), similar to the m^{1}A MeRIP-qPCR described in Figure 25.

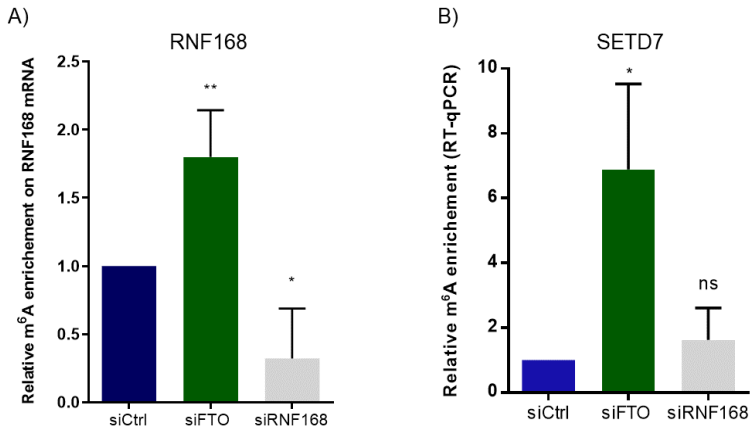

Figure 32. FTO depletion causes increased m^{6}A methylation marks on the *RNF168 transcript*.

U2OS cells treated with the above mentioned siRNAs for 48h followed by m^{6}A RNA immunoprecipitation assay. Graphs represent relative A) *RNF168* and B) *SETD7*mRNA levels from m^{6}A pulldown, expression normalized to GAPDH housekeeping gene. N=4, mean ± SD, One-way ANOVA.

RNF168 mRNA was found in both the control and FTO KD RNA immunoprecipitation samples. Knocking down FTO results in 1.8-fold increase of the *RNF168* levels when compared to control sample. These results indicate that the *RNF168* transcript is likely to contain a m^{6}A modification and that FTO is responsible for its removal. Interestingly, these results parallel the increased m^{1}A methylation marks on *RNF168* observed following ALKBH3 depletion in the m^{1}A MeRIP-qPCR assay (Figure 25). *SETD7* was used a positive control in m^{6}A MeRIP-qPCR assay as it had previously been shown to be m^{6}A methylated by Zeng et al and used as a positive control in their 2018 study of RNA

immunoprecipitation optimization (Zeng et al., 2018). FTO KD resulted in 6-fold increase of the *SETD7* mRNA when compared to control sample indicating the presence of m^{6}A on the *SETD7* transcript, thereby providing validation that the m^{6}A MeRIP-qPCR assay was successful.

To address the possibility of substrate overlaps between ALKBH3 and FTO, *RNF168*-m^{6}A levels were checked post ALKBH3 KD and *RNF168*-m^{1}A levels after FTO KD (Figure 33). This investigation was particularly relevant to investigate as both proteins have shown affinity for the opposite modification on tRNA (Ueda et al., 2017; Wei et al., 2018). Interestingly, ALKBH3 depletion did not affect m^{6}A levels nor did knocking down FTO affect m^{1}A levels pointing towards no substrate overlap between the two demethylases.

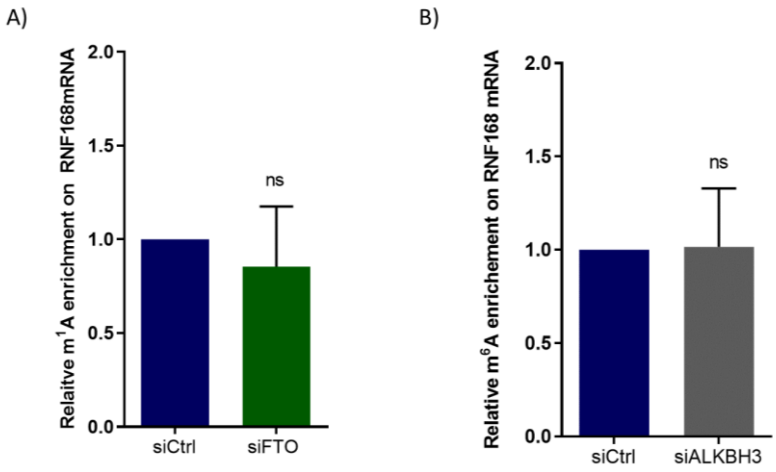

Figure 33. No substrate overlap between FTO and ALKBH3.

U2OS cells treated with the above mentioned siRNAs for 48h followed by A) m^{1}A MeRIP-qPCR assay and B) m^{6}A MeRIP-qPCR assay. Graphs represent relative *RNF168* mRNA expression from m^{1}A and m^{6}A pulldown, normalized to GAPDH housekeeping gene. N=3, mean ± SD, One-way ANOVA.

Having established that the loss of FTO causes an increase in m^{6}A methylation marks on the *RNF168* transcript, our next objective was to investigate if FTO regulates RNF168 in a manner similar to ALKBH3. To ensure the specificity of the observed phenotypical similarities between ALKBH3 and FTO-depleted cells, we systematically examined factors previously excluded in ALKBH3-depleted samples. The investigation included assessing *RNF168* mRNA expression post-FTO KD to understand transcriptional regulation. Additionally, we explored translational regulation through the evaluation of protein turnover and protein-protein interactions between RNF168 and FTO, using protein-protein co-IP followed by western blot analysis (Figure 34).

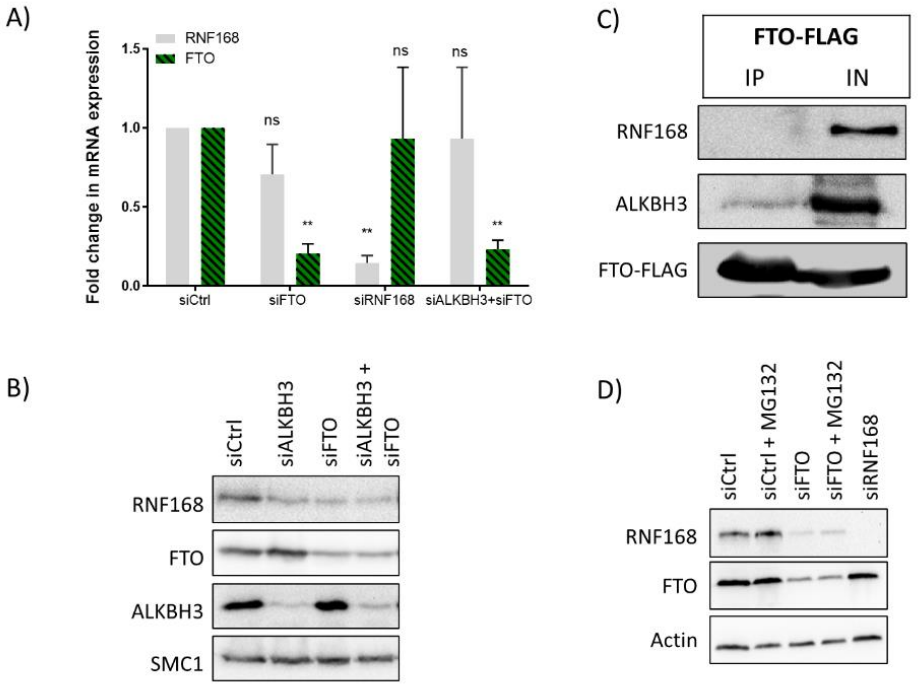

Figure 34. Deciphering FTO's Regulatory Impact on RNF168.

A) Total *FTO* and *RNF168* mRNA levels in U2OS cells treated with the indicated siRNAs for 48h followed by qPCR analysis, GAPDH used as housekeeping gene, n=3, mean±SD, One-way ANOVA. B) Western blot showing protein levels of RNF168, ALKBH3 and FTO in U2OS cells treated with the indicated siRNAs for 48h. C) Western blot analysis of protein-protein co-immunoprecipitation in U2OS cells transfected with FTO-FLAG tagged expression vector. Cell lysate was subjected to FLAG M2-pull down followed by immunoblotting using RNF168 ALKBH3 and FLAG antibody. Input sample (IN), immunoprecipitation sample (IP). D) Western blot showing the protein levels of RNF168 in U2OS cells treated with control and FTO targeting siRNAs for 48h, in the presence or absence of the proteasome inhibitor MG-132 (3h). SMC1 was used as a loading control.

Similar to the findings observed with ALKBH3, the depletion of FTO demonstrated no discernible effect on the mRNA expression of *RNF168*, and FTO did not confer protection against RNF168 protein degradation. Interestingly, when ALKBH3 and FTO were co-depleted, there was no cumulative impact on the downregulation of RNF168 protein or its mRNA expression. Moreover, no detectable protein-protein interaction was observed between FTO and RNF168. Intriguingly, the FTO-FLAG co-IP assay yielded noteworthy results, revealing a possible protein-protein interaction between FTO and ALKBH3 (Figure 34 C). To delve deeper into this interaction, we explored the reciprocal scenario by examining whether FTO could be detected in the ALKBH3-FLAG

co-IP (Figure 35). Indeed, a robust signal for FTO was observed in the immunoprecipitation sample from the ALKBH3-FLAG co-IP, suggesting a potential formation of a complex between these two demethylase proteins.

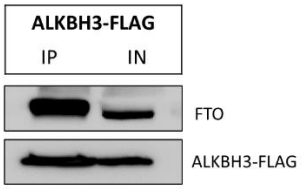

Figure 35. ALKBH3 and FTO interaction on protein level.

Western blot showing protein-protein co-immunoprecipitation in U2OS cells transfected with ALKBH3-FLAG tagged expression vector. Cell lysate was subjected to FLAG M2-pull down followed by immunoblotting using FTO and FLAG antibody. Input sample (IN), immunoprecipitation sample (IP).

4.1.8 FTO's influence on *RNF168* mRNA export

Having ruled out varied potential regulatory mechanisms and establishing FTO's involvement in modulating m^{6}A methylation marks on *RNF168* our subsequent focus was on exploring whether FTO depletion led to effects on *RNF168* mRNA export akin to those observed upon ALKBH3 depletion. After depleting U2OS cells of FTO, we proceeded to investigate both mRNA stability (Figure 36) and mRNA export of *RNF168* (Figure 37). To assess mRNA stability, we employed Actinomycin D treatment, while RNA cellular fractionation assay, followed by qPCR assay was used to study mRNA export.

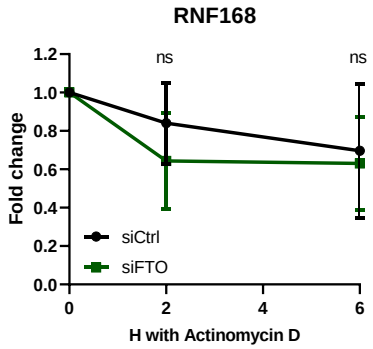

Figure 36.FTO knockdown has no effect on *RNF168* mRNA stability.

RNF168 mRNA stability in U2OS cells treated with control and siRNA for 48h followed by Actinomycin D treatment (8µg/ml) followed by qPCR, normalized to HPRT housekeeping gene. N=3, mean ± SD, two-tailed T-test.

The loss of FTO did not lead to significant increased *RNF168* mRNA instability compared to the control siRNA, even after prolonged Actinomycin D treatment (6h), suggesting that FTO has negligible influence on the stability of *RNF168* mRNA.

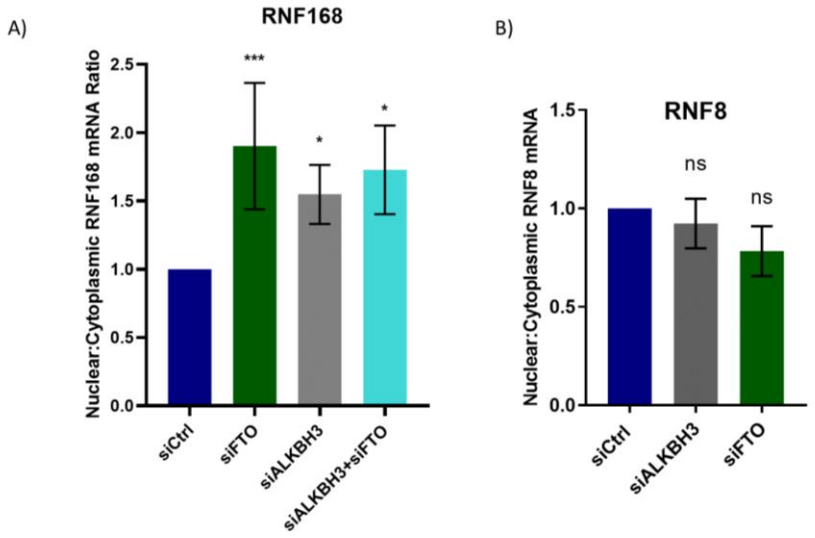

Figure 37. FTO knockdown results in increased nuclear retention of *RNF168* mRNA.

RNA fractionation assay. A) Ratio between nuclear and cytoplasmic *RNF168* mRNA expression in U2OS cells treated with control, ALKBH3, FTO and ALKBH3+FTO siRNAs for 48h followed by qPCR, expression normalized to housekeeping gene HPRT. B) Ratio between nuclear and cytoplasmic *RNF8* mRNA expression in U2OS cells treated with control, ALKBH3 and FTO siRNA for 48h followed by qPCR, expression normalized to housekeeping gene HPRT Ratio>1 indicates more mRNA expression in nucleus, ratio<1 demonstrates more mRNA expression in cytoplasm. N=3, mean±SD, One-way ANOVA.

In line with the effects observed in ALKBH3 KD, the loss of FTO led to elevated *RNF168* mRNA levels in the nucleus relative to the cytoplasm, indicating a potential defect in mRNA export for *RNF168*, possibly due to nuclear retention. Notably, the absence of FTO resulted in a more pronounced phenotype (1.8-fold nuclear retention) than the loss of ALKBH3 (1.5-fold nuclear retention) (Figure 37 A). In addition, *RNF8* nuclear and cytoplasmic levels were checked after depleting cells of either ALKBH3 or FTO to evaluate if ALKBH3 or FTO could influence other DNA repair factors via mRNA export. Neither loss of ALKBH3 nor FTO caused nuclear retention of *RNF8* mRNA (Figure 37 B). The double KD of ALKBH3 and FTO did not lead to increased nuclear retention of *RNF168* mRNA when compared to just knocking down ALKBH3 or FTO. The nuclear retention seen after RNA fractionation of siFTO treated cells was validated through the RNA Scope assay (Figure 38).

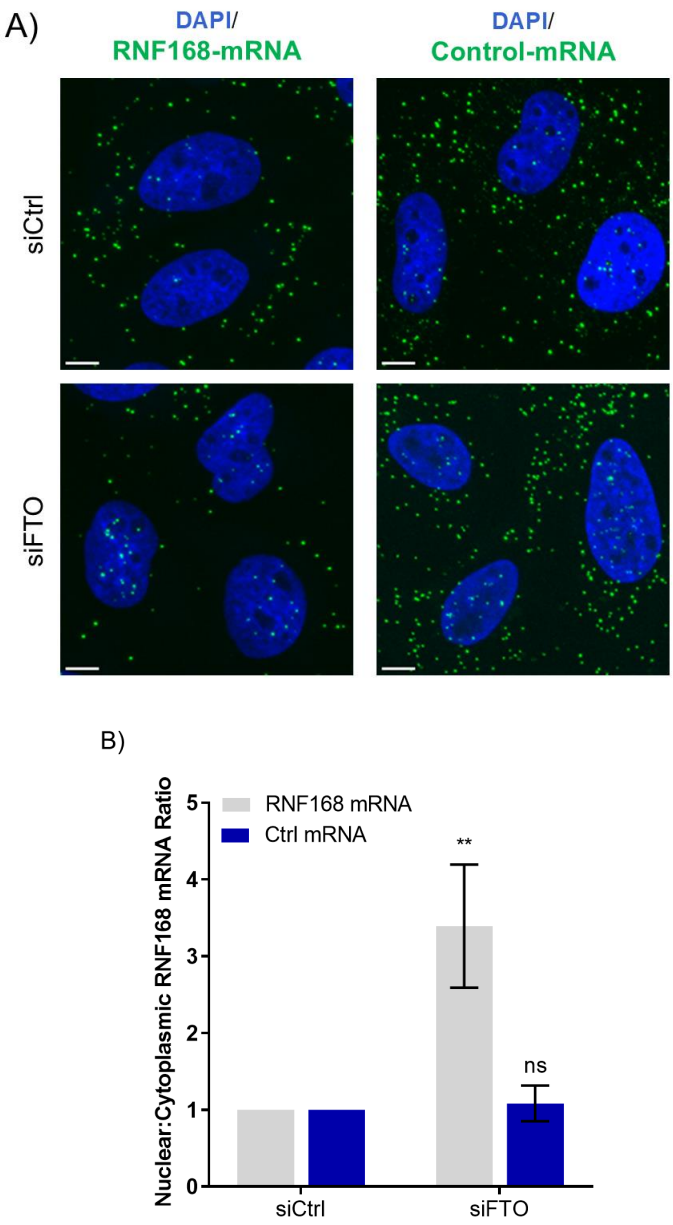

Figure 38. FTO promotes nuclear export of *RNF168* mRNA.

A) Representative pictures and B) quantification of RNA scope assay performed in U2OS cells treated with control and FTO siRNA for 48h followed by incubation with *RNF168* specific probes and control probes (green) and nucleus stain (DAPI). *PPIB* was used as control mRNA. Graph illustrates *RNF168* mRNA nuclear: cytoplasmic ratio where ratio>1 indicates more mRNA expression in nucleus, ratio<1 demonstrates more mRNA expression in cytoplasm. N=3, mean±SD, two-tailed T-test.

RNA Scope analysis confirmed the fractionation results (Figure 37 A) and further demonstrated that FTO depletion is affecting the mRNA export of *RNF168*. The nuclear retention caused by lack of FTO was 3.4-fold higher when compared to control sample, significantly surpassing the 2.3-fold nuclear retention observed when ALKBH3 is knocked down (Figure 28).

Results obtained thus far have revealed a strikingly similar RNF168 phenotype in the absence of both ALKBH3 and FTO. Analogous to ALKBH3, FTO appears to exert epitranscriptomic regulation on RNF168, potentially involving the removal of a methylation mark from its mRNA transcripts, thereby affecting efficient mRNA export and subsequent protein synthesis of RNF168.

4.1.9 FTO's substrate specificity in U2OS cells

In addition to removing the m^{6}A modification from mRNA, FTO has also demonstrated demethylation activity towards the m^{6}A$_m$ modification on mRNA. Notably, research indicates that FTO exhibits higher affinity for m^{6}A$_m$ then m^{6}A. The m^{6}A MeRIP-qPCR analysis (Figure 32) applied to assess the influence of FTO on m^{6}A methylation marks on *RNF168*, utilizes an m^{6}A antibody which is unable to distinguish between the m^{6}A and m^{6}A$_m$ modifications. Consequently, deciphering which modification FTO is interacting with on the *RNF168* transcript proved challenging, relying merely on the m^{6}A MeRIP data. To gain a better understanding of the specific modification FTO is removing from the *RNF168* transcript, we examined FTO's location within U2OS cells. FTO's cellular location has been proven to affect its target affinity, with FTO showing greater affinity for demethylating m^{6}A$_m$ in the cytoplasm but shifting its affinity towards m^{6}A in the nucleus (Wei et al., 2018) (Figure 39).

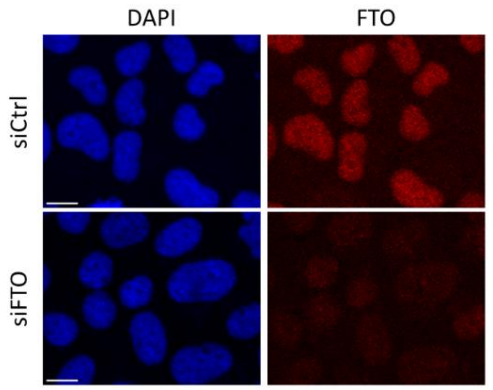

Figure 39. FTO expression in U2OS cells is predominantly in the nucleus.

U2OS cells treated with control and FTO siRNA for 48h followed by fixing and immunostaining with FTO specific antibody (red) and DAPI nucleus stain (blue). Scale bar: 10 µm.

Confocal microscopy results show that FTO localizes primarily in the nucleus in U2OS cells, suggesting that in our experimental model FTO is likely targeting the m^6A modification rather than m^6A_m.

4.1.10 Confirming RNF168 phenotype using CRISPR-Cas9 knockout models

So far, our findings indicate that the absence of either ALKBH3 or FTO results in increased nuclear retention of *RNF168* mRNA, leading to a reduction in RNF168 protein expression. To validate our observations regarding the involvement of ALKBH3 and FTO in the regulation of RNF168 and mitigate the potential for off-target effects associated with siRNA, we utilized CRISPR-Cas9 genome editing to establish stable KO U2OS cell line models for both ALKBH3 and FTO. Two KO cell lines were established for both ALKBH3 and FTO and RNF168 protein expression in the CRISPR-Cas9 KO cell line was analyzed using western blot (Figure 40 A). One KO cell line was chosen for each condition and *RNF168* mRNA export was assessed through the previously described RNA cellular fractionation assay (Figure 40 B).

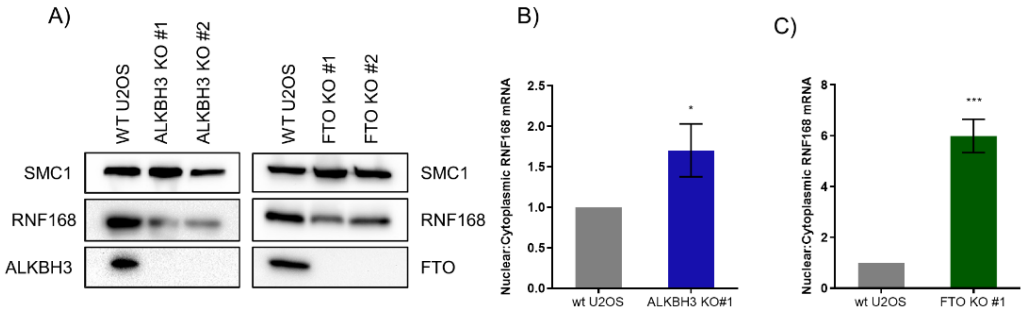

Figure 40. CRISPR-Cas9 KO cells display comparible RNF168 phenotype to siRNA treated cells.

A) Western blot analysis of ALKBH3, FTO and RNF168 expression CRISPR-Cas9 KO cell lines compared to wild type (WT) U2OS cells. SMC1 was used as loading control. B-C) RNA fractionation assay. Ratio between nuclear and cytoplasmic *RNF168* mRNA expression in WT U2OS cells and CRISPR-Cas9 KO cell lines. Followed by qPCR of *RNF168* mRNA expression, normalized to housekeeping gene HRPT. Ratio>1 indicates more mRNA expression in nucleus, ratio<1 demonstrates more mRNA expression in cytoplasm. N=3, mean±SD, two-tailed T-test.

CRISPR-Cas9-generated KO cell lines exhibited a comparable phenotype to siRNA-treated cells. Both ALKBH3 and FTO KO cell lines displayed reduced protein expression of RNF168 compared to wild-type U2OS cells. Additionally, both ALKBH3 and FTO KO cell lines unveiled increased *RNF168* mRNA levels in the nucleus

compared to the cytoplasm when compared to wild-type U2OS cells, once again suggesting impaired *RNF168* mRNA export in cells lacking FTO and ALKBH3.

4.1.11 Further investigations into the epitranscriptomic regulation of *RNF168* mRNA export

The work presented in this thesis so far has demonstrated that depletion of ALKBH3 and FTO impacts the mRNA export of *RNF168*. Both RNA Scope and RNA cellular fractionation experiments have revealed nuclear retention of *RNF168* mRNA following the KD of ALKBH3 and FTO. Our working hypothesis is that the observed impact is attributed to the epitranscriptomic regulation of RNF168 by ALKBH3 and FTO. This implies that for the normal mRNA export of *RNF168* and subsequent protein expression, both FTO and ALKBH3 play a crucial role in removing a methylation mark from the *RNF168* transcript, FTO the m^6A methylation and ALKBH3 the m^1A methylation. Whether these methylations are mainly a hindrance for efficient mRNA export or play a further role in the maturation of the *RNF168* mRNA still remains uncertain.

4.1.11.1 *mRNA methylations and mRNA export*

In recent years research has revealed a link between the mRNA export machinery and m^6A modification. Multiple members of the m^6A methylation complex have been found to interact with core components of the mRNA export machinery such as the Transcription-Export (TREX) complex and the NXF1-NXT1 heterodimer, strongly suggesting a functional interaction between the two processes (Lesbirel et al., 2019). Recent investigations have begun to unveil the intricate connections between the m^6A modification and the export of mRNA (Lesbirel et al., 2018; Roundtree Luo et al., 2017).

The m^6A (and m^1A) reader protein YTHDC1 has been shown to facilitate the nuclear export of mature m^6A-methylated transcripts by cooperating with the splicing factor and nuclear export adaptor protein SRSF3. This interaction facilitates the delivery of mRNA to the nuclear mRNA export receptor, NXF1, ensuring the normal process of mRNA export (Roundtree Luo et al., 2017). SRSF3 or YTHDC1 KD is known to result in a nuclear accumulation of a common set of transcripts, suggesting their involvement in the same pathway. Knocking down YTHDC1 results in mRNA export defects for specific transcripts, particularly m^6A-containing transcripts, indicating that YTHDC1 selectively exports m^6A-modified mRNAs, highlighting m^6A methylation as a mark for selective nuclear processing (Roundtree Luo et al., 2017). Furthermore, the m^6A writer machinery has been shown to recruit the TREX complex to m^6A-methylated mRNA and KD of components of the m^6A methyltransferase complex result in defective mRNA export (Lesbirel et al., 2018). Where the methylation eraser protein fit into the export process remains unclear.

From this we decided to investigate what influence major export factors along with YTH-proteins had on RNF168 protein expression (Figure 41). While our primary focus centered on YTHDC1 and SRSF3, we decided to incorporate other members of the YTH domain-containing family (YTHDF1-3) and an additional SR protein. YTHDC2 was excluded as its primary role is promoting transition from mitotic to meiotic divisions in stem cells (Wojtas et al., 2017). SRSF7, similar to SRSF3, is recognized for promoting NXF1 recruitment to mature mRNA *in vivo* (Muller-McNicoll et al., 2016) and interacting with YTHDC1 to facilitate nuclear export (Kasowitz et al., 2018).

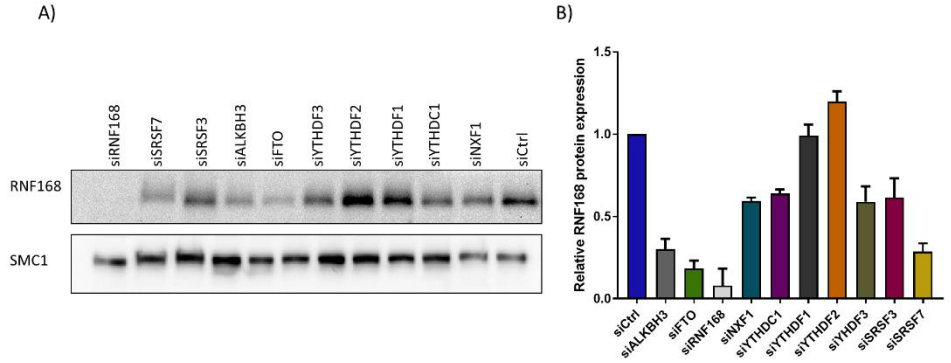

Figure 41. KD of nuclear export factors and m^{6}A/m^{1}A methylation readers affects RNF168 protein expression.

U2OS cells treated with the above-mentioned siRNAs for 48h. A) Western blot analysis to evaluate RNF168 expression. SMC1 was used as loading control. B) Relative quantification of RNF168 expression, compared to control siRNA. N=2, mean±SD.

Western blot analysis revealed a notable decrease in RNF168 protein expression upon depleting cells of SRSF7, SRSF3, YTHDC1, YTHDF3 and NXF1. Intriguingly, depleting U2OS cells of SRSF7 had the most pronounced effect, comparable to ALKBH3 and FTO depletion. The YTHDF1 and YTHDF2 proteins showed little to any noteworthy influence on RNF168 protein expression. NXF1 depletion led to decreased RNF168 protein levels, aligning with its recognized role in mRNA export. NXF1 KD is known to cause increased nuclear retention of poly(A)$^+$ mRNA, indicating a defect in mRNA export (Viphakone et al., 2012) and reduced mRNA export could lead to reduction in protein synthesis. Additionally, we see a small drop in SMC1 (loading control) when depleting cells of NXF1. These results indicate that YTHDC1 along with SRSF3 and SRSF7 might have a possible role in regulating RNF168 protein expression. Whether this is via mRNA export requires further investigations.

In addition to looking into methylation reader proteins and their influence on RNF168 protein expression our investigation extends to exploring the impact of m^{6}A and m^{1}A methylation writers on RNF168 protein expression along with using cellular fractionation assays to evaluate *RNF168* mRNA nuclear retention in cells depleted of YTHDC1, SRSF3, and SRSF7. These results are considered preliminary as they are composed of one biological replicate and can be found in Appendix C. Briefly, when m^{6}A and m^{1}A

methylation writers were silenced in U2OS cells using siRNA we noted diminished RNF168 protein expression. Additionally, cellular fractionating assay demonstrated that depleting cells of YTHDC1, SRFS3 and SRSF7 resulted in increased nuclear retention of *RNF168* mRNA. Further validation is required to confirm these initial findings, and additional experimental investigation is necessary to understand the involvement of m^1A/m^6A writers and readers in regulating *RNF168* mRNA export. However, our current data suggests that the methylation marks on *RNF168* may not solely hinder mRNA export, and proteins like YTDCH1, SRSF7, and to a lesser extent, SRSF3, might be involved in the export process. More details can be found in Appendix C.

4.1.12 ALKBH3 and FTO protein-protein interaction

To delve deeper into protein-protein interactions involving ALKBH3 and FTO and to validate the findings from the co-IP followed by western blot assay (Figure 34 C and Figure 35) a protein co-IP coupled with ultra-performance liquid chromatography–mass spectrometry was conducted in U2OS cells. Mass spectrometry analysis was performed using FLAG-tagged wild-type (WT) ALKBH3 and FTO plasmid along with catalytically dead (CD) ALKBH3 and FLAG tagged plasmids, each plasmid was done in triplicate.

The catalytically dead plasmids are as the name suggest catalytically inactive, meaning they are unable to demethylate nucleic acid. The iron-binding domain of the catalytic dead proteins has been altered which prevents binding of the Fe^{2+}ion. Since the AlkB protein family relies on the Fe^{2+} ion as a cofactor for their enzymatic activity, this alteration results in the loss of their demethylating capabilities. The DNA/RNA binding groove of the catalytic dead proteins remain unaffected, preserving their ability to bind to nucleic acid. We therefore hypothesized that the catalytic dead proteins could still bind to methyl groups on nucleic acid without the ability to demethylate them, which may lead to prolonged interaction durations between the catalytically inactive proteins and their targets, potentially facilitating the detection of additional protein-protein interactions in the mass spectrometry assay.

4.1.12.1 *Interesting binding partners found in co-IP/MS*

Mass spectrometry analysis confirmed our previous findings of protein interaction between ALKBH3 and FTO (Figure 34 C and Figure 35), as FTO scored fairly high on the list of interaction partners for both WT and CD ALKBH3 plasmids. ALKBH3 did not appear on the limited list of interaction partners for the WT-FTO plasmid. The reason for this is unknown but the FTO-WT co-IP/MS did overall not result in many protein interaction hits for FTO. ALKBH3 did however appear on the list for the CD FTO plasmid co-IP, providing a credible conformation of previously seen results in FTO co-IP (Figure 34 C). Notably, RNF168 did not appear as an interaction partner for either ALKBH3 or FTO in both WT and CD plasmids. This finding further strengthens the working hypothesis that both ALKBH3 and FTO are interacting with and regulating RNF168 at the mRNA level rather than the protein level.

The co-IP/MS analysis revealed numerous noteworthy protein-protein interactions associated with both ALKBH3 and FTO, presenting an extensive dataset that may be challenging to thoroughly discuss within the scope of this thesis. Nevertheless, the most relevant protein interactions identified in the co-IP/MS analysis, integral to the current research, are summarized in Table 13. For a full list of interactions found for each individual plasmid co-IP see Appendix D.

Table 13. Interesting protein interactions from co-IP/MS

Plasmid	Protein	Function
ALKBH3 WT / ALKBH3 CD	FTO	m^6A RNA demethylase
ALKBH3 WT	ZMYM2	Zinc finger protein, antagonizes 53BP1 to facilitate HR repair
ALKBH3 WT / ALKBH3 CD	PRMT5	Regulates RNF168 expression in glioblastomas. Activates transcription of DSB repair genes upon DNA damage
ALKBH3 WT	HNRNPF	RNA binding protein, known to regulate mRNA alternative splicing
ALKBH3 WT / ALKBH3 CD	WDR77	Forms a complex with PRMT5
ALKBH3 WT / ALKBH3 CD	HNRNPA2B1	RNA binding protein, known to regulate mRNA alternative splicing. A nuclear m^6A reader
ALKBH3 WT / ALKBH3 CD	HNRNPA1	m^6A reader protein. Transports of poly(A) mRNA from the nucleus to the cytoplasm and modulation of splice site selection
ALKBH3 WT	ALKBH5	m^6A RNA demethylase
ALKBH3 WT	HNRNPH1	RNA interacting protein. A component of an mRNA export complex, shuttles mature mRNA from the nucleus to the cytoplasm
ALKBH3 WT / ALKBH3 CD	HNRNPC	RNA interacting protein. Aids in stability and translation of bound mRNA and effects pre-mRNA splicing. Has also proven able to bind to m^6A and also to affect HR repair.
ALKBH3WT / ALKBH3 CD / FTO WT/ FTO CD	PRDX1	Antioxidant enzyme which reduces DNA damage and contributes to DNA Repair
ALKBH3 CD	SRSF3	A mRNA splicing factor. Interact with m^6A reader YTDHC1 to aid in mRNA export of m^6A methylated mRNA via NXF1.
ALKBH3 CD	TRIP12	Regulator of RNF168
ALKBH3 CD	SRSF1	A mRNA splicing regulator. Interacts with YTDHC1. Participates in mRNA export via NXF1.
FTO CD	ALKBH3	Alpha-ketoglutarate-dependent dioxygenase AlkB homolog 3
FTO CD	CHD2	PARP1 recruits CHD2 to rapidly expand chromatin and deposit H3.3 variants to initiate NHEJ repair
FTO CD	RBM6	Splicing factor involved in mRNA splicing. Promotes HR repair of DSB.
FTO CD	DHX9	RNA helicase, known to influence HR repair. RNF168 ubiquitinates DHX9 for resolution and removal of R-loops
FTO CD	RMBX / HNRNPG	RNA-binding. Influences DNA end resection. Activates ATR during replication stress response. M^6A reader protein that mediates splicing.
FTO CD	METTL14	m^6A methyltransferase.

The ALKBH3 protein, in both wild-type (WT) and catalytically dead (CD) forms, demonstrated interactions with various m^{6}A methylation-associated proteins, such as FTO, ALKBH5, hnRNPA2B1, hnRNPC and hnRNPA1. Additionally, ALKBH3 exhibited associations with well-known mRNA export factors, including SRSF1, SRSF3, and hnRNPH1. Interestingly, the catalytically dead ALKBH3 protein exhibited a distinct interaction with TRIP12, a recognized regulator of RNF168.

On the other hand, the FTO protein, in both WT and CD forms, displayed a comparatively smaller number of interaction partners than ALKBH3. While it did not interact with as many RNA-binding proteins, FTO was observed to bind to METTL14, a principal component of the m^{6}A methyltransferase complex, and hnRNPG, an m^{6}A methylation reader. Notably, both ALKBH3 and FTO demonstrated interactions with several proteins associated with DNA repair and the maintenance of genomic stability, including DHX9, PRMT5, ZMYM2, RBM6, and CHD2.

4.1.12.2 *Overlap between co-IP/MS*

Comparison of all four co-IP/MS analyses revealed some overlap among the samples, as summarized in Figure 42. Notably, there was significant overlap between the wild-type and catalytic dead versions of each plasmid. Eight proteins were consistently identified in all four co-IP/MS experiments, primarily consisting of ubiquitously expressed proteins like heat shock proteins, tubulin, and keratin proteins. Comparable results were seen for ALKBH3 and FTO WT overlap which consisted of 10 proteins, most of which were widely expressed in multiple cells such as GAPDH, keratin, annexin and heat shock proteins. The sole DNA repair related protein found interacting with both ALKBH3 and FTO was Peroxiredoxin 1 (PRDX1), an antioxidant enzyme known to prevent the accumulation of reactive oxygen species. Interestingly, when both ALKBH3 and FTO were rendered catalytically inactive, the number of proteins found to interact with them increased significantly which could be attributed to their ability to still bind to nucleic acid without being able to demethylate their targets. This circumstance may result in an extended binding duration to the nucleic acids, potentially allowing the proteins to interact for a prolonged period with other proteins arriving at the same site.

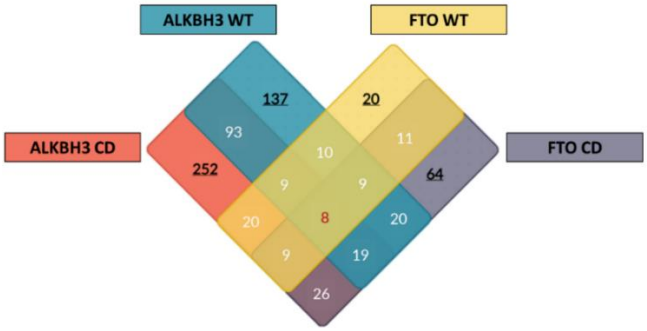

Figure 42. Overlap of protein detections in Co-IP/MS Analyses.

Venn diagram illustrating the overlap among proteins identified as interaction partners in the four co-IP/MS samples. Bold underlined numbers represent the total proteins detected in each sample, white numbers indicate the overlap between 2 or 3 samples, and red numbers indicate the overlap among all four samples.

4.2 ALKBH3's and FTO's effect on DNA DSB repair and genomic instability

4.2.1 ALKBH3 and DNA repair dynamics

RNF168 is widely recognized as a multifaceted regulator in the intricately orchestrated DDR pathway at damaged chromatin. This recognition stems from its established role in helping to recruit vital repair factors such as 53BP1 and BRCA1 to the damaged chromatin. To better understand the consequences of RNF168 loss due to ALKBH3 depletion for effective repair of DNA DSB we silenced ALKBH3 in U2OS cells. Subsequently, DSBs were induced using NCS, and MDC1 was utilized as a readout for DNA DSB repair dynamics (Figure 43). MDC1 is one of the first proteins to arrive at the site of DSBs where it directs the recruitment of other repair factors including RNF8 and RNF168. MDC1 is recruited to DSB before the initiation of ubiquitin-dependent steps in the DNA DSB signaling pathway. Over time MDC1 gradually disassociates from the DSB site as repair of the break progresses.

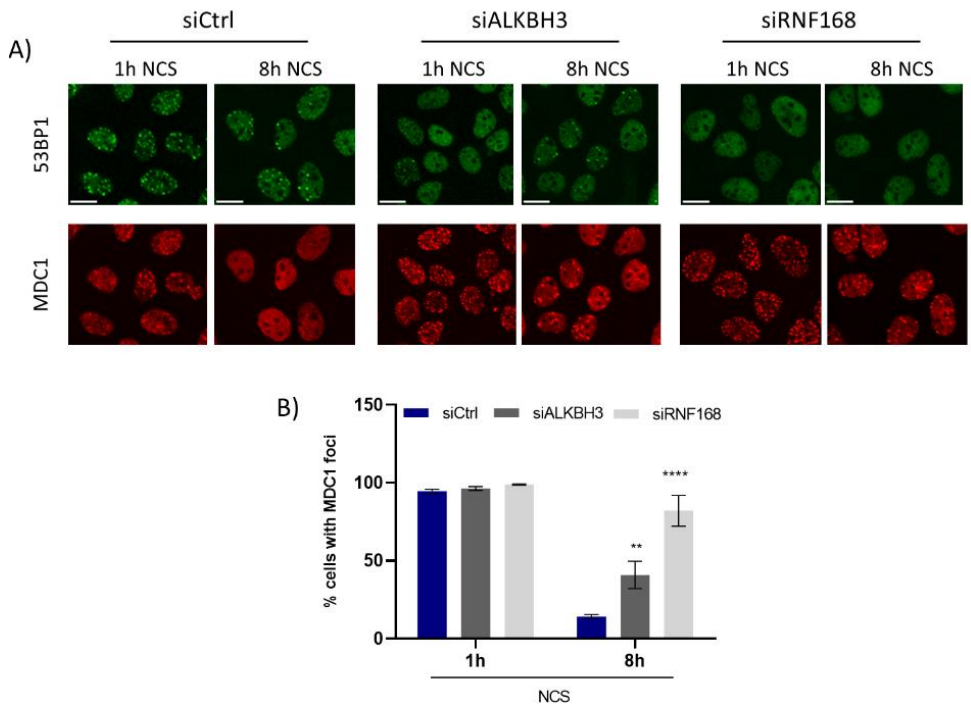

Figure 43. ALKBH3 depletion results in slow clearance of MDC1.

A) Representative images and B) quantification of U2OS cells treated with control, ALKBH3 and RNF168 siRNA for 48h followed by NCS (50 ng/mL) exposure for 1h. 1h and 8h later cells were fixed and stained with 53BP1 (green) and MDC1 (red) specific antibodies. Scale bar: 10μm. One-Way ANOVA, n=3 mean±SD.

In cells deficient in ALKBH3, a distinct decrease in the clearance of MDC1 foci was evident. Although the reduction was not as pronounced as observed in cells depleted of RNF168, it still represented a noteworthy decline when compared to cells subjected to control siRNA treatment. These results imply that the efficiency of DNA DSB repair is affected in cells depleted of ALKBH3.

4.2.2 ALKBH3's and FTO's effect on DNA DSB repair choice

Thus far the research presented in this thesis has shown that the loss of either ALKBH3 or FTO impacts DNA repair dynamics likely mediated through the epitranscriptomic regulation of RNF168. This influence is observed in the altered recruitment of 53BP1 to the site of DSB and in the case of ALKBH3 deficiency, causes less efficient DNA repair (Figure 19 and Figure 30) along with slower clearance of MDC1 foci in ALKBH3 depleted cells (Figure 43).

Integrating these findings with the known role of RNF168 ubiquitination in influencing the choice of DNA DSB repair, coupled with previous research demonstrating that loss of RNF168 drives cells to use the highly mutagenic repair pathway single strand

annealing (SSA) (Munoz et al., 2012; Ochs et al., 2016) prompts the question: Does knocking down ALKBH3 and FTO influence the choice of repair pathway? Specifically, does the depletion of ALKBH3 or FTO hinder cells from utilizing DNA DSB repair pathways such as HR or c-NHEJ, thereby potentially directing them towards the more error-prone and mutagenic SSA repair pathway, similar to cells lacking RNF168?

To answer this question fluorescence-activated cell sorting (FACS) analysis and established DSB GFP reporter system designed for HR, c-NHEJ, and SSA repair pathways (Bennardo et al., 2008; Gunn et al., 2012) were utilized to analyze repair rates in cells depleted of ALKBH3 or FTO. Each reporter system is specific for HR repair (DR-GFP), c-NHEJ (primEJ5-GFP), or SSA (hprtSA-GFP) repair, however they all contain similar constructs containing a disrupted GFP gene separated by an I-Sce1 restriction site. When the I-Sce1 restriction enzyme is introduced, it induces a DSB and repairing the DSB restores the GFP gene, enabling the detection of the corresponding DSB repair pathway.

U2OS cells stability expressing each reporter system were co-transfected with siRNAs and I-Sce1 restriction enzyme and repair rates of HR (Figure 44), NHEJ (Figure 45) and SSA (Figure 46) evaluated. For more information on DNA repair reporter systems see Appendix C.

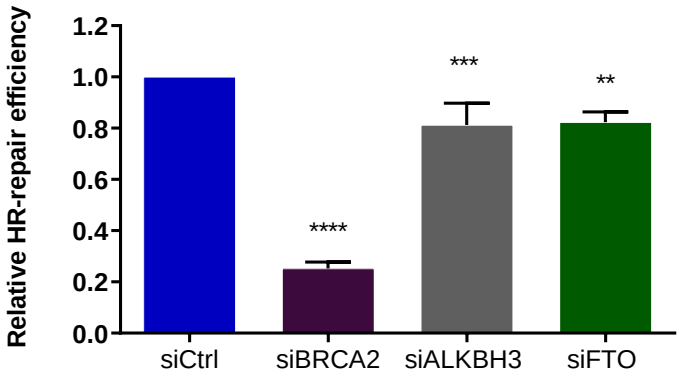

Figure 44.The influence of ALKBH3 and FTO depletion on HR repair efficiency in U2OS cells.

U2OS cells stably expressing HR-GFP plasmid were transfected with the indicated siRNAs for 24h followed by transfection of I-Sce1 plasmid to induce DSB. 24h post plasmid transfection cells were fixed and GFP signal analysis using FACS analysis. BRCA2 was used as positive control. N=4 mean±SD, One-way ANOVA. siFTO sample represents n=3.

In comparison to the control sample, the depletion of ALKBH3 in U2OS cells resulted in a 20% reduction in homologous recombination (HR) repair efficiency. A similar

reduction in HR repair efficiency was observed upon the depletion of FTO. Depleting cells of BRCA2 resulted in an 80% drop in HR repair efficiency; this was expected due to BRCA2's well defined role in HR repair. These results indicated that loss of either ALKBH3 or FTO contributes to small drop in the cells capacity to repair DSB using HR repair.

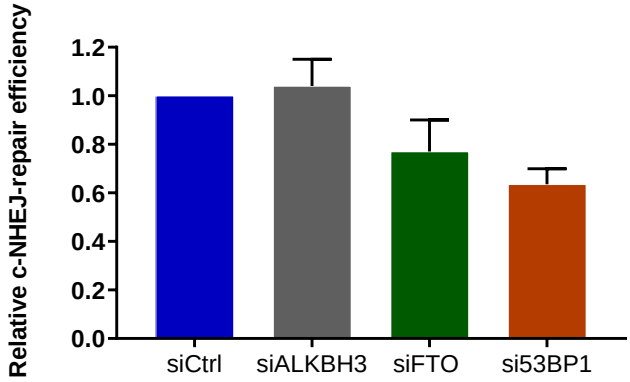

Figure 45. The influence of ALKBH3 and FTO depletion on c-NHEJ repair efficiency in U2OS cells.

U2OS cells stably expressing primEJ5-GFP plasmid were transfected with the indicated siRNAs for 24h followed by transfection of I-Sce1 plasmid to induce DSB. 24h post plasmid transfection cells were fixed and GFP signal analyzed using FACS analysis. N=2, mean ± SD.

Preliminary data on NHEJ repair efficiency indicates that cells depleted of FTO exhibited around 30% reduction in NHEJ repair efficiency compared to control cells, while positive control sample (cells depleted of 53BP1) resulted in 40% drop in c-NHEJ repair efficiency. Conversely, cells lacking ALKBH3 demonstrated no effect in c-NHEJ repair efficiency.

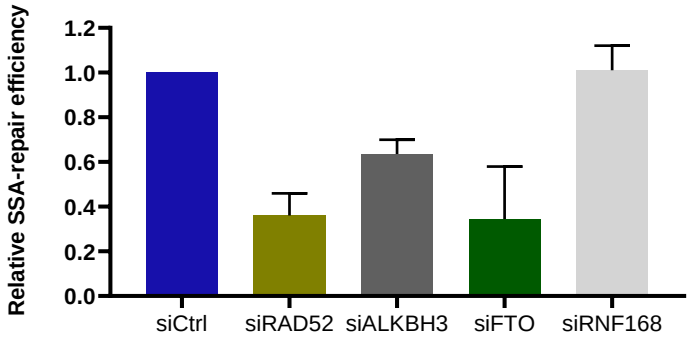

Figure 46. The influence of ALKBH3 and FTO depletion on SSA repair efficiency in U2OS cells.

U2OS cells stably expressing hprtSA-GFP plasmid were transfected with the indicated siRNAs for 24h followed by transfection of I-Sce1 plasmid to induce DSB. 24h post plasmid transfection cells were fixed and GFP signal analyzed using FACS analysis. RAD52 served as PCNn=2, mean ± SD.

Preliminary results from SSA repair efficiency revealed around 40% drop in SSA repair efficiency for cells lacking ALKBH3, 65% for cells lacking FTO when compared to control sample. As mentioned previously, loss of RNF168 has been linked to increased usages of SSA repair pathway (Munoz et al., 2012; Ochs et al., 2016), here we observe a negligible effect on SSA repair in the absence of RNF168, which is inconsistent with current literature. The reason for this discrepancy is unknown, and a more pronounced increase in SSA use was expected. As depletion of ALKBH3 and FTO has demonstrated loss of RNF168 protein expression (Figure 29) we would expect loss of ALKBH3 and FTO to result in increased usage of SSA, however we see the opposite.

RAD52 was used as a positive control of SSA repair efficiency as RAD52 is considered a key mediator of the SSA DNA repair mechanism (Grimme et al., 2010; Ivanov et al., 1996; Mortensen et al., 1996; Onaka et al., 2020; Reddy et al., 1997). As expected, depleting cells of RAD52 led to decrease SSA repair efficiency, or around 65% drop.

Cumulative data from DSB repair assays suggests that ALKBH3 and FTO can impact DNA DSB repair pathway choice. Cells deficient in ALKBH3 or FTO exhibit reduced capacity for DSB repair via HR, NHEJ and SSA pathways. It is noteworthy to mention that NHEJ and SSA data contain 2 biological replicates and are therefore considered preliminary and further research is needed to confirm these results.

4.2.3 Cells lacking ALKBH3 or FTO display increased genomic instability

DNA DSB are recognized as a significant source of genomic instability, with failure to repair or incorrect repair of these breaks known to result in cell death or chromosomal alterations, thereby increasing genomic instability and lead to cancer formation. Furthermore, the current literature supports a robust association between defects in the DNA DSB repair machinery and increased genomic instability. This includes RNF168 defects, as both human and murine cells lacking RNF168 have demonstrated increase in the frequency of genomic aberrations, this includes chromosomal aberrations and micronuclei (Bohgaki et al., 2011; Devgan et al., 2011; Stewart et al., 2009).

Our results have demonstrated that deficiency of ALKBH3 and FTO results in both the loss of RNF168 protein expression and affects the cell's ability to repair DSB (Figure 44-Figure 46). Given these observations, we sought to investigate whether cells devoid of FTO and ALKBH3 exhibited increased genomic instability. To assess whether the absence of ALKBH3 and FTO have any impact on genomic integrity spontaneously forming chromosomal aberrations were examined in U2OS cells through metaphase spread analysis (Figure 47).

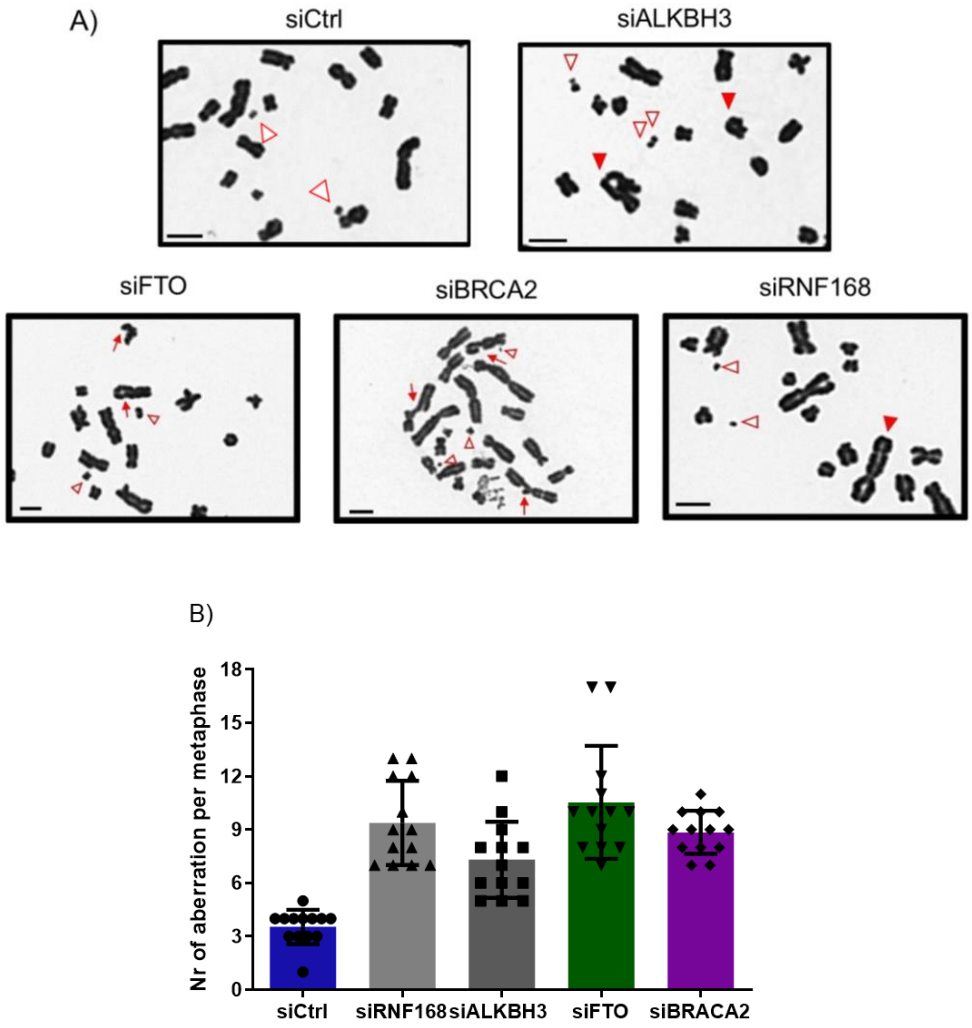

Figure 47. Increased chromosomal aberrations in cells depleted of ALKBH3 or FTO.

A) Representative images of chromosome metaphase spread in cells treated with above mentioned siRNAs, BRCA2 served as PC. DNA double strand breaks are shown with red arrows, DNA fragments with white triangles outlined in red and end fusion reprinted with red triangles. Scale bars: 10 µm. B) Quantification of the number of metaphase aberrations in U2OS cells treated with the specified siRNA for 48h. The graph shows the relative change in number of aberrations compared to control siRNA treated cells. 13 metaphases were analyzed per condition from 2 independent experiments.

An elevated frequency of spontaneous chromosomal aberrations was detected in both ALKBH3- and FTO-depleted samples as compared to the control sample. Intriguingly,

the absence of FTO led to a higher incidence of aberrations per metaphase spread in comparison with the ALKBH3 and RNF168 depleted samples.

Beyond the metaphase spread assay, genomic instability in U2OS cells subjected to ALKBH3 and FTO depletion was assessed using the micronuclei assay, a widely employed method for evaluating genomic instability. Additionally, a double KD involving both ALKBH3 and FTO was performed to investigate potential additive effects on genomic instability resulting from the simultaneous removal of both proteins (Figure 48).

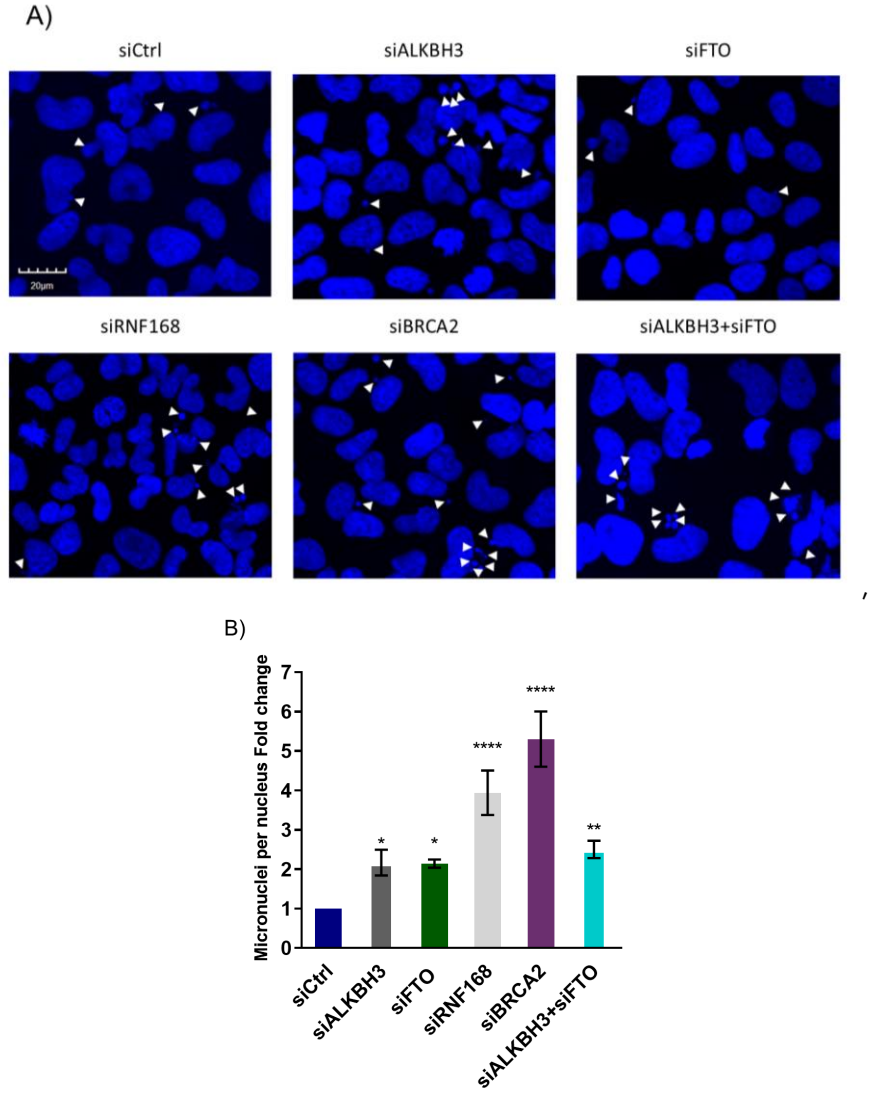

Figure 48. Depletion of ALKBH3 and FTO result in increased micronuclei formation.

A) Representative images of micronuclei assay in U2OS cells treated with above mentioned siRNAs for 48h followed by immunostaining by DAPI nuclei stain. BRCA2 and RNF168 served as PC. Micronuclei are represented by white arrows. Scale bars: 20 µm. B) Quantification of the number of micronuclei in cells. The graph shows the relative change in number of aberrations compared to control siRNA treated cells. N=3, mean ± SD, One-way ANOVA.

Knocking down either ALKBH3 or FTO resulted in 2-fold increase in micronuclei formation compared to control sample while the positive controls exhibited 4-fold (RNF168) and 5-fold (BRCA2) increase in micronuclei formation indicating increased genomic instability (Figure 48). Notably, the double KD of ALKBH3 and FTO did not yield an additive effect on genomic instability, with no statistical significance observed between the single and double KD conditions (Figure 49 A).

Co-depleting ALKBH3 and FTO findings have been consistent across multiple assays, encompassing western blot assay, micronuclei assay, cellular fractionation assay (evaluating *RNF168* expression in the nucleus and cytoplasm), and RT-qPCR (assessing total mRNA levels of *RNF168*). Double KD of ALKBH3 and FTO did not manifest in additive effect in any of the tested assays. A comprehensive summary of the data from the ALKBH3 and FTO double KD is presented in Figure 49.

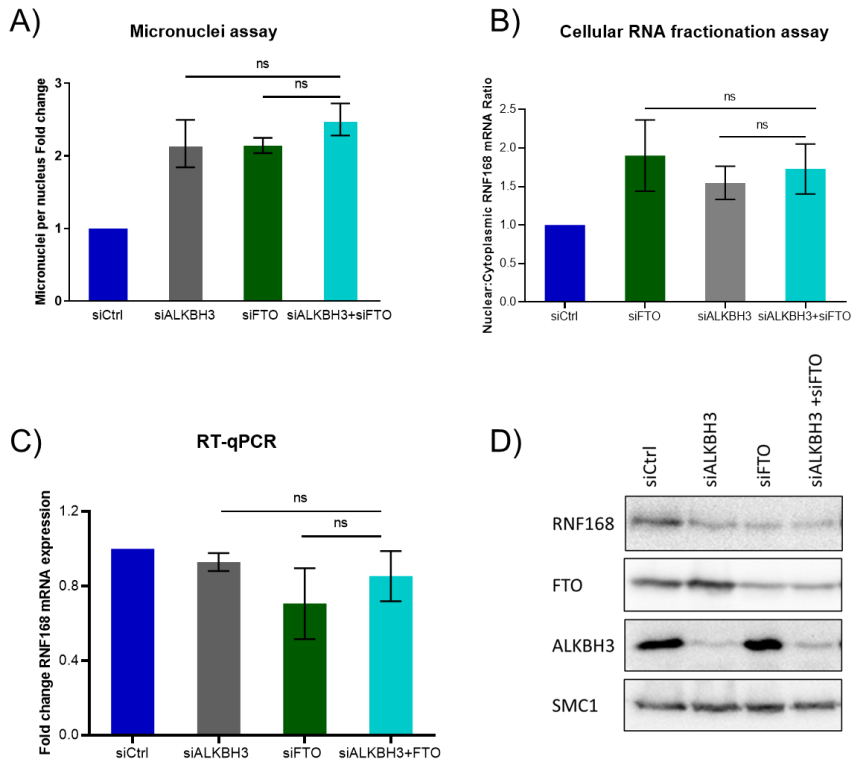

Figure 49. The double knockdown of ALKBH3 and FTO does not result in an additive effect on the RNF168 phenotype.

A) Micronuclei assay in U2OS cells treated with indicated siRNAs for 48h. N=3, mean ± SD, One-Way ANOVA. Each sample was normalized to siRNA control sample. B) RNA fractionation assay. Ratio between nuclear and cytoplasmic *RNF168* mRNA expression in U2OS cells treated with the indicated siRNAs for 48h followed by qPCR, expression normalized to housekeeping gene HPRT. Ratio>1 indicates more mRNA expression in nucleus, ratio<1 demonstrates more mRNA expression in cytoplasm. N=3, mean ± SD, One-way ANOVA. Each sample was normalized to siRNA control sample. C) Total *RNF168* mRNA levels in U2OS cells treated with the indicated siRNAs for 48h followed by qPCR analysis, expression normalized to housekeeping gene GAPHD, n=3, mean ± SD, One-way ANOVA. Each sample was normalized to siRNA control sample. D) Western blot showing the protein levels of RNF168, FTO and ALKBH3 in U2OS cells treated with indicated siRNAs for 48h. SMC1 was used as a loading control.

The last step in assessing the impact of depleting ALKBH3 and FTO on genomic instability involved the implementation of the micronuclei assay in our CRISPR/Cas9 established KO cell lines for ALKBH3 and FTO, compared against the wild-type U2OS cells (Figure 50). This step was undertaken with the additional objective of corroborating and validating the results obtained through siRNA-based experiments.

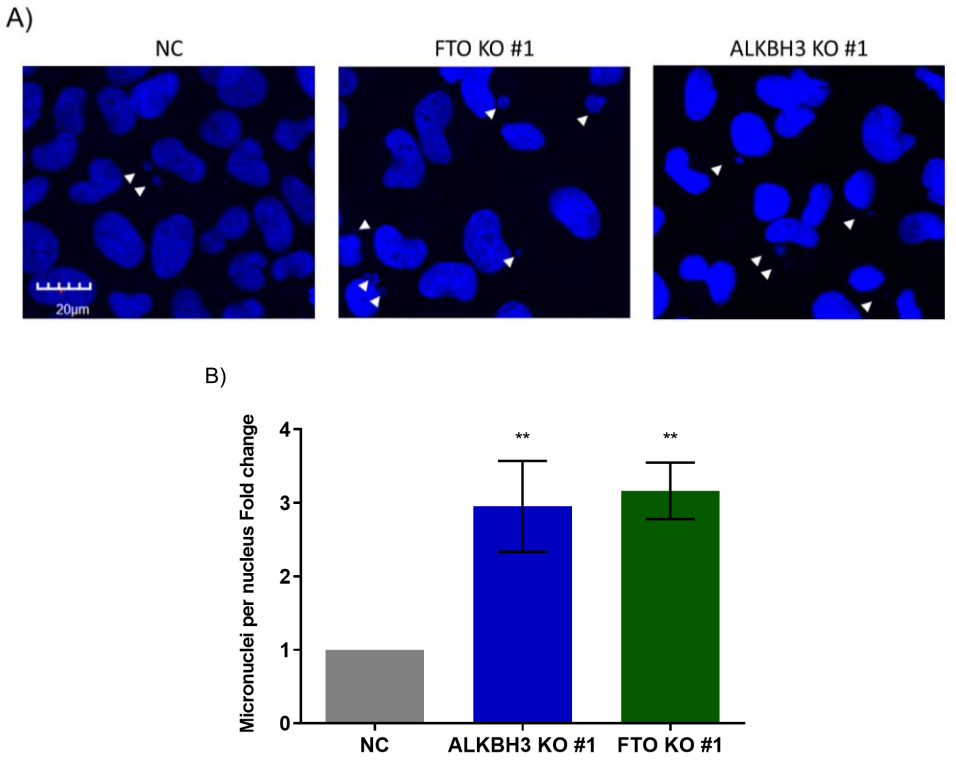

Figure 50. ALKBH3 and FTO CRISPR-Cas9 knockout cell lines display similar levels of genomic instability as siRNA-treated cells

A) Representative images of micronuclei assay in wild type U2OS cells (NC) and ALKBH3 and FTO CRISPR-Cas9 KO clones. Cells are fixed after growing for 48h followed by immunostaining by DAPI nuclei stain. Micronuclei are represented by white arrows. Scale bars: 20 µm. B) Quantification of the number of micronuclei in CRISPR-Cas9 KO clones. The graph shows the relative change in number of aberrations compared to wild type U2OS cells. N=3, mean ± SD, One-way ANOVA.

Both KO cell lines exhibited a notable increase in micronuclei formation, approximately a threefold rise compared to wild-type U2OS cells. This increase, while slightly greater than that observed in siRNA-treated cells (Figure 48), may be attributed to the complete removal of ALKBH3 and FTO in these CRISPR KO cell lines, potentially eliciting a more robust response.

4.2.4 Cells depleted of ALKBH3 and FTO show increased sensitivity to genotoxic agents

As previously discussed, RNF168 is a pivotal regulator of DNA repair, and plays a crucial role in promoting cell survival in response to genotoxic stress. This is evidenced by the hypersensitivity to ionizing irradiation observed in both human and murine systems in the absence of RNF168 (Bohgaki et al., 2011; Devgan et al., 2011; Stewart et al., 2009).

The loss of either ALKBH3 or FTO proteins has been demonstrated to influence DNA repair efficiency, induce alterations in the choice of DNA DSB repair pathways (Figure 44 – Figure 46) and lead to increased genomic instability (Figure 47-Figure 48). From this a hypothesis emerged suggesting that cells subjected to KD or KO of either ALKBH3 or FTO would prove vulnerable to DSB-inducing cancer therapy. To test this hypothesis, a clonogenic assay was conducted in U2OS cells depleted of ALKBH3 and FTO using siRNAs, followed by treatment with NCS (a radiomimetic drug and effective inducer of DSB) and Mitomycin C (MMC, a potent DNA crosslinking agent) (Figure 51).

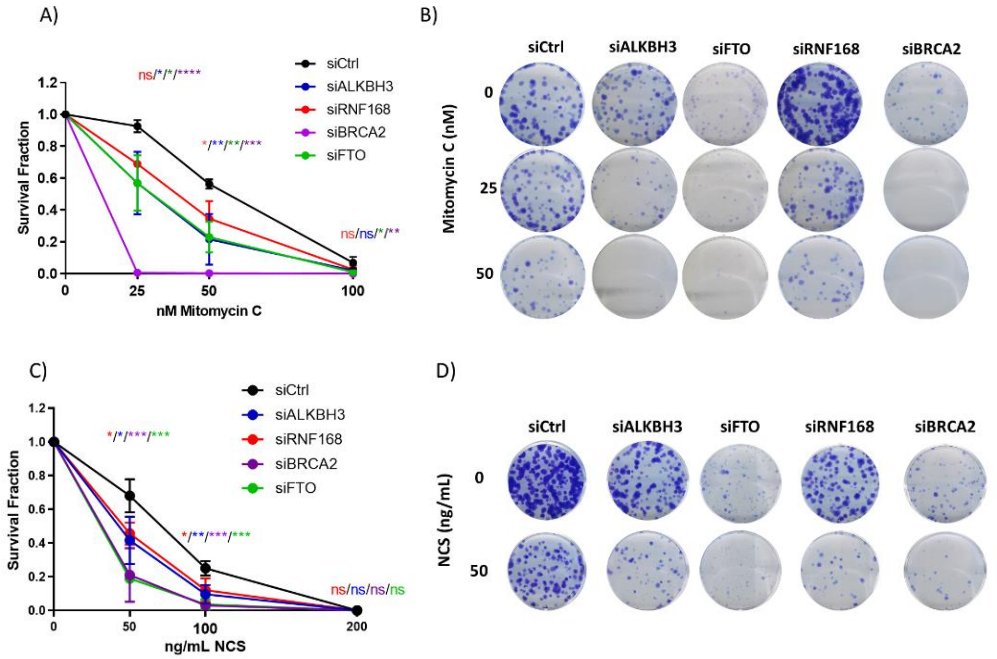

Figure 51. ALKBH3 and FTO depletion and sensitivity to genotoxic agents.

U2OS cells were treated with the indicated siRNAs for 48h, BRCA2 used as PC. Cells were seeded out in low density, treated with A-B) Mitomycin C and C-D) Neocarzinostatin. Cells grown for 11-14 days. N=3, mean ± SD, One-Way ANOVA.

Upon exposure to NCS and Mitomycin C treatments, cells depleted of ALKBH3 and FTO exhibited diminished survival compared to control cells. Cells depleted of ALKBH3 exhibited a similar response to NCS as cells lacking RNF168 but presented a small, although not-significant increase in response to MMC. Intriguingly, cells depleted of FTO had increased response to NCS in comparison to cells depleted of RNF168. Survival of cells depleted of FTO dropped to a similar level as the positive control sample, cells lacking BRCA2 when exposed to NCS. Similar to cells lacking ALKBH3, cells depleted of FTO showed increased drop in survival after MMC treatment when compared to cells deficient of RNF168.

To corroborate and substantiate the observed phenotype, the clonogenic assay was replicated using the ALKBH3 and FTO CRISPR-Cas9 KO clones and their response to NCS and MMC evaluated (Figure 52).

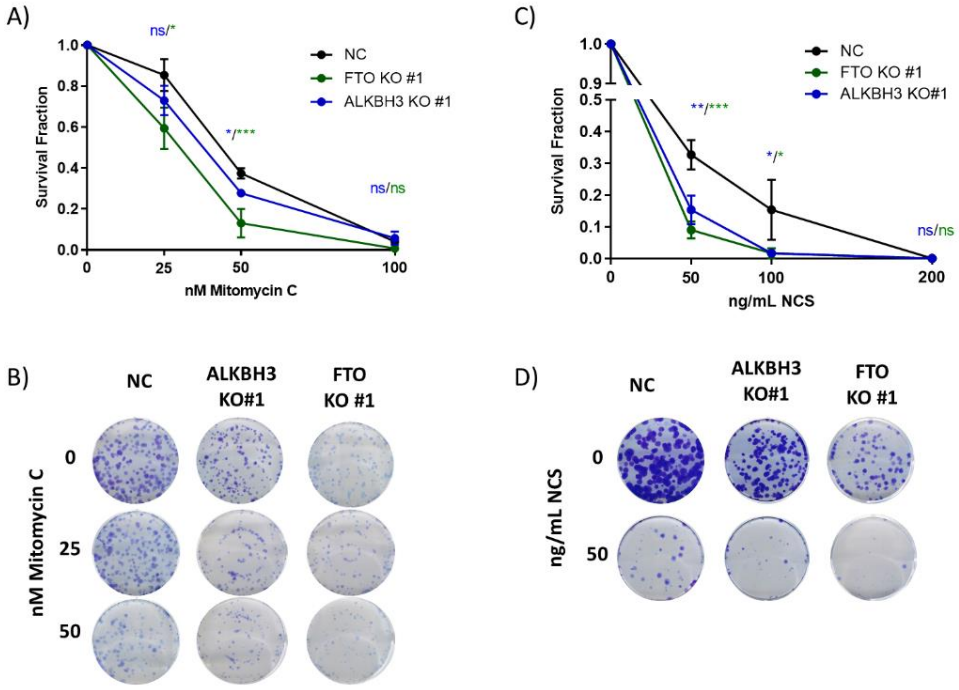

Figure 52. ALKBH3 and FTO CRISPR clones display comparable sensitivity to genotoxic agents as siRNA treated cells.

U2OS cells and ALKBH3 and FTO KO cells were seeded out in low density, treated with A-B) Mitomycin C or C-D) Neocarzinostatin and cells grown for 11-14 days. N=3, mean ± SD, One-Way ANOVA.

Both ALKBH3 and FTO KO cells exhibited increased susceptibility to both genotoxic agents when compared to wild-type U2OS cells, providing further confirmation to our hypothesis. Notably, FTO KO cells appear to exhibit greater susceptibility to MMC and NCS compared to ALKBH3 KO cells. These findings suggest a potential differential impact of FTO and ALKBH3 on cellular responses to genotoxic stress, highlighting the need for further exploration into their roles in DNA repair pathways and cellular survival mechanisms.

4.2.5 Exploring ALKBH3's and FTO's wider effect on genomic stability with RNA sequencing

The research conducted in this thesis has revealed that the depletion of ALKBH3 or FTO in cells leads to heightened genomic instability and increased sensitivity to genotoxic agents. Notably, in certain instances, cells lacking FTO exhibited a genomic instability phenotype that exceeded that of cells lacking RNF168, as evidenced by the metaphase spread assay (Figure 47) and NCS survival (Figure 51 C-D) assay. Likewise, while cells depleted of ALKBH3 did not consistently display as pronounced a phenotype as those

lacking FTO, in some cases, their response surpassed that of RNF168-depleted cells, as observed in the MMC response (Figure 51 A-B). It is worth noting that the increased response to MMC in ALKBH3-depleted cells did not reach statistical significance compared to cells lacking RNF168. Taken together these results suggest that FTO and to a lesser extent ALKBH3, might exert a more substantial influence on maintaining genome integrity that extends beyond their epitranscriptomic regulation of RNF168.

4.2.6 Differential gene expression analysis

In order to gain a deeper understanding of the potential expanding role of FTO and ALKBH3 in preserving genomic stability, U2OS cells were subjected to siRNA treatments targeting ALKBH3, FTO, and control siRNA. Following siRNA treatments, RNA sequencing was performed utilizing the Illumina platform. To gain a better understanding of the different gene expressions in FTO KD cells and ALKBH3 KD compared to control cells a differential gene expression (DEG) analysis was employed. Volcano plots were generated to visualize the significantly differentially expressed transcript in ALKBH3 and FTO samples vs control sample (Figure 53). Likelihood ratio and Wald test were utilized to determine significance and transcripts with p-value equal to or lower than 0.05 were deemed significantly differentially expressed.

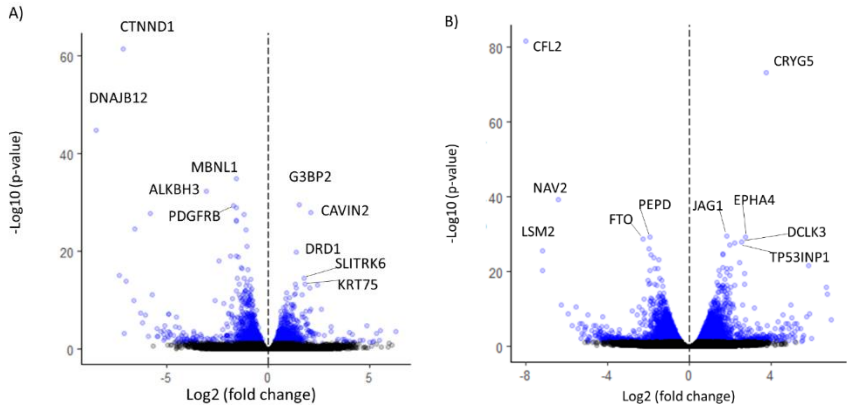

Figure 53. Volcano plot summarizing RNA sequencing differential gene expression analysis.

A) ALKBH3 and B) FTO depleted cells compared to cells treated with control cells. U2OS cells underwent treatment with control siRNA, FTO siRNA, and ALKBH3 siRNA for 48 hours, followed by Illumina RNA sequencing. Differential gene expression analysis was conducted using Sleuth. Significantly differentially expressed genes are marked with blue dots, while black dots represent non-statistically significantly differentially expressed transcripts. Top 10 most significantly altered transcripts by p-value are labelled in each picture. Volcano plots were made with data from 4 independent experiments.

4.2.7 Functional profiling

In order to examine the biological effect of FTO and ALKBH3 KD, it became imperative to study the biological processes taking place in cells depleted of either protein and discern potential disparities in these processes relative to control cells possessing fully functional ALKBH3 and FTO. Gene set enrichment analysis (GSEA) was performed, comparing firstly ALKBH3 KD cells to control cells and secondly FTO KD cells to control cells. Each KD sample was made up of four biological replicates and mean transcript per million (TPM) values were calculated and used to estimate fold change for each sample. Non-protein coding transcripts were excluded to ensure reliability of results along with any transcripts that did not have a p-value of ≤ 0.05. Using the Gene Ontology (GO) knowledgebase transcripts were assigned a biological function and categorized accordingly, allowing for GSEA (Figure 54 and Figure 55).

We identified 268 statistically significantly differentially expressed genes (90 upregulated and 178 downregulated) in cells lacking ALKBH3. In cells depleted FTO we identified 2716 (1476 upregulated and 1240 downregulated) significantly differentially expressed gens. The substantial increase in the number of differentially expressed genes in FTO-depleted cells, approximately tenfold more than cells lacking ALKBH3, underscores the broader impact on the overall transcriptional landscape by FTO when compared to ALKBH3. This observation could be associated with their functions as m^1A and m^6A demethylases, given that the m^6A modification is more prevalent than the m^1A modification on mRNA, however further research would be needed in order to gain a better understanding of ALKBH3 and FTO's influence on the transcriptome.

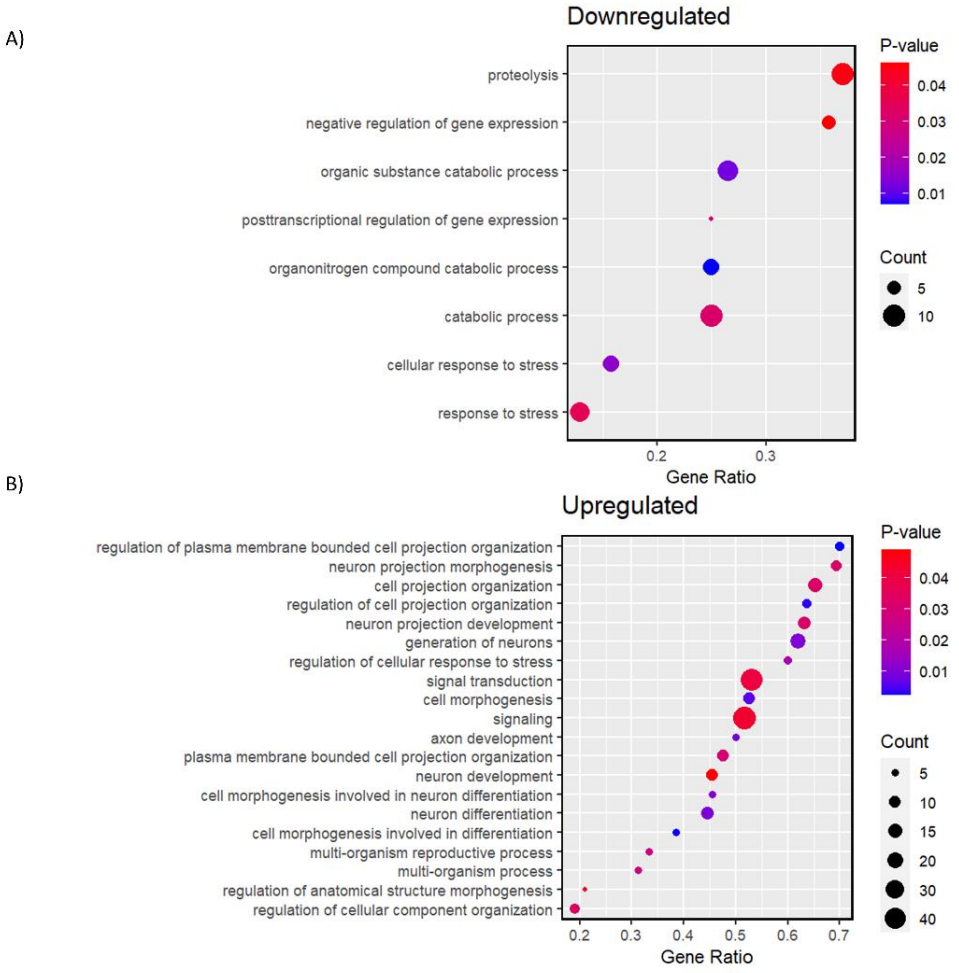

Figure 54. Dot plot functional enrichment analysis in ALKBH3 KD cells.

All significantly A) downregulated and B) upregulated biological processes in cells lacking ALKBH3. The color intensity of the nodes corresponds to p-value of the enrichment analysis. "Gene ratio" is the percentage of number of DEGs altered in the given GO term and "count" corresponds to the number of DEGs found to be differently expressed.

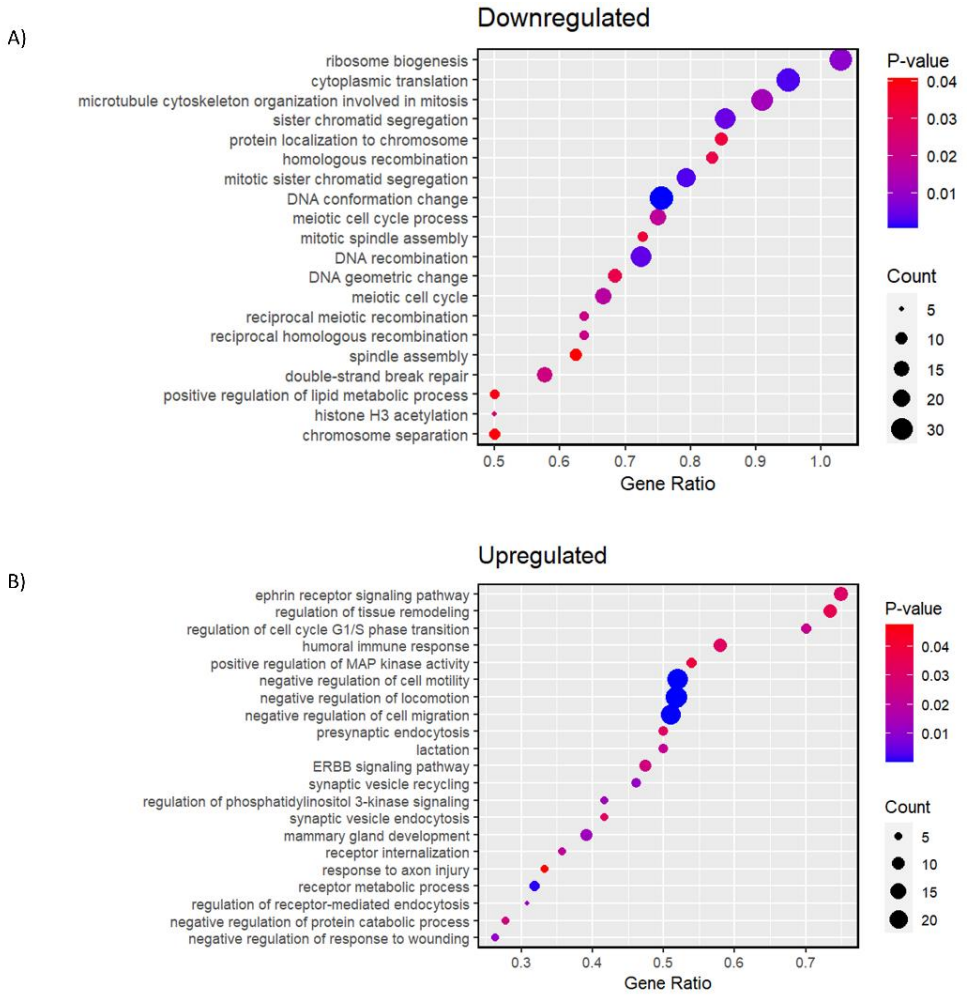

Figure 55. Dot plot functional enrichment analysis in FTO KD cells.

Top 20 most significantly A) downregulated and B) upregulated biological processes in cells depleted of FTO. The color intensity of the nodes corresponds to p-value of the enrichment analysis. "Gene ratio" is the percentage of number of DEGs altered in the given GO term and "count" corresponds to the number of DEGs found to be differently expressed.

When comparing ALKBH3 KD and control cells (Figure 54 A-B), the most distinctly repressed gene sets were primarily associated with cellular stress response and regulation of gene expression, whereas the significantly upregulated gene sets were related to neuron development. Interestingly while "Response to stress" was found downregulated in ALKBH3 KD cells, "Regulation of response to stress" was upregulated. Most significantly altered stress related genes, three downregulated stress-related genes and two upregulated, are displayed in Figure 56.

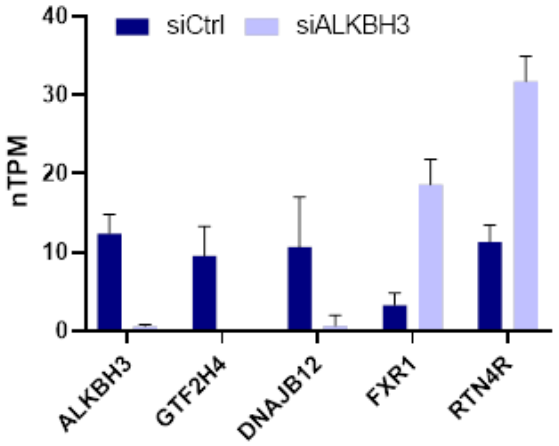

Figure 56. Stress response gene expression analysis in ALKBH3 KD cells.

Gene expression analysis was estimated with normalized mean TPM (nTPM) value from control and ALKBH3 KD cells. Graphs represent n=4 mean ± SD.

Results from comparison of FTO KD cells and control cells (Figure 55 A-B) revealed a broader spectrum of effects compared to the comparison between ALKBH3 KD and control cells. This outcome was anticipated, considering that FTO depletion had previously exhibited a tenfold greater impact on altered genes than ALKBH3-depleted cells. The top 20 most significantly altered GO terms were subsequently plotted, as depicted in Figure 55. Several interesting GO terms were found upregulated in FTO depleted cells including regulation of cell cycle G1/S phase transition, ERBB signaling pathway and negative regulation of cell migration. Downregulated biological processes in FTO depleted cells included chromosomal segregation, homologous recombination and most relevant to this project double strand break repair. By using GO annotation, DNA DSB repair genes could be filtered out and examined more thoroughly. When FTO KD cells were compared to control cells, 9 DNA DSB repair genes were significantly downregulated in FTO KD cells (Table 14 and Figure 57).

Table 14. Differently expressed DSB repair related genes in FTO KD cells.

ESCO2	SFR1	FANCD2
MCM2	BRCA1	FANCM
RAD21	GINS4	APTX

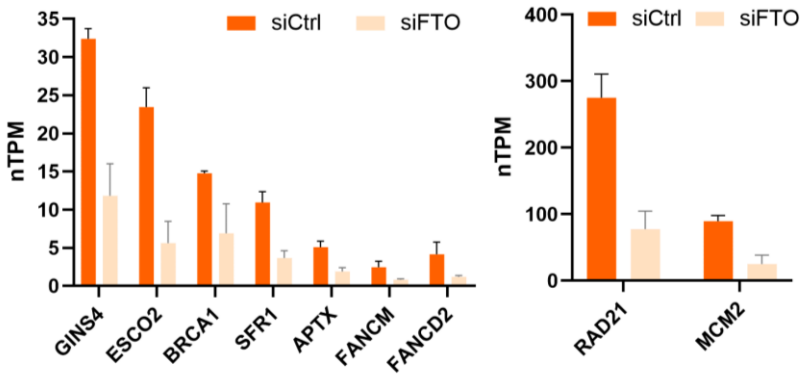

Figure 57. DNA DSB repair gene expression analysis in FTO KD cells.

Gene expression analysis was estimated with normalized mean TPM (nTPM) value from control and FTO KD cells. Graphs represent n=4 mean±SD.

The number of downregulated genes listed in Table 14 include several with recognized roles as effectors of DNA DSB repair. Five genes associated with the HR repair pathway were found to be downregulated; these include *BRCA1*, *FANCD2*, *FANCM, RAD21* and *SFR1*. Both *FANCD* and *FANCM* have a role in Fanconi anemia repair pathway. Additionally, one NHEJ related gene, *Aprataxin* (*APTX),* was downregulated in FTO-depleted cells. The DNA DSB recognition and recruitment factor, *ESCO2,* was found to be downregulated. *ESCO2* has been shown to be recruited to DSB in an ATM and MDC1 dependent manner and promotes 53BP1 recruitment (Fu et al., 2023). Lastly, *MCM2* and *GINS4* genes were found to be downregulated in FTO depleted cells. They are both part of the CMG (CDC45-MCM2-GINS) helicase complex which unwinds double-stranded DNA during DNA replication (Xiang et al., 2023).

4.2.7.1 *Confirming DNA DSB repair gene downregulation*

Among the nine downregulated genes identified in FTO-depleted cells, *BRCA1* was selected to further validate the gene expression analysis, using western blot. *BRCA1*, a well-established tumor suppressor gene, holds a crucial role in maintaining genomic stability. Its multifaceted functions encompass critical involvement in HR DSB repair, DNA damage signaling, activation of cell cycle checkpoints, protein ubiquitination, chromatin remodeling, as well as transcriptional regulation and apoptosis. U2OS cells were treated with FTO, ALKBH3, RNF168 and control siRNA followed by western blot analysis (Figure 58). The inclusion of ALKBH3 siRNA in the analysis was motivated by the absence of a significant difference in *BRCA1* expression in ALKBH3 KD cells. RNF168 served as a positive control, considering our previous research has demonstrated that ALKBH3 and FTO KD affect RNF168 protein expression.

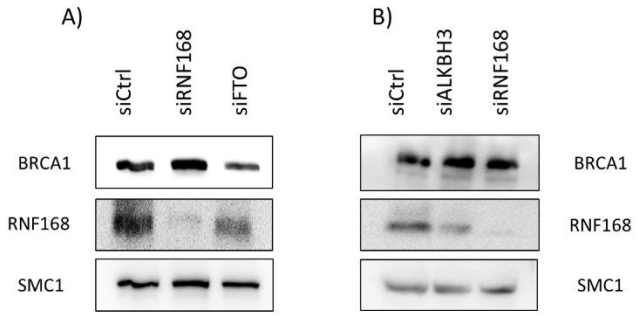

Figure 58. BRCA1 protein expression in FTO and ALKBH3 KD cells.

A-B) U2OS cells treated with the above-mentioned siRNAs for 48h followed by western blot analysis of BRCA1, BRCA2 and RNF168 and ALKBH3, SMC1 is used as loading control.

Upon depleting U2OS cells of FTO, a modest reduction in BRCA1 protein expression was observed compared to the control sample. In contrast, depleting cells of ALKBH3 and RNF168 did not impact the protein expression of either BRCA1. The downregulation of BRCA1 protein expression, along with the downregulation of other DNA DSB repair-related genes in FTO KD samples, may offer a plausible explanation for the heightened response of FTO-depleted cells to genotoxic reagent treatments and the observed increase in genomic instability.

5 Discussion and conclusions

5.1 Summary

The maintenance of genomic integrity is of great biological importance for the survival of living organisms. A network of mechanisms, collectively referred to as the DNA damage-response (DDR), collaborates to protect the integrity of the human genome. The crucial role of correctly functioning DNA damage response systems in human health becomes apparent through the severe consequences of inherited defects in DDR factors, leading to a spectrum of diseases, including neurological degeneration, premature aging, immune deficiency, and heightened susceptibility to severe forms of cancer (Hoeijmakers, 2001, 2009). Understanding the regulatory mechanisms governing DNA damage-response factors and their irregularities becomes crucial, especially in the context of cancer prevention. In-depth exploration in this field not only sheds light on the molecular basics of various diseases but also opens avenues for creating targeted therapeutic approaches, which is vital for developing interventions that can mitigate cancer risk and advance precision medicine, early detection, and treatment.

The work presented in this thesis has two major components. The first part unveils a novel form of regulation of the crucial DDR protein RNF168. We demonstrate that two dioxygenases, ALKBH3 and FTO, belonging to the AlkB protein family, influence protein expression of RNF168 conceivably via epitranscriptomic regulatory mechanisms. We find using siRNA mediated KD cells that cells depleted of ALKBH3 and FTO show increased methylation levels on the *RNF168* transcript defective *RNF168* mRNA export and reduced RNF168 protein expression. This defect in mRNA export and reduced RNF168 protein expression was later confirmed in CRISPR-Cas9 KO cell models. This presents a novel regulatory mechanism for RNF168, a protein that is already subject to extensive regulation thereby influencing the DNA DSB response. Notably, ALKBH3 and FTO exhibit similar regulatory effects on RNF168 despite targeting distinct methylation marks on its transcript, ALKBH3 targeting m^1A and FTO targeting m^6A. Depleting cells of either ALKBH3 or FTO results in remarkably similar phenotypic effects on RNF168, however, simultaneous depletion of both proteins did not produce an additive effect. Co-IP experiments unveiled a protein-protein interaction between ALKBH3 and FTO, suggesting a potential complex formation and their combined impact on RNF168 through a shared pathway. Furthermore, co-IP/MS analysis revealed interactions between ALKBH3 and FTO with several RNA-binding proteins involved in mRNA maturation, hinting at a potentially more nuanced role for these two demethylation proteins in mRNA processing.

The second part of this thesis was designed to gain a better understanding of the effect ALKBH3 and FTO have on the DNA DSB response through their influence on RNF168. We demonstrate that cells lacking ALKBH3 or FTO show diminished recruitment of crucial repair factors to the break sites, including 53BP1. Furthermore, loss of either ALKBH3 or FTO impacted DNA DSB repair dynamics, caused genomic instability, and increased susceptibility to genotoxic agents. RNA-sequencing analysis of cells with ALKBH3 or FTO KD unveiled an effect on various cellular functions. Particularly notable in FTO-depleted cells, gene ontology analysis highlighted significant downregulation of DNA double-strand break repair genes in FTO knockdowns, including *BRCA1*. Meanwhile, ALKBH3 knockdown cells showed a notable decrease in the cellular stress response, among other pathways.
Findings reported in this thesis could lead to new therapeutic insight as lack of either ALKBH3 or FTO may be used as a potential marker for cancer treatment response. The epitranscriptomic regulation of genome integrity demonstrated in this thesis presents a novel addition to the fast-growing field of epitranscriptomics and unveils a new role for mRNA methylations in governing DNA DSB repair signaling.

5.2 RNA modifications: A new layer of gene expression regulation

Post-transcriptional mRNA processing in eukaryotes involves modifying RNA after transcription but before protein translation. Among the prominent post-transcriptional processes are the 5′ capping and 3′ polyadenylation modifications, discovered over 50 years ago (Edmonds et al., 1971; Muthukrishnan et al., 1975; Wei et al., 1975). The exploration of RNA modifications predates the identification of the 5′ cap, with pseudouridine reported in 1957 followed by the discovery of m^1A in 1961 and m^6A in 1974 (Davis et al., 1957; Desrosiers et al., 1974; Dunn, 1961). The acknowledgment of the biological significance of RNA modifications, coupled with advancements in methodology, has given rise to the field of "epitranscriptomics." Comparable to epigenetics, epitranscriptomics explores functionally relevant chemical modifications on RNA that do not modify the genomic sequence.

5.2.1 Post-transcriptional regulation of RNF168

Methylations represent one of the most common forms of mRNA modifications and can significantly impact the life cycle of mRNA transcripts. These modifications have been identified as influential in initiating translation, stabilizing transcripts, splicing pre-mRNA, and facilitating mRNA export (Alarcon et al., 2015; N. Liu et al., 2015; X. Wang et al., 2014; Zheng et al., 2013). Several studies have suggested that methylation and demethylation of mRNA takes place co-transcriptionally (Adhikari et al., 2016; Akhtar et al., 2021; Slobodin et al., 2017).

Data presented in the first part of this thesis show epitranscriptomic regulation of the DDR factor, RNF168 by two demethylases or methylation erasers. Firstly, we note that loss of the alkylating repair enzyme, ALKBH3 leads to decreased protein expression of RNF168 in four different cell lines (Figure 20). The influence on RNF168 was found to be seemingly unrelated to ALKBH3's canonical role as an alkylating damage repair enzyme (Figure 22). Presenting a possible new distinct role for ALKBH3 in influencing the DDR, however further research is necessary to corroborate these findings. Beyond its role as an alkylating DNA damage repair enzyme, ALKBH3 has an established role as an RNA demethylase and is the only known m^1A mRNA demethylase. Our research demonstrated that depleting cells of ALKBH3 led to increased m^1A methylation levels on the *RNF168* transcript (Figure 25). The m^1A modification is known to affect mRNA translation by blocking Watson-Crick pairing (Aas et al., 2003) and to affect mRNA structural stability (Woo et al., 2019; Q. Zheng et al., 2020). Our results did not demonstrate any influence on mRNA transcription (Figure 24A) or mRNA stability (Figure 26) of *RNF168* in the absence of ALKBH3, but rather demonstrated in increased nuclear retention of the *RNF168* mRNA, indicating faulty mRNA export (Figure 27-Figure 28). These results connect the m^1A modification to mRNA export, indicating that m^1A demethylation by ALKBH3 influences mRNA export. This is to our knowledge the first reported case of ALKBH3 affecting nuclear export of m^1A methylated mRNA.

Further investigations demonstrated that ALKBH3 was not the only member of the AlkB family influencing RNF168 protein expression. Three different cell lines subjected to siRNA mediated KD of FTO (ALKBH9) (Figure 29) exhibited a reduction in RNF168 protein expression to a similar level as cells treated with siRNA for ALKBH3. Further research revealed that the depletion of FTO resulted in a comparable RNF168 phenotype as observed with the depletion of ALKBH3. FTO has a well-established role as a m^6A mRNA demethylase (Jia et al., 2011) and the depletion of FTO resulted in an increased levels of m^6A methylation on the *RNF168* transcript (Figure 32) and increased nuclear retention of the *RNF168* mRNA (Figure 37-Figure 38). ALKBH3 and FTOs influence on RNF168 protein expression and mRNA nuclear retention was further validated using CRISPR-Cas9 KO cell models (Figure 40).

Previous studies that have linked the m^6A modification to mRNA export (Lesbirel et al., 2018; Lesbirel et al., 2019; Roundtree Luo et al., 2017), however in contrast to previous findings which observed inhibition of mRNA export upon the removal of m^6A by ALKBH5 (Zheng et al., 2013), our results suggest that actively eliminating m^6A methylation induce stimulation of nuclear export. This discrepancy may stem from the mechanism through which ALKBH5 was found to affect mRNA export. In some instances, m^6A methylation enhances mRNA export by facilitating the recruitment of mRNA export factors or by promoting the formation of export-competent ribonucleoprotein complexes. Conversely, in other cases, m^6A modification may hinder mRNA export by altering RNA secondary structure or by regulating the binding of RNA-binding proteins involved in export, thus impeding the export process. In their

2013 publication Zheng et al., showed that ALKBH5 was affecting mRNA export by affecting the phosphorylation levels of SRSF1 by influencing the subcellular location of SRPK1. SRPK1 is one of the main kinases responsible for the phosphorylation of SRSF1. In its hyperphosphorylated state SRSF1 is thought to influence mRNA splicing while hypophosphorylated SRSF1 facilitates the interaction between the NXF1-P15 complex and mRNA cargo to promote mRNA export (Li et al., 2005). The modified subcellular localization of SRPK1 in ALKBH5-deficient cells may contribute partially to the altered phosphorylation status of SRSF1. It is plausible that the demethylation activity of FTO on m^{6}A has different effects on mRNA export compared to ALKBH5, e.g., aiding in the recruitment of other export factors. Additional research is required to uncover what role FTO m^{6}A demethylation plays in mRNA export.

5.2.2 The function of mRNA methylations in *RNF168* mRNA export

Nuclear mRNA export is a pivotal process in eukaryotic gene expression with majority of mRNA being transported from the nucleus through the nuclear heterodimeric export receptors NXF1-P15 and the TREX complex (Heath et al., 2016). During mRNA maturation, members of the TREX complex are sequentially added to the mRNA, ultimately forming a messenger ribonucleic complex which binds and transfers the mRNA to the export receptor NXF1 leading to export though the nuclear pore complexes (Dufu et al., 2010; Masuda et al., 2005; Viphakone et al., 2012).

Existing research has established a noteworthy connection between the m^{6}A methylation machinery and mRNA export. Firstly, specific factors related to the m^{6}A modification have been found to localize within nuclear speckles—regions in the nucleus housing mRNA export factors (Ping et al., 2014), this includes FTO which has demonstrated partial co-localization with nuclear speckles in HeLa and MCF7 cells (Berulava et al., 2013; Jia et al., 2011). Secondly, research has shown that knockdown experiments involving various m^{6}A associated proteins, including METTL3, WTAP, KIAAA1429, RBM15, YTHDC1, and ALKBH5, have consistently demonstrated to effect nuclear export of mRNA, including resulting in export defects (Fustin et al., 2013; Lesbirel et al., 2018; Roundtree Luo et al., 2017; Zheng et al., 2013; Zolotukhin et al., 2009). Lastly, co-IP and proteomics studies have unveiled multiple interactions between the core mRNA export machinery (TREX-NXF1) and m^{6}A methylation-associated proteins, strongly suggesting a functional connection between these two processes (Horiuchi et al., 2013; Lesbirel et al., 2018; Lindtner et al., 2006; Uranishi et al., 2009; Zolotukhin et al., 2009).

More recent investigations have begun to unveil the link between the molecular mechanisms of mRNA export and m^{6}A modifications. The methylation reader protein YTHDC1 has emerged as a pivotal player, helping transport mature m^{6}A-methylated transcripts to the nuclear mRNA export receptor NXF1 via its interaction with SRSF3. Notably, KD of SRSF3 or YTHDC1 leads to the nuclear accumulation of shared

transcripts, indicating their joint pathway involvement (Roundtree Luo et al., 2017). Additionally, research has shown that the association of the TREX complex with m^{6}A-methylated mRNA is contingent upon the m^{6}A methyltransferase complex. Subsequently, the TREX complex plays a crucial role in aiding the effective binding and stabilization of YTHDC1 with m^{6}A methylated mRNA. Cellular studies involving KD of TREX complex subunits result in diminished levels of YTHDC1 association with mRNA (Lesbirel et al., 2018). The involvement of the m^{6}A demethylase, FTO, in the export of methylated has yet to be elucidated.

The research presented in this study contributes additional evidence supporting the connection between the m^{6}A mRNA methylations and the export of mRNA from the nucleus, along with offering new evidence that suggest a link between demethylation of m^{1}A modification by ALKBH3 to mRNA export. The demethylation events of m^{6}A by FTO and m^{1}A by ALKBH3 appear to play a role in the maturation process of *RNF168* mRNA. Preliminary data employing siRNAs to suppress the expression of m^{6}A and m^{1}A methyltransferases (writers) did not lead to an elevation in RNF168 protein expression, as one might anticipate if the presence of m^{1}A or m^{6}A methylation marks on the *RNF168* transcript were merely a mechanism to impede mRNA export (Supplementary Figure 8). Indicating that these methylations may not serve solely as quality control measures requiring removal before mRNA export. It is however crucial to consider that methyltransferases exert influence on various mRNA maturation processes beyond mRNA export. This suggests the plausibility of their involvement in regulating RNF168 protein expression through alternative mechanisms, necessitating further investigation into the impact of mRNA methylations on the *RNF168* transcript.

Further investigations into other m^{1}A/m^{6}A-associated proteins revealed that suppressing the expression of the m^{6}A/m^{1}A interaction protein YTDHC1 and YTHDF3 along with RNA-binding proteins SRSF7 and SRSF3 using siRNAs significantly reduced the protein expression of RNF168 (Figure 41). The KD of the cytoplasmic m^{6}A reader YTHDF3 resulted in a decrease in the protein expression of RNF168 (Figure 41), which could be attributed to YTHDF3's role in aiding in mRNA translation. According to our working hypothesis FTO removes m^{6}A methylation from the *RNF168* transcript, facilitating regular mRNA export and protein expression. It is plausible that *RNF168* contains multiple m^{6}A-methylated bases, and FTO may not eliminate all of them, enabling YTHDF3 to bind to m^{6}A on *RNF168* mRNA upon its cytoplasmic entry and contribute to its translation. Similar to YTHDF3, the depletion of nuclear m^{6}A reader YTHDC1 and SRSF3 resulted in an approximate 40% reduction in RNF168 protein expression, while the absence of SRSF7 led to a 70% decrease (Figure 41). Furthermore, preliminary data derived from the RNA fractionation assay (Supplementary Figure 9) indicated that the KD of YTHDC1, SRSF3, and SRSF7 increase the nuclear accumulation of *RNF168* mRNA.

These results align with previous findings from Roundtree et al., which demonstrated using RIP-seq and PAR-CLIP experiments that *RNF168* mRNA is one of the numerous transcripts targeted by YTHDC1. Moreover, knocking down YTHDC1 using siRNA effects the subcellular location of its targets transcripts i.e., depleting cells of SRSF3 and YTHDC1 led to nuclear retention of m^{6}A methylated mRNA (Roundtree Luo et al., 2017). Our data further unveiled that SRSF7 exhibited a potentially stronger impact on the downregulation of RNF168 protein compared to SRSF3. Similar to SRSF3, SRSF7 functions as an adaptor in mRNA export, facilitating the recruitment of the export factor NXF1 to promote efficient mRNA export (Hargous et al., 2006; Muller-McNicoll et al., 2016; Reed et al., 2005). Moreover, SRSF7 has also been shown to interact with YTHCD1 and to be able to influence alternative polyadenylation and splicing (Kasowitz et al., 2018; Xiao et al., 2016). Recently, SRSF7 was identified as an m^{6}A regulator of a small portion of m^{6}A sites in glioblastoma cells by aiding in recruiting members of the methyltransferase complex (METTL3, METTL4, and WTAP) (Cun et al., 2023).

In their 2017 publication, Roundtree et al., propose a mechanism for the export of m^{6}A-methylated mRNA. According to their model YTDHC1-mediated mRNA export occurs in a manner dependent on m^{6}A methylation, independent of splicing, and takes place non-co-transcriptionally (Roundtree Luo et al., 2017). Considering the impact of YTHDC1 KD and SRSF3 KD on RNF168 protein expression (Figure 41) and *RNF168* mRNA nuclear accumulation (Figure 27 Figure 28, Figure 37, Figure 38 and Supplementary Figure 9), along with the observed increase in methylation levels on the *RNF168* mRNA following ALKBH3 KD and FTO KD (Figure 25 and Figure 32), it is reasonable to speculate that efficient *RNF168* mRNA export relies on both the presence and removal of these methylations. Another interesting point regarding export of m^{6}A methylated mRNA was put forward by Lesbirel et al in 2018 where they demonstrated that the m^{6}A methyltransferase complex was vital for the recruitment of the TREX complex to m^{6}A modified mRNA and its export. Moreover, they demonstrate that the efficient association of the m^{6}A reader YTHDC1 with mRNAs necessitated the presence of the TREX complex (Lesbirel et al., 2018).

One could hypothesize that placement of m^{6}A (and m^{1}A) on the *RNF168* transcript is important for the recruitment of the TREX complex which in turn aids in the recruitment of YTHDC1. YTHDC1 along with aid from SRSF3 and SRSF7 then aids in the export of the *RNF168* mRNA by interacting with NXF1 for efficient export. The removal of the m^{1}A and m^{6}A methylations occurs post-transcriptionally and after YTHDC1-SRSF3 interactions with the mRNA methylations. Failure to remove these methylations could potentially extend the nuclear lifespan of mRNA, rendering it vulnerable to further mRNA processing events. Alternatively, the presence of ALKBH3 and FTO might be crucial for recruitment of other mRNA-binding proteins or export factors important for the maturation of mRNA. It is important to acknowledge that these speculations warrant further investigation, as some conclusions are derived from preliminary data. To confirm our hypothesis and to precisely elucidate the mechanisms and functional implications of ALKBH3 and FTO demethylating activities within the intricate landscape of mRNA processing would necessitate further investigations.

5.2.3 Exploring the impact of RNA demethylases in mRNA export

To further explore the possibility of ALKBH3 and FTO playing a role in the mRNA export of *RNF168*, a co-IP/MS assay using FLAG tagged ALKBH3 or FTO plasmid was conducted to gain insight into the protein-protein interactions of ALKBH3 and FTO (Table 13 and Appendix D). The co-IP/MS data unveiled interactions between ALKBH3 and, to a lesser extent, FTO, with various RNA-binding proteins.

Members of the hnRNP protein family were identified as the most abundant RNA-binding proteins interacting with ALKBH3. The hnRNP proteins are recognized for their involvement in various aspects of RNA metabolic processes (Geuens et al., 2016), including mRNA export as a subset of these proteins are known to shuttle between the nucleus and cytoplasm (Izaurralde et al., 1997). Of the six hnRNP proteins found interacting with ALKBH3, hnRNPC, hnRNPA1 and hnRNPA2/B1 were of particular interest. Both hnRNPA1 and hnRNPA2/B1 are widely acknowledged for their roles in both mRNA export (Lu et al., 2023; Michael et al., 1995) and mRNA splicing (David et al., 2010; X. Y. Liu et al., 2015; Neubauer et al., 1998). Notably, all three hnRNP proteins have also been categorized as m^{6}A interaction proteins. hnRNPA2/B1 is classified as a nuclear reader of m^{6}A that can affect alternative splicing (Alarcon et al., 2015), while hnRNPA1 is recruited to m^{6}A-modified SARS-CoV-2 RNA, acting as an m^{6}A reader to enhance transcription (Kumar et al., 2022). hnRNPC has been found to bind to m^{6}A and effect alternative splicing and relative mRNA abundance of its target mRNA (N. Liu et al., 2015)

Another interesting set of proteins found to interact with ALKBH3 (catalytic dead version) were members of the serine-arginine rich (SR) protein family, SRSF1 and SRSF3. Like the hnRNP protein family, SR proteins are known to be involved in many mRNA processing steps, such as translation, splicing, export and stability (Huang et al., 2003; Sanford et al., 2005; Zhang et al., 2004). As previously mentioned, SRSF3 plays a role in nuclear export of m^{6}A methylated mRNA with YTDHC1. SRSF1 has also been found to interact with YTHDC1 on a protein level (Timcheva et al., 2022) but has not been linked to nuclear export of methylated mRNA in the same way SRSF3 has.

Discrepancies with the existing literature emerged when the ALKBH3 co-IP/MS assay failed to detect any interaction between ALKBH3 and established partners, including ASCC3, ASCC2, RIF1, or OTUD4 (Dango et al., 2011; Zhao et al., 2015). These studies employed a similar co-IP/MS assay with a FLAG-tagged ALKBH3 vector, albeit in different cell lines—HEK293T (Dango et al., 2011) and PC-3 (Zhao et al., 2015). These discrepancies may stem from a range of factors, including cell line differences, as higher endogenous ALKBH3 levels are found in both HEK293 and PC-3 cells than U2OS cells. Higher ALKBH3 levels may reflect the cell line-specific importance of ALKBH3 in the repair of alkylation damage and other cellular functions. In fact, Dango et al, demonstrated that loss of ALKBH3 in U2OS cells did not result in increased sensitivity to the alkylating agent MMS, in contrast to PC-3 cells where ALKBH3 is highly

expressed (Dango et al., 2011). Despite variations, some commonalities emerged between the co-IP/MS results presented in this thesis and previous ALKBH3 co-IP/MS studies. Specifically, PRMT5 (Protein Arginine Methyltransferase 5) emerged as a shared interaction partner of ALKBH3 in all three co-IP/MS analyses, while hnRNPH1 was a common factor between this study and the findings reported by Zhao et al., (Zhao et al., 2015), adding credibility to our findings.

FTO (catalytic dead version) was identified in interaction with three RNA-binding proteins, RBMX (also known as hnRNPG), RBMXL3 and RBM6, two of which RBMX and RBM6 have been associated with mRNA splicing (Bechara et al., 2013; Thonda et al., 2022). In addition, RBMX functions as an m^{6}A reader protein, binding to the m^{6}A modification on mRNA where it has been shown to associate with RNA polymerase II co-transcriptionally and modulates alternative splicing (Liu et al., 2017). Furthermore, RBMX has been shown to be a positive regulator of HR repair by influencing *BRCA2* expression (Adamson et al., 2012).

The established view on mRNA methylation, in particular m^{6}A, suggests that these modifications occur co-transcriptionally, with transcription influencing the catalytic activity of m^{6}A methyltransferases on mRNA (Slobodin et al., 2017). Similarly, pre-mRNA splicing is known to occur co-transcriptionally, as evidenced by multiple studies demonstrating the co-transcriptional nature of the splicing process (Herzel et al., 2017). Although mRNA export is not a co-transcriptional process, the prevailing notion is that the recruitment of the export machinery occurs in a co-transcriptional manner (Viphakone et al., 2019). Furthermore, the splicing machinery has been shown to aid in the recruitment of the TREX complex (Masuda et al., 2005) and as previously mentioned the m^{6}A methyltransferase complex has also been shown to play a role in recruitment of the TREX complex (Lesbirel et al., 2018). The potential integration of demethylation proteins into this intricate process is not implausible. However, the precise points of their involvement remain elusive, and the reasons behind the necessity of removing these methylations for efficient mRNA export are currently not well understood. Given the number of protein-protein interactions ALKBH3 and FTO were found to have with other RNA binding proteins it is possible to imagine that their presence is important for mRNA export, whether they aid in the recruitment of these RNA binding proteins or other important export factors, although further research is needed to establish their precise contribution in this process.

5.2.4 Crosstalk between mRNA Modification: Collaboration of ALKBH3 and FTO

Throughout the research conducted in this thesis, no additive effects on the RNF168 phenotype were observed following the double KD of ALKBH3 and FTO. Observations included no discernible impact on RNF168 protein expression, mRNA nuclear retention, mRNA levels, or levels of genomic instability (Figure 49).

Co-IP/ WB assay revealed an interaction between ALKBH3 and FTO, later confirmed co-IP/MS assay hinting at a possible complex formation between ALKBH3 and FTO. In both co-IP/WB assay (Figure 34 C, Figure 35) and co-IP/MS assay (Table 13 and Appendix D) FTO came up as a strong interaction partner of ALKBH3 while ALKBH3 interaction with FTO was significantly weaker (Figure 34C) and ALKBH3 did not come up as an interaction partner of WT FTO but did appear in co-IP/MS data for the catalytically dead version of FTO (Appendix D). The reason for these discrepancies remains unknown. It is noteworthy that the co-IP/MS analysis of WT FTO revealed limited interaction partners for FTO, with established partners such as SFPQ failing to emerge in the co-IP/MS results (Song et al., 2020). One possible explanation is that the FTO-FLAG tagged protein used for both co-IP assays may be immobilized in a manner that renders the protein-protein interaction site inaccessible. Alternatively, the overexpression of FTO might result in heightened protein aggregation or changes in protein shape, thereby rendering the FTO protein less accessible or unable to interact effectively. Another possibility is that a significant portion of FTO's protein interactions may be transient making them harder to detect using the WT FTO-plasmid. However, when the FTO protein is rendered catalytically inactive, it could lead to increased interaction time to its nucleic acid target, prolonging interactions with other proteins, making them detectible.

Despite weak FTO co-IP data the overall protein-protein interaction data presented in this study suggests collaboration between ALKBH3 and FTO within a shared pathway. From a mechanistic standpoint, the collaborative impact of ALKBH3 and FTO remains unclear and whether one functioned upstream or downstream of the other or if they worked at the same level, remains to be determined. Despite both belonging to the ALKBH gene family, these two proteins exhibit distinctions in substrate specificity and lack apparent functional overlap. Nevertheless, the absence of an additional influence on RNF168 phenotype upon the simultaneous depletion of ALKBH3 and FTO along with their protein-protein interaction suggests the possibility that ALKBH3 and FTO may influence RNF168 through a shared pathway, potentially involving crosstalk between distinct mRNA modifications.

In recent years, research has emerged demonstrating crosstalk between mRNA methylations including crosstalk between m^1A and m^6A where collaboration between the two modifications, along with their specific reader proteins, was essential for efficient mRNA degradation (Boo et al., 2022). Another recent example involves crosstalk between m^5C and m^6A to enhance protein translation (Q. Li et al., 2017).

Looking at co-IP/MS data revealed a surprising amount of m^6A associated proteins were found to be interacting with ALKBH3 (WT and CD) compared to the two found to be interacting with FTO (METTL14 and RBMX). ALKBH3 was found to interact with the two known m^6A demethylating proteins, FTO and ALKBH5 along with several m^6A reader proteins. This data suggests a potential association between ALKBH3 and m^6A-

mediated processing, providing further evidence for a possible crosstalk between m^6A and m^1A modification on the *RNF168* transcript. Furthermore, ALKBH3 had no impact on the m^6A levels on *RNF168* and FTO no impact on the m^1A levels (Figure 33) and both FTO and ALKBH3 seem to function fine in the absence of one another (neither impacted the protein level of the other, Figure 29) at least in the context of RNF168. From this, we hypothesized that demethylation by ALKBH3 and FTO could be two distinct steps in the same mRNA export pathway where both methylations must be removed for *RNF168* mRNA export to take place. Additional research is required to validate these findings, focusing on elucidating the specific mRNA methylation sites targeted by FTO and ALKBH3.

In conclusion, in the first segment of this thesis, the results indicated that both ALKBH3 and FTO exert an epitranscriptomic regulatory influence on RNF168. The depletion of ALKBH3 resulted in increased m^1A methylation levels on the *RNF168* transcripts, while depletion of FTO led to increased m^6A methylation levels. Furthermore, loss of either ALKBH3 or FTO leads to nuclear retention of *RNF168* mRNA, ultimately leading to reduction in RNF168 protein expression. These results provide further evidence of connection between the m^6A methylation machinery and mRNA export and establish a new connection between the demethylation activity of both FTO and ALKBH3 and mRNA export. Lastly, the observed protein-protein interactions between FTO and ALKBH3 suggest a potential collaboration between these demethylases within a shared pathway. These findings underscore the possibility of mRNA modification as a novel regulatory factor in DNA DSB repair signaling which contributes to the fine-tuning of RNF168 expression.

5.3 Novel epitranscriptomic regulation of RNF168

Ubiquitination is a crucial mechanism in governing cellular processes, encompassing DNA damage signaling and repair. RNF168 is considered the rate-limiting factor for the recruitment of key DDR factors to the damaged chromatin via the ubiquitination of histone H2A and H2AX at sites of DNA damage. Histone ubiquitination is a key step in the signaling cascade that attracts and facilitates the assembly of downstream DDR proteins to the damaged chromatin, including BRCA1, RAD18, BARD1 and 53BP1 (Becker et al., 2021; Doil et al., 2009; Mustofa et al., 2021; Tang et al., 2021). Considering RNF168's pivotal role in DDR signaling, its functions are meticulously regulated to uphold DDR balance and specificity. This regulatory mechanism ensures proper functionality while guarding against uncontrolled amplification of chromatin ubiquitylation which can have undesirable outcomes for genomic stability (Gudjonsson et al., 2012; Lancini et al., 2014; Mosbech et al., 2013).

Results presented in this thesis reveal an additional regulatory mechanism governing RNF168. This mechanism involves epitranscriptomic regulations orchestrated by two RNA demethylases, FTO and ALKBH3, which contribute to the regulation of RNF168.

This novel form of regulation involves the removal of a methylation mark from the *RNF168* transcript, subsequently enabling normal RNF168 protein production. This discovery adds an additional layer of complexity to the intricate control mechanisms governing RNF168 expression, and the chromatin ubiquitin response to damage, emphasizing the critical importance of precise regulation of RNF168 protein levels. In addition, our research provides evidence of a crosstalk between two DNA repair pathways, DSB repair and alkylation damage repair.

5.3.1 ALKBH3 and FTO: Implications for the DNA damage response

The precise structural and temporal control of mRNA methylation has in recent years emerged as an important regulatory mechanism in diverse biological processes, including the DNA damage response (Tsao et al., 2021; Xiang et al., 2017). The m^6A mRNA modification has previously been linked to the resolution of R-loops (Abakir et al., 2020; Yang et al., 2019) and to mediate repair of DSB by enabling recruitment of repair factors to DSB site to facilitate HR repair (Zhang et al., 2020). The connection between DNA repair and the m^1A modification is less clear, but research has indicated the potential involvement of m^1A in responding to DNA damage caused by alkylating agents (Tsao et al., 2021). However, to the best of our knowledge, no discernible correlations have been established between the m^1A modification and the repair of DSB. In part one of this thesis, we revealed the epitranscriptomic regulation of RNF168 mediated by FTO and ALKBH3, introducing a unique regulatory paradigm distinct from previously documented relationships between mRNA methylations and the DDR. Our investigation unveils a regulatory example between mRNA methylations and the DDR, where a specific DDR protein is regulated through epitranscriptomic mechanisms.

In the second part of this thesis our observations demonstrate that depleting cells of ALKBH3 led to loss of recruitment of both 53BP1 and its immediate binding partner RIF1 (Figure 19 B-E) to the site of DSB without affecting the protein expression (Figure 19 A) indicating ALKBH3 impacts the recruitment of these proteins via its regulation of RNF168. Moreover, loss of ALKBH3 led to slower clearing of MDC1 from DSB site indicating less efficient DNA DSB repair (Figure 43). Comparable results were seen in cells depleted of FTO where 53BP1 recruitment to DSB was decreased (Figure 30). In cells depleted of ALKBH3 and FTO, the defects in DNA DSB signaling were slightly less severe than in cells lacking RNF168, suggesting a partial loss of RNF168 function, consistent with the observed reduction in RNF168 protein expression (Figure 20 and Figure 29). From this we concluded that both ALKBH3 and FTO exert influence on the response to DSB repair, most likely through the regulation of RNF168.

5.3.2 ALKBH3 and FTO: Influence on DNA DSB repair pathway choice

When chromatin ubiquitination is impaired, the downstream events in DSB repair become compromised. The inability to efficiently recruit repair factors like 53BP1 and BRCA1 hinders the proper assembly of repair complexes, leading to defects in correct DNA DSB repair pathway choice. This can result in delayed or inefficient repair of DSBs, potentially leading to increased genomic instability and susceptibility to mutagenesis. Hence, ensuring proper chromatin ubiquitination is crucial for effective DSB repair. Previous studies have revealed that disrupting the RNF168-53BP1 pathway promotes the use of the very mutagenic SSA repair pathway (Munoz et al., 2012; Ochs et al., 2016). Considering the established role of RNF168 in the regulation and facilitation of DNA DSB repair, led to the obvious question whether the absence of either ALKBH3 or FTO would affect the balance of DNA DSB repair pathway choice. Specifically, whether cells lacking either ALKBH3 or FTO would exhibit reduced DSB repair through HR or NHEJ, consequently favoring the adoption of the mutagenic repair pathway, SSA?

5.3.2.1 *HR repair efficiency*

Utilizing single pathway GFP reporter systems to assess HR, NHEJ and SSA repair of DSBs in the absence of ALKBH3 or FTO, we observed an approximate 20% reduction in HR repair upon the depletion of ALKBH3 and FTO (Figure 44). This reduction in HR repair is likely to stem from the downregulation of RNF168 in cells depleted of FTO and ALKBH3. It is possible that partial depletion of RNF168 protein expression observed when FTO and ALKBH3 are KD using siRNA (Figure 29), permitting some HR repair to occur. However, additional investigations are warranted to elucidate these results further as the existing literature presents a varied perspective on the role of RNF168 in HR repair, with contradictory findings regarding its impact following depletion. Some studies using HR-reporter systems indicate that loss of RNF168 and RNF8 does not significantly affect HR (Meerang et al., 2011; Munoz et al., 2012; Sy et al., 2011), while others suggest that these proteins play a regulatory role in HR (Lu et al., 2012; Luijsterburg et al., 2017). More recent research has shed further light on RNF168's involvement in HR as RNF168 has been linked to BRCA1 recruitment to DSB via BARD1. BARD1 binds to RNF168 mediated ubiquitination of H2A/H2AX through its BURD motif which facilitate in the downstream recruitment of PALB2 and RAD51 to DSB (Becker et al., 2021; Krais et al., 2021). Additionally, RNF168 has been shown to recruit PALB2 to the damaged chromatin in a BRCA1 independent manner. Where RNF168 recruits PALB2 via H2A/H2AX ubiquitination and protein-protein interactions between RNF168 and PALB2. RNF168 siRNA mediated KD resulted in impaired PALB2 and RAD51 recruitment to DSB, defective HR repair and PARPi sensitivity, a hallmark of HR defect (Luijsterburg et al., 2017). This RNF168-PALB2 interaction has also been shown to mask BRCA1 haploinsufficiency and provide PALB2 dependent HR in *BRCA1* heterozygous

mouse cells (D. Zong et al., 2019). Additionally, RNF168 has been observed to assume an interesting role in BRCA1 null cells, where a downregulation of RNF168 protein expression has been noted in *BRCA1* mutated cell lines and primary tumors. This diminished expression of RNF168 protein has been associated with the facilitation of BRCA1 null cancer cell proliferation by balancing the levels of HR and NHEJ activity (Krais et al., 2020).

Considering these recently revealed associations between RNF168 and HR repair along with data presented in this thesis, demonstrating loss of RNF168 protein expression following ALKBH3 and FTO KD (Figure 20 and Figure 29), it is somewhat expected that the depletion of ALKBH3 and FTO would influence the HR repair efficiency in U2OS cells (Figure 44). The implications of decline in RNF168 protein expression due to ALKBH3 and FTO on the viability of BRCA1 null cells or for the promotion of PALB2-RAD51 dependent HR repair in *BRCA1* deficient cells remain to be fully elucidated but presents an interesting future research topic.

5.3.2.2 *c-NHEJ and SSA repair efficiency*

C-NHEJ was not affected by the loss of ALKBH3 whereas depletion of FTO resulted in an approximately 30% decrease c-NHEJ repair efficiency (Figure 45). The observation that ALKBH3 KD had little to no effect on NHEJ repair, while depletion of FTO led to a reduction, was surprising. Given that depletion of either ALKBH3 or FTO results in decreased RNF168 protein expression (Figure 20 and Figure 29) along with impaired recruitment of 53BP1 to DSB (Figure 19 and Figure 30) one would anticipate a more pronounced effect on c-NHEJ in the absence of ALKBH3, potentially comparable to the effect observed with FTO depletion. It is conceivable that during ALKBH3 KD, there might be sufficient RNF168 expression to sustain NHEJ while the impact of FTO KD could potentially have a broader effect on c-NHEJ besides influencing RNF168.

Another surprising result was observed when looking and SSA repair efficiency (Figure 46) as contrary to our expectations, the loss of ALKBH3 or FTO led to a reduction in SSA repair efficiency by 35% and 65%, respectively. This is in contrast with our hypothesized increase in SSA resulting from the downregulation of RNF168 and the reduced recruitment of 53BP1 to DSBs. Based on this preliminary data, both ALKBH3 and FTO appear to influence SSA DSB repair. Should this observation hold true, it is probable that this effect operates independently of their modulation of RNF168, as previous research has indicated an increased utilization of SSA repair mechanisms in the absence of RNF168 (Munoz et al., 2012, Ochs et al., 2016).

It is worth mentioning that the c-NHEJ and SSA repair assays are considered preliminary data (n=2) and should therefore be interpreted with caution. Further validation is required to confirm the accuracy of the results obtained from all three DSB repair reporter assays. The single pathway reporter systems, although widely used, present some limitations such as inability to capture all repair events and sensitivity to

experimental condition. Using siRNA to silence ALKBH3 or FTO could affect cell proliferation or cell cycle thereby exerting an indirect influence on the outcomes of DNA repair assays (Jiao et al., 2016; Li et al., 2024; Liefke et al., 2015; Liu et al., 2023; Shimada et al., 2012; Sun et al., 2023). DNA repair assay results would need to be confirmed using other models. SSA repair could be further evaluated by utilizing PCR setup as previously tested and described by Ochs et al (Ochs et al., 2016). Confocal microscopy could also be utilized to look at recruitment to DSB of pathway specific repair factors after ALKBH3 and FTO KD and induced DNA DSB damage, RAD51 foci (HR-repair), RAD52 foci (SSA-repair) and XRCC4 (c-NHEJ). Furthermore, an intriguing next step could involve the utilization of multi-pathway reporter systems to obtain a more comprehensive perspective on DSB repair pathway activity. This approach could clarify whether ALKBH3 or FTO operate in one or multiple pathways and aid in pinpointing where in the DSB repair network they function. This would be particularly interesting for FTO as it seems to affect all three tested repair pathways, indicating a potentially larger influence on DSB repair beyond influencing RNF168. RNA sequencing data in FTO KD cells (Figure 57) offered some valuable insight into FTO's broader impact on DNA DSB repair. It highlights the downregulation of DNA DSB repair pathways and crucial HR repair factors such as BRCA1 in the absence of FTO.

An important, yet underexplored question is how alt-NHEJ repair is affected by the absence of ALKBH3 and FTO. Alt-NHEJ is considered a backup repair mechanism when HR and c-NHEJ pathways are compromised (Iliakis et al., 2015). Our current findings indicate that the loss of ALKBH3 and FTO impairs HR repair and, in FTO-depleted cells, also affects c-NHEJ, without an increase in SSA repair. This suggests the possibility that cells deficient in ALKBH3 and FTO may rely on alt-NHEJ for double-strand break repair.

To recap, the preliminary DNA repair assay results suggest that depletion of either ALKBH3 or FTO leads to altered DNA DSB repair dynamics, likely linked, at least in part, to the observed downregulation of RNF168 in ALKBH3 and FTO KD cells. Silencing FTO and ALKBH3 with siRNAs induces a notable reduction in RNF168 protein expression, albeit not complete obliteration. This alteration in the cellular abundance of RNF168 is likely to affect the chromatin response to DNA DSBs. Both ALKBH3 and FTO may influence DSB repair by targeting factors beyond RNF168, as evidenced by FTO's impact on *BRCA1* expression (Figure 57). Given their role as mRNA demethylases, it is plausible that they affect additional DNA DSB repair factors which could provide potential explanation for the outcomes of DNA repair assays and underscores the necessity for further investigation.

5.3.3 ALKBH3 and FTO: Impact on genomic stability and response to genotoxic agents

Maintaining genome integrity relies on equilibrium in the choice of DNA DSB repair pathways. Disruption of this balance is a recognized source of genomic instability as each DSB repair pathway is tailored for specific circumstances, and an improper choice can result in inefficient repair (Ceccaldi et al., 2016). Our data so far has established that depleting cells of either ALKBH3 or FTO resulted in both loss of recruitment of 53BP1 (Figure 19 and Figure 30) and altered DNA DSB repair dynamics (Figure 44-Figure 46). From this we argued that loss of either ALKBH3 or FTO is likely to affect genomic stability of cells.

Using widely adopted genomic instability assays micronuclei assay and chromosome metaphase spread we establish an elevated level of genomic instability upon the depletion of either ALKBH3 or FTO (Figure 47-Figure 48). Lack of ALKBH3 and FTO resulted in approximately 2-fold increase in micronuclei formation compared to the control sample. Comparable findings were observed in CRISPR-Cas9 KO ALKBH3 and FTO clones, where a 3-fold increase in micronuclei was evident compared to WT U2OS cells (Figure 50), slightly exceeding the micronuclei formation observed in previous siRNA experiments. Similar outcomes were observed in the metaphase spread analysis for ALKBH3 depletion (Figure 47), with number of spontaneous chromosomal aberrations roughly doubling in cells lacking ALKBH3 compared to control cells. Intriguingly, the loss of FTO led to a higher number of chromosomal abnormalities than the loss of ALKBH3, reaching a comparative level with the positive control BRCA2.

Both FTO and ALKBH3 have previously been linked to maintenance of genomic integrity. ALKBH3's main role is catalyzing the demethylation of alkylating damage (m^3C) from ssDNA, thereby protecting the cellular genome from alkylating damage. This process preserves the integrity of DNA, contributing to the preservation of genomic stability (Dango et al., 2011). The results presented in this thesis demonstrate that ALKBH3 plays a role in efficient DNA DSB repair providing evidence of a crosstalk between DNA alkylation and DNA DSB repair. This is not the first instance where a connection between the alkylation repair and DSB repair pathways has been recognized, as ALKBH3 has previously been shown to have a direct protein-protein interaction with the RAD51 paralogue, RAD51C, a key player in HR. In their 2019 publication, Mohan and colleagues demonstrate that ALKBH3 interacts with RAD51C and that these interactions might enhance ALKBH3-mediated repair of alkyl-adducts in 3'-tailed DNA, indicating that a HR repair factor was influencing ALKBH3 mediated repair (Mohan et al., 2019). The findings presented in this thesis serve as juxtaposition, indicating that an alkylating repair factor may also influence DSB repair.

Unlike ALKBH3, FTO does not have an established role as an alkylating damage repair enzyme and has not been associated with DSB repair. Still, the loss of FTO in mouse spermatogonia has been demonstrated to result in elevated genomic instability as FTO

depletion led to aberrant chromosome segregation and G2/M cell cycle arrest (Huang et al., 2018). Furthermore, FTO has displayed a functional role in the genotoxic stress response as an m^6A associated protein (Xiang et al., 2017; Q. Zhang et al., 2019). Specifically, FTO is mobilized to sites of DNA damage induced by UV exposure, playing a crucial role in dynamically regulating a distinct m^6A RNA mark essential for the effective repair of DNA damage caused by UV radiation. More recently published research has demonstrated that FTO plays a more substantial role in the DNA damage response to a number of DNA damage stimuli by influencing cell-cycle progression (Liu et al., 2023). According to the results presented in this body of work, neither FTO nor ALKBH3 were observed to be localized to the DNA DSB site when DSB were induced, as indicated by the absence of overlap between FTO (Figure 31) or ALKBH3 (Figure 24C) and the DNA DSB marker γH2AX. This lack of co-localization along with the affect we note on mRNA export (Figure 27-Figure 28 and Figure 37-Figure 38) and protein levels of RNF168 (Figure 20 and Figure 29) in the absence of either ALKBH3 or FTO suggests that it is improbable for either of these demethylases to be involved in the local regulation of RNF168 at DNA damage sites.

Clonogenic assays performed in both siRNA-treated cells (Figure 51) and in ALKBH3- and FTO-CRISPR-Cas9 KO clones (Figure 52) demonstrated increased sensitivity to the genotoxic agents, NCS and MMC in cells lacking ALKBH3 and FTO, suggesting that both FTO and ALKBH3 contribute to survival in response to genotoxic stress. These results could be interesting from a clinical perspective as previous research by the Sigurdsson laboratory and others have demonstrated ALKBH3 expression is downregulated by promoter methylation across several different cancer types (Esteve-Puig et al., 2021; Knijnenburg et al., 2018; Stefansson et al., 2017) and that loss of ALKBH3 has been shown to be clinically relevant and to affect survival in breast cancer (Stefansson et al., 2017) and Hodgkin's lymphoma (Esteve-Puig et al., 2021). ALKBH3 deficiency might be a potent biomarker to predict treatment outcomes in cancer and be valuable contribution to personalized cancer management. Data presented in this body of work indicates that cancer patients with high ALKBH3 promoter methylation might benefit from cancer treatment using DNA-damaging agents or genotoxic agents which cause DSB and increase genomics instability. These include platinum-based chemotherapy agents, topoisomerase inhibitors or radiation therapy.

In contrast to ALKBH3, there have been no documented instances of FTO being silenced in cancer due to promoter methylations. Nevertheless, numerous examples exist of FTO gene variants linked to heightened cancer susceptibility (Lan et al., 2020) in particular breast cancer (Kaklamani et al., 2011), with the increased risk often being associated with obesity. There is however instance of increased cancer risk due to FTO variants without any links to obesity. These include melanomas and HER2 breast cancer. The increased risk is not well understood. However, given the results presented in this study including the increased genomic instability and response to genotoxic agents it could be possible that FTO regulation of RNF168 and influence on DBS signaling could

contribute to cancer formation meaning that loss of FTO could present as markers for cancer development. Similar to loss of ALKBH3, loss of FTO could present as possible targets for treatment using chemotherapy treatment causing DSB and increased genomic instability.

5.3.4 Exploring the extended role of FTO and ALKBH3 in genomic stability maintenance

An intriguing observation emerged when analyzing results from both the genomic instability assays and clonogenic survival assay, where the genomic instability phenotypes in FTO-depleted cells surpassed what could be solely attributed to decreased RNF168 expression. For instance, the levels of metaphase aberrations (Figure 47) and NCS-induced cell death (Figure 51 C-D) were higher in FTO KD cells compared to RNF168-deficient cells, approaching similar levels observed in the positive control of BRCA2-depleted cells. Additionally, while not as pronounced as the response to NCS-induced death, both ALKBH3 and FTO-depleted cells exhibited a slightly heightened response to MMC treatment compared to RNF168-depleted cells, although not statistically significant. Given that MMC is a known alkylating agent that induces alkylating damage, it is not unexpected that cells depleted of ALKBH3 exhibit an enhanced response to MMC (Dusre et al., 1989).

From these observations, we theorized that FTO (and possibly ALKBH3) might play a broader role in safeguarding genome integrity, beyond their epitranscriptomic regulation of RNF168. We therefore carried out RNA sequencing of U2OS cells treated with control, FTO and ALKBH3 siRNA. Differential expression analysis demonstrated 268 differentially expressed transcripts in cells depleted of ALKBH3 (Figure 53A) and 2716 in FTO depleted cells (Figure 53B). *RNF168* exhibited no significant differential expression in either sample, reinforcing the hypothesis that ALKBH3 and FTO do not influence transcription levels of *RNF168*, as previously observed through qPCR analysis (Figure 24A and Figure 34 A).

5.3.4.1 *FTO influence on BRCA1*

Analyzing the RNA sequencing data revealed that the DNA Double Strand Break Repair pathway was downregulated in cells depleted of FTO (Figure 55A). Looking further into the downregulated transcripts, revealed 9 DNA DSB repair related genes to be significantly downregulated in FTO KD cells, including *BRCA1*. When validating the *BRAC1* downregulation in FTO KD cells through western blot analysis, we observed a small decrease in BRCA1 protein expression when compared to control siRNA sample (Figure 58 A). *BRAC*1 is known to be alternatively spliced and has 40 different splice variants, 26 of which are protein coding (Ensembl, 2023). In our RNA sequencing dataset, a predominant proportion of the protein coding *BRCA1* transcripts were found to have a negative log fold change, however only one *BRCA1* transcript was found to be significantly downregulated when compared to control sample (p-value 0,035017).

This transcript produces one of the larger BRCA1 protein structures (1884 aa), labelled by the UniProt database as BRCA1 isoform 7 (UniProt ID: P38398-7) and is different from the chosen canonical *BRCA1* transcript (ENST00000357654.9) (UniProt ID: P38398-1) as it contains an alternatively spliced exon (aa residue 1453 – 1474). The inclusion of the alternative exon results in an extra 21 amino acids within the BRCA1 serine cluster domain (SCD), amino acids 1280-1524 (Clark et al., 2012). The SCD domain, rich in putative phosphorylation sites, undergoes phosphorylation by ATM/ATR kinases both *in vitro* and *in vivo* which facilitates the recruitment of BRCA1 to DSBs sites (Cortez et al., 1999).

Whether FTO is directly influencing alternative splicing of a specific *BRCA1* exon and thereby affecting BRCA1 localization to DNA damage or if FTO KD causes general downregulation of *BRCA1* remains unclear and demands further investigations. Current BRCA1 antibodies cannot distinguish between the BRCA1 isoforms making it hard for us to confirm if solely one *BRCA1* transcript is being affected by FTO KD (Figure 58). Other methodological limitations in our RNA sequencing approach include the relatively small number of replicates (n=4) and the absence of RT-qPCR assays to validate *BRCA1* downregulation post-FTO KD. While our four biological replicates exhibited general uniformity, a larger dataset would offer greater clarity regarding FTO's impact on BRCA1. However, the impact of FTO on *BRCA1* aligns with the slight reduction observed in HR repair in FTO-depleted cells (Figure 44). This correlation along with FTO's influence on other DSB repair genes (Table 14) may offer insights into the increased response to genotoxic agents and genomic instability phenotype observed in FTO-depleted cells compared to those lacking RNF168.

5.3.4.2 *ALKBH3's influence on cellular stress response.*

Gene ontology and functional enrichment analysis in cells depleted of ALKBH3 (Figure 54) revealed considerably lower number of affected targets compared to the depletion of FTO, which is in line with previous studies showing a moderate impact of ALKBH3 depletion on gene expression (Liefke et al., 2015). The disparity observed may be attributed to the distinct roles these proteins assume as mRNA demethylases, with FTO primarily involved in the removal of the more prevalent mRNA modification m^6A, in contrast to ALKBH3, which predominantly targets the less common m^1A modification.

Gene set enrichment analysis in ALKBH3 KD sample revealed that genes related to the cellular stress response were differentially expressed (Figure 54). Upon a more in-depth exploration of differentially expressed stress-related genes, our analysis identified three stress-related genes displaying significant downregulation and two exhibiting upregulation (Figure 56). Notably, the downregulated genes encompassed *ALKBH3* itself, alongside *GTF2H4* (General Transcription Factor IIH Subunit 4), which also plays a role in NER (Theil et al., 2023) and *DNAJB12* (DnaJ homolog subfamily B member 12), while the upregulated genes included *FXR1* (FMR1 Autosomal Homolog 1) and *RTN4R* (Reticulon-4 receptor).

In recent years, research has established a connection between the cellular stress response and the m^1A RNA modification, along with its associated proteins. ALKBH3 has previously demonstrated protective role against cellular stress through active participation in the demethylation of tRNA (Z. Chen et al., 2019) and the m^1A methyltransferase proteins TRMT6 and TRMT61A have been implicated in the formation of stress granules (SG). SG, which form as a response to stress, are transient and reversible structures involved in regulating gene expression and protecting cells during stress by sequestering and storing untranslated mRNAs (Protter et al., 2016). Loss of either TRMT6 or TRMT61A in HeLa cells impaired SGs formation and increased sensitivity to stress stimuli (Alriquet et al., 2021).

RNA sequencing data revealed alterations in cellular stress response subsequent to ALKBH3 KD, suggesting an influence on the stress response. The observed reduction in general transcriptional factors, such as GTF2H4, is a common occurrence in response to cellular stress (Himanen et al., 2019) and downregulation of the heat shock protein DNAJB12, which are known for their protective role against stress (Hu et al., 2022). Perhaps the most interesting stress related gene found differently expressed after ALKBH3 KD was *FXR1* which is considered a stress responsive gene that plays a role in SG dynamics and function (Didiot et al., 2009; Khan et al., 2024; Law et al., 2023). These findings suggest that cells lacking ALKBH3 may experience increased stress levels. This raises the possibility that ALKBH3 depletion could lead to the downregulation of protective stress-response proteins, such as DNAJB1, ultimately resulting in increased stress and the upregulation of a stress responsive proteins like FXR1.

Another possible explanation for the altered stress response in cells depleted of ALKBH3 could stem from the heightened genomic instability characteristic of ALKBH3 deficient cells (Figures 47, 48, and 50). Increased genomic instability is known to be a contributing factor to heightened cellular stress and the observed alterations in the expression of stress-related genes may be attributed, at least in part, to the increased genomic instability in cells lacking ALKBH3. One additional aspect to consider is that ALKBH3 may directly regulate these stress-responsive genes as an m^1A demethylase. Further investigations, including validation of ALKBH3's impact on stress response-related genes and its biological relevance are necessary to clarify these intricate interactions.

5.3.4.3 *Interactions of ALKBH3 and FTO with DNA repair proteins: A protein-protein perspective*

In addition to utilizing RNA sequencing findings to enhance our understanding of ALKBH3 and FTO's role in maintaining genomic stability, we revisited the results obtained from the co-IP/MS assay (Table 13 and Appendix D) to explore potential protein-protein interactions. Interestingly, the co-IP/MS data unveiled interactions

between ALKBH3 and FTO with various DNA repair-related proteins, providing further indications of their potential involvement in maintaining genomic stability and participating in DNA repair processes.

PRDX1 emerged as the sole shared DNA repair protein interacting with both ALKBH3 and FTO. As an antioxidant, PRDX1 protects cells from oxidative stress by catalyzing the reduction of various peroxides, including hydrogen peroxide. Recent research has established a connection between PRDX1 and DNA damage repair, specifically DSB repair. Deficiency of PRDX1 has been shown to compromise HR-induced DSB repair, resulting in heightened levels of DNA damage (Skoko et al., 2022). In a recent study Morett et al. identified PRDX1 as a DNA damage surveillance factor, relocating to the nucleus upon DNA damage to mitigate nuclear reactive oxygen species (Moretton et al., 2023). ALKBH3 was also found interacting with the previously discussed RNA binding protein hnRNPC which has been shown to be part of a nucleoprotein complex along with PALB2, BRCA1 and BRCA2. siRNA mediated KD of hnRNPC resulted in altered DSB repair dynamics as it reduced HR repair and caused downregulation of HR proteins such as RAD51, BRCA1, BRCA2 and BRIP1, partially due to diminished mRNA expression caused by altered mRNA splicing (Anantha et al., 2013).

Another interesting finding from the co-IP/MS assay were interactions between ALKBH3/FTO and proteins implicated in RNF168 regulation or regulated by RNF168, including PRMT5, TRIP12, and DHX9. ALKBH3 (catalytically dead version) was found to interact with TRIP12, a regulator of RNF168 known to modulate chromatin ubiquitination (Gudjonsson et al., 2012). Additionally, ALKBH3 (wild type) was found interacting with protein Arginine Methyltransferase 5 (PRMT5), a methyltransferase known to play a diverse role in the DDR and genomic stability maintenance by epigenetic, post-transcriptional, and post-translational mechanisms (Koh et al., 2015).

In glioblastomas PRMT5 has been found to promote *RNF168* transcription by maintaining a histone methylation mark on the RNF168 promoter region thereby enhancing the DNA damage response and induce chemo-radiant resistant in glioblastoma tumor (Du et al., 2019). In prostate cancer PRMT5 functions as an epigenetic activator that upregulates expression of various genes involved in DSB repair including *KU70/80*, *BRCA1*, *BRCA2* and *RAD51* (Owens et al., 2020). PRMT5 also influences DDR protein expression through targeted RNA modifications, contributing to doxorubicin resistance in breast cancer by facilitating the nuclear translocation of the RNA demethylase ALKBH5 which in turn removes m^6A from *BRCA1*, leading to mRNA stabilization and heightened DNA repair competency (Wu Wang et al., 2022). Additionally, PRMT5 regulates genomic stability via post-translational modifications of DDR proteins like p53 and 53BP1 (Hwang et al., 2021; Hwang et al., 2020). Overall, PRMT5 serves as a multifaceted regulator of genomic stability through diverse pathways. Whether ALKBH3 contributes to the PRMT5 mediated DDR response via their protein-protein interactions remains to be determined. Nonetheless, the intriguing

aspect lies in the interaction between ALKBH3 and a protein with such wide-reaching impact on genomic stability and the DDR. Further investigations are warranted to determine whether ALKBH3 can influence other aspects of the DDR beyond its known role in epitranscriptomic regulation of RNF168 through protein-protein interactions with PRMT5.

In its catalytically inactive state, FTO was found to interact with DHX9 (ATP-dependent RNA helicase A), a versatile protein with regulatory functions in various cellular processes, including DNA replication, transcription, translation, and the maintenance of genomic stability (Lee et al., 2016). DHX9 plays a role in DSB repair by recruiting BRCA1 to RNA generated by the RNA polymerase II transcription complex, where DHX9 along with BRCA1 facilitate end resection and the repair of DNA damage by HR. (Chakraborty et al., 2021). Recent research by Patel et al demonstrated that RNF168 suppresses R-loop formation in *BRCA1/BRCA2*-deficient cells by ubiquitinating DHX9, thereby facilitating its recruitment to R-loops and preventing their excessive accumulation and preserving genomic stability (Patel et al., 2021). The interaction between FTO and DHX9 presents intriguing possibilities and prompts questions about FTO's involvement in cellular processes in which DHX9 plays a role.

Another interesting interaction between FTO (catalytic dead version) worth mentioning is the heterogeneous nuclear ribonucleoprotein RBMX (also known as hnRNPG). While RBMX is predominantly recognized for its role in regulating pre- and post-transcriptional processes, such as pre-mRNA splicing, it has also been implicated in influencing DNA DSB repair. In a 2012 study RMBX was found to be recruited to DSB in a PARP1 dependent manner where it promoted HR repair by facilitating BRCA2 expression. Depleting U2OS cells of RMBX using siRNA resulted in loss of IR-induced RAD51 foci formation, downregulation of BRCA2 protein expression and decreased HR repair efficiency (Adamson et al., 2012). RMBX has also been connected to the maintenance of genomic stability in other ways then regulating HR repair. In a 2020 study RMBX was shown to be a pivotal factor in maintaining genome stability during replication as it was required for the activation of ATR in response to replication stress. Depletion of RBMX in cells results in replication defects, leading to increased genomic instability, such as elevated micronuclei formation and a high rate of sister-chromatid exchange (T. Zheng et al., 2020). As RBMX has also a m^6A reader it is interesting to speculate if its protein interaction with FTO is due to their m^6A connection or if FTO might be participating in any of RBMX many roles in maintaining genomic stability.

It is crucial to emphasize that the interaction observed between FTO and ALKBH3 and the DNA repair proteins identified needs validation to draw definitive conclusions regarding the potential involvement of ALKBH3 or FTO in DNA repair pathways associated with these proteins.

In conclusion, the results from the second part of this thesis have demonstrated that both ALKBH3 and FTO promote efficient DNA DSB chromatin signaling. The depletion of ALKBH3 or FTO results in the diminished recruitment of essential repair factors to damaged chromatin, thereby altering the dynamics of DSB repair. Consequently, cells

lacking ALKBH3 and FTO exhibit genomic instability and increased susceptibility to genotoxic agents inducing DSBs. Moreover, the interaction of both proteins with other DNA damage response proteins suggests a potential broader role in genomic stability maintenance. Finally, RNA sequencing data revealed that depletion of FTO causes downregulation of the DSB repair pathway, impacting crucial repair factors, including BRCA1. These findings point to a possible broader role for FTO in influencing the DNA damage response, surpassing its epitranscriptomic regulation of RNF168.

5.4 Future perspectives and limitations of study

5.4.1 Identification of methylation sites on the *RNF168* transcript

Data presented in this thesis indicates that RNF168 is epitranscriptomically regulated by the demethylases ALKBH3 and FTO where ALKBH3 removes m^1A and FTO m^6A from the *RNF168* mRNA to promote effective mRNA export and normal protein expression of RNF168. However, the current research is limited by the lack of precise identification of the m^1A and m^6A methylation sites on the *RNF168* transcript. Identification of the methylated sites on the *RNF168* transcript is crucial for validating the accuracy of our proposed model. Therefore, a necessary future step would be to determine the precise location of the m^6A and m^1A methylation sites within the *RNF168* transcript. Locating the methylation sites on *RNF168* would provide an opportunity to introduce mutations, rendering them unable to be methylated with m^1A or m^6A, and enable assessment of *RNF168* mRNA nuclear retention and reduced protein expression.

One weakness in our methodology is the MeRIP-qPCR assay used to identify methylation of the *RNF168* transcript due to the reliance on m^1A or m^6A methylation-specific antibodies whose specificity varies. Notably, the m^6A specific antibodies utilized in this study lack the capability to differentiate the m^6A and the m^6A_m modification, making it hard to definitively confirm that FTO's targeted modification removed from *RNF168* as m^6A rather than m^6A_m. Although FTO's cellular location has previously been shown to affect its substrate specificity (Wei et al., 2018), with FTO having more affinity towards m^6A in the nucleus an m^6A_m in the cytoplasm and in our experimental model, U2OS cells, FTO is mainly expressed in the nucleus it does not definitively exclude the possibility that m^6A_m might be influencing RNF168. Future investigations should focus on elucidating FTO's specific methylation target on *RNF168*. A possible next step entails employing advanced sequencing techniques such as third-generation sequencing, notably Nanopore sequencing, to confirm the presence and precise localization of m^6A modifications on the *RNF168* transcript. Previous studies have demonstrated the capability of Nanopore sequencing to detect m^6A modifications on RNA (Liu et al., 2019). In the Sigurdsson laboratory, a master's project has been started to investigate this matter and preliminary Nanopore sequencing runs have commenced using mRNA isolated from U2OS cells treated with both FTO and control siRNA. The primary objective is to verify the presence and precise location of m^6A

modifications on the R*NF168* transcript utilizing the PromethIon Nanopore platform for sequencing analysis.

The m^1A antibody (MBL life science #D345-3) used in the m^1A-RIP-qPCR has also come under scrutiny for being unspecific as research from 2019 demonstrated that the m^1A antibody which has been used in many m^1A-RIP-seq analysis was also able to bind to the m^7G-cap resulting in false-positive hits in the 5'UTR (Grozhik et al., 2019). To verify the presence of m^1A on the *RNF168* transcript, a potential future approach could involve replicating the m^1A-RIP-qPCR assay using alternative m^1A antibodies as advancements in m^1A antibody development have expanded the range of available options. As of the present writing, third-generation sequencing methods are not capable of identifying the m^1A modification. Consequently, Nanopore sequencing is not suitable for pinpointing the m^1A methylation site on the *RNF168* transcript. Alternatively, non-antibody-dependent second-generation RNA sequencing methods, such as m^1A-quant-seq could be used for m^1A detection. These sequencing approach rely on reverse transcriptase that introduce mutations at specific RNA modification sites during reverse transcription, facilitating the precise identification of the m^1A modification site (Zhou et al., 2019).

To further strengthen our hypothesis regarding the regulatory role of FTO and ALKBH3 in RNF168 expression through their demethylase activities, rescue experiments would provide further validation. These experiments involve reintroducing ALKBH3 or FTO into cells previously depleted of these enzymes and examining RNF168 protein expression. Multiple rescue experiments have been attempted by the Sigurdsson laboratory but have unfortunately proved challenging. Attempts have been made using siRNA-treatment in conjunction with siRNA-resistant ALKBH3 or FTO plasmids, and confocal microscopy to assess 53BP1 and RNF168 recruitment to DSB site. Unfortunately, over expression of ALKBH3 and FTO using FLAG-tagged plasmid in combination with siRNA treatment and induction of DSB using NCS proved too toxic, rendering it difficult to observe a healthy DNA damage response in the cells. In an effort to try and circumvent the toxic effect of combined siRNA and plasmids treatment current rescue experiments have focused on utilizing the established ALKBH3 and FTO CRISPR-Cas9 KO cells models along with WT and catalytically inactive mutants of FTO or ALKBH3 plasmids. Preliminary confocal microscopy data on 53BP1 recruitment to DSB in ALKBH3 and FTO KO cells transfected with WT and CD plasmids have been attempted and preliminary data looks promising, however further optimization is required.

5.4.2 Validation of protein-mRNA interaction

An additional next step in future research entails the validation of the protein-RNA interaction between *RNF168* mRNA and ALKBH3 and FTO. The research outlined in this thesis has presented evidence suggesting that ALKBH3 and FTO do not engage with

RNF168 at the protein level (Table 13, Figure 24 B and Figure 34 C). Our current working hypothesis suggests that they influence RNF168 by demethylating its mRNA transcript and confirming the mRNA-protein interaction between *RNF168*-mRNA and ALKBH3/FTO would strengthen our hypothesis. Present methodologies employed to identify RNA-protein interactions include RNA immunoprecipitation (RNA-RIP) or UV/chemical crosslinking and immunoprecipitation (CLIP). RNA-RIP or selectively extract RNA-protein complex from samples and typically involve using high-affinity tags like biotin, where biotinylated RNA probes bind to proteins from cell lysates, followed by purification via agarose or magnetic beads. Proteins are identified via western blotting or mass spectrometry. Alternatively, antibodies specific to the protein of interest can be used to label or isolate the RNA-protein complex, followed by RNA detection through northern blot, RT-PCR or RNA sequencing. CLIP methods function by cross-link RNA and protein, then purify the protein of interest and identify bound RNAs using RT-PCR or high-throughput RNA sequencing. Both methods have advantages and disadvantages, with CLIP potentially allowing for the identification of the RNA consensus motifs for ALKBH3 and FTO.

5.4.3 mRNA demethylases and mRNA maturation

The initial segment of this thesis presents evidence suggesting that methylations on the *RNF168* transcript are important to its mRNA maturation. Our findings illustrate that the depletion of ALKBH3 and FTO leads to increased nuclear retention of RNF168 mRNA, underscoring the significance of methylation removal for normal *RNF168* mRNA export. Moreover, other proteins associated with m^1A and m^6A have shown similar effects on RNF168 protein expression and nuclear retention, supporting our hypothesis regarding the involvement of m^1A and m^6A methylation in *RNF168* mRNA maturation. As previously discussed, confirming the location of methylations on the *RNF168* transcript is crucial for validating our hypothesis along with gathering additional biological replicates from preliminary data (Appendix C).

Both ALKBH3 and FTO were found to interact with numerous RNA binding proteins, including members of the hnRNP and SR protein families, known for their roles in important mRNA processes such as splicing, translation, and export. Further validation of these protein interactions would be prudent, along with efforts to elucidate their implications, particularly regarding if other mRNA maturation processes are influenced by ALKBH3 and FTO. Investigating whether depleting ALKBH3 or FTO affects pre-mRNA splicing of *RNF168* would be advisable as defects in mRNA export might be caused by the accumulation of un-spliced mRNA forms (Bartosovic et al., 2017). As of the current literature, there is no documented evidence supporting the existence of alternative spliced forms of *RNF168*. However, this absence of information does not diminish the significance of investigating this aspect or the notion that mRNA methylations could play a role in constitutive or alternative splicing of *RNF168*. Notably, a brief *in silico* analysis of the 3′ and 5′ splice sites across the six exons constituting the

RNF168 transcript revealed a potential 3′ weak splice site on exon 2 (data not shown), suggesting the possibility of an alternatively spliced exon (Yeo et al., 2004). The potential involvement of methylation marks on the *RNF168* transcript in both splicing and export, and the possible roles of FTO and ALKBH3 within the intricate network of proteins required for *RNF168* mRNA processing, merit consideration.

5.4.4 Impact of FTO and ALKBH3 on DNA repair: Potential cancer targets and biomarkers

An intriguing path for future exploration involves investigating our findings within a pathological context. As has been previously described both ALKBH3 and FTO are found aberrantly expressed in numerous cancers, each with distinct implications, therefore ALKBH and FTO represent intriguing candidates as potential biomarkers in cancer diagnosis and prognosis. Their aberrant expression patterns, with upregulation in some cancers and downregulation in others, highlight their complex roles in cancer biology. Furthermore, the correlation between their downregulation and poorer patient survival underscores their potential as therapeutic targets. Future research efforts aimed at elucidating the precise mechanisms underlying the dual functions of ALKBH3 and FTO could pave the way for their utilization as novel diagnostic tools and therapeutic targets in the fight against cancer.

In some instances, as has been previously mentioned, downregulation of ALKBH3 expression has been linked with reduced survival in cancer as reported by the Sigurdsson laboratory and others (Esteve-Puig et al., 2021; Knijnenburg et al., 2018; Stefansson et al., 2017). Downregulation of FTO has also been observed in number of cancers correlating with worse survival, this is mostly related to its m^6A demethylase activity or due to increased risk of obesity (Jeschke et al., 2021; Lan et al., 2020; Ruan et al., 2021; Wu et al., 2019). However genetic variants in FTO have also been associated with an increased risk of cancer independent of obesity, including melanoma and HER2-positive breast cancer (Iles et al., 2013; Montazeri et al., 2022) where the mechanism behind increased risk of melanoma or HER2 in not well understood. Similarly, the mechanisms underlying the relationship between elevated levels of ALKBH3 promoter methylation (>20%) in breast cancer and the subsequent decrease in patient survival remain poorly understood. Considering the findings presented in current thesis, which demonstrate that depleting cells of ALKBH3 or FTO leads to increased genomic instability—a well-established hallmark of cancer—it is conceivable that lack of either ALKBH3 or FTO play contributory roles in cancer formation.

An intriguing avenue for further exploration in ALKBH3 and FTO research involves conducting functional analyses of the FTO gene variants identified in melanoma and HER2-positive cancers. This would entail investigating how these genetic alterations influence the functionality of FTO and its impact on cancer development and

progression. Similarly, investigations into the role of high ALKBH3 promoter methylation in breast cancer could shed light on whether could ALKBH3 functions as a tumor suppressor gene in breast cancer. Understanding the implications of ALKBH3 loss, potentially leading to increased alkylating damage and heightened DSB damage, as suggested by results from this thesis, could provide valuable insights into cancer pathogenesis. The goal of this analysis is to gain insights into the molecular mechanisms underlying cancer development, identifying if ALKBH3 or FTO presents as potential therapeutic targets, and inform personalized treatment strategies for cancer patients.

Another interesting direction for future inquiry in this project entails investigating the possibility of targeting ALKBH3 or FTO to restore synthetic lethality in HR-deficient cancers, given their influence on RNF168. As previously noted, in the absence of BRCA1 or when BRCA1 fails to interact with PALB2, RNF168 becomes essential for PALB2 recruitment (Krais et al., 2021; Luijsterburg et al., 2017; D. Zong et al., 2019). Restoring HR in BRCA1-deficient cells by relying on RNF168 ubiquitin dependent backup pathway to recruit PALB2 could lead to weaknesses that might be targeted to induced synthetic lethality in *BRCA1* deficient cells. Targeting the RNF168-PALB2 axis could potentially mitigate or overcome PARP inhibitor resistance in a substantial subset of *BRCA1* mutant cancers. RNF168 deficiency has been shown to suppress BRCA1-associated mammary tumorigenesis in a mouse model, while low *RNF168* mRNA levels in HR-defective human breast cancer correlate with improved patient survival. Moreover, loss of RNF168 suppresses *in vitro* and *in vivo* growth of BRCA1 and BRCA2-deficient tumors and enhances their sensitivity to PARP inhibitors (Patel et al., 2021) and targeting RNF168 in *BRCA1* and *53BP1* null cells has been shown to reverse PARPi resistance (D. Zong et al., 2019). The potential impact of targeting ALKBH3 or FTO to overcome PARPi resistance through their epitranscriptomic regulation of RNF168 remains unexplored, yet it represents a compelling area for further investigation. To address this, a master's project was initiated within the Sigurdsson laboratory to investigate the impact of ALKBH3 and FTO on cellular response to PARPi and assess whether targeting either enzyme could restore synthetic lethality to PARPi. Additionally, diminished RNF168 protein expression due to ALKBH3 or FTO KD might hold significant implication for *BRCA1* mutation carriers. The factors contributing to cancer formation in *BRCA1* mutation carriers are not fully understood, however evidence suggests that cells carrying one germline mutated *BRCA1* allele experience increased replication stress and genomic instability (Pathania et al., 2014). As *BRCA1* haploinsufficiency can be masked by RNF168 mediated PALB2 recruitment (D. L. Zong et al., 2019), RNF168 protein expression might become a crucial factor for maintaining genomic stability in *BRCA1* mutation carriers.

Lastly, a limitation to the methodology used in this body of work is the lack of validation of findings *in vivo*. To date, all genetic stability assays and assessments of cell survival following genotoxic exposure have been conducted *in vitro*. Employing *in vivo* assays to

corroborate our findings would bolster the credibility of our hypothesis. Currently, knockout mouse models for FTO and ALKBH3 are accessible, presenting an opportunity to validate our data and to assess ALKBH3 and FTO as potential biomarkers for genotoxic drug treatment.

5.4.5 Exploring novel directions: Expanding the scope of FTO and ALKBH3 research

Numerous avenues for future research exist within this project. ALKBH3 and FTO exhibit a diverse array of effects on various cellular function as RNA demethylases. Data from both RNA sequencing and co-IP/MS provide an excellent starting point to expand the scope of this project in multiple directions.

Firstly, an intriguing pathway for future investigation entails investigating the role of ALKBH3 in the cellular stress response. This includes examining whether the depletion of ALKBH3 and the heightened m^1A methylation has an impact on stress granule formation and overall cellular stress response mechanisms. Secondly, a promising opportunity for investigation involves delving deeper into the impact of FTO on the general maintenance of genomic stability within cells. RNA sequencing data presented in this study has revealed that depleting cells of FTO influence the expression of *BRCA1*. Elucidating if and how FTO is influencing *BRCA1* would be a very interesting future research as FTO has been found aberrantly expressed in breast cancer (Kaklamani et al., 2011; Niu et al., 2019; Wu et al., 2019). Nanopore sequencing techniques (5.4.1) could shed light on potential epitranscriptomic regulation of *BRCA1* by FTO.

Thirdly, the co-IP/MS data unveiled numerous intriguing protein interactions, with a notable emphasis on ALKBH3. Among ALKBH3's binding partners, PRMT5 stands out, given its significant role in DNA repair and genomic maintenance, as previously discussed. Further investigation into the nature of their interaction could prove interesting for the field of DNA repair. PRMT5 represents merely one among several intriguing proteins that engage in interactions with ALKBH3, pointing to a variety of potential research directions for this project. Despite the data for FTO interactions being relatively limited some interesting binding partners such as RMBX and DHX9 were discovered and their interaction with FTO would be an interesting research area. It might prove beneficial to repeat the FTO co-IP/MS assay and consider relocating the FLAG tag to the C-terminus to improve results. An interesting experiment to perform would be replicating the co-IP/MS assay after inducing DNA damage in cells. This approach could be of significant importance in ascertaining whether ALKBH3 and FTO exhibit increased interaction with specific repair factors following the induction of DNA damage. Such findings would provide further insight into the importance of the identified protein-protein interaction and the potential differential roles of ALKBH3 and FTO in DNA repair and maintenance of genomic stability.

Fourthly, an under explored avenue in this project is what role if any mRNA methylations have in the cell's response to DNA damage. For instance, it remains to be determined whether RNF168 exhibits altered methylation patterns on its mRNA following DNA damage induction. Given that the significance of RNF168 becomes the most relevant following DNA damage, it would be interesting to investigate whether inducing DNA damage impacts the methylation levels of RNF168. This inquiry arises from the possibility that induced DNA damage might elevate the expression of ALKBH3 or FTO, resulting in increased demethylation of RNF168. Consequently, this could lead to increased protein expression and a swifter response to DNA damage. Evaluating m^6A and m^1A methylation levels on RNF168 post induction of DSB might give us interesting insight into the significance of mRNA demethylation as a regulatory factor in the response to DSB. This could be accomplished through established methodologies such as MeRIP-qPCR or by the previously described Nanopore sequencing or m^1A-quant-seq approaches.

In recent years growing evidence has unveiled an unexpected and significant role of RNA across different stages of the DDR, sensing damage, guiding repair enzymes to damaged sites and regulating repair gene expression (Vagbo et al., 2020). Recent research has demonstrated that DNA DSB and reactive oxygen species can induce DNA:RNA hybrids (Wei et al., 2015). These hybrids have been found to facilitate the recruitment of particular DNA repair proteins, thus boosting the effectiveness and accuracy of DSB repair processes (Crossley et al., 2019; Teng et al., 2018; Yasuhara et al., 2018). Interestingly the function of RNA in recruiting DNA repair factors bears resemblance to the chromatin surrounding DSB raising the interesting question if like the chromatin, RNA can undergo modifications at the site of DSB and whether the enzymes responsible for writing, reading, and erasing RNA modifications play a crucial role in DSB repair.
Emerging evidence suggests that post-transcriptional RNA modifications may function as a regulatory mechanism influencing DNA repair pathways, thus underscoring the significance of exploring this avenue. In 2020 Chen et al., published a paper suggesting that post-transcriptional modifications of RNA could act as DNA damage codes to regulate DNA repair. They demonstrated that the m^5C methyltransferase, TRDMT1, was recruited to the site of DNA damage where it prompted mRNA m^5C methylation. Loss of TRDMT1 led to loss of RAD51 and RAD52 recruitment and compromises HR repair, revealing that HR repair was influenced by RNA m^5C. Furthermore, loss of TRDMT1 confers PARPi sensitivity both *in vitro* and *in vivo* (Chen et al., 2020). This is not the first recorded instance of RNA methylation influencing the DNA damage response. As we have previously mentioned, the m^6A methylation and its associated proteins have been implicated in DNA damage repair by regulating the UV damage response (Xiang et al., 2017), promote HR repair by aiding in BRCA1 and RAD51 recruitment (Zhang et al., 2020) and to regulate the DNA damage response to reactive oxygen species (Yu et al., 2021).

A promising path for further investigation could involve investigating whether the absence of ALKBH3 or FTO influences RNA methylation at DNA damage sites. Our current findings indicate that neither protein localizes to DSB sites upon their induction (Figure 24 C and Figure 31). However, it raises the question of whether they might be recruited in response to other forms of DNA damage, participating in RNA demethylation to facilitate DNA repair. In their 2017 publication, Xiang et al. demonstrated FTO's localization to sites of UV damage, where it demethylates m^6A from RNA to enhance the repair of UV-induced DNA damage. Thus, it would be intriguing to examine whether the loss of ALKBH3 or FTO affects RNA methylation levels in response to various types of DNA damage.

Additionally, a compelling area for future investigation entails exploring whether ALKBH3 and FTO regulate other mRNA targets similarly to RNF168. Existing research has demonstrated that other DNA repair factors can undergo epitranscriptomic regulation, as exemplified by a recent investigation conducted Wu et al. This study provided evidence of m^6A modification on BRCA1, which is removed by ALKBH5 to maintain *BRCA1* mRNA stability and function (Wu Wang et al., 2022). Utilizing techniques such as Nanopore sequencing and m^1A-quant-sequencing may provide insights into additional mRNA targets influenced by the demethylation activity of FTO and ALKBH3. Furthermore, could ALKBH3 and FTO be regulating other proteins via mRNA demethylation and impaired nuclear mRNA export? The Sigurdsson laboratory has started investigating this using an RNA subcellular isolation kit in conjunction with second-generation RNA sequencing. U2OS cells are subjected to treatment with FTO-siRNA, ALKBH3-siRNA, or a double knockdown of ALKBH3 and FTO, followed by cellular fractionation to isolate RNA from both the cytoplasm and nucleus.

Finally, research has demonstrated that RNF168 mediated ubiquitination is important for other pathways responsible for maintaining genomic integrity, this include resolving R-loops (Patel et al., 2021), DNA crosslinks repair (Katsuki et al., 2021), facilitating (Schmid et al., 2018) and promoting (Yang et al., 2024) DNA replication. What role if any silencing FTO and ALKBH3 has these processes remains unknown, presenting an intriguing avenue for future research.

5.4.6 Final conclusion

The work presented in this thesis provides evidence that ALKBH3 and FTO, members of the AlkB protein family, exert regulatory control over the E3 ubiquitin ligase RNF168, plausibly in an epitranscriptomic manner. The removal of mRNA methylations from the *RNF168* transcript by ALKBH3 and FTO demonstrates how mRNA methylation can influence mRNA export and protein expression of RNF168. These findings thereby reveal how mRNA export can impact the effectiveness of DNA DSB chromatin signaling and additionally provide evidence of crosstalk between two DNA repair pathways, alkylation repair and DNA DSB repair.

Furthermore, our data demonstrates the absence of ALKBH3 or FTO results in impaired recruitment of crucial repair factors to break sites, compromised DNA DSB repair dynamics, genomic instability, and increased susceptibility to genotoxic agents. These findings suggest that the absence of ALKBH3 or FTO may serve as potential markers for cancer treatment response. Overall, this research expands our understanding of epitranscriptomic gene regulation and reveals a novel role for mRNA methylations in governing DNA DSB repair signaling.

This project opens up numerous avenues for future research. The epitranscriptomic regulation of RNF168 by ALKBH3 and FTO represents only the beginning in the exploration of potential targets influenced by these enzymes. It is my hope that the results presented in this thesis will open up opportunities for further research into both DNA damage response and signaling, as well as epitranscriptomics, fostering a deeper understanding of these intricate processes and their implications in health and disease.

References

Aas, P. A., Otterlei, M., Falnes, P. O., Vagbo, C. B., Skorpen, F., Akbari, M., . . . Krokan, H. E. (2003). Human and bacterial oxidative demethylases repair alkylation damage in both RNA and DNA. *Nature*, *421*(6925), 859-863. https://doi.org/10.1038/nature01363

Abakir, A., Giles, T. C., Cristini, A., Foster, J. M., Dai, N., Starczak, M., . . . Ruzov, A. (2020). N(6)-methyladenosine regulates the stability of RNA:DNA hybrids in human cells. *Nat Genet*, *52*(1), 48-55. https://doi.org/10.1038/s41588-019-0549-x

Adamson, B., Smogorzewska, A., Sigoillot, F. D., King, R. W., & Elledge, S. J. (2012). A genome-wide homologous recombination screen identifies the RNA-binding protein RBMX as a component of the DNA-damage response. *Nat Cell Biol*, *14*(3), 318-328. https://doi.org/10.1038/ncb2426

Adhikari, S., Xiao, W., Zhao, Y. L., & Yang, Y. G. (2016). m(6)A: Signaling for mRNA splicing. *RNA Biol*, *13*(9), 756-759. https://doi.org/10.1080/15476286.2016.1201628

Ahnesorg, P., Smith, P., & Jackson, S. P. (2006). XLF interacts with the XRCC4-DNA ligase IV complex to promote DNA nonhomologous end-joining. *Cell*, *124*(2), 301-313. https://doi.org/10.1016/j.cell.2005.12.031

Akhtar, J., Lugoboni, M., & Junion, G. (2021). m(6)A RNA modification in transcription regulation. *Transcription*, *12*(5), 266-276. https://doi.org/10.1080/21541264.2022.2057177

Akichika, S., Hirano, S., Shichino, Y., Suzuki, T., Nishimasu, H., Ishitani, R., . . . Suzuki, T. (2019). Cap-specific terminal N (6)-methylation of RNA by an RNA polymerase II-associated methyltransferase. *Science*, *363*(6423). https://doi.org/10.1126/science.aav0080

Al-Minawi, A. Z., Lee, Y. F., Hakansson, D., Johansson, F., Lundin, C., Saleh-Gohari, N., . . . Helleday, T. (2009). The ERCC1/XPF endonuclease is required for completion of homologous recombination at DNA replication forks stalled by inter-strand cross-links. *Nucleic Acids Res*, *37*(19), 6400-6413. https://doi.org/10.1093/nar/gkp705

Alarcon, C. R., Goodarzi, H., Lee, H., Liu, X., Tavazoie, S., & Tavazoie, S. F. (2015). HNRNPA2B1 Is a Mediator of m(6)A-Dependent Nuclear RNA Processing Events. *Cell*, *162*(6), 1299-1308. https://doi.org/10.1016/j.cell.2015.08.011

Alemu., E. A., He., C., & Klungland., A. (2016). ALKBHs-facilitated RNA modifications and de-modifications. *DNA Repair (Amst)*, *44*, 87-91. https://doi.org/10.1016/j.dnarep.2016.05.026

Alexander, J. L., & Orr-Weaver, T. L. (2016). Replication fork instability and the consequences of fork collisions from rereplication. *Genes Dev*, *30*(20), 2241-2252. https://doi.org/10.1101/gad.288142.116

Alriquet, M., Calloni, G., Martinez-Limon, A., Delli Ponti, R., Hanspach, G., Hengesbach, M., . . . Vabulas, R. M. (2021). The protective role of m1A during stress-induced granulation. *J Mol Cell Biol*, *12*(11), 870-880. https://doi.org/10.1093/jmcb/mjaa023

Altmann, T., & Gennery, A. R. (2016). DNA ligase IV syndrome; a review. *Orphanet J Rare Dis*, *11*(1), 137. https://doi.org/10.1186/s13023-016-0520-1

Altmeyer, M., & Lukas, J. (2013). To spread or not to spread--chromatin modifications in response to DNA damage. *Curr Opin Genet Dev*, *23*(2), 156-165. https://doi.org/10.1016/j.gde.2012.11.001

Anantha, R. W., Alcivar, A. L., Ma, J., Cai, H., Simhadri, S., Ule, J., . . . Xia, B. (2013). Requirement of heterogeneous nuclear ribonucleoprotein C for BRCA gene expression and homologous recombination. *PLoS One*, *8*(4), e61368. https://doi.org/10.1371/journal.pone.0061368

Anderson, J., Phan, L., & Hinnebusch, A. G. (2000). The Gcd10p/Gcd14p complex is the essential two-subunit tRNA(1-methyladenosine) methyltransferase of Saccharomyces cerevisiae. *Proc Natl Acad Sci U S A*, *97*(10), 5173-5178. https://doi.org/10.1073/pnas.090102597

Antoniou, A. C., Foulkes, W. D., & Tischkowitz, M. (2014). Breast-cancer risk in families with mutations in PALB2. *N Engl J Med*, *371*(17), 1651-1652. https://doi.org/10.1056/NEJMc1410673

Ao, J. Y., Zhu, X. D., Chai, Z. T., Cai, H., Zhang, Y. Y., Zhang, K. Z., . . . Sun, H. C. (2017). Colony-Stimulating Factor 1 Receptor Blockade Inhibits Tumor Growth by Altering the Polarization of Tumor-Associated Macrophages in Hepatocellular Carcinoma. *Mol Cancer Ther*, *16*(8), 1544-1554. https://doi.org/10.1158/1535-7163.MCT-16-0866

Arana, M. E., Seki, M., Wood, R. D., Rogozin, I. B., & Kunkel, T. A. (2008). Low-fidelity DNA synthesis by human DNA polymerase theta. *Nucleic Acids Res*, *36*(11), 3847-3856. https://doi.org/10.1093/nar/gkn310

Arnoult, N., Correia, A., Ma, J., Merlo, A., Garcia-Gomez, S., Maric, M., . . . Karlseder, J. (2017). Regulation of DNA repair pathway choice in S and G2 phases by the NHEJ inhibitor CYREN. *Nature*, *549*(7673), 548-552. https://doi.org/10.1038/nature24023

Arribas-Hernandez, L., Rennie, S., Schon, M., Porcelli, C., Enugutti, B., Andersson, R., . . . Brodersen, P. (2021). The YTHDF proteins ECT2 and ECT3 bind largely overlapping target sets and influence target mRNA abundance, not alternative polyadenylation. *Elife*, *10*. https://doi.org/10.7554/eLife.72377

Aylon, Y., Liefshitz, B., & Kupiec, M. (2004). The CDK regulates repair of double-strand breaks by homologous recombination during the cell cycle. *EMBO J*, *23*(24), 4868-4875. https://doi.org/10.1038/sj.emboj.7600469

Ayoub, N., Jeyasekharan, A. D., Bernal, J. A., & Venkitaraman, A. R. (2009). Paving the way for H2AX phosphorylation: chromatin changes in the DNA damage response. *Cell Cycle*, *8*(10), 1494-1500. https://doi.org/10.4161/cc.8.10.8501

Bar-Yaacov, D., Frumkin, I., Yashiro, Y., Chujo, T., Ishigami, Y., Chemla, Y., . . . Mishmar, D. (2016). Mitochondrial 16S rRNA Is Methylated by tRNA Methyltransferase TRMT61B in All Vertebrates. *PLoS Biol*, *14*(9), e1002557. https://doi.org/10.1371/journal.pbio.1002557

Barbieri, I., Tzelepis, K., Pandolfini, L., Shi, J., Millan-Zambrano, G., Robson, S. C., . . . Kouzarides, T. (2017). Promoter-bound METTL3 maintains myeloid leukaemia by m(6)A-dependent translation control. *Nature*, *552*(7683), 126-131. https://doi.org/10.1038/nature24678

Bartek, J., & Lukas, J. (2003). Chk1 and Chk2 kinases in checkpoint control and cancer. *Cancer Cell*, *3*(5), 421-429. https://doi.org/10.1016/s1535-6108(03)00110-7

Bartek, J., & Lukas, J. (2007). DNA damage checkpoints: from initiation to recovery or adaptation. *Curr Opin Cell Biol*, *19*(2), 238-245. https://doi.org/10.1016/j.ceb.2007.02.009

Bartosovic, M., Molares, H. C., Gregorova, P., Hrossova, D., Kudla, G., & Vanacova, S. (2017). N6-methyladenosine demethylase FTO targets pre-mRNAs and regulates alternative splicing and 3′-end processing. *Nucleic Acids Res*, *45*(19), 11356-11370. https://doi.org/10.1093/nar/gkx778

Batista, P. J., Molinie, B., Wang, J., Qu, K., Zhang, J., Li, L., . . . Chang, H. Y. (2014). m(6)A RNA modification controls cell fate transition in mammalian embryonic stem cells. *Cell Stem Cell*, *15*(6), 707-719. https://doi.org/10.1016/j.stem.2014.09.019

Bechara, E. G., Sebestyen, E., Bernardis, I., Eyras, E., & Valcarcel, J. (2013). RBM5, 6, and 10 differentially regulate NUMB alternative splicing to control cancer cell proliferation. *Mol Cell*, *52*(5), 720-733. https://doi.org/10.1016/j.molcel.2013.11.010

Becker, J. R., Clifford, G., Bonnet, C., Groth, A., Wilson, M. D., & Chapman, J. R. (2021). BARD1 reads H2A lysine 15 ubiquitination to direct homologous recombination. *Nature*, *596*(7872), 433-+. https://doi.org/10.1038/s41586-021-03776-w

Bekker-Jensen, S., & Mailand, N. (2010). Assembly and function of DNA double-strand break repair foci in mammalian cells. *DNA Repair (Amst)*, *9*(12), 1219-1228. https://doi.org/10.1016/j.dnarep.2010.09.010

Benitez, A., Liu, W., Palovcak, A., Wang, G., Moon, J., An, K., . . . Zhang, Y. (2018). FANCA Promotes DNA Double-Strand Break Repair by Catalyzing Single-Strand Annealing and Strand Exchange. *Mol Cell*, *71*(4), 621-628 e624. https://doi.org/10.1016/j.molcel.2018.06.030

Bennardo, N., Cheng, A., Huang, N., & Stark, J. M. (2008). Alternative-NHEJ is a mechanistically distinct pathway of mammalian chromosome break repair. *PLoS Genet*, *4*(6), e1000110. https://doi.org/10.1371/journal.pgen.1000110

Berlivet, S., Scutenaire, J., Deragon, J. M., & Bousquet-Antonelli, C. (2019). Readers of the m(6)A epitranscriptomic code. *Biochim Biophys Acta Gene Regul Mech*, *1862*(3), 329-342. https://doi.org/10.1016/j.bbagrm.2018.12.008

Berulava, T., Ziehe, M., Klein-Hitpass, L., Mladenov, E., Thomale, J., Ruther, U., & Horsthemke, B. (2013). FTO levels affect RNA modification and the transcriptome. *Eur J Hum Genet*, *21*(3), 317-323. https://doi.org/10.1038/ejhg.2012.168

Beucher, A., Birraux, J., Tchouandong, L., Barton, O., Shibata, A., Conrad, S., . . . Lobrich, M. (2009). ATM and Artemis promote homologous recombination of radiation-induced DNA double-strand breaks in G2. *EMBO J*, *28*(21), 3413-3427. https://doi.org/10.1038/emboj.2009.276

Bhargava, R., Onyango, D. O., & Stark, J. M. (2016). Regulation of Single-Strand Annealing and its Role in Genome Maintenance. *Trends Genet*, *32*(9), 566-575. https://doi.org/10.1016/j.tig.2016.06.007

Bjornstad, L. G., Zoppellaro, G., Tomter, A. B., Falnes, P. O., & Andersson, K. K. (2011). Spectroscopic and magnetic studies of wild-type and mutant forms of the Fe(II)- and 2-oxoglutarate-dependent decarboxylase ALKBH4. *Biochem J*, *434*(3), 391-398. https://doi.org/10.1042/BJ20101667

Bohgaki, T., Bohgaki, M., Cardoso, R., Panier, S., Zeegers, D., Li, L., . . . Hakem, R. (2011). Genomic instability, defective spermatogenesis, immunodeficiency, and cancer in a mouse model of the RIDDLE syndrome. *PLoS Genet*, *7*(4), e1001381. https://doi.org/10.1371/journal.pgen.1001381

Boissel, S., Reish, O., Proulx, K., Kawagoe-Takaki, H., Sedgwick, B., Yeo, G. S., . . . Colleaux, L. (2009). Loss-of-function mutation in the dioxygenase-encoding FTO gene causes severe growth retardation and multiple malformations. *Am J Hum Genet*, *85*(1), 106-111. https://doi.org/10.1016/j.ajhg.2009.06.002

Boo, S. H., Ha, H., & Kim, Y. K. (2022). m(1)A and m(6)A modifications function cooperatively to facilitate rapid mRNA degradation. *Cell Rep*, *40*(10), 111317. https://doi.org/10.1016/j.celrep.2022.111317

Botuyan, M. V., Lee, J., Ward, I. M., Kim, J. E., Thompson, J. R., Chen, J., & Mer, G. (2006). Structural basis for the methylation state-specific recognition of histone H4-K20 by 53BP1 and Crb2 in DNA repair. *Cell*, *127*(7), 1361-1373. https://doi.org/10.1016/j.cell.2006.10.043

Boulias, K., Toczydlowska-Socha, D., Hawley, B. R., Liberman, N., Takashima, K., Zaccara, S., . . . Greer, E. L. (2019). Identification of the m(6)Am Methyltransferase PCIF1 Reveals the Location and Functions of m(6)Am in the Transcriptome. *Mol Cell*, *75*(3), 631-643 e638. https://doi.org/10.1016/j.molcel.2019.06.006

Bray, N. L., Pimentel, H., Melsted, P., & Pachter, L. (2016). Near-optimal probabilistic RNA-seq quantification. *Nat Biotechnol*, *34*(5), 525-527. https://doi.org/10.1038/nbt.3519

Bryant, H. E., Schultz, N., Thomas, H. D., Parker, K. M., Flower, D., Lopez, E., . . . Helleday, T. (2005). Specific killing of BRCA2-deficient tumours with inhibitors of poly(ADP-ribose) polymerase. *Nature*, *434*(7035), 913-917. https://doi.org/10.1038/nature03443

Buck, D., Malivert, L., de Chasseval, R., Barraud, A., Fondaneche, M. C., Sanal, O., . . . Revy, P. (2006). Cernunnos, a novel nonhomologous end-joining factor, is mutated in human immunodeficiency with microcephaly. *Cell*, *124*(2), 287-299. https://doi.org/10.1016/j.cell.2005.12.030

Bunting, S. F., Callen, E., Wong, N., Chen, H. T., Polato, F., Gunn, A., . . . Nussenzweig, A. (2010). 53BP1 inhibits homologous recombination in Brca1-deficient cells by blocking resection of DNA breaks. *Cell*, *141*(2), 243-254. https://doi.org/10.1016/j.cell.2010.03.012

Burma, S., Chen, B. P., Murphy, M., Kurimasa, A., & Chen, D. J. (2001). ATM phosphorylates histone H2AX in response to DNA double-strand breaks. *J Biol Chem*, *276*(45), 42462-42467. https://doi.org/10.1074/jbc.C100466200

Cai, X., Wang, X., Cao, C., Gao, Y., Zhang, S., Yang, Z., . . . Ye, L. (2018). HBXIP-elevated methyltransferase METTL3 promotes the progression of breast cancer via inhibiting tumor suppressor let-7g. *Cancer Lett*, *415*, 11-19. https://doi.org/10.1016/j.canlet.2017.11.018

Callen, E., Di Virgilio, M., Kruhlak, M. J., Nieto-Soler, M., Wong, N., Chen, H. T., . . . Nussenzweig, A. (2013). 53BP1 mediates productive and mutagenic DNA repair through distinct phosphoprotein interactions. *Cell*, *153*(6), 1266-1280. https://doi.org/10.1016/j.cell.2013.05.023

Cannan, W. J., & Pederson, D. S. (2016). Mechanisms and Consequences of Double-Strand DNA Break Formation in Chromatin. *J Cell Physiol*, *231*(1), 3-14. https://doi.org/10.1002/jcp.25048

Cappannini, A., Ray, A., Purta, E., Mukherjee, S., Boccaletto, P., Moafinejad, S. N., . . . Bujnicki, J. M. (2023). MODOMICS: a database of RNA modifications and related information. 2023 update. *Nucleic Acids Res*, *52*(D1), D239-D244. https://doi.org/10.1093/nar/gkad1083

Carlile, T. M., Rojas-Duran, M. F., Zinshteyn, B., Shin, H., Bartoli, K. M., & Gilbert, W. V. (2014). Pseudouridine profiling reveals regulated mRNA pseudouridylation in yeast and human cells. *Nature*, *515*(7525), 143-146. https://doi.org/10.1038/nature13802

Ceccaldi, R., Rondinelli, B., & D'Andrea, A. D. (2016). Repair Pathway Choices and Consequences at the Double-Strand Break. *Trends Cell Biol*, *26*(1), 52-64. https://doi.org/10.1016/j.tcb.2015.07.009

Ceppi, I., Howard, S. M., Kasaciunaite, K., Pinto, C., Anand, R., Seidel, R., & Cejka, P. (2020). CtIP promotes the motor activity of DNA2 to accelerate long-range DNA end resection. *Proc Natl Acad Sci U S A*, *117*(16), 8859-8869. https://doi.org/10.1073/pnas.2001165117

Chakraborty, P., & Hiom, K. (2021). DHX9-dependent recruitment of BRCA1 to RNA promotes DNA end resection in homologous recombination. *Nat Commun*, *12*(1), 4126. https://doi.org/10.1038/s41467-021-24341-z

Chanut, P., Britton, S., Coates, J., Jackson, S. P., & Calsou, P. (2016). Coordinated nuclease activities counteract Ku at single-ended DNA double-strand breaks. *Nature Communications*, *7*. https://doi.org/ARTN 12889

10.1038/ncomms12889

Chapman, J. R., Barral, P., Vannier, J. B., Borel, V., Steger, M., Tomas-Loba, A., . . . Boulton, S. J. (2013). RIF1 is essential for 53BP1-dependent nonhomologous end joining and suppression of DNA double-strand break resection. *Mol Cell*, *49*(5), 858-871. https://doi.org/10.1016/j.molcel.2013.01.002

Chapman, J. R., Taylor, M. R., & Boulton, S. J. (2012). Playing the end game: DNA double-strand break repair pathway choice. *Mol Cell*, *47*(4), 497-510. https://doi.org/10.1016/j.molcel.2012.07.029

Chen, H., Yang, H., Zhu, X., Yadav, T., Ouyang, J., Truesdell, S. S., . . . Lan, L. (2020). m(5)C modification of mRNA serves a DNA damage code to promote homologous recombination. *Nat Commun*, *11*(1), 2834. https://doi.org/10.1038/s41467-020-16722-7

Chen, J., Feng, W., Jiang, J., Deng, Y., & Huen, M. S. (2012). Ring finger protein RNF169 antagonizes the ubiquitin-dependent signaling cascade at sites of DNA damage. *J Biol Chem*, *287*(33), 27715-27722. https://doi.org/10.1074/jbc.M112.373530

Chen, Y., Peng, C., Chen, J., Chen, D., Yang, B., He, B., . . . Zheng, S. (2019). WTAP facilitates progression of hepatocellular carcinoma via m6A-HuR-dependent epigenetic silencing of ETS1. *Mol Cancer*, *18*(1), 127. https://doi.org/10.1186/s12943-019-1053-8

Chen, Z., Qi, M., Shen, B., Luo, G., Wu, Y., Li, J., . . . Wang, H. (2019). Transfer RNA demethylase ALKBH3 promotes cancer progression via induction of tRNA-derived small RNAs. *Nucleic Acids Res*, *47*(5), 2533-2545. https://doi.org/10.1093/nar/gky1250

Chen, Z., Zhong, X., Xia, M., & Zhong, J. (2021). The roles and mechanisms of the m6A reader protein YTHDF1 in tumor biology and human diseases. *Mol Ther Nucleic Acids*, *26*, 1270-1279. https://doi.org/10.1016/j.omtn.2021.10.023

Cheng, M., Sheng, L., Gao, Q., Xiong, Q., Zhang, H., Wu, M., . . . Li, Y. (2019). The m(6)A methyltransferase METTL3 promotes bladder cancer progression via AFF4/NF-kappaB/MYC signaling network. *Oncogene*, *38*(19), 3667-3680. https://doi.org/10.1038/s41388-019-0683-z

Choe, J., Lin, S., Zhang, W., Liu, Q., Wang, L., Ramirez-Moya, J., . . . Gregory, R. I. (2018). mRNA circularization by METTL3-eIF3h enhances translation and promotes oncogenesis. *Nature*, *561*(7724), 556-560. https://doi.org/10.1038/s41586-018-0538-8

Chu, X., Erdman, R., Susek, M., Gerst, H., Derr, K., Al-Agha, M., . . . Gerhard, G. S. (2008). Association of morbid obesity with FTO and INSIG2 allelic variants. *Arch Surg*, *143*(3), 235-240; discussion 241. https://doi.org/10.1001/archsurg.2007.77

Clark, S. L., Rodriguez, A. M., Snyder, R. R., Hankins, G. D., & Boehning, D. (2012). Structure-Function Of The Tumor Suppressor BRCA1. *Comput Struct Biotechnol J*, *1*(1). https://doi.org/10.5936/csbj.201204005

Coleman, K. A., & Greenberg, R. A. (2011). The BRCA1-RAP80 complex regulates DNA repair mechanism utilization by restricting end resection. *J Biol Chem*, *286*(15), 13669-13680. https://doi.org/10.1074/jbc.M110.213728

Cortez, D., Wang, Y., Qin, J., & Elledge, S. J. (1999). Requirement of ATM-dependent phosphorylation of brca1 in the DNA damage response to double-strand breaks. *Science*, *286*(5442), 1162-1166. https://doi.org/10.1126/science.286.5442.1162

Cozen, A. E., Quartley, E., Holmes, A. D., Hrabeta-Robinson, E., Phizicky, E. M., & Lowe, T. M. (2015). ARM-seq: AlkB-facilitated RNA methylation sequencing reveals a complex landscape of modified tRNA fragments. *Nat Methods*, *12*(9), 879-884. https://doi.org/10.1038/nmeth.3508

Crossley, M. P., Bocek, M., & Cimprich, K. A. (2019). R-Loops as Cellular Regulators and Genomic Threats. *Mol Cell*, *73*(3), 398-411. https://doi.org/10.1016/j.molcel.2019.01.024

Cui, Q., Shi, H., Ye, P., Li, L., Qu, Q., Sun, G., . . . Shi, Y. (2017). m(6)A RNA Methylation Regulates the Self-Renewal and Tumorigenesis of Glioblastoma Stem Cells. *Cell Rep*, *18*(11), 2622-2634. https://doi.org/10.1016/j.celrep.2017.02.059

Cun, Y., An, S., Zheng, H., Lan, J., Chen, W., Luo, W., . . . Li, J. (2023). Specific Regulation of m(6)A by SRSF7 Promotes the Progression of Glioblastoma. *Genomics Proteomics Bioinformatics*, *21*(4), 707-728. https://doi.org/10.1016/j.gpb.2021.11.001

Dai, D., Wang, H., Zhu, L., Jin, H., & Wang, X. (2018). N6-methyladenosine links RNA metabolism to cancer progression. *Cell Death Dis*, *9*(2), 124. https://doi.org/10.1038/s41419-017-0129-x

Dai, Q., Moshitch-Moshkovitz, S., Han, D., Kol, N., Amariglio, N., Rechavi, G., . . . He, C. (2017). Nm-seq maps 2′-O-methylation sites in human mRNA with base precision. *Nat Methods*, *14*(7), 695-698. https://doi.org/10.1038/nmeth.4294

Dai, X., Wang, T., Gonzalez, G., & Wang, Y. (2018). Identification of YTH Domain-Containing Proteins as the Readers for N1-Methyladenosine in RNA. *Anal Chem*, *90*(11), 6380-6384. https://doi.org/10.1021/acs.analchem.8b01703

Daley, J. M., & Sung, P. (2013). RIF1 in DNA break repair pathway choice. *Mol Cell*, *49*(5), 840-841. https://doi.org/10.1016/j.molcel.2013.02.019

Daley, J. M., & Sung, P. (2014). 53BP1, BRCA1, and the choice between recombination and end joining at DNA double-strand breaks. *Mol Cell Biol*, *34*(8), 1380-1388. https://doi.org/10.1128/MCB.01639-13

Dango, S., Mosammaparast, N., Sowa, M. E., Xiong, L. J., Wu, F., Park, K., . . . Shi, Y. (2011). DNA unwinding by ASCC3 helicase is coupled to ALKBH3-dependent DNA alkylation repair and cancer cell proliferation. *Mol Cell*, *44*(3), 373-384. https://doi.org/10.1016/j.molcel.2011.08.039

David, C. J., Chen, M., Assanah, M., Canoll, P., & Manley, J. L. (2010). HnRNP proteins controlled by c-Myc deregulate pyruvate kinase mRNA splicing in cancer. *Nature*, *463*(7279), 364-368. https://doi.org/10.1038/nature08697

Davis, A. J., & Chen, D. J. (2013). DNA double strand break repair via non-homologous end-joining. *Transl Cancer Res*, *2*(3), 130-143. https://doi.org/10.3978/j.issn.2218-676X.2013.04.02

Davis, F. F., & Allen, F. W. (1957). Ribonucleic acids from yeast which contain a fifth nucleotide. *J Biol Chem*, *227*(2), 907-915. https://www.ncbi.nlm.nih.gov/pubmed/13463012

Deniz, M., Romashova, T., Kostezka, S., Faul, A., Gundelach, T., Moreno-Villanueva, M., . . . Wiesmuller, L. (2017). Increased single-strand annealing rather than non-homologous end-joining predicts hereditary ovarian carcinoma. *Oncotarget*, *8*(58), 98660-98676. https://doi.org/10.18632/oncotarget.21720

Desrosiers, R., Friderici, K., & Rottman, F. (1974). Identification of methylated nucleosides in messenger RNA from Novikoff hepatoma cells. *Proc Natl Acad Sci U S A*, *71*(10), 3971-3975. https://doi.org/10.1073/pnas.71.10.3971

Devgan, S. S., Sanal, O., Doil, C., Nakamura, K., Nahas, S. A., Pettijohn, K., . . . Gatti, R. A. (2011). Homozygous deficiency of ubiquitin-ligase ring-finger protein RNF168 mimics the radiosensitivity syndrome of ataxia-telangiectasia. *Cell Death Differ*, *18*(9), 1500-1506. https://doi.org/10.1038/cdd.2011.18

Didiot, M. C., Subramanian, M., Flatter, E., Mandel, J. L., & Moine, H. (2009). Cells lacking the fragile X mental retardation protein (FMRP) have normal RISC activity but exhibit altered stress granule assembly. *Molecular Biology of the Cell*, *20*(1), 428-437. https://doi.org/10.1091/mbc.e08-07-0737

Do, A. T., Brooks, J. T., Le Neveu, M. K., & LaRocque, J. R. (2014). Double-strand break repair assays determine pathway choice and structure of gene conversion events in Drosophila melanogaster. *G3 (Bethesda)*, *4*(3), 425-432. https://doi.org/10.1534/g3.113.010074

Doil, C., Mailand, N., Bekker-Jensen, S., Menard, P., Larsen, D. H., Pepperkok, R., . . . Lukas, C. (2009). RNF168 Binds and Amplifies Ubiquitin Conjugates on Damaged Chromosomes to Allow Accumulation of Repair Proteins. *Cell*, *136*(3), 435-446. https://doi.org/10.1016/j.cell.2008.12.041

Dominissini, D., Moshitch-Moshkovitz, S., Salmon-Divon, M., Amariglio, N., & Rechavi, G. (2013). Transcriptome-wide mapping of N(6)-methyladenosine by m(6)A-seq based on immunocapturing and massively parallel sequencing. *Nat Protoc*, *8*(1), 176-189. https://doi.org/10.1038/nprot.2012.148

Dominissini, D., Moshitch-Moshkovitz, S., Schwartz, S., Salmon-Divon, M., Ungar, L., Osenberg, S., . . . Rechavi, G. (2012). Topology of the human and mouse m6A RNA methylomes revealed by m6A-seq. *Nature*, *485*(7397), 201-206. https://doi.org/10.1038/nature11112

Dominissini, D., Nachtergaele, S., Moshitch-Moshkovitz, S., Peer, E., Kol, N., Ben-Haim, M. S., . . . He, C. (2016). The dynamic N1-methyladenosine methylome in eukaryotic messenger RNA. *Nature*, *530*(7591), 441-446. https://doi.org/10.1038/nature16998

Doyle, J. M., Gao, J. L., Wang, J. W., Yang, M. J., & Potts, P. R. (2010). MAGE-RING Protein Complexes Comprise a Family of E3 Ubiquitin Ligases. *Molecular Cell*, *39*(6), 963-974. https://doi.org/10.1016/j.molcel.2010.08.029

Du, C., Hansen, L. J., Singh, S. X., Wang, F., Sun, R., Moure, C. J., . . . He, Y. (2019). A PRMT5-RNF168-SMURF2 Axis Controls H2AX Proteostasis. *Cell Rep*, *28*(12), 3199-3211 e3195. https://doi.org/10.1016/j.celrep.2019.08.031

Du, H., Zhao, Y., He, J., Zhang, Y., Xi, H., Liu, M., . . . Wu, L. (2016). YTHDF2 destabilizes m(6)A-containing RNA through direct recruitment of the CCR4-NOT deadenylase complex. *Nat Commun*, *7*, 12626. https://doi.org/10.1038/ncomms12626

Dufu, K., Livingstone, M. J., Seebacher, J., Gygi, S. P., Wilson, S. A., & Reed, R. (2010). ATP is required for interactions between UAP56 and two conserved mRNA export proteins, Aly and CIP29, to assemble the TREX complex. *Genes Dev*, *24*(18), 2043-2053. https://doi.org/10.1101/gad.1898610

Duncan, T., Trewick, S. C., Koivisto, P., Bates, P. A., Lindahl, T., & Sedgwick, B. (2002). Reversal of DNA alkylation damage by two human dioxygenases. *Proc Natl Acad Sci U S A*, *99*(26), 16660-16665. https://doi.org/10.1073/pnas.262589799

Dunn, D. B. (1961). The occurrence of 1-methyladenine in ribonucleic acid. *Biochim Biophys Acta*, *46*, 198-200. https://doi.org/10.1016/0006-3002(61)90668-0

Dusre, L., Covey, J. M., Collins, C., & Sinha, B. K. (1989). DNA damage, cytotoxicity and free radical formation by mitomycin C in human cells. *Chem Biol Interact*, *71*(1), 63-78. https://doi.org/10.1016/0009-2797(89)90090-2

Edmonds, M., Vaughan, M. H., Jr., & Nakazato, H. (1971). Polyadenylic acid sequences in the heterogeneous nuclear RNA and rapidly-labeled polyribosomal RNA of HeLa cells: possible evidence for a precursor relationship. *Proc Natl Acad Sci U S A*, *68*(6), 1336-1340. https://doi.org/10.1073/pnas.68.6.1336

Edo, K., & Koide, Y. (1997). Neocarzinostatin Chromophore: Structure and Mechanism of DNA Cleavage. In H. Maeda, K. Edo, & N. Ishida (Eds.), *Neocarzinostatin: The Past, Present, and Future of an Anticancer Drug* (pp. 23-45). Springer Japan. https://doi.org/10.1007/978-4-431-66914-2_3

Ensembl. (2023, July 2023). *Gene: BRCA1*. ensembl.org. https://www.ensembl.org/Homo_sapiens/Gene/Summary?db=core;g=ENSG00000012048;r=17:43044295-43170245;t=ENST00000471181

Escribano-Diaz, C., Orthwein, A., Fradet-Turcotte, A., Xing, M., Young, J. T., Tkac, J., . . . Durocher, D. (2013). A cell cycle-dependent regulatory circuit composed of 53BP1-RIF1 and BRCA1-CtIP controls DNA repair pathway choice. *Mol Cell*, *49*(5), 872-883. https://doi.org/10.1016/j.molcel.2013.01.001

Esteve-Puig, R., Climent, F., Pineyro, D., Domingo-Domenech, E., Davalos, V., Encuentra, M., . . . Esteller, M. (2021). Epigenetic loss of m(1)A RNA demethylase ALKBH3 in Hodgkin lymphoma targets collagen, conferring poor clinical outcome. *Blood*, *137*(7), 994-999. https://doi.org/10.1182/blood.2020005823

Falnes, P. O., Bjoras, M., Aas, P. A., Sundheim, O., & Seeberg, E. (2004). Substrate specificities of bacterial and human AlkB proteins. *Nucleic Acids Res*, *32*(11), 3456-3461. https://doi.org/10.1093/nar/gkh655

Falnes, P. O., Johansen, R. F., & Seeberg, E. (2002). AlkB-mediated oxidative demethylation reverses DNA damage in Escherichia coli. *Nature*, *419*(6903), 178-182. https://doi.org/10.1038/nature01048

Falnes, P. O., Klungland, A., & Alseth, I. (2007). Repair of methyl lesions in DNA and RNA by oxidative demethylation. *Neuroscience*, *145*(4), 1222-1232. https://doi.org/10.1016/j.neuroscience.2006.11.018

Fedeles, B. I., Singh, V., Delaney, J. C., Li, D., & Essigmann, J. M. (2015). The AlkB Family of Fe(II)/alpha-Ketoglutarate-dependent Dioxygenases: Repairing Nucleic Acid Alkylation Damage and Beyond. *J Biol Chem*, *290*(34), 20734-20742. https://doi.org/10.1074/jbc.R115.656462

Feng, L., Fong, K. W., Wang, J., Wang, W., & Chen, J. (2013). RIF1 counteracts BRCA1-mediated end resection during DNA repair. *J Biol Chem*, *288*(16), 11135-11143. https://doi.org/10.1074/jbc.M113.457440

Ferretti, L. P., Lafranchi, L., & Sartori, A. A. (2013). Controlling DNA-end resection: a new task for CDKs. *Front Genet*, *4*, 99. https://doi.org/10.3389/fgene.2013.00099

Fischer, J., Koch, L., Emmerling, C., Vierkotten, J., Peters, T., Bruning, J. C., & Ruther, U. (2009). Inactivation of the Fto gene protects from obesity. *Nature*, *458*(7240), 894-898. https://doi.org/10.1038/nature07848

Fradet-Turcotte, A., Canny, M. D., Escribano-Diaz, C., Orthwein, A., Leung, C. C., Huang, H., . . . Durocher, D. (2013). 53BP1 is a reader of the DNA-damage-induced H2A Lys 15 ubiquitin mark. *Nature*, *499*(7456), 50-54. https://doi.org/10.1038/nature12318

Franken, N. A., Rodermond, H. M., Stap, J., Haveman, J., & van Bree, C. (2006). Clonogenic assay of cells in vitro. *Nat Protoc*, *1*(5), 2315-2319. https://doi.org/10.1038/nprot.2006.339

Frayling, T. M., Timpson, N. J., Weedon, M. N., Zeggini, E., Freathy, R. M., Lindgren, C. M., . . . McCarthy, M. I. (2007). A common variant in the FTO gene is associated with body mass index and predisposes to childhood and adult obesity. *Science*, *316*(5826), 889-894. https://doi.org/10.1126/science.1141634

Fu, D., Brophy, J. A., Chan, C. T., Atmore, K. A., Begley, U., Paules, R. S., . . . Samson, L. D. (2010). Human AlkB homolog ABH8 Is a tRNA methyltransferase required for wobble uridine modification and DNA damage survival. *Mol Cell Biol*, *30*(10), 2449-2459. https://doi.org/10.1128/MCB.01604-09

Fu, J., Zhou, S., Xu, H., Liao, L., Shen, H., Du, P., & Zheng, X. (2023). ATM-ESCO2-SMC3 axis promotes 53BP1 recruitment in response to DNA damage and safeguards genome integrity by stabilizing cohesin complex. *Nucleic Acids Res*, *51*(14), 7376-7391. https://doi.org/10.1093/nar/gkad533

Fu, Y., Jia, G., Pang, X., Wang, R. N., Wang, X., Li, C. J., . . . He, C. (2013). FTO-mediated formation of N6-hydroxymethyladenosine and N6-formyladenosine in mammalian RNA. *Nat Commun*, *4*, 1798. https://doi.org/10.1038/ncomms2822

Fustin, J. M., Doi, M., Yamaguchi, Y., Hida, H., Nishimura, S., Yoshida, M., . . . Okamura, H. (2013). RNA-methylation-dependent RNA processing controls the speed of the circadian clock. *Cell*, *155*(4), 793-806. https://doi.org/10.1016/j.cell.2013.10.026

Gao, L., Wang, A., Chen, Y., Cai, X., Li, Y., Zhao, J., . . . Huang, J. A. (2023). FTO facilitates cancer metastasis by modifying the m(6)A level of FAP to induce integrin/FAK signaling in non-small cell lung cancer. *Cell Commun Signal*, *21*(1), 311. https://doi.org/10.1186/s12964-023-01343-6

Gao, S., Li, X., Zhang, M., Zhang, N., Wang, R., & Chang, J. (2021). Structural characteristics of small-molecule inhibitors targeting FTO demethylase. *Future Med Chem*, *13*(17), 1475-1489. https://doi.org/10.4155/fmc-2021-0132

Gao, Y., Wang, H., Li, H., Ye, X., Xia, Y., Yuan, S., . . . Zhang, J. (2021). Integrated analyses of m(1)A regulator-mediated modification patterns in tumor microenvironment-infiltrating immune cells in colon cancer. *Oncoimmunology*, *10*(1), 1936758. https://doi.org/10.1080/2162402X.2021.1936758

Garg, R., Melstrom, L., Chen, J., He, C., & Goel, A. (2022). Targeting FTO Suppresses Pancreatic Carcinogenesis via Regulating Stem Cell Maintenance and EMT Pathway. *Cancers (Basel)*, *14*(23). https://doi.org/10.3390/cancers14235919

Gatti, M., Pinato, S., Maiolica, A., Rocchio, F., Prato, M. G., Aebersold, R., & Penengo, L. (2015). RNF168 promotes noncanonical K27 ubiquitination to signal DNA damage. *Cell Rep*, *10*(2), 226-238. https://doi.org/10.1016/j.celrep.2014.12.021

Gatti, M., Pinato, S., Maspero, E., Soffientini, P., Polo, S., & Penengo, L. (2012). A novel ubiquitin mark at the N-terminal tail of histone H2As targeted by RNF168 ubiquitin ligase. *Cell Cycle*, *11*(13), 2538-2544. https://doi.org/10.4161/cc.20919

Gerken, T., Girard, C. A., Tung, Y. C., Webby, C. J., Saudek, V., Hewitson, K. S., . . . Schofield, C. J. (2007). The obesity-associated FTO gene encodes a 2-oxoglutarate-dependent nucleic acid demethylase. *Science*, *318*(5855), 1469-1472. https://doi.org/10.1126/science.1151710

Germani, A., Prabel, A., Mourah, S., Podgorniak, M. P., Di Carlo, A., Ehrlich, R., . . . Bruzzoni-Giovanelli, H. (2003). SIAH-1 interacts with CtIP and promotes its degradation by the proteasome pathway. *Oncogene*, *22*(55), 8845-8851. https://doi.org/10.1038/sj.onc.1206994

Geuens, T., Bouhy, D., & Timmerman, V. (2016). The hnRNP family: insights into their role in health and disease. *Hum Genet*, *135*(8), 851-867. https://doi.org/10.1007/s00439-016-1683-5

Giglia-Mari, G., Zotter, A., & Vermeulen, W. (2011). DNA damage response. *Cold Spring Harb Perspect Biol*, *3*(1), a000745. https://doi.org/10.1101/cshperspect.a000745

Gilar, M., Belenky, A., & Wang, B. H. (2001). High-throughput biopolymer desalting by solid-phase extraction prior to mass spectrometric analysis. *J Chromatogr A*, *921*(1), 3-13. https://doi.org/10.1016/s0021-9673(01)00833-0

Gottlieb, T. M., & Jackson, S. P. (1993). The DNA-dependent protein kinase: requirement for DNA ends and association with Ku antigen. *Cell*, *72*(1), 131-142. https://doi.org/10.1016/0092-8674(93)90057-w

Grimme, J. M., Honda, M., Wright, R., Okuno, Y., Rothenberg, E., Mazin, A. V., . . . Spies, M. (2010). Human Rad52 binds and wraps single-stranded DNA and mediates annealing via two hRad52-ssDNA complexes. *Nucleic Acids Res*, *38*(9), 2917-2930. https://doi.org/10.1093/nar/gkp1249

Grosjean, H., Szweykowska-Kulinska, Z., Motorin, Y., Fasiolo, F., & Simos, G. (1997). Intron-dependent enzymatic formation of modified nucleosides in eukaryotic tRNAs: a review. *Biochimie*, *79*(5), 293-302. https://doi.org/10.1016/s0300-9084(97)83517-1

Grozhik, A. V., Olarerin-George, A. O., Sindelar, M., Li, X., Gross, S. S., & Jaffrey, S. R. (2019). Antibody cross-reactivity accounts for widespread appearance of m(1)A in 5'UTRs. *Nat Commun*, *10*(1), 5126. https://doi.org/10.1038/s41467-019-13146-w

Gudjonsson, T., Altmeyer, M., Savic, V., Toledo, L., Dinant, C., Grofte, M., . . . Lukas, C. (2012). TRIP12 and UBR5 suppress spreading of chromatin ubiquitylation at damaged chromosomes. *Cell*, *150*(4), 697-709. https://doi.org/10.1016/j.cell.2012.06.039

Gunn, A., & Stark, J. M. (2012). I-SceI-based assays to examine distinct repair outcomes of mammalian chromosomal double strand breaks. *Methods Mol Biol*, *920*, 379-391. https://doi.org/10.1007/978-1-61779-998-3_27

Hahnel, P. S., Enders, B., Sasca, D., Roos, W. P., Kaina, B., Bullinger, L., . . . Kindler, T. (2014). Targeting components of the alternative NHEJ pathway sensitizes KRAS mutant leukemic cells to chemotherapy. *Blood*, *123*(15), 2355-2366. https://doi.org/10.1182/blood-2013-01-477620

Haince, J. F., McDonald, D., Rodrigue, A., Dery, U., Masson, J. Y., Hendzel, M. J., & Poirier, G. G. (2008). PARP1-dependent kinetics of recruitment of MRE11 and NBS1 proteins to multiple DNA damage sites. *J Biol Chem*, *283*(2), 1197-1208. https://doi.org/10.1074/jbc.M706734200

Haince, J. F., McDonald, D., Rodrigue, A., Déry, U., Masson, J. Y., Hendzel, M. J., & Poirier, G. G. (2008). PARP1-dependent kinetics of recruitment of MRE11 and NBS1 proteins to multiple DNA damage sites. *Journal of Biological Chemistry*, *283*(2), 1197-1208. https://doi.org/10.1074/jbc.M706734200

Han, L., & Yu, K. (2008). Altered kinetics of nonhomologous end joining and class switch recombination in ligase IV-deficient B cells. *J Exp Med*, *205*(12), 2745-2753. https://doi.org/10.1084/jem.20081623

Hanahan, D., & Weinberg, R. A. (2011). Hallmarks of cancer: the next generation. *Cell*, *144*(5), 646-674. https://doi.org/10.1016/j.cell.2011.02.013

Hargous, Y., Hautbergue, G. M., Tintaru, A. M., Skrisovska, L., Golovanov, A. P., Stevenin, J., . . . Allain, F. H. (2006). Molecular basis of RNA recognition and TAP binding by the SR proteins SRp20 and 9G8. *EMBO J*, *25*(21), 5126-5137. https://doi.org/10.1038/sj.emboj.7601385

Harper, J. W., & Elledge, S. J. (2007). The DNA damage response: ten years after. *Mol Cell*, *28*(5), 739-745. https://doi.org/10.1016/j.molcel.2007.11.015

Harrison, J. C., & Haber, J. E. (2006). Surviving the breakup: the DNA damage checkpoint. *Annu Rev Genet*, *40*, 209-235. https://doi.org/10.1146/annurev.genet.40.051206.105231

Hauer, M. H., Seeber, A., Singh, V., Thierry, R., Sack, R., Amitai, A., . . . Gasser, S. M. (2017). Histone degradation in response to DNA damage enhances chromatin dynamics and recombination rates. *Nat Struct Mol Biol*, *24*(2), 99-107. https://doi.org/10.1038/nsmb.3347

He, L., Li, H., Wu, A., Peng, Y., Shu, G., & Yin, G. (2019). Functions of N6-methyladenosine and its role in cancer. *Mol Cancer*, *18*(1), 176. https://doi.org/10.1186/s12943-019-1109-9

He, L., Li, J., Wang, X., Ying, Y., Xie, H., Yan, H., . . . Xie, L. (2018). The dual role of N6-methyladenosine modification of RNAs is involved in human cancers. *J Cell Mol Med*, *22*(10), 4630-4639. https://doi.org/10.1111/jcmm.13804

He, Y., Hu, H., Wang, Y., Yuan, H., Lu, Z., Wu, P., . . . Miao, Y. (2018). ALKBH5 Inhibits Pancreatic Cancer Motility by Decreasing Long Non-Coding RNA KCNK15-AS1 Methylation. *Cell Physiol Biochem*, *48*(2), 838-846. https://doi.org/10.1159/000491915

Heath, C. G., Viphakone, N., & Wilson, S. A. (2016). The role of TREX in gene expression and disease. *Biochem J*, *473*(19), 2911-2935. https://doi.org/10.1042/BCJ20160010

Hefferin, M. L., & Tomkinson, A. E. (2005). Mechanism of DNA double-strand break repair by non-homologous end joining. *DNA Repair (Amst)*, *4*(6), 639-648. https://doi.org/10.1016/j.dnarep.2004.12.005

Herzel, L., Ottoz, D. S. M., Alpert, T., & Neugebauer, K. M. (2017). Splicing and transcription touch base: co-transcriptional spliceosome assembly and function. *Nat Rev Mol Cell Biol*, *18*(10), 637-650. https://doi.org/10.1038/nrm.2017.63

Heyer, W. D., Ehmsen, K. T., & Liu, J. (2010). Regulation of homologous recombination in eukaryotes. *Annu Rev Genet*, *44*, 113-139. https://doi.org/10.1146/annurev-genet-051710-150955

Himanen, S. V., & Sistonen, L. (2019). New insights into transcriptional reprogramming during cellular stress. *J Cell Sci*, *132*(21). https://doi.org/10.1242/jcs.238402

Hoeijmakers, J. H. (2001). Genome maintenance mechanisms for preventing cancer. *Nature*, *411*(6835), 366-374. https://doi.org/10.1038/35077232

Hoeijmakers, J. H. (2009). DNA damage, aging, and cancer. *N Engl J Med*, *361*(15), 1475-1485. https://doi.org/10.1056/NEJMra0804615

Horiuchi, K., Kawamura, T., Iwanari, H., Ohashi, R., Naito, M., Kodama, T., & Hamakubo, T. (2013). Identification of Wilms' tumor 1-associating protein complex and its role in alternative splicing and the cell cycle. *J Biol Chem*, *288*(46), 33292-33302. https://doi.org/10.1074/jbc.M113.500397

Hotta, K., Sho, M., Fujimoto, K., Shimada, K., Yamato, I., Anai, S., . . . Nakajima, Y. (2015). Clinical significance and therapeutic potential of prostate cancer antigen-1/ALKBH3 in human renal cell carcinoma. *Oncol Rep*, *34*(2), 648-654. https://doi.org/10.3892/or.2015.4017

Hu, C., Yang, J., Qi, Z., Wu, H., Wang, B., Zou, F., . . . Liu, Q. (2022). Heat shock proteins: Biological functions, pathological roles, and therapeutic opportunities. *MedComm (2020)*, *3*(3), e161. https://doi.org/10.1002/mco2.161

Hu, Q., Botuyan, M. V., Cui, G., Zhao, D., & Mer, G. (2017). Mechanisms of Ubiquitin-Nucleosome Recognition and Regulation of 53BP1 Chromatin Recruitment by RNF168/169 and RAD18. *Mol Cell*, *66*(4), 473-487 e479. https://doi.org/10.1016/j.molcel.2017.04.009

Hua, W., Zhao, Y., Jin, X., Yu, D., He, J., Xie, D., & Duan, P. (2018). METTL3 promotes ovarian carcinoma growth and invasion through the regulation of AXL translation and epithelial to mesenchymal transition. *Gynecologic Oncology*, *151*(2), 356-365. https://doi.org/10.1016/j.ygyno.2018.09.015

Huang, H., Weng, H., & Chen, J. (2020). m(6)A Modification in Coding and Non-coding RNAs: Roles and Therapeutic Implications in Cancer. *Cancer Cell*, *37*(3), 270-288. https://doi.org/10.1016/j.ccell.2020.02.004

Huang, T., Gao, Q., Feng, T., Zheng, Y., Guo, J., & Zeng, W. (2018). FTO Knockout Causes Chromosome Instability and G2/M Arrest in Mouse GC-1 Cells. *Front Genet*, *9*, 732. https://doi.org/10.3389/fgene.2018.00732

Huang, Y., Gattoni, R., Stevenin, J., & Steitz, J. A. (2003). SR splicing factors serve as adapter proteins for TAP-dependent mRNA export. *Mol Cell*, *11*(3), 837-843. https://doi.org/10.1016/s1097-2765(03)00089-3

Huen, M. S., & Chen, J. (2008). The DNA damage response pathways: at the crossroad of protein modifications. *Cell Res*, *18*(1), 8-16. https://doi.org/10.1038/cr.2007.109

Huen, M. S., Grant, R., Manke, I., Minn, K., Yu, X., Yaffe, M. B., & Chen, J. (2007). RNF8 transduces the DNA-damage signal via histone ubiquitylation and checkpoint protein assembly. *Cell*, *131*(5), 901-914. https://doi.org/10.1016/j.cell.2007.09.041

Huff, S., Tiwari, S. K., Gonzalez, G. M., Wang, Y., & Rana, T. M. (2021). m(6)A-RNA Demethylase FTO Inhibitors Impair Self-Renewal in Glioblastoma Stem Cells. *ACS Chem Biol*, *16*(2), 324-333. https://doi.org/10.1021/acschembio.0c00841

Hustedt, N., & Durocher, D. (2016). The control of DNA repair by the cell cycle. *Nat Cell Biol*, *19*(1), 1-9. https://doi.org/10.1038/ncb3452

Hwang, J. W., Cho, Y., Bae, G. U., Kim, S. N., & Kim, Y. K. (2021). Protein arginine methyltransferases: promising targets for cancer therapy. *Exp Mol Med*, *53*(5), 788-808. https://doi.org/10.1038/s12276-021-00613-y

Hwang, J. W., Kim, S.-N., Myung, N., Song, D., Han, G., Bae, G.-U., . . . Kim, Y. K. (2020). PRMT5 promotes DNA repair through methylation of 53BP1 and is regulated by Src-mediated phosphorylation. *Communications Biology*, *3*(1), 428. https://doi.org/10.1038/s42003-020-01157-z

Ikels, K., Kuschel, S., Fischer, J., Kaisers, W., Eberhard, D., & Ruther, U. (2014). FTO is a relevant factor for the development of the metabolic syndrome in mice. *PLoS One*, *9*(8), e105349. https://doi.org/10.1371/journal.pone.0105349

Iles, M. M., Law, M. H., Stacey, S. N., Han, J., Fang, S., Pfeiffer, R., . . . Investigators, A. (2013). A variant in FTO shows association with melanoma risk not due to BMI. *Nat Genet*, *45*(4), 428-432, 432e421. https://doi.org/10.1038/ng.2571

Iliakis, G., Murmann, T., & Soni, A. (2015). Alternative end-joining repair pathways are the ultimate backup for abrogated classical non-homologous end-joining and homologous recombination repair: Implications for the formation of chromosome translocations. *Mutat Res Genet Toxicol Environ Mutagen*, *793*, 166-175. https://doi.org/10.1016/j.mrgentox.2015.07.001

Ira, G., Pellicioli, A., Balijja, A., Wang, X., Fiorani, S., Carotenuto, W., . . . Foiani, M. (2004). DNA end resection, homologous recombination and DNA damage checkpoint activation require CDK1. *Nature*, *431*(7011), 1011-1017. https://doi.org/10.1038/nature02964

Ivanov, E. L., Sugawara, N., Fishman-Lobell, J., & Haber, J. E. (1996). Genetic requirements for the single-strand annealing pathway of double-strand break repair in Saccharomyces cerevisiae. *Genetics*, *142*(3), 693-704. https://www.ncbi.nlm.nih.gov/pubmed/8849880

Izaurralde, E., Jarmolowski, A., Beisel, C., Mattaj, I. W., Dreyfuss, G., & Fischer, U. (1997). A role for the M9 transport signal of hnRNP A1 in mRNA nuclear export. *J Cell Biol*, *137*(1), 27-35. https://doi.org/10.1083/jcb.137.1.27

Jackson, S. P., & Bartek, J. (2009). The DNA-damage response in human biology and disease. *Nature*, *461*(7267), 1071-1078. https://doi.org/10.1038/nature08467

Jadav, R. S., Chanduri, M. V., Sengupta, S., & Bhandari, R. (2013). Inositol pyrophosphate synthesis by inositol hexakisphosphate kinase 1 is required for homologous recombination repair. *J Biol Chem*, *288*(5), 3312-3321. https://doi.org/10.1074/jbc.M112.396556

Janin, M., Coll-SanMartin, L., & Esteller, M. (2020). Disruption of the RNA modifications that target the ribosome translation machinery in human cancer. *Mol Cancer*, *19*(1), 70. https://doi.org/10.1186/s12943-020-01192-8

Jensen, R. B., Ozes, A., Kim, T., Estep, A., & Kowalczykowski, S. C. (2013). BRCA2 is epistatic to the RAD51 paralogs in response to DNA damage. *DNA Repair (Amst)*, *12*(4), 306-311. https://doi.org/10.1016/j.dnarep.2012.12.007

Jeschke, J., Collignon, E., Al Wardi, C., Krayem, M., Bizet, M., Jia, Y., . . . Fuks, F. (2021). Downregulation of the FTO m(6)A RNA demethylase promotes EMT-mediated progression of epithelial tumors and sensitivity to Wnt inhibitors. *Nat Cancer*, *2*(6), 611-628. https://doi.org/10.1038/s43018-021-00223-7

Jia, G., Fu, Y., Zhao, X., Dai, Q., Zheng, G., Yang, Y., . . . He, C. (2011). N6-methyladenosine in nuclear RNA is a major substrate of the obesity-associated FTO. *Nat Chem Biol*, *7*(12), 885-887. https://doi.org/10.1038/nchembio.687

Jiao, Y., Zhang, J., Lu, L., Xu, J., & Qin, L. (2016). The Fto Gene Regulates the Proliferation and Differentiation of Pre-Adipocytes in Vitro. *Nutrients*, *8*(2), 102. https://doi.org/10.3390/nu8020102

Jin, H., Huo, C., Zhou, T., & Xie, S. (2022). m(1)A RNA Modification in Gene Expression Regulation. *Genes (Basel)*, *13*(5). https://doi.org/10.3390/genes13050910

Kaklamani, V., Yi, N., Sadim, M., Siziopikou, K., Zhang, K., Xu, Y., . . . Mantzoros, C. (2011). The role of the fat mass and obesity associated gene (FTO) in breast cancer risk. *BMC Med Genet*, *12*, 52. https://doi.org/10.1186/1471-2350-12-52

Karanam, K., Kafri, R., Loewer, A., & Lahav, G. (2012). Quantitative live cell imaging reveals a gradual shift between DNA repair mechanisms and a maximal use of HR in mid S phase. *Mol Cell*, *47*(2), 320-329. https://doi.org/10.1016/j.molcel.2012.05.052

Kasowitz, S. D., Ma, J., Anderson, S. J., Leu, N. A., Xu, Y., Gregory, B. D., . . . Wang, P. J. (2018). Nuclear m6A reader YTHDC1 regulates alternative polyadenylation and splicing during mouse oocyte development. *PLoS Genet*, *14*(5), e1007412. https://doi.org/10.1371/journal.pgen.1007412

Kass, E. M., & Jasin, M. (2010). Collaboration and competition between DNA double-strand break repair pathways. *FEBS Lett*, *584*(17), 3703-3708. https://doi.org/10.1016/j.febslet.2010.07.057

Katsuki, Y., Abe, M., Park, S. Y., Wu, W., Yabe, H., Yabe, M., . . . Takata, M. (2021). RNF168 E3 ligase participates in ubiquitin signaling and recruitment of SLX4 during DNA crosslink repair. *Cell Rep*, *37*(4), 109879. https://doi.org/10.1016/j.celrep.2021.109879

Kauffmann, A., Rosselli, F., Lazar, V., Winnepenninckx, V., Mansuet-Lupo, A., Dessen, P., . . . Sarasin, A. (2008). High expression of DNA repair pathways is associated with metastasis in melanoma patients. *Oncogene*, *27*(5), 565-573. https://doi.org/10.1038/sj.onc.1210700

Kawarada, L., Suzuki, T., Ohira, T., Hirata, S., Miyauchi, K., & Suzuki, T. (2017). ALKBH1 is an RNA dioxygenase responsible for cytoplasmic and mitochondrial tRNA modifications. *Nucleic Acids Res*, *45*(12), 7401-7415. https://doi.org/10.1093/nar/gkx354

Kent, T., Chandramouly, G., McDevitt, S. M., Ozdemir, A. Y., & Pomerantz, R. T. (2015). Mechanism of microhomology-mediated end-joining promoted by human DNA polymerase theta. *Nat Struct Mol Biol*, *22*(3), 230-237. https://doi.org/10.1038/nsmb.2961

Khan, F. A., Fang, N., Zhang, W., & Ji, S. (2024). The multifaceted role of Fragile X-Related Protein 1 (FXR1) in cellular processes: an updated review on cancer and clinical applications. *Cell Death Dis*, *15*(1), 72. https://doi.org/10.1038/s41419-023-06413-8

Kluyver, T., Ragan-Kelley, B., Pérez, F., Granger, B., Bussonnier, M., Frederic, J., . . . Jupyter development team. (2016). *Jupyter Notebooks – a publishing format for reproducible computational workflows* 20th International Conference on Electronic Publishing (01/01/16), https://eprints.soton.ac.uk/403913/

Knijnenburg, T. A., Wang, L., Zimmermann, M. T., Chambwe, N., Gao, G. F., Cherniack, A. D., . . . Wang, C. (2018). Genomic and Molecular Landscape of DNA Damage Repair Deficiency across The Cancer Genome Atlas. *Cell Rep*, *23*(1), 239-254 e236. https://doi.org/10.1016/j.celrep.2018.03.076

Koh, C. M., Bezzi, M., & Guccione, E. (2015). The Where and the How of PRMT5. *Current Molecular Biology Reports*, *1*(1), 19-28. https://doi.org/10.1007/s40610-015-0003-5

Konishi, N., Nakamura, M., Ishida, E., Shimada, K., Mitsui, E., Yoshikawa, R., . . . Tsujikawa, K. (2005). High expression of a new marker PCA-1 in human prostate carcinoma. *Clin Cancer Res*, *11*(14), 5090-5097. https://doi.org/10.1158/1078-0432.CCR-05-0195

Kontur, C., Jeong, M., Cifuentes, D., & Giraldez, A. J. (2020). Ythdf m(6)A Readers Function Redundantly during Zebrafish Development. *Cell Rep*, *33*(13), 108598. https://doi.org/10.1016/j.celrep.2020.108598

Koole, W., van Schendel, R., Karambelas, A. E., van Heteren, J. T., Okihara, K. L., & Tijsterman, M. (2014). A Polymerase Theta-dependent repair pathway suppresses extensive genomic instability at endogenous G4 DNA sites. *Nat Commun*, *5*, 3216. https://doi.org/10.1038/ncomms4216

Korn, S. M., Ulshofer, C. J., Schneider, T., & Schlundt, A. (2021). Structures and target RNA preferences of the RNA-binding protein family of IGF2BPs: An overview. *Structure*, *29*(8), 787-803. https://doi.org/10.1016/j.str.2021.05.001

Krais, J. J., Wang, Y., Bernhardy, A. J., Clausen, E., Miller, J. A., Cai, K. Q., . . . Johnson, N. (2020). RNF168-Mediated Ubiquitin Signaling Inhibits the Viability of BRCA1-Null Cancers. *Cancer Res*, *80*(13), 2848-2860. https://doi.org/10.1158/0008-5472.CAN-19-3033

Krais, J. J., Wang, Y., Patel, P., Basu, J., Bernhardy, A. J., & Johnson, N. (2021). RNF168-mediated localization of BARD1 recruits the BRCA1-PALB2 complex to DNA damage. *Nat Commun*, *12*(1), 5016. https://doi.org/10.1038/s41467-021-25346-4

Kuang, W., Jin, H., Yang, F., Chen, X., Liu, J., Li, T., . . . Zhou, T. (2022). ALKBH3-dependent m(1)A demethylation of Aurora A mRNA inhibits ciliogenesis. *Cell Discov*, *8*(1), 25. https://doi.org/10.1038/s41421-022-00385-3

Kumar, R., Khandelwal, N., Chander, Y., Nagori, H., Verma, A., Barua, A., . . . Kumar, N. (2022). S-adenosylmethionine-dependent methyltransferase inhibitor DZNep blocks transcription and translation of SARS-CoV-2 genome with a low tendency to select for drug-resistant viral variants. *Antiviral Res*, *197*, 105232. https://doi.org/10.1016/j.antiviral.2021.105232

Lan, N., Lu, Y., Zhang, Y., Pu, S., Xi, H., Nie, X., . . . Yuan, W. (2020). FTO - A Common Genetic Basis for Obesity and Cancer. *Front Genet*, *11*, 559138. https://doi.org/10.3389/fgene.2020.559138

Lancini, C., van den Berk, P. C., Vissers, J. H., Gargiulo, G., Song, J. Y., Hulsman, D., . . . Citterio, E. (2014). Tight regulation of ubiquitin-mediated DNA damage response by USP3 preserves the functional integrity of hematopoietic stem cells. *J Exp Med*, *211*(9), 1759-1777. https://doi.org/10.1084/jem.20131436

Langerak, P., Mejia-Ramirez, E., Limbo, O., & Russell, P. (2011). Release of Ku and MRN from DNA ends by Mre11 nuclease activity and Ctp1 is required for homologous recombination repair of double-strand breaks. *PLoS Genet*, *7*(9), e1002271. https://doi.org/10.1371/journal.pgen.1002271

Larsen, D. H., Poinsignon, C., Gudjonsson, T., Dinant, C., Payne, M. R., Hari, F. J., . . . Lukas, J. (2010). The chromatin-remodeling factor CHD4 coordinates signaling and repair after DNA damage. *J Cell Biol*, *190*(5), 731-740. https://doi.org/10.1083/jcb.200912135

Lasman, L., Krupalnik, V., Viukov, S., Mor, N., Aguilera-Castrejon, A., Schneir, D., . . . Hanna, J. H. (2020). Context-dependent functional compensation between Ythdf m(6)A reader proteins. *Genes Dev*, *34*(19-20), 1373-1391. https://doi.org/10.1101/gad.340695.120

Law, J. O., Jones, C. M., Stevenson, T., Williamson, T. A., Turner, M. S., Kusumaatmaja, H., & Grellscheid, S. N. (2023). A bending rigidity parameter for stress granule condensates. *Sci Adv*, *9*(20), eadg0432. https://doi.org/10.1126/sciadv.adg0432

Lee, J. H., Hong, J., Zhang, Z., de la Pena Avalos, B., Proietti, C. J., Deamicis, A. R., . . . Xu, K. (2021). Regulation of telomere homeostasis and genomic stability in cancer by N (6)-adenosine methylation (m(6)A). *Sci Adv*, *7*(31). https://doi.org/10.1126/sciadv.abg7073

Lee, J. H., & Paull, T. T. (2004). Direct activation of the ATM protein kinase by the Mre11/Rad50/Nbs1 complex. *Science*, *304*(5667), 93-96. https://doi.org/10.1126/science.1091496

Lee, M. N., Tseng, R. C., Hsu, H. S., Chen, J. Y., Tzao, C., Ho, W. L., & Wang, Y. C. (2007). Epigenetic inactivation of the chromosomal stability control genes BRCA1, BRCA2, and XRCC5 in non-small cell lung cancer. *Clin Cancer Res*, *13*(3), 832-838. https://doi.org/10.1158/1078-0432.CCR-05-2694

Lee, S. O., Kelliher, J. L., Song, W., Tengler, K., Sarkar, A., Dray, E., & Leung, J. W. C. (2023). UBA80 and UBA52 fine-tune RNF168-dependent histone ubiquitination and DNA repair. *J Biol Chem*, *299*(8), 105043. https://doi.org/10.1016/j.jbc.2023.105043

Lee, T., & Pelletier, J. (2016). The biology of DHX9 and its potential as a therapeutic target. *Oncotarget*, *7*(27), 42716-42739. https://doi.org/10.18632/oncotarget.8446

Lee, Y. J., Park, S. J., Ciccone, S. L., Kim, C. R., & Lee, S. H. (2006). An in vivo analysis of MMC-induced DNA damage and its repair. *Carcinogenesis*, *27*(3), 446-453. https://doi.org/10.1093/carcin/bgi254

Lesbirel, S., Viphakone, N., Parker, M., Parker, J., Heath, C., Sudbery, I., & Wilson, S. A. (2018). The m(6)A-methylase complex recruits TREX and regulates mRNA export. *Sci Rep*, *8*(1), 13827. https://doi.org/10.1038/s41598-018-32310-8

Lesbirel, S., & Wilson, S. A. (2019). The m(6)A-methylase complex and mRNA export. *Biochim Biophys Acta Gene Regul Mech*, *1862*(3), 319-328. https://doi.org/10.1016/j.bbagrm.2018.09.008

Li, A., Chen, Y. S., Ping, X. L., Yang, X., Xiao, W., Yang, Y., . . . Yang, Y. G. (2017). Cytoplasmic m(6)A reader YTHDF3 promotes mRNA translation. *Cell Res*, *27*(3), 444-447. https://doi.org/10.1038/cr.2017.10

Li, D., Zhou, L., Liu, Z., Zhang, Z., Mao, W., Shi, W., . . . Wan, Y. (2024). FTO demethylates regulates cell-cycle progression by controlling CCND1 expression in luteinizing goat granulosa cells. *Theriogenology*, *216*, 20-29. https://doi.org/10.1016/j.theriogenology.2023.12.029

Li, H., Liu, Z. Y., Wu, N., Chen, Y. C., Cheng, Q., & Wang, J. (2020). PARP inhibitor resistance: the underlying mechanisms and clinical implications. *Mol Cancer*, *19*(1), 107. https://doi.org/10.1186/s12943-020-01227-0

Li, H., Ren, Y., Mao, K., Hua, F., Yang, Y., Wei, N., . . . Zhang, H. (2018). FTO is involved in Alzheimer's disease by targeting TSC1-mTOR-Tau signaling. *Biochem Biophys Res Commun*, *498*(1), 234-239. https://doi.org/10.1016/j.bbrc.2018.02.201

Li, J., Han, Y., Zhang, H., Qian, Z., Jia, W., Gao, Y., . . . Li, B. (2019). The m6A demethylase FTO promotes the growth of lung cancer cells by regulating the m6A level of USP7 mRNA. *Biochem Biophys Res Commun*, *512*(3), 479-485. https://doi.org/10.1016/j.bbrc.2019.03.093

Li, J., Yang, X., Qi, Z., Sang, Y., Liu, Y., Xu, B., . . . Deng, Y. (2019). The role of mRNA m(6)A methylation in the nervous system. *Cell Biosci*, *9*, 66. https://doi.org/10.1186/s13578-019-0330-y

Li, J., Zuo, Z., Lai, S., Zheng, Z., Liu, B., Wei, Y., & Han, T. (2021). Differential analysis of RNA methylation regulators in gastric cancer based on TCGA data set and construction of a prognostic model. *J Gastrointest Oncol*, *12*(4), 1384-1397. https://doi.org/10.21037/jgo-21-325

Li, Q., Li, X., Tang, H., Jiang, B., Dou, Y., Gorospe, M., & Wang, W. (2017). NSUN2-Mediated m5C Methylation and METTL3/METTL14-Mediated m6A Methylation Cooperatively Enhance p21 Translation. *J Cell Biochem*, *118*(9), 2587-2598. https://doi.org/10.1002/jcb.25957

Li, Q., Wang, C., Dong, W., Su, Y., & Ma, Z. (2021). WTAP facilitates progression of endometrial cancer via CAV-1/NF-kappaB axis. *Cell Biol Int*, *45*(6), 1269-1277. https://doi.org/10.1002/cbin.11570

Li, X., & Manley, J. L. (2005). Inactivation of the SR protein splicing factor ASF/SF2 results in genomic instability. *Cell*, *122*(3), 365-378. https://doi.org/10.1016/j.cell.2005.06.008

Li, X., Peng, J., & Yi, C. (2017). Transcriptome-Wide Mapping of N (1)-Methyladenosine Methylome. *Methods Mol Biol*, *1562*, 245-255. https://doi.org/10.1007/978-1-4939-6807-7_16

Li, X., Xiong, X., Wang, K., Wang, L., Shu, X., Ma, S., & Yi, C. (2016). Transcriptome-wide mapping reveals reversible and dynamic N(1)-methyladenosine methylome. *Nat Chem Biol*, *12*(5), 311-316. https://doi.org/10.1038/nchembio.2040

Li, X., Xiong, X., Zhang, M., Wang, K., Chen, Y., Zhou, J., . . . Yi, C. (2017). Base-Resolution Mapping Reveals Distinct m(1)A Methylome in Nuclear- and Mitochondrial-Encoded Transcripts. *Mol Cell*, *68*(5), 993-1005 e1009. https://doi.org/10.1016/j.molcel.2017.10.019

Li, Y., Bedi, R. K., Moroz-Omori, E. V., & Caflisch, A. (2020). Structural and Dynamic Insights into Redundant Function of YTHDF Proteins. *J Chem Inf Model*, *60*(12), 5932-5935. https://doi.org/10.1021/acs.jcim.0c01029

Li, Y., Su, R., Deng, X., Chen, Y., & Chen, J. (2022). FTO in cancer: functions, molecular mechanisms, and therapeutic implications. *Trends Cancer*, *8*(7), 598-614. https://doi.org/10.1016/j.trecan.2022.02.010

Li, Y., Zheng, D., Wang, F., Xu, Y., Yu, H., & Zhang, H. (2019). Expression of Demethylase Genes, FTO and ALKBH1, Is Associated with Prognosis of Gastric Cancer. *Dig Dis Sci*, *64*(6), 1503-1513. https://doi.org/10.1007/s10620-018-5452-2

Li, Z., Weng, H., Su, R., Weng, X., Zuo, Z., Li, C., . . . Chen, J. (2017). FTO Plays an Oncogenic Role in Acute Myeloid Leukemia as a N(6)-Methyladenosine RNA Demethylase. *Cancer Cell*, *31*(1), 127-141. https://doi.org/10.1016/j.ccell.2016.11.017

Lieber, M. R. (2010). The mechanism of double-strand DNA break repair by the nonhomologous DNA end-joining pathway. *Annu Rev Biochem*, *79*, 181-211. https://doi.org/10.1146/annurev.biochem.052308.093131

Liefke, R., Windhof-Jaidhauser, I. M., Gaedcke, J., Salinas-Riester, G., Wu, F., Ghadimi, M., & Dango, S. (2015). The oxidative demethylase ALKBH3 marks hyperactive gene promoters in human cancer cells. *Genome Med*, *7*(1), 66. https://doi.org/10.1186/s13073-015-0180-0

Lin, F. L., Sperle, K., & Sternberg, N. (1984). Model for homologous recombination during transfer of DNA into mouse L cells: role for DNA ends in the recombination process. *Mol Cell Biol*, *4*(6), 1020-1034. https://doi.org/10.1128/mcb.4.6.1020-1034.1984

Lin, Z., Hsu, P. J., Xing, X., Fang, J., Lu, Z., Zou, Q., . . . Tong, M. H. (2017). Mettl3-/Mettl14-mediated mRNA N(6)-methyladenosine modulates murine spermatogenesis. *Cell Res*, *27*(10), 1216-1230. https://doi.org/10.1038/cr.2017.117

Lindahl, T. (1993). Instability and decay of the primary structure of DNA. *Nature*, *362*(6422), 709-715. https://doi.org/10.1038/362709a0

Linder, B., Grozhik, A. V., Olarerin-George, A. O., Meydan, C., Mason, C. E., & Jaffrey, S. R. (2015). Single-nucleotide-resolution mapping of m6A and m6Am throughout the transcriptome. *Nat Methods*, *12*(8), 767-772. https://doi.org/10.1038/nmeth.3453

Lindtner, S., Zolotukhin, A. S., Uranishi, H., Bear, J., Kulkarni, V., Smulevitch, S., . . . Pavlakis, G. N. (2006). RNA-binding motif protein 15 binds to the RNA transport element RTE and provides a direct link to the NXF1 export pathway. *J Biol Chem*, *281*(48), 36915-36928. https://doi.org/10.1074/jbc.M608745200

Liu, C., Mou, S., & Cai, Y. (2013). FTO gene variant and risk of overweight and obesity among children and adolescents: a systematic review and meta-analysis. *PLoS One*, *8*(11), e82133. https://doi.org/10.1371/journal.pone.0082133

Liu, E., Lee, A. Y., Chiba, T., Olson, E., Sun, P., & Wu, X. (2007). The ATR-mediated S phase checkpoint prevents rereplication in mammalian cells when licensing control is disrupted. *J Cell Biol*, *179*(4), 643-657. https://doi.org/10.1083/jcb.200704138

Liu, F., Clark, W., Luo, G., Wang, X., Fu, Y., Wei, J., . . . He, C. (2016). ALKBH1-Mediated tRNA Demethylation Regulates Translation. *Cell*, *167*(7), 1897. https://doi.org/10.1016/j.cell.2016.11.045

Liu, H., Begik, O., Lucas, M. C., Ramirez, J. M., Mason, C. E., Wiener, D., . . . Novoa, E. M. (2019). Accurate detection of m(6)A RNA modifications in native RNA sequences. *Nat Commun*, *10*(1), 4079. https://doi.org/10.1038/s41467-019-11713-9

Liu, J., Ren, D., Du, Z., Wang, H., Zhang, H., & Jin, Y. (2018). m(6)A demethylase FTO facilitates tumor progression in lung squamous cell carcinoma by regulating MZF1 expression. *Biochem Biophys Res Commun*, *502*(4), 456-464. https://doi.org/10.1016/j.bbrc.2018.05.175

Liu, N., Dai, Q., Zheng, G., He, C., Parisien, M., & Pan, T. (2015). N(6)-methyladenosine-dependent RNA structural switches regulate RNA-protein interactions. *Nature*, *518*(7540), 560-564. https://doi.org/10.1038/nature14234

Liu, N., & Pan, T. (2016). N6-methyladenosine-encoded epitranscriptomics. *Nat Struct Mol Biol*, *23*(2), 98-102. https://doi.org/10.1038/nsmb.3162

Liu, N., Zhou, K. I., Parisien, M., Dai, Q., Diatchenko, L., & Pan, T. (2017). N6-methyladenosine alters RNA structure to regulate binding of a low-complexity protein. *Nucleic Acids Res*, *45*(10), 6051-6063. https://doi.org/10.1093/nar/gkx141

Liu, T., & Huang, J. (2014). Quality control of homologous recombination. *Cell Mol Life Sci*, *71*(19), 3779-3797. https://doi.org/10.1007/s00018-014-1649-5

Liu, T., & Huang, J. (2016). DNA End Resection: Facts and Mechanisms. *Genomics Proteomics Bioinformatics*, *14*(3), 126-130. https://doi.org/10.1016/j.gpb.2016.05.002

Liu, W., Yasui, M., Sassa, A., You, X., Wan, J., Cao, Y., . . . Luan, Y. (2023). FTO regulates the DNA damage response via effects on cell-cycle progression. *Mutat Res Genet Toxicol Environ Mutagen*, *887*, 503608. https://doi.org/10.1016/j.mrgentox.2023.503608

Liu, X. Y., Li, H. L., Su, J. B., Ding, F. H., Zhao, J. J., Chai, F., . . . Chen, X. H. (2015). Regulation of RAGE splicing by hnRNP A1 and Tra2beta-1 and its potential role in AD pathogenesis. *Journal of Neurochemistry*, *133*(2), 187-198. https://doi.org/10.1111/jnc.13069

Livak, K. J., & Schmittgen, T. D. (2001). Analysis of relative gene expression data using real-time quantitative PCR and the 2(-Delta Delta C(T)) Method. *Methods*, *25*(4), 402-408. https://doi.org/10.1006/meth.2001.1262

Longhese, M. P., Bonetti, D., Manfrini, N., & Clerici, M. (2010). Mechanisms and regulation of DNA end resection. *EMBO J*, *29*(17), 2864-2874. https://doi.org/10.1038/emboj.2010.165

Lu, C. S., Truong, L. N., Aslanian, A., Shi, L. Z., Li, Y., Hwang, P. Y., . . . Wu, X. (2012). The RING finger protein RNF8 ubiquitinates Nbs1 to promote DNA double-strand break repair by homologous recombination. *J Biol Chem*, *287*(52), 43984-43994. https://doi.org/10.1074/jbc.M112.421545

Lu, Y., Zou, R., Gu, Q., Wang, X., Zhang, J., Ma, R., . . . Zhang, Y. (2023). CRNDE mediated hnRNPA2B1 stability facilitates nuclear export and translation of KRAS in colorectal cancer. *Cell Death Dis*, *14*(9), 611. https://doi.org/10.1038/s41419-023-06137-9

Luijsterburg, M. S., Typas, D., Caron, M. C., Wiegant, W. W., van den Heuvel, D., Boonen, R. A., . . . van Attikum, H. (2017). A PALB2-interacting domain in RNF168 couples homologous recombination to DNA break-induced chromatin ubiquitylation. *Elife*, *6*. https://doi.org/10.7554/eLife.20922

Ma, J. Z., Yang, F., Zhou, C. C., Liu, F., Yuan, J. H., Wang, F., . . . Sun, S. H. (2017). METTL14 suppresses the metastatic potential of hepatocellular carcinoma by modulating N(6) -methyladenosine-dependent primary MicroRNA processing. *Hepatology*, *65*(2), 529-543. https://doi.org/10.1002/hep.28885

Macari, F., El-Houfi, Y., Boldina, G., Xu, H., Khoury-Hanna, S., Ollier, J., . . . Joubert, D. (2016). TRM6/61 connects PKCalpha with translational control through tRNAi(Met) stabilization: impact on tumorigenesis. *Oncogene*, *35*(14), 1785-1796. https://doi.org/10.1038/onc.2015.244

Mailand, N., Bekker-Jensen, S., Faustrup, H., Melander, F., Bartek, J., Lukas, C., & Lukas, J. (2007). RNF8 ubiquitylates histones at DNA double-strand breaks and promotes assembly of repair proteins. *Cell*, *131*(5), 887-900. https://doi.org/10.1016/j.cell.2007.09.040

Marechal, A., & Zou, L. (2013). DNA damage sensing by the ATM and ATR kinases. *Cold Spring Harb Perspect Biol*, *5*(9). https://doi.org/10.1101/cshperspect.a012716

Masani, S., Han, L., Meek, K., & Yu, K. (2016). Redundant function of DNA ligase 1 and 3 in alternative end-joining during immunoglobulin class switch recombination. *Proc Natl Acad Sci U S A*, *113*(5), 1261-1266. https://doi.org/10.1073/pnas.1521630113

Masuda, S., Das, R., Cheng, H., Hurt, E., Dorman, N., & Reed, R. (2005). Recruitment of the human TREX complex to mRNA during splicing. *Genes Dev*, *19*(13), 1512-1517. https://doi.org/10.1101/gad.1302205

Mateos-Gomez, P. A., Gong, F., Nair, N., Miller, K. M., Lazzerini-Denchi, E., & Sfeir, A. (2015). Mammalian polymerase theta promotes alternative NHEJ and suppresses recombination. *Nature*, *518*(7538), 254-257. https://doi.org/10.1038/nature14157

Mathiyalagan, P., Adamiak, M., Mayourian, J., Sassi, Y., Liang, Y., Agarwal, N., . . . Sahoo, S. (2019). FTO-Dependent N(6)-Methyladenosine Regulates Cardiac Function During Remodeling and Repair. *Circulation*, *139*(4), 518-532. https://doi.org/10.1161/CIRCULATIONAHA.118.033794

Matos, J., & West, S. C. (2014). Holliday junction resolution: regulation in space and time. *DNA Repair (Amst)*, *19*(100), 176-181. https://doi.org/10.1016/j.dnarep.2014.03.013

Mattiroli, F., Vissers, J. H., van Dijk, W. J., Ikpa, P., Citterio, E., Vermeulen, W., . . . Sixma, T. K. (2012). RNF168 ubiquitinates K13-15 on H2A/H2AX to drive DNA damage signaling. *Cell*, *150*(6), 1182-1195. https://doi.org/10.1016/j.cell.2012.08.005

Mauer, J., Luo, X., Blanjoie, A., Jiao, X., Grozhik, A. V., Patil, D. P., . . . Jaffrey, S. R. (2017a). Reversible methylation of m(6)A(m) in the 5′ cap controls mRNA stability. *Nature*, *541*(7637), 371-375. https://doi.org/10.1038/nature21022

Mauer, J., Luo, X., Blanjoie, A., Jiao, X., Grozhik, A. V., Patil, D. P., . . . Jaffrey, S. R. (2017b). Reversible methylation of m(6)Am in the 5′ cap controls mRNA stability. *Nature*, *541*(7637), 371-375. https://doi.org/10.1038/nature21022

Mauer, J., Sindelar, M., Despic, V., Guez, T., Hawley, B. R., Vasseur, J. J., . . . Jaffrey, S. R. (2019). FTO controls reversible m(6)Am RNA methylation during snRNA biogenesis. *Nat Chem Biol*, *15*(4), 340-347. https://doi.org/10.1038/s41589-019-0231-8

McHugh, P. J., Spanswick, V. J., & Hartley, J. A. (2001). Repair of DNA interstrand crosslinks: molecular mechanisms and clinical relevance. *Lancet Oncol*, *2*(8), 483-490. https://doi.org/10.1016/S1470-2045(01)00454-5

Meerang, M., Ritz, D., Paliwal, S., Garajova, Z., Bosshard, M., Mailand, N., . . . Ramadan, K. (2011). The ubiquitin-selective segregase VCP/p97 orchestrates the response to DNA double-strand breaks. *Nat Cell Biol*, *13*(11), 1376-1382. https://doi.org/10.1038/ncb2367

Meyer, K. D., Patil, D. P., Zhou, J., Zinoviev, A., Skabkin, M. A., Elemento, O., . . . Jaffrey, S. R. (2015). 5′ UTR m(6)A Promotes Cap-Independent Translation. *Cell*, *163*(4), 999-1010. https://doi.org/10.1016/j.cell.2015.10.012

Meyer, K. D., Saletore, Y., Zumbo, P., Elemento, O., Mason, C. E., & Jaffrey, S. R. (2012). Comprehensive analysis of mRNA methylation reveals enrichment in 3′ UTRs and near stop codons. *Cell*, *149*(7), 1635-1646. https://doi.org/10.1016/j.cell.2012.05.003

Michael, W. M., Choi, M., & Dreyfuss, G. (1995). A nuclear export signal in hnRNP A1: a signal-mediated, temperature-dependent nuclear protein export pathway. *Cell*, *83*(3), 415-422. https://doi.org/10.1016/0092-8674(95)90119-1

Mills, K. D., Ferguson, D. O., & Alt, F. W. (2003). The role of DNA breaks in genomic instability and tumorigenesis. *Immunol Rev*, *194*, 77-95. https://doi.org/10.1034/j.1600-065x.2003.00060.x

Mimitou, E. P., & Symington, L. S. (2008). Sae2, Exo1 and Sgs1 collaborate in DNA double-strand break processing. *Nature*, *455*(7214), 770-774. https://doi.org/10.1038/nature07312

Mimitou, E. P., & Symington, L. S. (2010). Ku prevents Exo1 and Sgs1-dependent resection of DNA ends in the absence of a functional MRX complex or Sae2. *EMBO J*, *29*(19), 3358-3369. https://doi.org/10.1038/emboj.2010.193

Mirman, Z., & de Lange, T. (2020). 53BP1: a DSB escort. *Genes Dev*, *34*(1-2), 7-23. https://doi.org/10.1101/gad.333237.119

Mohan, M., Akula, D., Dhillon, A., Goyal, A., & Anindya, R. (2019). Human RAD51 paralogue RAD51C fosters repair of alkylated DNA by interacting with the ALKBH3 demethylase. *Nucleic Acids Res*, *47*(22), 11729-11745. https://doi.org/10.1093/nar/gkz938

Montazeri, F., Hatami, H., Fathi, S., Hasanpour Ardekanizadeh, N., Bourbour, F., Rastgoo, S., . . . Doaei, S. (2022). FTO genotype was associated with breast cancer in HER2 negative patients. *Clin Nutr ESPEN*, *49*, 495-498. https://doi.org/10.1016/j.clnesp.2022.02.122

Moretton, A., Kourtis, S., Ganez Zapater, A., Calabro, C., Espinar Calvo, M. L., Fontaine, F., . . . Sdelci, S. (2023). A metabolic map of the DNA damage response identifies PRDX1 in the control of nuclear ROS scavenging and aspartate availability. *Mol Syst Biol*, *19*(7), e11267. https://doi.org/10.15252/msb.202211267

Mortensen, U. H., Bendixen, C., Sunjevaric, I., & Rothstein, R. (1996). DNA strand annealing is promoted by the yeast Rad52 protein. *Proc Natl Acad Sci U S A*, *93*(20), 10729-10734. https://doi.org/10.1073/pnas.93.20.10729

Mosbech, A., Lukas, C., Bekker-Jensen, S., & Mailand, N. (2013). The deubiquitylating enzyme USP44 counteracts the DNA double-strand break response mediated by the RNF8 and RNF168 ubiquitin ligases. *J Biol Chem*, *288*(23), 16579-16587. https://doi.org/10.1074/jbc.M113.459917

Moshous, D., Callebaut, I., de Chasseval, R., Corneo, B., Cavazzana-Calvo, M., Le Deist, F., . . . de Villartay, J. P. (2001). Artemis, a novel DNA double-strand break repair/V(D)J recombination protein, is mutated in human severe combined immune deficiency. *Cell*, *105*(2), 177-186. https://doi.org/10.1016/s0092-8674(01)00309-9

Motycka, T. A., Bessho, T., Post, S. M., Sung, P., & Tomkinson, A. E. (2004). Physical and functional interaction between the XPF/ERCC1 endonuclease and hRad52. *J Biol Chem*, *279*(14), 13634-13639. https://doi.org/10.1074/jbc.M313779200

Muller-McNicoll, M., Botti, V., de Jesus Domingues, A. M., Brandl, H., Schwich, O. D., Steiner, M. C., . . . Neugebauer, K. M. (2016). SR proteins are NXF1 adaptors that link alternative RNA processing to mRNA export. *Genes Dev*, *30*(5), 553-566. https://doi.org/10.1101/gad.276477.115

Munoz, M. C., Laulier, C., Gunn, A., Cheng, A., Robbiani, D. F., Nussenzweig, A., & Stark, J. M. (2012). Ring Finger Nuclear Factor RNF168 Is Important for Defects in Homologous Recombination Caused by Loss of the Breast Cancer Susceptibility Factor BRCA1. *Journal of Biological Chemistry*, *287*(48), 40618-40628. https://doi.org/10.1074/jbc.M112.410951

Mustofa, M. K., Tanoue, Y., Chirifu, M., Shimasaki, T., Tateishi, C., Nakamura, T., & Tateishi, S. (2021). RAD18 mediates DNA double-strand break-induced ubiquitination of chromatin protein. *J Biochem*, *170*(1), 33-40. https://doi.org/10.1093/jb/mvab010

Muthukrishnan, S., Both, G. W., Furuichi, Y., & Shatkin, A. J. (1975). 5'-Terminal 7-methylguanosine in eukaryotic mRNA is required for translation. *Nature*, *255*(5503), 33-37. https://doi.org/10.1038/255033a0

Neubauer, G., King, A., Rappsilber, J., Calvio, C., Watson, M., Ajuh, P., . . . Mann, M. (1998). Mass spectrometry and EST-database searching allows characterization of the multi-protein spliceosome complex. *Nat Genet*, *20*(1), 46-50. https://doi.org/10.1038/1700

Newman, E. A., Lu, F., Bashllari, D., Wang, L., Opipari, A. W., & Castle, V. P. (2015). Alternative NHEJ Pathway Components Are Therapeutic Targets in High-Risk Neuroblastoma. *Mol Cancer Res*, *13*(3), 470-482. https://doi.org/10.1158/1541-7786.MCR-14-0337

Nick McElhinny, S. A., Snowden, C. M., McCarville, J., & Ramsden, D. A. (2000). Ku recruits the XRCC4-ligase IV complex to DNA ends. *Mol Cell Biol*, *20*(9), 2996-3003. https://doi.org/10.1128/MCB.20.9.2996-3003.2000

Nimonkar, A. V., Genschel, J., Kinoshita, E., Polaczek, P., Campbell, J. L., Wyman, C., . . . Kowalczykowski, S. C. (2011). BLM-DNA2-RPA-MRN and EXO1-BLM-RPA-MRN constitute two DNA end resection machineries for human DNA break repair. *Genes Dev*, *25*(4), 350-362. https://doi.org/10.1101/gad.2003811

Niu, F., Che, P., Yang, Z., Zhang, J., Yang, L., Zhuang, M., . . . Ji, S. J. (2022). m(6)A regulation of cortical and retinal neurogenesis is mediated by the redundant m(6)A readers YTHDFs. *iScience*, *25*(9), 104908. https://doi.org/10.1016/j.isci.2022.104908

Niu, Y., Lin, Z., Wan, A., Chen, H., Liang, H., Sun, L., . . . Wan, G. (2019). RNA N6-methyladenosine demethylase FTO promotes breast tumor progression through inhibiting BNIP3. *Mol Cancer*, *18*(1), 46. https://doi.org/10.1186/s12943-019-1004-4

Noordermeer, S. M., Adam, S., Setiaputra, D., Barazas, M., Pettitt, S. J., Ling, A. K., . . . Durocher, D. (2018). The shieldin complex mediates 53BP1-dependent DNA repair. *Nature*, *560*(7716), 117-121. https://doi.org/10.1038/s41586-018-0340-7

Nowsheen, S., & Lou, Z. (2018). Calling RNF168 to action. *Cell Stress*, *2*(5), 113-114. https://doi.org/10.15698/cst2018.05.135

O'Connor, M. J. (2015). Targeting the DNA Damage Response in Cancer. *Mol Cell*, *60*(4), 547-560. https://doi.org/10.1016/j.molcel.2015.10.040

Ochi, T., Blackford, A. N., Coates, J., Jhujh, S., Mehmood, S., Tamura, N., . . . Jackson, S. P. (2015). DNA repair. PAXX, a paralog of XRCC4 and XLF, interacts with Ku to promote DNA double-strand break repair. *Science*, *347*(6218), 185-188. https://doi.org/10.1126/science.1261971

Ochs, F., Somyajit, K., Altmeyer, M., Rask, M. B., Lukas, J., & Lukas, C. (2016). 53BP1 fosters fidelity of homology-directed DNA repair. *Nat Struct Mol Biol*, *23*(8), 714-721. https://doi.org/10.1038/nsmb.3251

Ogi, T., & Lehmann, A. R. (2006). The Y-family DNA polymerase kappa (pol kappa) functions in mammalian nucleotide-excision repair. *Nat Cell Biol*, *8*(6), 640-642. https://doi.org/10.1038/ncb1417

Onaka, A. T., Su, J., Katahira, Y., Tang, C., Zafar, F., Aoki, K., . . . Nakagawa, T. (2020). DNA replication machinery prevents Rad52-dependent single-strand annealing that leads to gross chromosomal rearrangements at centromeres. *Commun Biol*, *3*(1), 202. https://doi.org/10.1038/s42003-020-0934-0

Orel, N., Kyryk, A., & Puchta, H. (2003). Different pathways of homologous recombination are used for the repair of double-strand breaks within tandemly arranged sequences in the plant genome. *Plant J*, *35*(5), 604-612. https://doi.org/10.1046/j.1365-313x.2003.01832.x

Ougland, R., Rognes, T., Klungland, A., & Larsen, E. (2015). Non-homologous functions of the AlkB homologs. *J Mol Cell Biol*, *7*(6), 494-504. https://doi.org/10.1093/jmcb/mjv029

Owens, J. L., Beketova, E., Liu, S., Tinsley, S. L., Asberry, A. M., Deng, X., . . . Hu, C. D. (2020). PRMT5 Cooperates with pICln to Function as a Master Epigenetic Activator of DNA Double-Strand Break Repair Genes. *iScience*, *23*(1), 100750. https://doi.org/10.1016/j.isci.2019.100750

Ozkurede, U., Kala, R., Johnson, C., Shen, Z., Miller, R. A., & Garcia, G. G. (2019). Cap-independent mRNA translation is upregulated in long-lived endocrine mutant mice. *J Mol Endocrinol*, *63*(2), 123-138. https://doi.org/10.1530/JME-19-0021

Pandey, R. R., Delfino, E., Homolka, D., Roithova, A., Chen, K. M., Li, L., . . . Pillai, R. S. (2020). The Mammalian Cap-Specific m(6)Am RNA Methyltransferase PCIF1 Regulates Transcript Levels in Mouse Tissues. *Cell Rep*, *32*(7), 108038. https://doi.org/10.1016/j.celrep.2020.108038

Pannunzio, N. R., Li, S., Watanabe, G., & Lieber, M. R. (2014). Non-homologous end joining often uses microhomology: implications for alternative end joining. *DNA Repair (Amst)*, *17*, 74-80. https://doi.org/10.1016/j.dnarep.2014.02.006

Paques, F., & Haber, J. E. (1999). Multiple pathways of recombination induced by double-strand breaks in Saccharomyces cerevisiae. *Microbiol Mol Biol Rev*, *63*(2), 349-404. https://doi.org/10.1128/MMBR.63.2.349-404.1999

Pardo, B., Gomez-Gonzalez, B., & Aguilera, A. (2009). DNA repair in mammalian cells: DNA double-strand break repair: how to fix a broken relationship. *Cell Mol Life Sci*, *66*(6), 1039-1056. https://doi.org/10.1007/s00018-009-8740-3

Park, O. H., Ha, H., Lee, Y., Boo, S. H., Kwon, D. H., Song, H. K., & Kim, Y. K. (2019). Endoribonucleolytic Cleavage of m(6)A-Containing RNAs by RNase P/MRP Complex. *Mol Cell*, *74*(3), 494-507 e498. https://doi.org/10.1016/j.molcel.2019.02.034

Patel, P. S., Abraham, K. J., Guturi, K. K. N., Halaby, M. J., Khan, Z., Palomero, L., . . . Hakem, R. (2021). RNF168 regulates R-loop resolution and genomic stability in BRCA1/2-deficient tumors. *J Clin Invest*, *131*(3). https://doi.org/10.1172/JCI140105

Pathania, S., Bade, S., Le Guillou, M., Burke, K., Reed, R., Bowman-Colin, C., . . . Livingston, D. M. (2014). BRCA1 haploinsufficiency for replication stress suppression in primary cells. *Nat Commun*, *5*, 5496. https://doi.org/10.1038/ncomms6496

Peifer, C., Sharma, S., Watzinger, P., Lamberth, S., Kotter, P., & Entian, K. D. (2013). Yeast Rrp8p, a novel methyltransferase responsible for m1A 645 base modification of 25S rRNA. *Nucleic Acids Res*, *41*(2), 1151-1163. https://doi.org/10.1093/nar/gks1102

Petri, B. J., & Klinge, C. M. (2023). m6A readers, writers, erasers, and the m6A epitranscriptome in breast cancer. *J Mol Endocrinol*, *70*(2). https://doi.org/10.1530/JME-22-0110

Peuscher, M. H., & Jacobs, J. J. (2011). DNA-damage response and repair activities at uncapped telomeres depend on RNF8. *Nat Cell Biol*, *13*(9), 1139-1145. https://doi.org/10.1038/ncb2326

Pimentel, H., Bray, N. L., Puente, S., Melsted, P., & Pachter, L. (2017). Differential analysis of RNA-seq incorporating quantification uncertainty. *Nat Methods*, *14*(7), 687-690. https://doi.org/10.1038/nmeth.4324

Pinato, S., Scandiuzzi, C., Arnaudo, N., Citterio, E., Gaudino, G., & Penengo, L. (2009). RNF168, a new RING finger, MIU-containing protein that modifies chromatin by ubiquitination of histones H2A and H2AX. *BMC Mol Biol*, *10*, 55. https://doi.org/10.1186/1471-2199-10-55

Ping, X. L., Sun, B. F., Wang, L., Xiao, W., Yang, X., Wang, W. J., . . . Yang, Y. G. (2014). Mammalian WTAP is a regulatory subunit of the RNA N6-methyladenosine methyltransferase. *Cell Res*, *24*(2), 177-189. https://doi.org/10.1038/cr.2014.3

Polo, S. E., & Jackson, S. P. (2011). Dynamics of DNA damage response proteins at DNA breaks: a focus on protein modifications. *Genes Dev*, *25*(5), 409-433. https://doi.org/10.1101/gad.2021311

Pontier, D. B., & Tijsterman, M. (2009). A robust network of double-strand break repair pathways governs genome integrity during C. elegans development. *Curr Biol*, *19*(16), 1384-1388. https://doi.org/10.1016/j.cub.2009.06.045

Popovic, D., Vucic, D., & Dikic, I. (2014). Ubiquitination in disease pathogenesis and treatment. *Nat Med*, *20*(11), 1242-1253. https://doi.org/10.1038/nm.3739

Poulsen, M., Lukas, C., Lukas, J., Bekker-Jensen, S., & Mailand, N. (2012). Human RNF169 is a negative regulator of the ubiquitin-dependent response to DNA double-strand breaks. *J Cell Biol*, *197*(2), 189-199. https://doi.org/10.1083/jcb.201109100

Protter, D. S. W., & Parker, R. (2016). Principles and Properties of Stress Granules. *Trends Cell Biol*, *26*(9), 668-679. https://doi.org/10.1016/j.tcb.2016.05.004

Qi, Z., Zhang, C., Jian, H., Hou, M., Lou, Y., Kang, Y., . . . Zhou, H. (2023). N(1)-Methyladenosine modification of mRNA regulates neuronal gene expression and oxygen glucose deprivation/reoxygenation induction. *Cell Death Discov*, *9*(1), 159. https://doi.org/10.1038/s41420-023-01458-2

Qiu, S., & Huang, J. (2021). MRN complex is an essential effector of DNA damage repair. *J Zhejiang Univ Sci B*, *22*(1), 31-37. https://doi.org/10.1631/jzus.B2000289

Rai, R., Li, J. M., Zheng, H., Lok, G. T., Deng, Y., Huen, M. S., . . . Chang, S. (2011). The E3 ubiquitin ligase Rnf8 stabilizes Tpp1 to promote telomere end protection. *Nat Struct Mol Biol*, *18*(12), 1400-1407. https://doi.org/10.1038/nsmb.2172

Ramanathan, A., Robb, G. B., & Chan, S. H. (2016). mRNA capping: biological functions and applications. *Nucleic Acids Res*, *44*(16), 7511-7526. https://doi.org/10.1093/nar/gkw551

Rass, E., Grabarz, A., Plo, I., Gautier, J., Bertrand, P., & Lopez, B. S. (2009). Role of Mre11 in chromosomal nonhomologous end joining in mammalian cells. *Nat Struct Mol Biol*, *16*(8), 819-824. https://doi.org/10.1038/nsmb.1641

Reczek, C. R., Szabolcs, M., Stark, J. M., Ludwig, T., & Baer, R. (2013). The interaction between CtIP and BRCA1 is not essential for resection-mediated DNA repair or tumor suppression. *J Cell Biol*, *201*(5), 693-707. https://doi.org/10.1083/jcb.201302145

Reddy, G., Golub, E. I., & Radding, C. M. (1997). Human Rad52 protein promotes single-strand DNA annealing followed by branch migration. *Mutat Res*, *377*(1), 53-59. https://doi.org/10.1016/s0027-5107(97)00057-2

Reed, R., & Cheng, H. (2005). TREX, SR proteins and export of mRNA. *Curr Opin Cell Biol*, *17*(3), 269-273. https://doi.org/10.1016/j.ceb.2005.04.011

Riches, L. C., Lynch, A. M., & Gooderham, N. J. (2008). Early events in the mammalian response to DNA double-strand breaks. *Mutagenesis*, *23*(5), 331-339. https://doi.org/10.1093/mutage/gen039

Roost, C., Lynch, S. R., Batista, P. J., Qu, K., Chang, H. Y., & Kool, E. T. (2015). Structure and thermodynamics of N6-methyladenosine in RNA: a spring-loaded base modification. *J Am Chem Soc*, *137*(5), 2107-2115. https://doi.org/10.1021/ja513080v

Rothenberg, E., Grimme, J. M., Spies, M., & Ha, T. (2008). Human Rad52-mediated homology search and annealing occurs by continuous interactions between overlapping nucleoprotein complexes. *Proc Natl Acad Sci U S A*, *105*(51), 20274-20279. https://doi.org/10.1073/pnas.0810317106

Roundtree, I. A., Evans, M. E., Pan, T., & He, C. (2017). Dynamic RNA Modifications in Gene Expression Regulation. *Cell*, *169*(7), 1187-1200. https://doi.org/10.1016/j.cell.2017.05.045

Roundtree, I. A., Luo, G. Z., Zhang, Z., Wang, X., Zhou, T., Cui, Y., . . . He, C. (2017). YTHDC1 mediates nuclear export of N(6)-methyladenosine methylated mRNAs. *Elife*, *6*. https://doi.org/10.7554/eLife.31311

Rouse, J., & Jackson, S. P. (2002). Interfaces between the detection, signaling, and repair of DNA damage. *Science*, *297*(5581), 547-551. https://doi.org/10.1126/science.1074740

Ruan, D. Y., Li, T., Wang, Y. N., Meng, Q., Li, Y., Yu, K., . . . Xu, R. H. (2021). FTO downregulation mediated by hypoxia facilitates colorectal cancer metastasis. *Oncogene*, *40*(33), 5168-5181. https://doi.org/10.1038/s41388-021-01916-0

Ruis, B. L., Fattah, K. R., & Hendrickson, E. A. (2008). The catalytic subunit of DNA-dependent protein kinase regulates proliferation, telomere length, and genomic stability in human somatic cells. *Mol Cell Biol*, *28*(20), 6182-6195. https://doi.org/10.1128/MCB.00355-08

Rydberg, B., & Lindahl, T. (1982). Nonenzymatic methylation of DNA by the intracellular methyl group donor S-adenosyl-L-methionine is a potentially mutagenic reaction. *EMBO J*, *1*(2), 211-216. https://doi.org/10.1002/j.1460-2075.1982.tb01149.x

Sabarneh, A., Ereqat, S., Cauchi, S., AbuShamma, O., Abdelhafez, M., Ibrahim, M., & Nasereddin, A. (2018). Common FTO rs9939609 variant and risk of type 2 diabetes in Palestine. *BMC Med Genet*, *19*(1), 156. https://doi.org/10.1186/s12881-018-0668-8

Safra, M., Sas-Chen, A., Nir, R., Winkler, R., Nachshon, A., Bar-Yaacov, D., . . . Schwartz, S. (2017). The m1A landscape on cytosolic and mitochondrial mRNA at single-base resolution. *Nature*, *551*(7679), 251-255. https://doi.org/10.1038/nature24456

Saletore, Y., Meyer, K., Korlach, J., Vilfan, I. D., Jaffrey, S., & Mason, C. E. (2012). The birth of the Epitranscriptome: deciphering the function of RNA modifications. *Genome Biol*, *13*(10), 175. https://doi.org/10.1186/gb-2012-13-10-175

Samson, L., & Cairns, J. (1977). A new pathway for DNA repair in Escherichia coli. *Nature*, *267*(5608), 281-283. https://doi.org/10.1038/267281a0

Sanford, J. R., Ellis, J. D., Cazalla, D., & Caceres, J. F. (2005). Reversible phosphorylation differentially affects nuclear and cytoplasmic functions of splicing factor 2/alternative splicing factor. *Proc Natl Acad Sci U S A*, *102*(42), 15042-15047. https://doi.org/10.1073/pnas.0507827102

Schibler, U., Kelley, D. E., & Perry, R. P. (1977). Comparison of methylated sequences in messenger RNA and heterogeneous nuclear RNA from mouse L cells. *J Mol Biol*, *115*(4), 695-714. https://doi.org/10.1016/0022-2836(77)90110-3

Schlacher, K., Christ, N., Siaud, N., Egashira, A., Wu, H., & Jasin, M. (2011). Double-strand break repair-independent role for BRCA2 in blocking stalled replication fork degradation by MRE11. *Cell*, *145*(4), 529-542. https://doi.org/10.1016/j.cell.2011.03.041

Schmid, J. A., Berti, M., Walser, F., Raso, M. C., Schmid, F., Krietsch, J., . . . Penengo, L. (2018). Histone Ubiquitination by the DNA Damage Response Is Required for Efficient DNA Replication in Unperturbed S Phase. *Mol Cell*, *71*(6), 897-910 e898. https://doi.org/10.1016/j.molcel.2018.07.011

Schwartz, S. (2018). m(1)A within cytoplasmic mRNAs at single nucleotide resolution: a reconciled transcriptome-wide map. *RNA*, *24*(11), 1427-1436. https://doi.org/10.1261/rna.067348.118

Schwartz, S., Agarwala, S. D., Mumbach, M. R., Jovanovic, M., Mertins, P., Shishkin, A., . . . Regev, A. (2013). High-resolution mapping reveals a conserved, widespread, dynamic mRNA methylation program in yeast meiosis. *Cell*, *155*(6), 1409-1421. https://doi.org/10.1016/j.cell.2013.10.047

Schwertman, P., Bekker-Jensen, S., & Mailand, N. (2016). Regulation of DNA double-strand break repair by ubiquitin and ubiquitin-like modifiers. *Nat Rev Mol Cell Biol*, *17*(6), 379-394. https://doi.org/10.1038/nrm.2016.58

Scully, R., Panday, A., Elango, R., & Willis, N. A. (2019). DNA double-strand break repair-pathway choice in somatic mammalian cells. *Nat Rev Mol Cell Biol*, *20*(11), 698-714. https://doi.org/10.1038/s41580-019-0152-0

Sedgwick, B., Bates, P. A., Paik, J., Jacobs, S. C., & Lindahl, T. (2007). Repair of alkylated DNA: recent advances. *DNA Repair (Amst)*, *6*(4), 429-442. https://doi.org/10.1016/j.dnarep.2006.10.005

Sendinc, E., Valle-Garcia, D., Dhall, A., Chen, H., Henriques, T., Navarrete-Perea, J., . . . Shi, Y. (2019). PCIF1 Catalyzes m6Am mRNA Methylation to Regulate Gene Expression. *Mol Cell*, *75*(3), 620-630 e629. https://doi.org/10.1016/j.molcel.2019.05.030

Seo, K. W., & Kleiner, R. E. (2020). YTHDF2 Recognition of N(1)-Methyladenosine (m(1)A)-Modified RNA Is Associated with Transcript Destabilization. *ACS Chem Biol*, *15*(1), 132-139. https://doi.org/10.1021/acschembio.9b00655

Sfeir, A., & Symington, L. S. (2015). Microhomology-Mediated End Joining: A Back-up Survival Mechanism or Dedicated Pathway? *Trends in Biochemical Sciences*, *40*(11), 701-714. https://doi.org/10.1016/j.tibs.2015.08.006

Shafik, A. M., Zhou, H., Lim, J., Dickinson, B., & Jin, P. (2022). Dysregulated mitochondrial and cytosolic tRNA m1A methylation in Alzheimer's disease. *Hum Mol Genet*, *31*(10), 1673-1680. https://doi.org/10.1093/hmg/ddab357

Shanbhag, N. M., Rafalska-Metcalf, I. U., Balane-Bolivar, C., Janicki, S. M., & Greenberg, R. A. (2010). ATM-dependent chromatin changes silence transcription in cis to DNA double-strand breaks. *Cell*, *141*(6), 970-981. https://doi.org/10.1016/j.cell.2010.04.038

Sharma, A., Alswillah, T., Singh, K., Chatterjee, P., Willard, B., Venere, M., . . . Almasan, A. (2018). USP14 regulates DNA damage repair by targeting RNF168-dependent ubiquitination. *Autophagy*, *14*(11), 1976-1990. https://doi.org/10.1080/15548627.2018.1496877

Sharma, R., Lewis, S., & Wlodarski, M. W. (2020). DNA Repair Syndromes and Cancer: Insights Into Genetics and Phenotype Patterns. *Frontiers in Pediatrics*, *8*, 570084. https://doi.org/10.3389/fped.2020.570084

Shen, C., Sheng, Y., Zhu, A. C., Robinson, S., Jiang, X., Dong, L., . . . Chen, J. (2020). RNA Demethylase ALKBH5 Selectively Promotes Tumorigenesis and Cancer Stem Cell Self-Renewal in Acute Myeloid Leukemia. *Cell Stem Cell*, *27*(1), 64-80 e69. https://doi.org/10.1016/j.stem.2020.04.009

Shi, H., Wang, X., Lu, Z., Zhao, B. S., Ma, H., Hsu, P. J., . . . He, C. (2017). YTHDF3 facilitates translation and decay of N(6)-methyladenosine-modified RNA. *Cell Res*, *27*(3), 315-328. https://doi.org/10.1038/cr.2017.15

Shi, H., Zhao, J., Han, L., Xu, M., Wang, K., Shi, J., & Dong, Z. (2020). Retrospective study of gene signatures and prognostic value of m6A regulatory factor in non-small cell lung cancer using TCGA database and the verification of FTO. *Aging (Albany NY)*, *12*(17), 17022-17037. https://doi.org/10.18632/aging.103622

Shi, L., Chen, W., Zhang, Z., Chen, J., & Xue, M. (2021). N1-methyladenosine profiling of long non-coding RNA in colorectal cancer. *IUBMB Life*, *73*(10), 1235-1243. https://doi.org/10.1002/iub.2534

Shi, L., Yang, X. M., Tang, D. D., Liu, G., Yuan, P., Yang, Y., . . . Song, D. K. (2015). Expression and significance of m1A transmethylase, hTrm6p/hTrm61p and its related gene hTrm6/hTrm61 in bladder urothelial carcinoma. *Am J Cancer Res*, *5*(7), 2169-2179. https://www.ncbi.nlm.nih.gov/pubmed/26328247

Shi, Q. M., Xue, C., Yuan, X., He, Y. T., & Yu, Z. J. (2020). Gene signatures and prognostic values of m1A-related regulatory genes in hepatocellular carcinoma. *Scientific Reports*, *10*(1). https://doi.org/ARTN 15083 10.1038/s41598-020-72178-1

Shibata, A. (2017). Regulation of repair pathway choice at two-ended DNA double-strand breaks. *Mutat Res*, *803-805*, 51-55. https://doi.org/10.1016/j.mrfmmm.2017.07.011

Shibata, A., & Jeggo, P. A. (2021). ATM's Role in the Repair of DNA Double-Strand Breaks. *Genes (Basel)*, *12*(9). https://doi.org/10.3390/genes12091370

Shimada, K., Fujii, T., Tsujikawa, K., Anai, S., Fujimoto, K., & Konishi, N. (2012). ALKBH3 contributes to survival and angiogenesis of human urothelial carcinoma cells through NADPH oxidase and tweak/Fn14/VEGF signals. *Clin Cancer Res*, *18*(19), 5247-5255. https://doi.org/10.1158/1078-0432.CCR-12-0955

Shivange, G., Monisha, M., Nigam, R., Kodipelli, N., & Anindya, R. (2016). RecA stimulates AlkB-mediated direct repair of DNA adducts. *Nucleic Acids Res*, *44*(18), 8754-8763. https://doi.org/10.1093/nar/gkw611

Shrivastav, N., Li, D., & Essigmann, J. M. (2010). Chemical biology of mutagenesis and DNA repair: cellular responses to DNA alkylation. *Carcinogenesis*, *31*(1), 59-70. https://doi.org/10.1093/carcin/bgp262

Shu, J., Wang, X., Yang, X., & Zhao, G. (2023). Author Correction: ATM inhibitor KU60019 synergistically sensitizes lung cancer cells to topoisomerase II poisons by multiple mechanisms. *Sci Rep*, *13*(1), 13850. https://doi.org/10.1038/s41598-023-40952-6

Sikorski, P. J., Warminski, M., Kubacka, D., Ratajczak, T., Nowis, D., Kowalska, J., & Jemielity, J. (2020). The identity and methylation status of the first transcribed nucleotide in eukaryotic mRNA 5′ cap modulates protein expression in living cells. *Nucleic Acids Res*, *48*(4), 1607-1626. https://doi.org/10.1093/nar/gkaa032

Skoko, J. J., Cao, J., Gaboriau, D., Attar, M., Asan, A., Hong, L., . . . Neumann, C. A. (2022). Redox regulation of RAD51 Cys319 and homologous recombination by peroxiredoxin 1. *Redox Biol*, *56*, 102443. https://doi.org/10.1016/j.redox.2022.102443

Slobodin, B., Han, R., Calderone, V., Vrielink, J., Loayza-Puch, F., Elkon, R., & Agami, R. (2017). Transcription Impacts the Efficiency of mRNA Translation via Co-transcriptional N6-adenosine Methylation. *Cell*, *169*(2), 326-337 e312. https://doi.org/10.1016/j.cell.2017.03.031

Sobhian, B., Shao, G., Lilli, D. R., Culhane, A. C., Moreau, L. A., Xia, B., . . . Greenberg, R. A. (2007). RAP80 targets BRCA1 to specific ubiquitin structures at DNA damage sites. *Science*, *316*(5828), 1198-1202. https://doi.org/10.1126/science.1139516

Song, H. P., Wang, Y., Wang, R. X., Zhang, X., Liu, Y. P., Jia, G. F., & Chen, P. R. (2020). SFPQ Is an FTO-Binding Protein that Facilitates the Demethylation Substrate Preference. *Cell Chemical Biology*, *27*(3), 283-+. https://doi.org/10.1016/j.chembiol.2020.01.002

Songe-Moller, L., van den Born, E., Leihne, V., Vagbo, C. B., Kristoffersen, T., Krokan, H. E., . . . Klungland, A. (2010). Mammalian ALKBH8 possesses tRNA methyltransferase activity required for the biogenesis of multiple wobble uridine modifications implicated in translational decoding. *Mol Cell Biol*, *30*(7), 1814-1827. https://doi.org/10.1128/MCB.01602-09

Stark, J. M., Pierce, A. J., Oh, J., Pastink, A., & Jasin, M. (2004). Genetic steps of mammalian homologous repair with distinct mutagenic consequences. *Mol Cell Biol*, *24*(21), 9305-9316. https://doi.org/10.1128/MCB.24.21.9305-9316.2004

Stefansson, O. A., Hermanowicz, S., van der Horst, J., Hilmarsdottir, H., Staszczak, Z., Jonasson, J. G., . . . Sigurdsson, S. (2017). CpG promoter methylation of the ALKBH3 alkylation repair gene in breast cancer. *BMC Cancer*, *17*(1), 469. https://doi.org/10.1186/s12885-017-3453-8

Stephen C West , M. G. B., Ying Wai Chan, Joao Matos, Shriparna Sarbajna, Haley D M Wyatt (2015). Resolution of Recombination Intermediates: Mechanisms and Regulation *Cold Spring Harb Symp Quant Biol*.

Stewart, G. S., Panier, S., Townsend, K., Al-Hakim, A. K., Kolas, N. K., Miller, E. S., . . . Durocher, D. (2009). The RIDDLE syndrome protein mediates a ubiquitin-dependent signaling cascade at sites of DNA damage. *Cell*, *136*(3), 420-434. https://doi.org/10.1016/j.cell.2008.12.042

Stewart, G. S., Stankovic, T., Byrd, P. J., Wechsler, T., Miller, E. S., Huissoon, A., . . . Taylor, A. M. (2007). RIDDLE immunodeficiency syndrome is linked to defects in 53BP1-mediated DNA damage signaling. *Proc Natl Acad Sci U S A*, *104*(43), 16910-16915. https://doi.org/10.1073/pnas.0708408104

Sugiyama, T., Zaitseva, E. M., & Kowalczykowski, S. C. (1997). A single-stranded DNA-binding protein is needed for efficient presynaptic complex formation by the Saccharomyces cerevisiae Rad51 protein. *J Biol Chem*, *272*(12), 7940-7945. https://doi.org/10.1074/jbc.272.12.7940

Sun, H., Zhang, M., Li, K., Bai, D., & Yi, C. (2019). Cap-specific, terminal N(6)-methylation by a mammalian m(6)Am methyltransferase. *Cell Res*, *29*(1), 80-82. https://doi.org/10.1038/s41422-018-0117-4

Sun, Z., Sun, X., Qin, G., Li, Y., Zhou, G., & Jiang, X. (2023). FTO promotes proliferation and migration of bladder cancer via enhancing stability of STAT3 mRNA in an m6A-dependent manner. *Epigenetics*, *18*(1), 2242688. https://doi.org/10.1080/15592294.2023.2242688

Sundheim, O., Vagbo, C. B., Bjoras, M., Sousa, M. M., Talstad, V., Aas, P. A., . . . Slupphaug, G. (2006). Human ABH3 structure and key residues for oxidative demethylation to reverse DNA/RNA damage. *EMBO J*, *25*(14), 3389-3397. https://doi.org/10.1038/sj.emboj.7601219

Suszynska, M., Ratajska, M., & Kozlowski, P. (2020). BRIP1, RAD51C, and RAD51D mutations are associated with high susceptibility to ovarian cancer: mutation prevalence and precise risk estimates based on a pooled analysis of ~30,000 cases. *J Ovarian Res*, *13*(1), 50. https://doi.org/10.1186/s13048-020-00654-3

Sy, S. M., Jiang, J., Dong, S. S., Lok, G. T., Wu, J., Cai, H., . . . Huen, M. S. (2011). Critical roles of ring finger protein RNF8 in replication stress responses. *J Biol Chem*, *286*(25), 22355-22361. https://doi.org/10.1074/jbc.M111.232041

Symington, L. S., & Gautier, J. (2011). Double-strand break end resection and repair pathway choice. *Annu Rev Genet*, *45*, 247-271. https://doi.org/10.1146/annurev-genet-110410-132435

Takata, M., Sasaki, M. S., Sonoda, E., Morrison, C., Hashimoto, M., Utsumi, H., . . . Takeda, S. (1998). Homologous recombination and non-homologous end-joining pathways of DNA double-strand break repair have overlapping roles in the maintenance of chromosomal integrity in vertebrate cells. *EMBO J*, *17*(18), 5497-5508. https://doi.org/10.1093/emboj/17.18.5497

Tang, C., Klukovich, R., Peng, H., Wang, Z., Yu, T., Zhang, Y., . . . Yan, W. (2018). ALKBH5-dependent m6A demethylation controls splicing and stability of long 3'-UTR mRNAs in male germ cells. *Proc Natl Acad Sci U S A*, *115*(2), E325-E333. https://doi.org/10.1073/pnas.1717794115

Tang, M., Li, S., & Chen, J. (2021). Ubiquitylation in DNA double-strand break repair. *DNA Repair (Amst)*, *103*, 103129. https://doi.org/10.1016/j.dnarep.2021.103129

Tao, L., Mu, X., Chen, H., Jin, D., Zhang, R., Zhao, Y., . . . Zhou, Z. (2021). FTO modifies the m6A level of MALAT and promotes bladder cancer progression. *Clin Transl Med*, *11*(2), e310. https://doi.org/10.1002/ctm2.310

Tarsounas, M., & Sung, P. (2020). The antitumorigenic roles of BRCA1-BARD1 in DNA repair and replication. *Nat Rev Mol Cell Biol*, *21*(5), 284-299. https://doi.org/10.1038/s41580-020-0218-z

Tasaki, M., Shimada, K., Kimura, H., Tsujikawa, K., & Konishi, N. (2011). ALKBH3, a human AlkB homologue, contributes to cell survival in human non-small-cell lung cancer. *Br J Cancer*, *104*(4), 700-706. https://doi.org/10.1038/sj.bjc.6606012

Taylor, A. M. R., Rothblum-Oviatt, C., Ellis, N. A., Hickson, I. D., Meyer, S., Crawford, T. O., . . . Stewart, G. S. (2019). Chromosome instability syndromes. *Nat Rev Dis Primers*, *5*(1), 64. https://doi.org/10.1038/s41572-019-0113-0

Teng, Y., Yadav, T., Duan, M., Tan, J., Xiang, Y., Gao, B., . . . Lan, L. (2018). ROS-induced R loops trigger a transcription-coupled but BRCA1/2-independent homologous recombination pathway through CSB. *Nat Commun*, *9*(1), 4115. https://doi.org/10.1038/s41467-018-06586-3

Thacker, J. (2005). The RAD51 gene family, genetic instability and cancer. *Cancer Lett*, *219*(2), 125-135. https://doi.org/10.1016/j.canlet.2004.08.018

Theil, A. F., Hackes, D., & Lans, H. (2023). TFIIH central activity in nucleotide excision repair to prevent disease. *DNA Repair (Amst)*, *132*, 103568. https://doi.org/10.1016/j.dnarep.2023.103568

Thompson, L. H. (2012). Recognition, signaling, and repair of DNA double-strand breaks produced by ionizing radiation in mammalian cells: the molecular choreography. *Mutat Res*, *751*(2), 158-246. https://doi.org/10.1016/j.mrrev.2012.06.002

Thonda, S., Vinnakota, R. L., Kona, S. V., & Kalivendi, S. V. (2022). Identification of RBMX as a splicing regulator in Parkinsonian mimetic induced alternative splicing of alpha-synuclein. *Biochim Biophys Acta Gene Regul Mech*, *1865*(4), 194825. https://doi.org/10.1016/j.bbagrm.2022.194825

Timcheva, K., Dufour, S., Touat-Todeschini, L., Burnard, C., Carpentier, M. C., Chuffart, F., . . . Verdel, A. (2022). Chromatin-associated YTHDC1 coordinates heat-induced reprogramming of gene expression. *Cell Rep*, *41*(11), 111784. https://doi.org/10.1016/j.celrep.2022.111784

Tobin, L. A., Robert, C., Nagaria, P., Chumsri, S., Twaddell, W., Ioffe, O. B., . . . Rassool, F. V. (2012). Targeting abnormal DNA repair in therapy-resistant breast cancers. *Mol Cancer Res*, *10*(1), 96-107. https://doi.org/10.1158/1541-7786.MCR-11-0255

Tomasz, M. (1995). Mitomycin C: small, fast and deadly (but very selective). *Chem Biol*, *2*(9), 575-579. https://doi.org/10.1016/1074-5521(95)90120-5

Trewick, S. C., Henshaw, T. F., Hausinger, R. P., Lindahl, T., & Sedgwick, B. (2002). Oxidative demethylation by Escherichia coli AlkB directly reverts DNA base damage. *Nature*, *419*(6903), 174-178. https://doi.org/10.1038/nature00908

Tsao, N., Brickner, J. R., Rodell, R., Ganguly, A., Wood, M., Oyeniran, C., . . . Mosammaparast, N. (2021). Aberrant RNA methylation triggers recruitment of an alkylation repair complex. *Mol Cell*, *81*(20), 4228-4242 e4228. https://doi.org/10.1016/j.molcel.2021.09.024

Ueda, Y., Ooshio, I., Fusamae, Y., Kitae, K., Kawaguchi, M., Jingushi, K., . . . Tsujikawa, K. (2017). AlkB homolog 3-mediated tRNA demethylation promotes protein synthesis in cancer cells. *Sci Rep*, *7*, 42271. https://doi.org/10.1038/srep42271

Uranishi, H., Zolotukhin, A. S., Lindtner, S., Warming, S., Zhang, G. M., Bear, J., . . . Felber, B. K. (2009). The RNA-binding motif protein 15B (RBM15B/OTT3) acts as cofactor of the nuclear export receptor NXF1. *J Biol Chem*, *284*(38), 26106-26116. https://doi.org/10.1074/jbc.M109.040113

Uziel, T., Lerenthal, Y., Moyal, L., Andegeko, Y., Mittelman, L., & Shiloh, Y. (2003). Requirement of the MRN complex for ATM activation by DNA damage. *EMBO J*, *22*(20), 5612-5621. https://doi.org/10.1093/emboj/cdg541

Vagbo, C. B., & Slupphaug, G. (2020). RNA in DNA repair. *DNA Repair (Amst)*, *95*, 102927. https://doi.org/10.1016/j.dnarep.2020.102927

Valdiglesias, V., Giunta, S., Fenech, M., Neri, M., & Bonassi, S. (2013). gammaH2AX as a marker of DNA double strand breaks and genomic instability in human population studies. *Mutat Res*, *753*(1), 24-40. https://doi.org/10.1016/j.mrrev.2013.02.001

van de Kooij, B., Schreuder, A., Pavani, R. S., Garzero, V., Van Hoeck, A., San Martin Alonso, M., . . . Noordermeer, S. M. (2023). EXO1-mediated DNA repair by single-strand annealing is essential for BRCA1-deficient cells. *bioRxiv*. https://doi.org/10.1101/2023.02.24.529205

Venkitaraman, A. R. (2002). Cancer susceptibility and the functions of BRCA1 and BRCA2. *Cell*, *108*(2), 171-182. https://doi.org/10.1016/s0092-8674(02)00615-3

Vilardo, E., Nachbagauer, C., Buzet, A., Taschner, A., Holzmann, J., & Rossmanith, W. (2012). A subcomplex of human mitochondrial RNase P is a bifunctional methyltransferase–extensive moonlighting in mitochondrial tRNA biogenesis. *Nucleic Acids Res*, *40*(22), 11583-11593. https://doi.org/10.1093/nar/gks910

Viphakone, N., Hautbergue, G. M., Walsh, M., Chang, C. T., Holland, A., Folco, E. G., . . . Wilson, S. A. (2012). TREX exposes the RNA-binding domain of Nxf1 to enable mRNA export. *Nat Commun*, *3*, 1006. https://doi.org/10.1038/ncomms2005

Viphakone, N., Sudbery, I., Griffith, L., Heath, C. G., Sims, D., & Wilson, S. A. (2019). Co-transcriptional Loading of RNA Export Factors Shapes the Human Transcriptome. *Mol Cell*, *75*(2), 310-323 e318. https://doi.org/10.1016/j.molcel.2019.04.034

Visvanathan, A., Patil, V., Arora, A., Hegde, A. S., Arivazhagan, A., Santosh, V., & Somasundaram, K. (2018). Essential role of METTL3-mediated m(6)A modification in glioma stem-like cells maintenance and radioresistance. *Oncogene*, *37*(4), 522-533. https://doi.org/10.1038/onc.2017.351

Vu, L. P., Pickering, B. F., Cheng, Y., Zaccara, S., Nguyen, D., Minuesa, G., . . . Kharas, M. G. (2017). The N(6)-methyladenosine (m(6)A)-forming enzyme METTL3 controls myeloid differentiation of normal hematopoietic and leukemia cells. *Nat Med*, *23*(11), 1369-1376. https://doi.org/10.1038/nm.4416

Walker, J. R., Corpina, R. A., & Goldberg, J. (2001). Structure of the Ku heterodimer bound to DNA and its implications for double-strand break repair. *Nature*, *412*(6847), 607-614. https://doi.org/Doi 10.1038/35088000

Wang, B., & Elledge, S. J. (2007). Ubc13/Rnf8 ubiquitin ligases control foci formation of the Rap80/Abraxas/Brca1/Brcc36 complex in response to DNA damage. *Proc Natl Acad Sci U S A*, *104*(52), 20759-20763. https://doi.org/10.1073/pnas.0710061104

Wang, C., & Lees-Miller, S. P. (2013). Detection and repair of ionizing radiation-induced DNA double strand breaks: new developments in nonhomologous end joining. *Int J Radiat Oncol Biol Phys*, *86*(3), 440-449. https://doi.org/10.1016/j.ijrobp.2013.01.011

Wang, C. Y., Shie, S. S., Hsieh, I. C., Tsai, M. L., & Wen, M. S. (2015). FTO modulates circadian rhythms and inhibits the CLOCK-BMAL1-induced transcription. *Biochem Biophys Res Commun*, *464*(3), 826-832. https://doi.org/10.1016/j.bbrc.2015.07.046

Wang, H., Perrault, A. R., Takeda, Y., Qin, W., Wang, H., & Iliakis, G. (2003). Biochemical evidence for Ku-independent backup pathways of NHEJ. *Nucleic Acids Res*, *31*(18), 5377-5388. https://doi.org/10.1093/nar/gkg728

Wang, J., Aroumougame, A., Lobrich, M., Li, Y., Chen, D., Chen, J., & Gong, Z. (2014). PTIP associates with Artemis to dictate DNA repair pathway choice. *Genes Dev*, *28*(24), 2693-2698. https://doi.org/10.1101/gad.252478.114

Wang, M., Chen, S., & Ao, D. (2021). Targeting DNA repair pathway in cancer: Mechanisms and clinical application. *MedComm (2020)*, *2*(4), 654-691. https://doi.org/10.1002/mco2.103

Wang, M., Zhu, Y., Wang, C., Fan, X., Jiang, X., Ebrahimi, M., . . . Li, X. (2016). Crystal structure of the two-subunit tRNA m(1)A58 methyltransferase TRM6-TRM61 from Saccharomyces cerevisiae. *Sci Rep*, *6*, 32562. https://doi.org/10.1038/srep32562

Wang, P., Doxtader, K. A., & Nam, Y. (2016). Structural Basis for Cooperative Function of Mettl3 and Mettl14 Methyltransferases. *Mol Cell*, *63*(2), 306-317. https://doi.org/10.1016/j.molcel.2016.05.041

Wang, Q., Wang, G., Wang, Y., Liu, C., & He, X. (2018). Association of AlkB homolog 3 expression with tumor recurrence and unfavorable prognosis in hepatocellular carcinoma. *J Gastroenterol Hepatol*. https://doi.org/10.1111/jgh.14117

Wang, S., Chai, P., Jia, R., & Jia, R. (2018). Novel insights on m(6)A RNA methylation in tumorigenesis: a double-edged sword. *Mol Cancer*, *17*(1), 101. https://doi.org/10.1186/s12943-018-0847-4

Wang, X., Lu, Z., Gomez, A., Hon, G. C., Yue, Y., Han, D., . . . He, C. (2014). N6-methyladenosine-dependent regulation of messenger RNA stability. *Nature*, *505*(7481), 117-120. https://doi.org/10.1038/nature12730

Wang, X., Zhao, B. S., Roundtree, I. A., Lu, Z., Han, D., Ma, H., . . . He, C. (2015). N(6)-methyladenosine Modulates Messenger RNA Translation Efficiency. *Cell*, *161*(6), 1388-1399. https://doi.org/10.1016/j.cell.2015.05.014

Wang, Y., Li, Y., Yue, M., Wang, J., Kumar, S., Wechsler-Reya, R. J., . . . Zhao, J. C. (2018). Publisher Correction: N(6)-methyladenosine RNA modification regulates embryonic neural stem cell self-renewal through histone modifications. *Nat Neurosci*, *21*(8), 1139. https://doi.org/10.1038/s41593-018-0169-2

Wang, Y., Wang, J., Li, X., Xiong, X., Wang, J., Zhou, Z., . . . Fan, Z. (2021). N(1)-methyladenosine methylation in tRNA drives liver tumourigenesis by regulating cholesterol metabolism. *Nat Commun*, *12*(1), 6314. https://doi.org/10.1038/s41467-021-26718-6

Weber, A. M., & Ryan, A. J. (2015). ATM and ATR as therapeutic targets in cancer. *Pharmacol Ther*, *149*, 124-138. https://doi.org/10.1016/j.pharmthera.2014.12.001

Wei, C. M., Gershowitz, A., & Moss, B. (1975). Methylated nucleotides block 5′ terminus of HeLa cell messenger RNA. *Cell*, *4*(4), 379-386. https://doi.org/10.1016/0092-8674(75)90158-0

Wei, J., Liu, F., Lu, Z., Fei, Q., Ai, Y., He, P. C., . . . He, C. (2018). Differential m(6)A, m(6)A(m), and m(1)A Demethylation Mediated by FTO in the Cell Nucleus and Cytoplasm. *Mol Cell*, *71*(6), 973-985 e975. https://doi.org/10.1016/j.molcel.2018.08.011

Wei, L., Nakajima, S., Bohm, S., Bernstein, K. A., Shen, Z., Tsang, M., . . . Lan, L. (2015). DNA damage during the G0/G1 phase triggers RNA-templated, Cockayne syndrome B-dependent homologous recombination. *Proc Natl Acad Sci U S A*, *112*(27), E3495-3504. https://doi.org/10.1073/pnas.1507105112

Weidong Xiong, Y. Z., Zilun Wei, Chaofu Li, Ranzun Zhao, Junbo Ge, Bei Shi,. (2023). N1-methyladenosine formation, gene regulation, biological functions, and clinical relevance. *Molecular Therapy*, *31*(2), 308-330. https://doi.org/10.1016/j.ymthe.2022.10.015.

Wickramasinghe, V. O., & Laskey, R. A. (2015). Control of mammalian gene expression by selective mRNA export. *Nat Rev Mol Cell Biol*, *16*(7), 431-442. https://doi.org/10.1038/nrm4010

Willems, P., Claes, K., Baeyens, A., Vandersickel, V., Werbrouck, J., De Ruyck, K., . . . Vral, A. (2008). Polymorphisms in nonhomologous end-joining genes associated with breast cancer risk and chromosomal radiosensitivity. *Genes Chromosomes Cancer*, *47*(2), 137-148. https://doi.org/10.1002/gcc.20515

Wojtas, M. N., Pandey, R. R., Mendel, M., Homolka, D., Sachidanandam, R., & Pillai, R. S. (2017). Regulation of m(6)A Transcripts by the 3′–>5′ RNA Helicase YTHDC2 Is Essential for a Successful Meiotic Program in the Mammalian Germline. *Mol Cell*, *68*(2), 374-387 e312. https://doi.org/10.1016/j.molcel.2017.09.021

Woo, H. H., & Chambers, S. K. (2019). Human ALKBH3-induced m(1)A demethylation increases the CSF-1 mRNA stability in breast and ovarian cancer cells. *Biochimica Et Biophysica Acta-Gene Regulatory Mechanisms*, *1862*(1), 35-46. https://doi.org/10.1016/j.bbagrm.2018.10.008

Wood, R. D., & Doublie, S. (2016). DNA polymerase theta (POLQ), double-strand break repair, and cancer. *DNA Repair (Amst)*, *44*, 22-32. https://doi.org/10.1016/j.dnarep.2016.05.003

Wu, L., Wu, D., Ning, J., Liu, W., & Zhang, D. (2019). Changes of N6-methyladenosine modulators promote breast cancer progression. *BMC Cancer*, *19*(1), 326. https://doi.org/10.1186/s12885-019-5538-z

Wu, T., Hu, E., Xu, S., Chen, M., Guo, P., Dai, Z., . . . Yu, G. (2021). clusterProfiler 4.0: A universal enrichment tool for interpreting omics data. *Innovation (Camb)*, *2*(3), 100141. https://doi.org/10.1016/j.xinn.2021.100141

Wu, Y., Chen, Z., Xie, G., Zhang, H., Wang, Z., Zhou, J., . . . Wang, H. (2022). RNA m(1)A methylation regulates glycolysis of cancer cells through modulating ATP5D. *Proc Natl Acad Sci U S A*, *119*(28), e2119038119. https://doi.org/10.1073/pnas.2119038119

Wu, Y., Jiang, D., Zhang, H., Yin, F., Guo, P., Zhang, X., . . . Han, Y. (2022). N1-Methyladenosine (m1A) Regulation Associated With the Pathogenesis of Abdominal Aortic Aneurysm Through YTHDF3 Modulating Macrophage Polarization. *Front Cardiovasc Med*, *9*, 883155. https://doi.org/10.3389/fcvm.2022.883155

Wu, Y., Li, J., Li, C., Lu, S., Wei, X., Li, Y., . . . Hu, Z. (2023). Fat mass and obesity-associated factor (FTO)-mediated N6-methyladenosine regulates spermatogenesis in an age-dependent manner. *J Biol Chem*, *299*(6), 104783. https://doi.org/10.1016/j.jbc.2023.104783

Wu, Y., Wang, Z., Han, L., Guo, Z., Yan, B., Guo, L., . . . Zhang, J. (2022). PRMT5 regulates RNA m6A demethylation for doxorubicin sensitivity in breast cancer. *Mol Ther*, *30*(7), 2603-2617. https://doi.org/10.1016/j.ymthe.2022.03.003

Xiang, S., Reed, D. R., & Alexandrow, M. G. (2023). The CMG helicase and cancer: a tumor "engine" and weakness with missing mutations. *Oncogene*, *42*(7), 473-490. https://doi.org/10.1038/s41388-022-02572-8

Xiang, Y., Laurent, B., Hsu, C. H., Nachtergaele, S., Lu, Z., Sheng, W., . . . Shi, Y. (2017). Corrigendum: RNA m(6)A methylation regulates the ultraviolet-induced DNA damage response. *Nature*, *552*(7685), 430. https://doi.org/10.1038/nature24007

Xiao, W., Adhikari, S., Dahal, U., Chen, Y. S., Hao, Y. J., Sun, B. F., . . . Yang, Y. G. (2016). Nuclear m(6)A Reader YTHDC1 Regulates mRNA Splicing. *Mol Cell*, *61*(4), 507-519. https://doi.org/10.1016/j.molcel.2016.01.012

Xie, A., Kwok, A., & Scully, R. (2009). Role of mammalian Mre11 in classical and alternative nonhomologous end joining. *Nat Struct Mol Biol*, *16*(8), 814-818. https://doi.org/10.1038/nsmb.1640

Xiong, X., Du, Z., Wang, Y., Feng, Z., Fan, P., Yan, C., . . . Zhang, J. (2015). 53BP1 promotes microhomology-mediated end-joining in G1-phase cells. *Nucleic Acids Res*, *43*(3), 1659-1670. https://doi.org/10.1093/nar/gku1406

Xiong, X., Li, X., Wang, K., & Yi, C. (2018). Perspectives on topology of the human m(1)A methylome at single nucleotide resolution. *RNA*, *24*(11), 1437-1442. https://doi.org/10.1261/rna.067694.118

Xu, B., Liu, D., Wang, Z., Tian, R., & Zuo, Y. (2021). Multi-substrate selectivity based on key loops and non-homologous domains: new insight into ALKBH family. *Cell Mol Life Sci*, *78*(1), 129-141. https://doi.org/10.1007/s00018-020-03594-9

Xu, L., Liu, X., Sheng, N., Oo, K. S., Liang, J., Chionh, Y. H., . . . Fu, X. Y. (2017). Three distinct 3-methylcytidine (m(3)C) methyltransferases modify tRNA and mRNA in mice and humans. *J Biol Chem*, *292*(35), 14695-14703. https://doi.org/10.1074/jbc.M117.798298

Yamato, I., Sho, M., Shimada, K., Hotta, K., Ueda, Y., Yasuda, S., . . . Nakajima, Y. (2012). PCA-1/ALKBH3 contributes to pancreatic cancer by supporting apoptotic resistance and angiogenesis. *Cancer Res*, *72*(18), 4829-4839. https://doi.org/10.1158/0008-5472.CAN-12-0328

Yan, C. T., Boboila, C., Souza, E. K., Franco, S., Hickernell, T. R., Murphy, M., . . . Alt, F. W. (2007). IgH class switching and translocations use a robust non-classical end-joining pathway. *Nature*, *449*(7161), 478-482. https://doi.org/10.1038/nature06020

Yang, G., Liu, C., Chen, S. H., Kassab, M. A., Hoff, J. D., Walter, N. G., & Yu, X. (2018). Super-resolution imaging identifies PARP1 and the Ku complex acting as DNA double-strand break sensors. *Nucleic Acids Res*, *46*(7), 3446-3457. https://doi.org/10.1093/nar/gky088

Yang, W., Meng, J., Liu, J., Ding, B., Tan, T., Wei, Q., & Yu, Y. (2020). The N(1)-Methyladenosine Methylome of Petunia mRNA. *Plant Physiol*, *183*(4), 1710-1724. https://doi.org/10.1104/pp.20.00382

Yang, X., Liu, Q. L., Xu, W., Zhang, Y. C., Yang, Y., Ju, L. F., . . . Yang, Y. G. (2019). m(6)A promotes R-loop formation to facilitate transcription termination. *Cell Res*, *29*(12), 1035-1038. https://doi.org/10.1038/s41422-019-0235-7

Yang, X., Yang, Y., Sun, B. F., Chen, Y. S., Xu, J. W., Lai, W. Y., . . . Yang, Y. G. (2017). *5*-methylcytosine promotes mRNA export - NSUN2 as the methyltransferase and ALYREF as an m(*5*)C reader. *Cell Res*, *27*(*5*), 606-625. https://doi.org/10.1038/cr.2017.*55*

Yang, Y., Hsu, P. J., Chen, Y. S., & Yang, Y. G. (2018). Dynamic transcriptomic m(6)A decoration: writers, erasers, readers and functions in RNA metabolism. *Cell Res*, *28*(6), 616-624. https://doi.org/10.1038/s41422-018-0040-8

Yang, Y., Li, Q., Ling, Y., Leng, L., Ma, Y., Xue, L., . . . Tao, S. (2022). m6A eraser FTO modulates autophagy by targeting SQSTM1/P62 in the prevention of canagliflozin against renal fibrosis. *Front Immunol*, *13*, 1094556. https://doi.org/10.3389/fimmu.2022.1094556

Yap, T. A., O'Carrigan, B., Penney, M. S., Lim, J. S., Brown, J. S., de Miguel Luken, M. J., . . . de Bono, J. S. (2020). Phase I Trial of First-in-Class ATR Inhibitor M6620 (VX-970) as Monotherapy or in Combination With Carboplatin in Patients With Advanced Solid Tumors. *J Clin Oncol*, *38*(27), 3195-3204. https://doi.org/10.1200/JCO.19.02404

Yasuhara, T., Kato, R., Hagiwara, Y., Shiotani, B., Yamauchi, M., Nakada, S., . . . Miyagawa, K. (2018). Human Rad*5*2 Promotes XPG-Mediated R-loop Processing to Initiate Transcription-Associated Homologous Recombination Repair. *Cell*, *175*(2), *5*58-570 e511. https://doi.org/10.1016/j.cell.2018.08.056

Yeo, G., & Burge, C. B. (2004). Maximum entropy modeling of short sequence motifs with applications to RNA splicing signals. *J Comput Biol*, *11*(2-3), 377-394. https://doi.org/10.1089/1066527041410418

Yin, M., Liao, Z., Liu, Z., Wang, L. E., O'Reilly, M., Gomez, D., . . . Wei, Q. (2012). Genetic variants of the nonhomologous end joining gene LIG4 and severe radiation pneumonitis in nonsmall cell lung cancer patients treated with definitive radiotherapy. *Cancer*, *118*(2), *5*28-535. https://doi.org/10.1002/cncr.26214

Yoon, J. H., Prakash, L., & Prakash, S. (2009). Highly error-free role of DNA polymerase eta in the replicative bypass of UV-induced pyrimidine dimers in mouse and human cells. *Proc Natl Acad Sci U S A*, *106*(43), 18219-18224. https://doi.org/10.1073/pnas.0910121106

Yu, F., Wei, J., Cui, X., Yu, C., Ni, W., Bungert, J., . . . Qian, Z. (2021). Post-translational modification of RNA m6A demethylase ALKBH*5* regulates ROS-induced DNA damage response. *Nucleic Acids Res*, *49*(10), *5*779-*5*797. https://doi.org/10.1093/nar/gkab415

Yu, X., & Chen, J. (2004). DNA damage-induced cell cycle checkpoint control requires CtIP, a phosphorylation-dependent binding partner of BRCA1 C-terminal domains. *Mol Cell Biol*, *24*(21), 9478-9486. https://doi.org/10.1128/MCB.24.21.9478-9486.2004

Zaccara, S., & Jaffrey, S. R. (2020). A Unified Model for the Function of YTHDF Proteins in Regulating m(6)A-Modified mRNA. *Cell*, *181*(7), 1582-1595 e1518. https://doi.org/10.1016/j.cell.2020.05.012

Zeng, J., Zhang, H., Tan, Y., Wang, Z., Li, Y., & Yang, X. (2021). m6A demethylase FTO suppresses pancreatic cancer tumorigenesis by demethylating PJA2 and inhibiting Wnt signaling. *Mol Ther Nucleic Acids*, *25*, 277-292. https://doi.org/10.1016/j.omtn.2021.06.005

Zeng, Y., Wang, S., Gao, S., Soares, F., Ahmed, M., Guo, H., . . . He, H. H. (2018). Refined RIP-seq protocol for epitranscriptome analysis with low input materials. *PLoS Biol*, *16*(9), e2006092. https://doi.org/10.1371/journal.pbio.2006092

Zhang, C., Chen, L., Peng, D., Jiang, A., He, Y., Zeng, Y., . . . Zhao, Y. (2020). METTL3 and N6-Methyladenosine Promote Homologous Recombination-Mediated Repair of DSBs by Modulating DNA-RNA Hybrid Accumulation. *Mol Cell*, *79*(3), 425-442 e427. https://doi.org/10.1016/j.molcel.2020.06.017

Zhang, C., Samanta, D., Lu, H., Bullen, J. W., Zhang, H., Chen, I., . . . Semenza, G. L. (2016). Hypoxia induces the breast cancer stem cell phenotype by HIF-dependent and ALKBH5-mediated m(6)A-demethylation of NANOG mRNA. *Proc Natl Acad Sci U S A*, *113*(14), E2047-2056. https://doi.org/10.1073/pnas.1602883113

Zhang, L. S., Xiong, Q. P., Pena Perez, S., Liu, C., Wei, J., Le, C., . . . He, C. (2021). ALKBH7-mediated demethylation regulates mitochondrial polycistronic RNA processing. *Nat Cell Biol*, *23*(7), 684-691. https://doi.org/10.1038/s41556-021-00709-7

Zhang, Q., Riddle, R. C., Yang, Q., Rosen, C. R., Guttridge, D. C., Dirckx, N., . . . Clemens, T. L. (2019). The RNA demethylase FTO is required for maintenance of bone mass and functions to protect osteoblasts from genotoxic damage. *Proc Natl Acad Sci U S A*, *116*(36), 17980-17989. https://doi.org/10.1073/pnas.1905489116

Zhang, S., Zhao, B. S., Zhou, A., Lin, K., Zheng, S., Lu, Z., . . . Huang, S. (2017). m(6)A Demethylase ALKBH5 Maintains Tumorigenicity of Glioblastoma Stem-like Cells by Sustaining FOXM1 Expression and Cell Proliferation Program. *Cancer Cell*, *31*(4), 591-606 e596. https://doi.org/10.1016/j.ccell.2017.02.013

Zhang, X., Wei, L. H., Wang, Y., Xiao, Y., Liu, J., Zhang, W., . . . Jia, G. (2019). Structural insights into FTO's catalytic mechanism for the demethylation of multiple RNA substrates. *Proc Natl Acad Sci U S A*, *116*(8), 2919-2924. https://doi.org/10.1073/pnas.1820574116

Zhang, Z., & Krainer, A. R. (2004). Involvement of SR proteins in mRNA surveillance. *Mol Cell*, *16*(4), 597-607. https://doi.org/10.1016/j.molcel.2004.10.031

Zhao, L., Kong, X., Zhong, W., Wang, Y., & Li, P. (2020). FTO accelerates ovarian cancer cell growth by promoting proliferation, inhibiting apoptosis, and activating autophagy. *Pathol Res Pract*, *216*(9), 153042. https://doi.org/10.1016/j.prp.2020.153042

Zhao, L. Y., Song, J., Liu, Y., Song, C. X., & Yi, C. (2020). Mapping the epigenetic modifications of DNA and RNA. *Protein Cell*, *11*(11), 792-808. https://doi.org/10.1007/s13238-020-00733-7

Zhao, S., Devega, R., Francois, A., & Kidane, D. (2021). Human ALKBH6 Is Required for Maintenance of Genomic Stability and Promoting Cell Survival During Exposure of Alkylating Agents in Pancreatic Cancer. *Front Genet*, *12*, 635808. https://doi.org/10.3389/fgene.2021.635808

Zhao, X., Yang, Y., Sun, B. F., Shi, Y., Yang, X., Xiao, W., . . . Yang, Y. G. (2014). FTO-dependent demethylation of N6-methyladenosine regulates mRNA splicing and is required for adipogenesis. *Cell Res*, *24*(12), 1403-1419. https://doi.org/10.1038/cr.2014.151

Zhao, Y., Majid, M. C., Soll, J. M., Brickner, J. R., Dango, S., & Mosammaparast, N. (2015). Noncanonical regulation of alkylation damage resistance by the OTUD4 deubiquitinase. *EMBO J*, *34*(12), 1687-1703. https://doi.org/10.15252/embj.201490497

Zhao, Y., Zhao, Q., Kaboli, P. J., Shen, J., Li, M., Wu, X., . . . Xiao, Z. (2019). m1A Regulated Genes Modulate PI3K/AKT/mTOR and ErbB Pathways in Gastrointestinal Cancer. *Transl Oncol*, *12*(10), 1323-1333. https://doi.org/10.1016/j.tranon.2019.06.007

Zheng, G., Dahl, J. A., Niu, Y., Fedorcsak, P., Huang, C. M., Li, C. J., . . . He, C. (2013). ALKBH5 is a mammalian RNA demethylase that impacts RNA metabolism and mouse fertility. *Mol Cell*, *49*(1), 18-29. https://doi.org/10.1016/j.molcel.2012.10.015

Zheng, Q., Gan, H., Yang, F., Yao, Y., Hao, F., Hong, L., & Jin, L. (2020). Cytoplasmic m(1)A reader YTHDF3 inhibits trophoblast invasion by downregulation of m(1)A-methylated IGF1R. *Cell Discov*, *6*, 12. https://doi.org/10.1038/s41421-020-0144-4

Zheng, T., Zhou, H., Li, X., Peng, D., Yang, Y., Zeng, Y., . . . Zhao, Y. (2020). RBMX is required for activation of ATR on repetitive DNAs to maintain genome stability. *Cell Death Differ*, *27*(11), 3162-3176. https://doi.org/10.1038/s41418-020-0570-8

Zhong, S., Li, H., Bodi, Z., Button, J., Vespa, L., Herzog, M., & Fray, R. G. (2008). MTA is an Arabidopsis messenger RNA adenosine methylase and interacts with a homolog of a sex-specific splicing factor. *Plant Cell*, *20*(5), 1278-1288. https://doi.org/10.1105/tpc.108.058883

Zhou, H., Rauch, S., Dai, Q., Cui, X., Zhang, Z., Nachtergaele, S., . . . Dickinson, B. C. (2019). Evolution of a reverse transcriptase to map N(1)-methyladenosine in human messenger RNA. *Nat Methods*, *16*(12), 1281-1288. https://doi.org/10.1038/s41592-019-0550-4

Zhou, J., Wan, J., Shu, X. E., Mao, Y., Liu, X. M., Yuan, X., . . . Qian, S. B. (2018). N(6)-Methyladenosine Guides mRNA Alternative Translation during Integrated Stress Response. *Mol Cell*, *69*(4), 636-647 e637. https://doi.org/10.1016/j.molcel.2018.01.019

Zhou, L. L., Xu, H., Huang, Y., & Yang, C. G. (2021). Targeting the RNA demethylase FTO for cancer therapy. *RSC Chem Biol*, *2*(5), 1352-1369. https://doi.org/10.1039/d1cb00075f

Zhou, S., Bai, Z. L., Xia, D., Zhao, Z. J., Zhao, R., Wang, Y. Y., & Zhe, H. (2018). FTO regulates the chemo-radiotherapy resistance of cervical squamous cell carcinoma (CSCC) by targeting beta-catenin through mRNA demethylation. *Mol Carcinog*, *57*(5), 590-597. https://doi.org/10.1002/mc.22782

Zhu, Q., Sharma, N., He, J., Wani, G., & Wani, A. A. (2015). USP7 deubiquitinase promotes ubiquitin-dependent DNA damage signaling by stabilizing RNF168. *Cell Cycle*, *14*(9), 1413-1425. https://doi.org/10.1080/15384101.2015.1007785

Zhuang, C., Zhuang, C., Luo, X., Huang, X., Yao, L., Li, J., . . . Gui, Y. (2019). N6-methyladenosine demethylase FTO suppresses clear cell renal cell carcinoma through a novel FTO-PGC-1alpha signalling axis. *J Cell Mol Med*, *23*(3), 2163-2173. https://doi.org/10.1111/jcmm.14128

Zhuang, J., Jiang, G., Willers, H., & Xia, F. (2009). Exonuclease function of human Mre11 promotes deletional nonhomologous end joining. *J Biol Chem*, *284*(44), 30565-30573. https://doi.org/10.1074/jbc.M109.059444

Zolotukhin, A. S., Uranishi, H., Lindtner, S., Bear, J., Pavlakis, G. N., & Felber, B. K. (2009). Nuclear export factor RBM15 facilitates the access of DBP5 to mRNA. *Nucleic Acids Res*, *37*(21), 7151-7162. https://doi.org/10.1093/nar/gkp782

Zong, D., Adam., S., Yifan Wang, Hiroyuki Sasanuma, Elsa Callén, Matilde Murga, . . . Nussenzweig, A. (2019). BRCA1 Haploinsufficiency Is Masked by RNF168-Mediated Chromatin Ubiquitylation. *Mol Cell*, *73*(6), 1267-1281 e1267. https://doi.org/10.1016/j.molcel.2018.12.010

Zong, D., Callen, E., Pegoraro, G., Lukas, C., Lukas, J., & Nussenzweig, A. (2015). Ectopic expression of RNF168 and 53BP1 increases mutagenic but not physiological non-homologous end joining. *Nucleic Acids Res*, *43*(10), 4950-4961. https://doi.org/10.1093/nar/gkv336

Zong, D. L., Adam, S., Wang, Y. F., Sasanuma, H., Callen, E., Murga, M., . . . Nussenzweig, A. (2019). BRCA1 Haploinsufficiency Is Masked by RNF168-Mediated Chromatin Ubiquitylation. *Molecular Cell*, *73*(6), 1267-+. https://doi.org/10.1016/j.molcel.2018.12.010

Zou, D., Dong, L., Li, C., Yin, Z., Rao, S., & Zhou, Q. (2019). The m(6)A eraser FTO facilitates proliferation and migration of human cervical cancer cells. *Cancer Cell Int*, *19*, 321. https://doi.org/10.1186/s12935-019-1045-1

Original Publications

Paper I

The oxidative demethylases ALKBH3 and FTO contribute to efficient RNF168 dependent DNA double-strand break signaling.

Authors

Thorkell Guðjónsson (TG) [1,2,3¶], Karen Kristjánsdóttir (KK)[1,2¶], Stefan Thor Hermanowicz (SH)[1,2] Kritika Kirty (KR)[1,2], Arnar Ingi Vilhjálmsson (AV)[1,2], Snædís Ragnarsdóttir (SR) [1,2], Drífa Hrund Guðmundsdóttir (DG)[1,2], Birta Dröfn Jónsdóttir (BJ)[1,2], Erla Sveinbjörnsdóttir (ES)[4] and Stefán Sigurðsson (SS) [1,2,5*].

1.Cancer Research Laboratory, Biomedical Center, Sturlugata 8, 101, Reykjavik, Iceland.

2.Faculty of Medicine, University of Iceland, Vatnsmyrarvegur 16, 101, Reykjavik, Iceland

3. Biotech Research & Innovation Centre, University of Copenhagen, Ole Maaløes Vej 5, 2200 Copenhagen, Denmark

4. Department of Genetics and Molecular Medicine at University Hospital (Landspitali), Hringbraut, 101 Reykjavík, Iceland

5. Department of Biochemistry and Molecular Biology, Biomedical Center, Sturlugata 8, 101, Reykjavik, Iceland

¶ These authors contributed equally to this work

*Corresponding author stefsi@hi.is

Summary

DNA double-strand breaks (DSBs) are one of the most harmful forms of DNA damage as incorrectly repaired DSBs can lead to severe genome instability and increased risk of cancer development. Histone ubiquitination, mediated by the E3 ubiquitin ligase RNF168, plays a central role in the recruitment of repair factors to DNA DSBs. Here we report that ALKBH3 and FTO, dioxygenases with well-described functions in repair of alkylation damage, promote efficient DNA DSB chromatin signaling. Depletion of ALKBH3 and FTO leads to increased RNF168 mRNA methylation, resulting in impaired mRNA nuclear export and reduced RNF168 protein expression. Consequently, ALKBH3 or FTO deficient cells show strong signs of RNF168 dysfunction, including impaired 53BP1 recruitment to DNA DSBs, genome instability and hypersensitivity to genotoxic agents. Our findings uncover the role of mRNA modifications in regulations of DNA DSB repair signaling and provide evidence for crosstalk between alkylation repair and DNA DSB repair.

Keywords

DNA Double strand break repair; mRNA methylations; epitranscriptomics; genomic stability; RNF168; ALKBH3; FTO

Introduction

The integrity of the genome is constantly being challenged by intrinsic and extrinsic factors that damage the DNA. Unrepaired, or incorrectly repaired lesions, can lead to severe genomic aberrations, which can have life-threatening consequences. To counteract these harmful events cells have evolved a comprehensive network of

pathways commonly referred to as the DNA damage response (DDR). Inherited defects in DDR genes predispose to diverse human diseases, including cancer, immune deficiencies, and neurodegenerative disorders, highlighting the importance of genome maintenance in safeguarding normal cellular functions [1]

DNA double strand breaks (DSB) are one of the most cytotoxic forms of DNA damage. Failure in repairing DSBs has the potential to cause severe genome instability and mutations in key members of the DNA DSB repair pathways predispose to several types of cancer, including breast and ovarian cancer [2-4]. The chromatin ubiquitination pathway orchestrated by the E3 ubiquitin ligases RNF8 and RNF168 plays an essential role in the stepwise assembly of key DNA DSB repair factors at damaged chromatin, including 53BP1 and BRCA1 [5-7]. The RNF8/RNF168 pathway has a known role in promoting non-homologous end joining (NHEJ) repair and class switch recombination [8], although more recently, it has also been implicated in homologous recombination (HR) repair [9-11]. Studies from mice suggest that RNF168 activity supports HR repair in cells with decreased BRCA1 activity [12], and serves as an important barrier against genome instability and tumorigenesis in BRCA1 heterozygote mice [11,12], demonstrating the important role of RNF168 in tumorigenesis. Mutations in RNF168 are known to cause a rare genetic disorder Radiosensitivity, immunodeficiency, dysmorphic features and learning difficulties (RIDDLE) syndrome, first reported in 2007 [13], and associated with defective DSB repair as patients suffering from this disease are unable to recruit 53BP1 to the site of DSBs [7,14].

In addition to its role in DNA DSB repair, the chromatin ubiquitination pathway contributes to several other genome maintenance pathways, including R-loop resolution [15], DNA replication [16], telomere maintenance [17], DNA crosslinking repair [18] and preventing access of the transcription machinery at sites of DNA damage [19]. Despite this general positive impact on genome maintenance, studies have shown that excessive activation of RNF8/RNF168 dependent chromatin signaling can have

deleterious consequences on cell function [20,21], which in some cases can drive tumorigenesis [15]. Changes in the nuclear pool of RNF168 result in dramatic changes in DNA DSB repair dynamics, with increased usage of mutagenic DSB repair [22] and activation of NHEJ at uncapped telomere ends [23], increasing the risk of introducing mutations and chromosome end fusions. In line with that, cells have evolved a series of mechanisms, which counteract the activity of RNF168 at damaged chromatin [24].

In recent years, mRNA modifications have emerged as an important regulatory mechanism of gene expression. mRNA modifications have been shown to influence several stages of the mRNA life cycle, thereby affecting the function, structure, and catalytic activity of mRNAs [25,26]. One of the most common forms of mRNA-modification is methylations and two of the most well-known methylations are N^6-methyladenosine (m^6A) and N^1-methyladenosine (m^1A). Both modifications have a set of specific writers (methyltransferases), readers and erasers (demethylases), demonstrating the dynamic nature of mRNA methylation.

Two such erasers are the fat mass and obesity associated protein (FTO) and AlkB homolog 3 (ALKBH3). These proteins are two out of nine members of the Fe (II) -ketoglutarate-dependent dioxygenase (AlkB) family which is a part of the cells DDR network that removes alkylating lesions from DNA and RNA [27,28]. FTO (also known as ALKBH9) was the first discovered mRNA demethylase and has been reported to catalyze the demethylation of m^6A both *in vitro* and *in vivo* [29,30], thereby providing the first evidence of reversible post-transcriptional modifications on mRNA. Subsequent studies showed that FTO can also catalyze demethylation of N^6,2′O-diomethyladenosine (m^6A_m), located at the *5′* end of mRNA, showing greater affinity towards m^6A_m compared to m^6A [31]. This discovery was reproduced by Wei et al who also demonstrated that FTO has increased preference for m^6A_m in *in vitro* experiments. In this context, however, it has been shown that the intracellular localization of FTO

dictates its substrate specificity. In the nucleus, FTO predominantly targets m^6A, whereas m^6A_m is the primary target of FTO in the cytoplasm [32].

ALKBH3 is known to demethylate *N*-methylated bases from both RNA and DNA with single strand substrate preference [27,28] and is best known for removing 3-methylcytocine (m^3C) from ssDNA [33] with the aid of ASCC3 helicase [34]. Additionally, ALKBH3 has proven capable of removing m^1A methylation from mRNA [35-37]. Previously, we and others have shown that ALKBH3 expression is silenced by promoter methylation across several different cancer types [38-40]. Furthermore, loss of ALKBH3 has been shown to be clinically relevant and significantly affect survival of both breast cancer [38] and Hodgkin lymphoma patients [40].

Transcriptome-wide mapping of m^6A and m^1A mRNA modifications have demonstrated that the RNF168 transcript contains both modifications [41,42]. However, the functional importance of these mRNA methylations on the RNF168 transcript is unknown. Here, we show that the RNA demethylases ALKBH3 and FTO play a significant role in promoting efficient RNF168 expression. We find that depletion of ALKBH3 and FTO results in increased RNF168 mRNA methylation and defective mRNA nuclear export, which results in decreased RNF168 protein expression. This translates into reduced recruitment of key genome caretakers such as 53BP1 and RIF1 to sites of DNA damage, increased genome instability and impaired cell survival in response to genotoxic stress inducing agents. This data indicates that ALKBH3 and FTO play a role in the epitranscriptomic regulation of RNF168 and presents mRNA modifications as a novel regulatory mechanism in DNA DSB repair signaling.

Results

ALKBH3 promotes efficient expression of RNF168.

Results from two independent previously published, mass spectrometry proteomics studies, have reported an interaction between ALKBH3 and RIF1 [34,43] which is a key

effector in the chromatin ubiquitination pathway [44]. Inspired by this, we analyzed the recruitment of RIF1 and its immediate upstream functional partner, 53BP1, to sites of DNA DSBs, in naïve and ALKBH3 depleted U2OS cells. Interestingly, siRNA mediated knockdown of ALKBH3 suppressed the focal accumulation of both 53BP1 and RIF1 at sites of DNA DSBs (Figure 1A, 1B and Figure S1A, S1B), without affecting γ-H2AX formation, which is upstream of the ubiquitin dependent DSB signaling pathway. Further analysis revealed a clear reduction in RNF168 protein levels following ALKBH3 depletion, a phenotype reproduced by independent siRNAs in several different cancer cell lines (Figure 1C and Figure S1C,S1D). Importantly, no decrease was detected in the protein levels of other key genome maintenance factors; including RNF8, RIF1 and 53BP1 (Figure S1E, S1F) suggesting that decreased RNF168 expression is not caused by a global decrease in gene expression. This is further supported by previously published transcriptomic analysis in ALKBH3 knockdown cells, which indicates that ALKBH3 does not directly regulate gene transcription [45].

To determine the consequence of decreased RNF168 expression in ALKBH3 knockdown cells, we first turned to one of the main functions of RNF168, promoting efficient DNA DSB repair. Following RNAi mediated silencing of ALKBH3, we treated U2OS cells with neocarzinostatin (NCS) to induce DNA DSBs and followed in time the number of DNA DSB nuclear foci. As a readout for DNA DSB repair dynamics, we used MDC1 accumulation at sites of DNA DSBs. MDC1 is one of the first proteins to arrive at DNA DSB sites, where it directs the recruitment of downstream repair factors to DNA DSBs. It is upstream of the ubiquitin dependent steps in the DNA DSB repair-signaling pathway, and gradually dissociates from DSBs with ongoing DNA repair [46]. In line with its key role in promoting efficient DNA DSB repair, inactivation of RNF168 results in slower clearance of MDC1 foci following DNA damage (Figure. 1D and Figure. S1G), as seen in previous publications [6,20]. Interestingly this was also the case in ALKBH3 knockdown cells, where there was a significant increase in cells with MDC1

foci, compared to control cells, 8h following NCS treatment, indicating less efficient DNA DSB repair.

DNA DSB repair defects are an important source of genome instability in cancer. Human and mouse cells lacking RNF168 show an increase in the frequency of genomic aberrations, including increased frequency of micronuclei and chromosomal aberrations [15,47,48]. To determine if the effects of ALKBH3 knockdown on genome integrity are comparable to RNF168 deficiency, we examined the numbers of spontaneous chromosomal aberrations in metaphase spreads in U2OS cells (Figure 1E, 1F). Compared to control cells, both RNF168 and ALKBH3 knockdown cells displayed a significant increase in spontaneous chromosomal aberrations suggesting increased genome instability. Collectively, these findings suggest that there are phenotypic similarities between RNF168 and ALKBH3 deficient cells, suggesting that downregulation of RNF168 in ALKBH3 deficient cells has deleterious effects on normal cell function.

ALKBH3 plays a central role in DNA alkylation repair, preferably on single stranded DNA [27]. In DNA alkylation repair, ALKBH3 interacts with the DNA helicase ASCC3, which unwinds DNA and creates the single-stranded DNA substrate needed for the DNA repair activity of ALKBH3 [34]. Interestingly, siRNA mediated depletion of ASCC3 has no impact on RNF168 protein levels or 53BP1 recruitment to sites of DNA DSBs. Furthermore, silencing ALKBH2, which together with ALKBH3 is the functional homolog of the AlkB enzyme in E. coli, did not affect RNF168 protein expression (Figure S1H, S1I). This suggests that ALKBH3 is regulating the expression of RNF168, independent of its well-described role in DNA alkylation repair.

ALKBH3 promotes the nuclear export of RNF168 mRNA.

RNF168 is a rate-limiting factor in the chromatin response to DNA DSBs; therefore, keeping RNF168 expression levels in balance is important for normal cellular function. In this context, one of the best-described mechanisms is the dynamic regulation of RNF168 protein turnover, which involves a sequence of factors involved in the ubiquitin-proteasome pathway of protein degradation. To determine if ALKBH3 depletion affects RNF168 protein turnover, we treated ALKBH3 knockdown cells with the proteasome inhibitor MG-132, followed by western blot analysis to determine RNF168 protein expression. MG-132 treatment did not restore RNF168 levels in ALKBH3 depleted cells (Figure 2A), which indicates that the decrease observed in RNF168 expression is not a result of protein degradation.

In addition to its role in DNA alkylation repair, ALKBH3 has been shown to influence gene expression by removing m^1A methylation marks of mRNAs [35,41,49]. Previous transcriptome-wide mapping of m^1A modifications in human cell lines (HEK293, HELA and HEPG2) identified RNF168 among thousands of transcripts containing the modifications [41]. There is however some uncertainty regarding the exact prevalence of m^1A mRNA modifications on RNF168, since it was not reported as a m^1A containing transcript in a second transcriptome-wide study [35,49]. To address this in our experimental system, we performed an antibody based m^1A-RNA immunoprecipitation (RIP) assay in U2OS cells, followed by a qPCR to determine the abundance of RNF168 associated with m^1A in control and ALKBH3 depleted cells. m^1A-RIP was based on previously described methylations specific IP [35,50,51]. In both the control sample and ALKBH3 depleted sample, we detected RNF168 in the m^1A pulled-down RNA population; however, ALKBH3 knockdown resulted in a substantial increase in RNF168 levels (Figure 2B). This suggests that the m^1A modification is present on RNF168 mRNAs, and that upon decreased ALKBH3 expression, there is an increase in the overall levels of m^1A-modified RNF168 RNA.

Inspired by this, we set out to analyze the potential impact of ALKBH3 on the RNF168 mRNA molecule. mRNA modifications influence several stages of the mRNA life cycle, including mRNA transcription, stability, translation, splicing and intracellular mRNA dynamics [25,26]. RNF168 gene expression analysis by quantitative PCR (qPCR) revealed no change in total RNF168 mRNA levels following ALKBH3 depletion (Figure 2C), indicating that decreased transcription does not explain the drop in RNF168 protein levels.

Next, we performed a cellular RNA fractionation analysis, followed by qPCR, to evaluate the potential impact of ALKBH3 on the intracellular distribution of the RNF168 mRNA pool. Strikingly, we observed a clear enrichment of the RNF168 transcript in the nuclear fraction following ALKBH3 depletion (Figure 2D), indicating increased nuclear retention of RNF168 mRNA molecules. To validate these findings, we used RNA scope, an RNA *in situ* hybridization assay, to visualize and quantify any potential changes in the intracellular distribution of individual RNF168 molecules, in ALKBH3 depleted cells. Consistently, the results from the RNA scope analysis also showed an increase in nuclear RNF168 transcripts, and associated decrease in the cytoplasmic fraction (Figure 2E, 2F). Collectively, these data suggest that in ALKBH3 depleted cells, there is increased nuclear accumulation of RNF168 mRNA, which could indicate problems with the nuclear export of the RNF168 mRNA.

The potential role of additional AlkB family members in RNF168 regulation.

When combined, our results suggest that active removal of RNA methylation marks might play an important role in promoting efficient RNF168 expression, which is to our knowledge, a novel regulatory mechanism for RNF168. This encouraged us to explore the role of RNA de-methylation enzymes in RNF168 regulation further. In addition to ALKBH3, other members of the AlkB gene family are known to have RNA demethylase activity [52]. This includes FTO and ALKBH5, which both catalyze oxidative demethylation

of mRNA. Depletion of ALKBH5, which has previously been implicated in the regulation of mRNA nuclear export via m^{6}A demethylation [53], had no impact on RNF168 expression (Figure 3A). Remarkably, however, FTO knockdown dramatically reduced RNF168 protein levels, comparable to the downregulation observed in ALKBH3 depletion cells (Figure 3A). This was observed with multiple independent siRNAs in U2OS cells (Figure S2A) and confirmed in PC-3 cells. (Figure S2B). Interestingly, no additive effect on RNF168 protein levels was detected upon co-depletion of ALKBH3 and FTO (Figure 3B), suggesting that ALKBH3 and FTO might be regulating RNF168 expression via the same pathway. Similar to previous results when depleting cells of ALKBH3, decreased FTO expression did not affect total mRNA levels of RNF168 (Figure S2C), or RNF168 protein turnover (Figure S2D).

Subsequent experiments showed that comparable to ALKBH3 depletion, FTO knockdown resulted in reduced number of 53BP1 foci following NCS treatment (Figure 3C) and increased chromosomal aberrations (Figure 3D and Figure. S2E), with no effect on key repair factors protein expression (Figure. S2F). Importantly, we also detected increased nuclear accumulation of RNF168 mRNA following FTO depletion (Figure 3E,3F,3G), suggesting that FTO promotes nuclear RNF168 mRNA export.

Previous studies have shown that in the nucleus FTO has a preference for m^{6}A mRNA [32]. Immunofluorescence analysis showed that in U2OS cells FTO protein expression is predominantly confined to the nucleus (Figure S2G). Based on this, we hypothesized that defects in m^{6}A mRNA demethylation might explain the increased nuclear retention of RNF168 mRNA in FTO knockdown cells. To elucidate if FTO influences the levels of RNF168 m^{6}A modified mRNA we used a previously described m^{6}A-RNA immunoprecipitation assay [50], which is based on the same principle as the m^{1}A-RIP assay described above.

Compared to control cells, we observed a significant increase in m^6A interacting RNF168 mRNA following FTO depleted cells (Figure 3H). These results indicate that m^6A methylated RNF168 mRNA is a substrate for FTO, which could potentially explain the observed nuclear export defect. As expected, no increase in m^6A associated mRNA was detected following ALKBH3 depletion, nor was there any change in m^1A-modified RNF168 RNA in FTO knockdown cells (Figure S2H, S2I). Together, this suggests that although FTO and ALKBH3 are both important for RNF168 mRNA export, there is currently no evidence for mRNA substrate overlap between the two proteins.

Genomic instability and increased sensitivity to genotoxic drugs in ALKBH3 and FTO knockout cell lines.

To further confirm the role of ALKBH3 and FTO in RNF168 regulation and minimize the chances of siRNA off-target effects we turned to CRISPR-Cas9 genome editing to establish stable knockout cell line models. As expected, ALKBH3 and FTO knockout, respectively, caused reduced RNF168 protein expression (Figure 4A). Additionally, we detected increased micronuclei formation in both ALKBH3 and FTO knockout cell lines, which is a clear sign of genome instability (Figure 4B). This observation was further confirmed using siRNA mediated ALKBH3 and FTO knockdown (Figure S3A, S3B). Furthermore, compared to control cells, there was a clear enrichment of RNF168 mRNA in the nucleus in both knockout cell lines (Figure 4C, 4D), strongly supporting that ALKBH3 and FTO are involved in the RNF168 mRNA nuclear export process.

As a central regulator of DNA repair, RNF168 plays an important role in promoting survival after genotoxic stress [6,18]. In line with that, one of the hallmarks of RNF168 deficiency in mice and humans is hypersensitivity to ionizing irradiation (IR) [7,14,48]. To determine if this was also the case in ALKBH3 and FTO deficient cells, we performed a clonogenic survival assay in ALKBH3 and FTO knockout cell lines treated with NCS, which is a radiomimetic drug and a potent inducer of DNA DSBs.

Compared to control cells, both knockout cell lines displayed reduced survival following NCS treatment (Figure 4E). Likewise, both the FTO and ALKBH3 knockout cell lines were hypersensitivity to the DNA crosslinking agent Mitomycin C (MMC) (Figure 4F), which is in line with what has previously been reported in RNF168 deficient cells [18]. Increased sensitivity to NCS and MMC was also observed following siRNA mediated knockdown of ALKBH3 and FTO (Figure. S3C, S3D). Taken together, these findings indicate that similar to RNF168, ALKBH3 and FTO are important for genomic stability and survival in response to genotoxic agents.

Discussion

In recent years, precise spatial and temporal control of mRNA methylation has emerged as an important regulatory mechanism in diverse biological processes, including the DNA damage response [54,55]. For DNA double strand break repair, this has been linked to the role of m^6A modification enzymes in RNA:DNA hybrids and R-loop resolution, which in return has important implications for genome maintenance and recruitment of critical repair factors to sites of DNA double strand breaks [56,57]. In this study, we provide an example of a more specific form of regulation, with two known mRNA demethylation enzymes, ALKBH3 and FTO, directly influencing the activity of a key DNA DSB signaling factor by regulating its expression. These findings provide several additions to the current concept of mRNA methylation and DNA repair. First, our results indicate that active removal of mRNA methylation marks can in specific cases stimulate mRNA nuclear export, which is in contrast to previous reports showing that ALKBH5 dependent removal of m^6A marks inhibits mRNA export [53]. Second, our results suggest that in addition to the predominantly studied m^6A modification, m^1A mRNA methylation might potentially also be involved in maintaining genome stability and the regulation of mRNA export which is to our knowledge the first reported case of m^1A

influencing mRNA export. Finally, we for the first time show that mRNA eraser enzymes are important for efficient DNA DSB signaling and subsequent DNA repair.

ALKBH3 has previously been shown to promote genome stability through its role in DNA alkylation repair [34]. Here, we show that ALKBH3 might have a broader role in genome maintenance than previously anticipated. ALKBH3 via its impact on RNF168 also contributes to DNA DSB repair, suggesting there is a functional crosstalk between the two essential cellular defense mechanisms. Recently, an interesting example of such crosstalk was published by [58], where they show interaction between RAD51C and ALKBH3 stimulated the DNA alkylation repair function of ALKBH3 *in vitro*. Here we show that ALKBH3 promotes efficient DNA DSB repair, which further supports the functional overlap between DNA alkylation and DNA DSB repair.

In contrast to ALKBH3, there are no reports of a direct function for FTO in DNA alkylation repair there is, however, a link between FTO, m^6A and genotoxic stress responses, especially the ultraviolet-induced DNA damage response [54,59]. Xiang et al reported that FTO localizes to sites of UV damage, where it is involved in the dynamic regulation of a specific m^6A RNA mark, needed for efficient repair of UV-induced DNA damage. Interestingly, no recruitment of FTO to sites of DNA double strand breaks was detected, which is in line with our findings where we did not see any co-localization between FTO and the DNA DSB marker H2AX (data not shown). Therefore, it is highly unlikely that FTO is regulating RNF168 mRNA methylation locally at sites of DNA damage. However, since the need for RNF168 is most pressing in response to DNA double strand breaks formation, it would be interesting to study whether DNA damaging agents affect the levels of RNF168 mRNA methylation.

Previously we reported ALKBH3 gene inactivation through promoter methylation in over 20 % of breast cancer cases, and that ALKBH3 loss is associated with reduced patient survival [38]. Following studies revealed that epigenetic silencing of

ALKBH3 is not restricted to breast cancer, in fact it is a frequent event across cancer types, detected in 8 % of all tumor samples in The Cancer Genome Atlas (TCGA) database [39]. Interestingly, here we show that ALKBH3 deficiency is associated with increased sensitivity to NCS and MMC (Figure 4D-4G and Figure S3B-S3E), suggesting ALKBH3 contributes to survival in response to genotoxic stress. From the clinical perspective, this might potentially be an important finding, since it raises the possibility that ALKBH3 deficiency might be a potent biomarker to predict treatment outcomes in cancer and be a valuable contribution to personalized cancer management, although further studies are necessary to explore this in greater detail. Currently, there are no publications that show FTO epigenetic silencing in cancer. There are, however, several examples of FTO gene variants associated with increased cancer risk [60] in particular breast cancer [61]. In many cases, the increased cancer risk can be directly linked with obesity, where FTO mutations are considered a major risk factor. Nevertheless, there are some examples where there is no apparent link to obesity. Work from Iles et al suggests an association between two FTO variants and melanoma risk, independent of increased body mass index [62]. A more recent example demonstrated a connection between FTO genotype and breast cancer risk in HER2-negative patients, unrelated to obesity [63]. The mechanism behind the increased risk is not understood; however, given the strong connection between genome instability and cancer, it might be possible that the FTO's role in genome maintenance presented here, and in previous publications, contributes to cancer formation. Intriguingly, several FTO inhibitors are showing promising results in animal and cell line models, as potential therapeutic targets in cancer [60,64] stressing the need for further research on FTO and its contribution to cancer formation.

Compared to RNF168 deficient cells, the DNA DSB signaling defects were slightly milder in ALKBH3 and FTO depleted cells, indicating a partial loss of RNF168 function, which is in line with the level of reduction we observe in RNF168 protein expression.

This indicates that even in the absence of ALKBH3 and FTO, cells can still express RNF168 to some extent, suggesting there are additional mechanisms available to support RNF168 mRNA export. In certain cases, however, the genome instability phenotypes in FTO depleted cells extended beyond what can be explained by decreased RNF168 expression. For instance, the level of metaphase aberrations and NCS induced cell death is somewhat higher in FTO knockdown cells, compared to RNF168 deficient cells, suggesting a broader role in safeguarding genome integrity. This highlights the need for further research on the role of FTO in maintaining genome stability.

RNF168 is a rate-limiting factor in DNA DSB repair signaling and aberrant RNF168 expression has important implications for human disease. It is therefore not surprising that RNF168 functions have many layers of regulation, which include stepwise regulation of recruitment to sites of DNA damage, and multiple factors controlling protein abundance. Likely, the dynamic regulation of RNF168 mRNA methylation levels is a novel example of a mechanism, which contributes to the fine-tuning of RNF168 expression.

The connection between mRNA methylations and mRNA export has become more evident in recent years, primarily due to the discovery of robust interactions between multiple constituents of the m^6A methylation complex, methylation reader proteins and the core mRNA export machinery, indicating a functional interplay between these two processes [65-67]. The precise role of the methylation eraser proteins, ALKBH3 and FTO, in the mRNA export process remains ambiguous and requires additional investigation. It is plausible that the removal of m^6A and m^1A modifications serves as a quality control mechanism as the extended presence of methylation marks on mRNA transcripts may inhibit their nuclear export.

Notably, the antibody used in the m^6A RNA-immunoprecipitation analysis cannot distinguish between m^6A and m^6A_m. However, as previously noted experimental

evidence highlights FTO's selective affinity for m^6A within the cell nucleus [32]. Given that in our experimental model, U2OS cells, FTO localizes in the nucleus, the likelihood leans towards m^6A being the methylation target instead of m^6A_m. To confirm this, locating specific methylation sites on RNF168 mRNA transcripts through advanced sequencing techniques, such as Nanopore direct RNA sequencing would be needed. Furthermore, information on specific FTO and ALKBH3 target sites, and how these residues impact mRNA-protein interactions, could hold the key to elucidating the mechanism behind how the removal of m^6A and m^1A regulates mRNA exports. Mechanistically, we do not fully understand the cooperative effect of ALKBH3 and FTO. Apart from being members of the ALKBH gene family, the two genes differ in substrate specificity, and have no apparent functional overlap. It is however interesting, that we see no additional impact on RNF168 protein levels following co-depletion of ALKBH3 and FTO, which might suggest ALKBH3 and FTO promote RNF168 mRNA export via the same pathway, potentially involving crosstalk between different mRNA modifications.

Recently, several examples of crosstalk between different mRNA methylation marks have been reported, for instance in protein translation where m^6A and m^5C cooperate to enhance protein translation [68]. Another example of such crosstalk comes from studies on mRNA degradation, where crosstalk between m^1A and m^6A modifications, and their specific reader proteins, is needed to facilitate efficient mRNA degradation [69]. Here, we envisage a comparable mechanism, where FTO and ALKBH3 dependent removal of m^6A and m^1A, respectively, are two distinct steps in the same mRNA export pathway.

In this study, we uncover mRNA export as an important regulatory mechanism involved in DNA DSB repair signalling. More specifically, our results indicate that two RNA demethylases, ALKBH3 and FTO, promote efficient RNF168 mRNA export, and play

important roles in genome maintenance and cell survival in response to genotoxic stress.

Material and methods

Cell culture: U2OS, MCF7 and PC-3 were maintained in DMEM (Dulbecco's Modified Eagle Medium) with GlutaMAX with pyruvate (Thermo Fisher, LT-31966-021) supplemented fetal bovine serum (FBS, 10% Thermo Scientific, 10500064) penicillin (20 U/mL) and streptomycin (20 µg/mL) (Thermo Scientific, 15070-063) and cultured in 95% air with 5% CO2 at 37°C. MCF7 were additionally cultured with 0,01mg/mL insulin (Sigma Aldrich, SA-I6634-100MG)

RNA extraction: RNA was extracted from human osteosarcoma U2OS cells using Tri-Reagent (Thermo Fisher Scientific) according to manufacturer's instruction. The concentration of total RNA was measured on Nanodrop One (Thermo Fisher, AM9738).

Quantitative real time PCR (qPCR): Following cDNA synthesized; qPCR assay was conducted using SYBR Green master mix (Thermo Fisher, A25742) in Bio-Rad system CFX384. Downstream analysis was performed using Bio-Rad CFX manager version 3.0. The threshold cycle number (Cq) was analyzed in triplicates for each sample. Gene expression for genes of interest were normalized to housekeeping genes (HPRT, beta actin or GAPDH) and calculated using the using the $2^{-\Delta\Delta CT}$ method for relative quantification.

siRNA transfection: Using Lipofectamine RNAiMAX transfection reagent (Thermo Fisher, 13778075) cells were transfected with 10nM siRNA (Thermo Fisher) according to the manufacturer's instructions.

FLAG co-immunoprecipitation: U2OS cells were harvested 48h post plasmid transfection with GenJet™ In Vitro DNA Transfection Reagent for U2OS Cells (SignaGene Laboratories, SL100489-OS) using 1mL FLAG-IP lysis buffer (50 mM Tris

HCl pH 7.4, 150 mM NaCl, 1mM EDTA and 1% TRITON X-100) with added protease inhibitor cocktail 1:100. Plates were incubated with lysis buffer for 30 minutes on a shaker at 4°C. Cell debris were removed by centrifugation at 14.000 rpm for 10 min. Supernatant was transferred to a chilled 1.5 mL tube, with 100 µL being preserved as an input control (IN). The remaining lysate was added to Anti-FLAG conjugated agarose beads (Sigma-Aldrich,2220) and rotated at 4°C overnight. Agarose-beads were washed three times in ice cold TBS buffer (50 mM Tris HCl pH 7.4, 150 mM NaCl), with 1 min centrifuging between each spin. For elution 100µL of 300ng/µL 3xFLAG peptide (Sigma, F4799) was added to sample and incubated at 4°C ON with gentile shaking. Samples were then centrifuged at 7000g for 1 min and supernatant was gathered as immunoprecipitation sample (IP). Samples were mixed with 2xLaemmmli sample buffer (Santa Cruz, sc-286963) in 1:1 ratio and boiled at 95°C for 5 minutes and analyzed with immunoblotting.

Immunoblotting: Proteins were extracted from cells at 80-90% confluency using 2xLaemmmli sample buffer (Santa Cruz,sc-286963) and treated with Benzonase nuclease (Sigma Aldrich, E1014). Samples were electrophoresed using 6, 8 or 10% acrylamide gel followed by transfer to nitrocellulose membrane. Primary antibodies were incubated with membrane overnight at 4°C followed by washing with 1xPBS+0,2% Tween for 5 min. Secondary antibodies (1:10.000 dilution) were incubated for 1h at RT. The membrane was developed with Luminol Reagent (Santa Cruz, sc-2048) and visualized in a ChemiDoc XRS+ system (Bio-Rad).

Immunofluorescence confocal microscopy: Cells were grown on coverslips and fixed with 4% paraformaldehyde for 15 min followed by permeabilization with 0,2% Triton-X for 5 min and 1h of blocking with DMEM with 10% FBS. Primary antibodies were incubated for 1h at RT (dilutions 1:250, 1:500 or 1:1000) followed by secondary antibodies Alexa-Fluor 488 goat anti rabbit/mouse, Alexa-Fluor 555 goat anti-

rabbit/mouse (1:1000) and nuclear DNA was stained by DAPI (1:5000) for 1h. Coverslips were mounted on glass slides using Fluoroshield (Sigma Aldrich, F6182) mounting medium.

FV1200 Olympus inverted confocal microscope was used to acquire images. Dual color confocal images were attained with standard settings using laser lines 488 nm and 543 nm for excitation of Alexa Fluor 488 and Alexa Fluor 555 dyes. Nuclear DAPI staining was imaged using excitation by the 405 nm laser. For each condition 5-10 images were randomly obtained with the 20X objective and imported into ImageJ and Cell Profiler for downstream image analysis. For each data point, at least 200 cells (identified by DAPI staining) were analyzed.

m^6A and m^1A RNA immunoprecipitation (MeRIP): MeRIP was based on previously described m^6A-sequencing protocol [50] [51]with a few alterations.

300µg of total RNA was incubated with 30µL of both protein A and protein G magnetic beads (Thermo Fisher, 10002D, 10004D,) along with m^6A or m^1A antibody, 10% of RNA was saved as input.

IP-RNA was eluted with 300µL of elution buffer (100mM KCl, 5mMmgCl2, 10mM HEPES, 0.5% Tween-20, 1mM DTT, 0.1% SDS, RNase inhibitor 100U and 15 µg/mL proteinase K) for 2 min at RT followed by 30 min at 50°C. Magnetic rack was used to separate RNA from beads, supernatant was collected into a new tubes and IP-RNA extracted using phenol-chloroform (P3803, Sigma). IP-RNA was precipitated using 100% ethanol, 3M sodium acetate pH 5,2 and 20µg glycogen (R0561T, Thermo Fisher).

MeRIP real time qPCR: Real time qPCR was performed to assess the relative expression of RNF168 in IP-RNA and input RNA samples. cDNA was synthesized from using Oligo$(dT)_{12-18}$ primers (Thermo Fisher, SO132) and Superscript II (18064022,

Thermo Fisher) following manufacture´s protocol. Quantitative analysis of the PCR products was performed using SYBR Green master mix (A25742, Thermo Fisher) in Bio-Rad system CFX384. Downstream analysis was performed using Bio-Rad CFX manager version 3.0.

The pulldown efficiency was calculated as % of input by computing the difference in the Ct as follows: $2^{\wedge-(Ct[IP]-Ct[Input-logDF])} *10$, where DF stands for input dilution factor. GAPDH expression was used to normalize target gene expression in IP sample.

Cellular fractionation: Following siRNA treatment for 48h, cellular fractionation was completed were cytoplasmic and nuclear RNA was isolated using the RNA Subcellular Isolation Kit from Active Motive (25501) following manufacturer's instruction and qPCR performed as described above. Nuclear:cytoplasmic ratio was defined as the ratio of mRNA expression in nucleus vs mRNA expression in cytoplasm.

RNA Scope: Following a 48h incubation with siRNAs U2OS cells were fixed with 4% paraformaldehyde for 30 minutes followed by protease digestion (Pretreat protease III, ACD Bio 322340) for 10 min at RT. Cells were incubated with target probes (ACD Bio 300031/320861) for 2h at 40°C and washed two times with 1xRNAScope wash buffer (ACD Bio ,310091). Next primary, secondary, tertiary, and fluorescent probes (ACD bio, 320850) were placed on for 30, 15, 30 and 15 minutes respectively, each with two 5 min washes in the wash buffer. Finally, cells were treated with DAPI nuclear stain for 60 sec followed immediately by mounting samples on glass slips with mounting medium. Images were acquired with confocal microscopy, using Olympus FLV1200 under the 60X oil immersion objective in an unbiased manner, based on DAPI staining rather than the RNAScope foci and analyzed using Image J and Cell Profiler 3.0. Approximately 200 cells were counted for each treatment.

Proteasome Inhibition: U2OS cells were treated with 10 μM MG-132 (Sigma Aldrich, 1211877-36-9) a peptide aldehyde that blocks proteolytic activity of the 26S the major protease in eukaryotic cells for 3h. Cells were treated according to manufacturer's instruction.

Clonogenic assay: Following a 48h incubation with siRNA (10nM) cells were counted in seeded out in triplicates in six well plates (500 cells, 2500 cells for siFTO). After 24h cells were treated with NCS (Sigma-Aldrich, N9162) for 1h or with Mitomycin C (Biotechne,3258/2) for 24h. Cells were cultured for an additional 7-11 days. Colonies were stained with crystal violet and counted. Survival fraction was calculated according to [70]. CRISPR-Cas9 KO cells were seeded out in low density (500 cells) in six well plates and treated as described above.

CRISPR cell line generation: Using RNAiMAX transfection reagent (Thermo Fisher, 13778030) U2OS cells were transfected with three single-guide RNA (sgRNA) with CRISPR/Cas9 system to induce knockout of either FTO or ALKBH3. TRAC gene used as a positive control. 72h after transfection, cells were plated out in single cell density after which individual clones were isolated. Inference of CRISPR edits (ICE) analysis tool provided by Synthego Inc was used to analyze specific fragment deletions or indels and to evaluate overall knockout score for each sample. The knockout was verified by western blot and Sanger sequencing.

Metaphase chromosome spread: Following 48h incubation with siRNA U2OS cells were treated with 500ng/μL of Colcemid (Invitrogen, 15212-012) to cause metaphase arrest. Cells were trypsinized, swollen with 75mM KCl solution for 20 min at 37 °C, followed by centrifugation at 1000 rpm, supernatant removed, and pellet resuspend in fixing solution (3:1 methanol: acidic acid). Fixing step was repeated 3 times and chromosomes suspended in 200μL fixing solution. Microscope slides were created by dropping the cell suspension on the slides in HANABI metaphase spreader from ADS

Biotech and stained with Giemsa staining. The slides were scanned, and images automatically captured using DUET-3 automated imaging system from BioView. The images were analyzed using Solo software from BioView and aberration counted.

Micronuclei assay: Following 48h incubation with siRNA, U2Os cells were fixed with 4% paraformaldehyde for 15 min followed by permeabilization with 0,2% Triton-X for 5 min and 1h of blocking with DMEM with 10% FBS. Cells were stained with Nuclear DNA was stained, DAPI (Sigma-Aldrich, D9542) diluted 1:5000 for 1h at RT. Coverslips were mounted on glass slides using Fluoroshield (SIGMA, F6182) mounting medium. CRISPR clones were grown on coverslips and fixed and stained as described above.

FV1200 Olympus inverted confocal microscope was used to acquire images. Nuclear DAPI staining was imaged using excitation by the 405 nm laser. For each condition 5 images were randomly obtained with the 20X objective and imported into ImageJ and Cell Profiler for downstream image analysis. Approximately 200-300 cells were counted for each treatment.

Statistical analysis: All data generated were taken from distinct samples and presented as mean±SD. All experiments were performed in a minimum of three biological replicates. The statistical significance of experimental data was assessed using two-tailed unpaired students T-test or two-tailed Mann-Whitney T-test (metaphase spread data), using Graph Pad Prism 6 for windows.

P-values are as follows: ****p<0.0001, ***p<0.001, **p<0.01, *p<0.05.

Data availability: The authors declare that the data supporting the findings of this study are available from the corresponding authors upon request.

References

1. Lukas, J., Lukas, C., and Bartek, J. (2011). More than just a focus: The chromatin response to DNA damage and its role in genome integrity maintenance. Nat Cell Biol 13, 1161-1169, 10.1038/ncb2344.

2. Song, H., Dicks, E., Ramus, S.J., Tyrer, J.P., Intermaggio, M.P., Hayward, J., Edlund, C.K., Conti, D., Harrington, P., Fraser, L. et al. (2015). Contribution of Germline Mutations in the RAD51B, RAD51C, and RAD51D Genes to Ovarian Cancer in the Population. J Clin Oncol 33, 2901-2907, 10.1200/JCO.2015.61.2408.

3. Bartkova, J., Tommiska, J., Oplustilova, L., Aaltonen, K., Tamminen, A., Heikkinen, T., Mistrik, M., Aittomaki, K., Blomqvist, C., Heikkila, P. et al. (2008). Aberrations of the MRE11-RAD50-NBS1 DNA damage sensor complex in human breast cancer: MRE11 as a candidate familial cancer-predisposing gene. Mol Oncol 2, 296-316, 10.1016/j.molonc.2008.09.007.

4. Heeke, A.L., Pishvaian, M.J., Lynce, F., Xiu, J., Brody, J.R., Chen, W.J., Baker, T.M., Marshall, J.L., and Isaacs, C. (2018). Prevalence of Homologous Recombination-Related Gene Mutations Across Multiple Cancer Types. JCO Precis Oncol 2018, 10.1200/PO.17.00286.

5. Mailand, N., Bekker-Jensen, S., Faustrup, H., Melander, F., Bartek, J., Lukas, C., and Lukas, J. (2007). RNF8 ubiquitylates histones at DNA double-strand breaks and promotes assembly of repair proteins. Cell 131, 887-900, 10.1016/j.cell.2007.09.040.

6. Doil, C., Mailand, N., Bekker-Jensen, S., Menard, P., Larsen, D.H., Pepperkok, R., Ellenberg, J., Panier, S., Durocher, D., Bartek, J. et al. (2009). RNF168 Binds and Amplifies Ubiquitin Conjugates on Damaged Chromosomes to Allow Accumulation of Repair Proteins. Cell 136, 435-446, 10.1016/j.cell.2008.12.041.

7. Stewart, G.S., Panier, S., Townsend, K., Al-Hakim, A.K., Kolas, N.K., Miller, E.S., Nakada, S., Ylanko, J., Olivarius, S., Mendez, M. et al. (2009). The RIDDLE syndrome protein mediates a ubiquitin-dependent signaling cascade at sites of DNA damage. Cell 136, 420-434, 10.1016/j.cell.2008.12.042.

8. Bohgaki, M., Bohgaki, T., El Ghamrasni, S., Srikumar, T., Maire, G., Panier, S., Fradet-Turcotte, A., Stewart, G.S., Raught, B., Hakem, A. et al. (2013). RNF168 ubiquitylates 53BP1 and controls its response to DNA double-strand breaks. Proceedings of the National Academy of Sciences of the United States of America 110, 20982-20987, 10.1073/pnas.1320302111.

9. Luijsterburg, M.S., Typas, D., Caron, M.C., Wiegant, W.W., van den Heuvel, D., Boonen, R.A., Couturier, A.M., Mullenders, L.H., Masson, J.Y., and van Attikum, H.

(2017). A PALB2-interacting domain in RNF168 couples homologous recombination to DNA break-induced chromatin ubiquitylation. Elife 6, 10.7554/eLife.20922.

10. Ochs, F., Somyajit, K., Altmeyer, M., Rask, M.B., Lukas, J., and Lukas, C. (2016). 53BP1 fosters fidelity of homology-directed DNA repair. Nature structural & molecular biology 23, 714-721, 10.1038/nsmb.3251.

11. Krais, J.J., Wang, Y., Patel, P., Basu, J., Bernhardy, A.J., and Johnson, N. (2021). RNF168-mediated localization of BARD1 recruits the BRCA1-PALB2 complex to DNA damage. Nat Commun 12, 5016, 10.1038/s41467-021-25346-4.

12. Zong, D., Adam, S., Wang, Y., Sasanuma, H., Callen, E., Murga, M., Day, A., Kruhlak, M.J., Wong, N., Munro, M. et al. (2019). BRCA1 Haploinsufficiency Is Masked by RNF168-Mediated Chromatin Ubiquitylation. Mol Cell 73, 1267-1281 e1267, 10.1016/j.molcel.2018.12.010.

13. Stewart, G.S., Stankovic, T., Byrd, P.J., Wechsler, T., Miller, E.S., Huissoon, A., Drayson, M.T., West, S.C., Elledge, S.J., and Taylor, A.M. (2007). RIDDLE immunodeficiency syndrome is linked to defects in 53BP1-mediated DNA damage signaling. Proceedings of the National Academy of Sciences of the United States of America 104, 16910-16915, 10.1073/pnas.0708408104.

14. Devgan, S.S., Sanal, O., Doil, C., Nakamura, K., Nahas, S.A., Pettijohn, K., Bartek, J., Lukas, C., Lukas, J., and Gatti, R.A. (2011). Homozygous deficiency of ubiquitin-ligase ring-finger protein RNF168 mimics the radiosensitivity syndrome of ataxia-telangiectasia. Cell Death Differ 18, 1500-1506, 10.1038/cdd.2011.18.

15. Patel, P.S., Abraham, K.J., Guturi, K.K.N., Halaby, M.J., Khan, Z., Palomero, L., Ho, B., Duan, S., St-Germain, J., Algouneh, A. et al. (2021). RNF168 regulates R-loop resolution and genomic stability in BRCA1/2-deficient tumors. The Journal of clinical investigation 131, 10.1172/JCI140105.

16. Schmid, J.A., Berti, M., Walser, F., Raso, M.C., Schmid, F., Krietsch, J., Stoy, H., Zwicky, K., Ursich, S., Freire, R. et al. (2018). Histone Ubiquitination by the DNA Damage Response Is Required for Efficient DNA Replication in Unperturbed S Phase. Mol Cell 71, 897-910 e898, 10.1016/j.molcel.2018.07.011.

17. Rai, R., Li, J.M., Zheng, H., Lok, G.T., Deng, Y., Huen, M.S., Chen, J., Jin, J., and Chang, S. (2011). The E3 ubiquitin ligase Rnf8 stabilizes Tpp1 to promote telomere end protection. Nature structural & molecular biology 18, 1400-1407, 10.1038/nsmb.2172.

18. Katsuki, Y., Abe, M., Park, S.Y., Wu, W., Yabe, H., Yabe, M., van Attikum, H., Nakada, S., Ohta, T., Seidman, M.M. et al. (2021). RNF168 E3 ligase participates in ubiquitin signaling and recruitment of SLX4 during DNA crosslink repair. Cell Rep 37, 109879, 10.1016/j.celrep.2021.109879.

19. Shanbhag, N.M., Rafalska-Metcalf, I.U., Balane-Bolivar, C., Janicki, S.M., and Greenberg, R.A. (2010). ATM-dependent chromatin changes silence transcription in cis to DNA double-strand breaks. Cell 141, 970-981, 10.1016/j.cell.2010.04.038.

20. Gudjonsson, T., Altmeyer, M., Savic, V., Toledo, L., Dinant, C., Grofte, M., Bartkova, J., Poulsen, M., Oka, Y., Bekker-Jensen, S. et al. (2012). TRIP12 and UBR5 suppress spreading of chromatin ubiquitylation at damaged chromosomes. Cell 150, 697-709, 10.1016/j.cell.2012.06.039.

21. Altmeyer, M., and Lukas, J. (2013). To spread or not to spread--chromatin modifications in response to DNA damage. Curr Opin Genet Dev 23, 156-165, 10.1016/j.gde.2012.11.001.

22. Zong, D., Callen, E., Pegoraro, G., Lukas, C., Lukas, J., and Nussenzweig, A. (2015). Ectopic expression of RNF168 and 53BP1 increases mutagenic but not physiological non-homologous end joining. Nucleic acids research 43, 4950-4961, 10.1093/nar/gkv336.

23. Peuscher, M.H., and Jacobs, J.J. (2011). DNA-damage response and repair activities at uncapped telomeres depend on RNF8. Nat Cell Biol 13, 1139-1145, 10.1038/ncb2326.

24. Panier, S., and Durocher, D. (2013). Push back to respond better: regulatory inhibition of the DNA double-strand break response. Nat Rev Mol Cell Biol 14, 661-672, 10.1038/nrm3659.

25. Zaccara, S., Ries, R.J., and Jaffrey, S.R. (2019). Reading, writing and erasing mRNA methylation. Nat Rev Mol Cell Biol 20, 608-624, 10.1038/s41580-019-0168-5.

26. Zhou, Y., Kong, Y., Fan, W., Tao, T., Xiao, Q., Li, N., and Zhu, X. (2020). Principles of RNA methylation and their implications for biology and medicine. Biomed Pharmacother 131, 110731, 10.1016/j.biopha.2020.110731.

27. Aas, P.A., Otterlei, M., Falnes, P.O., Vagbo, C.B., Skorpen, F., Akbari, M., Sundheim, O., Bjoras, M., Slupphaug, G., Seeberg, E. et al. (2003). Human and bacterial oxidative demethylases repair alkylation damage in both RNA and DNA. Nature 421, 859-863, 10.1038/nature01363.

28. Falnes, P.O., Bjoras, M., Aas, P.A., Sundheim, O., and Seeberg, E. (2004). Substrate specificities of bacterial and human AlkB proteins. Nucleic acids research 32, 3456-3461, 10.1093/nar/gkh655.

29. Jia, G., Fu, Y., Zhao, X., Dai, Q., Zheng, G., Yang, Y., Yi, C., Lindahl, T., Pan, T., Yang, Y.G. et al. (2011). N6-methyladenosine in nuclear RNA is a major substrate of the obesity-associated FTO. Nat Chem Biol 7, 885-887, 10.1038/nchembio.687.

30. Fu, Y., Jia, G., Pang, X., Wang, R.N., Wang, X., Li, C.J., Smemo, S., Dai, Q., Bailey, K.A., Nobrega, M.A. et al. (2013). FTO-mediated formation of N6-hydroxymethyladenosine and N6-formyladenosine in mammalian RNA. Nat Commun 4, 1798, 10.1038/ncomms2822.

31. Mauer, J., Luo, X., Blanjoie, A., Jiao, X., Grozhik, A.V., Patil, D.P., Linder, B., Pickering, B.F., Vasseur, J.J., Chen, Q. et al. (2017). Reversible methylation of m(6)A(m) in the 5′ cap controls mRNA stability. Nature 541, 371-375, 10.1038/nature21022.

32. Wei, J., Liu, F., Lu, Z., Fei, Q., Ai, Y., He, P.C., Shi, H., Cui, X., Su, R., Klungland, A. et al. (2018). Differential m(6)A, m(6)A(m), and m(1)A Demethylation Mediated by FTO in the Cell Nucleus and Cytoplasm. Mol Cell 71, 973-985 e975, 10.1016/j.molcel.2018.08.011.

33. Duncan, T., Trewick, S.C., Koivisto, P., Bates, P.A., Lindahl, T., and Sedgwick, B. (2002). Reversal of DNA alkylation damage by two human dioxygenases. Proceedings of the National Academy of Sciences of the United States of America 99, 16660-16665, 10.1073/pnas.262589799.

34. Dango, S., Mosammaparast, N., Sowa, M.E., Xiong, L.J., Wu, F., Park, K., Rubin, M., Gygi, S., Harper, J.W., and Shi, Y. (2011). DNA unwinding by ASCC3 helicase is coupled to ALKBH3-dependent DNA alkylation repair and cancer cell proliferation. Mol Cell 44, 373-384, 10.1016/j.molcel.2011.08.039.

35. Li, X., Xiong, X., Wang, K., Wang, L., Shu, X., Ma, S., and Yi, C. (2016). Transcriptome-wide mapping reveals reversible and dynamic N(1)-methyladenosine methylome. Nat Chem Biol 12, 311-316, 10.1038/nchembio.2040.

36. Kuang, W., Jin, H., Yang, F., Chen, X., Liu, J., Li, T., Chang, Y., Liu, M., Xu, Z., Huo, C. et al. (2022). ALKBH3-dependent m(1)A demethylation of Aurora A mRNA inhibits ciliogenesis. Cell Discov 8, 25, 10.1038/s41421-022-00385-3.

37. Woo, H.H., and Chambers, S.K. (2019). Human ALKBH3-induced m(1)A demethylation increases the CSF-1 mRNA stability in breast and ovarian cancer cells. Bba-Gene Regul Mech 1862, 35-46, 10.1016/j.bbagrm.2018.10.008.

38. Stefansson, O.A., Hermanowicz, S., van der Horst, J., Hilmarsdottir, H., Staszczak, Z., Jonasson, J.G., Tryggvadottir, L., Gudjonsson, T., and Sigurdsson, S. (2017). CpG promoter methylation of the ALKBH3 alkylation repair gene in breast cancer. BMC Cancer 17, 469, 10.1186/s12885-017-3453-8.

39. Knijnenburg, T.A., Wang, L., Zimmermann, M.T., Chambwe, N., Gao, G.F., Cherniack, A.D., Fan, H., Shen, H., Way, G.P., Greene, C.S. et al. (2018). Genomic

and Molecular Landscape of DNA Damage Repair Deficiency across The Cancer Genome Atlas. Cell Rep 23, 239-254 e236, 10.1016/j.celrep.2018.03.076.

40. Esteve-Puig, R., Climent, F., Pineyro, D., Domingo-Domenech, E., Davalos, V., Encuentra, M., Rea, A., Espejo-Herrera, N., Soler, M., Lopez, M. et al. (2021). Epigenetic loss of m(1)A RNA demethylase ALKBH3 in Hodgkin lymphoma targets collagen, conferring poor clinical outcome. Blood 137, 994-999, 10.1182/blood.2020005823.

41. Dominissini, D., Nachtergaele, S., Moshitch-Moshkovitz, S., Peer, E., Kol, N., Ben-Haim, M.S., Dai, Q., Di Segni, A., Salmon-Divon, M., Clark, W.C. et al. (2016). The dynamic N1-methyladenosine methylome in eukaryotic messenger RNA. Nature 530, 441-446, 10.1038/nature16998.

42. Hawley, B.R., and Jaffrey, S.R. (2019). Transcriptome-Wide Mapping of m(6) A and m(6) Am at Single-Nucleotide Resolution Using miCLIP. Curr Protoc Mol Biol 126, e88, 10.1002/cpmb.88.

43. Zhao, Y., Majid, M.C., Soll, J.M., Brickner, J.R., Dango, S., and Mosammaparast, N. (2015). Noncanonical regulation of alkylation damage resistance by the OTUD4 deubiquitinase. EMBO J 34, 1687-1703, 10.15252/embj.201490497.

44. Daley, J.M., and Sung, P. (2013). RIF1 in DNA break repair pathway choice. Mol Cell 49, 840-841, 10.1016/j.molcel.2013.02.019.

45. Liefke, R., Windhof-Jaidhauser, I.M., Gaedcke, J., Salinas-Riester, G., Wu, F., Ghadimi, M., and Dango, S. (2015). The oxidative demethylase ALKBH3 marks hyperactive gene promoters in human cancer cells. Genome Med 7, 66, 10.1186/s13073-015-0180-0.

46. Lukas, C., Melander, F., Stucki, M., Falck, J., Bekker-Jensen, S., Goldberg, M., Lerenthal, Y., Jackson, S.P., Bartek, J., and Lukas, J. (2004). Mdc1 couples DNA double-strand break recognition by Nbs1 with its H2AX-dependent chromatin retention. EMBO J 23, 2674-2683, 10.1038/sj.emboj.7600269.

47. Guturi, K.K.N., Bohgaki, M., Bohgaki, T., Srikumar, T., Ng, D., Kumareswaran, R., El Ghamrasni, S., Jeon, J., Patel, P., Eldin, M.S. et al. (2016). RNF168 and USP10 regulate topoisomerase IIalpha function via opposing effects on its ubiquitylation. Nat Commun 7, 12638, 10.1038/ncomms12638.

48. Bohgaki, T., Bohgaki, M., Cardoso, R., Panier, S., Zeegers, D., Li, L., Stewart, G.S., Sanchez, O., Hande, M.P., Durocher, D. et al. (2011). Genomic instability, defective spermatogenesis, immunodeficiency, and cancer in a mouse model of the RIDDLE syndrome. PLoS Genet 7, e1001381, 10.1371/journal.pgen.1001381.

49. Li, X., Xiong, X., Zhang, M., Wang, K., Chen, Y., Zhou, J., Mao, Y., Lv, J., Yi, D., Chen, X.W. et al. (2017). Base-Resolution Mapping Reveals Distinct m(1)A Methylome in Nuclear- and Mitochondrial-Encoded Transcripts. Mol Cell 68, 993-1005 e1009, 10.1016/j.molcel.2017.10.019.

50. Zeng, Y., Wang, S., Gao, S., Soares, F., Ahmed, M., Guo, H., Wang, M., Hua, J.T., Guan, J., Moran, M.F. et al. (2018). Refined RIP-seq protocol for epitranscriptome analysis with low input materials. PLoS Biol 16, e2006092, 10.1371/journal.pbio.2006092.

51. Dominissini, D., Moshitch-Moshkovitz, S., Salmon-Divon, M., Amariglio, N., and Rechavi, G. (2013). Transcriptome-wide mapping of N(6)-methyladenosine by m(6)A-seq based on immunocapturing and massively parallel sequencing. Nature protocols 8, 176-189, 10.1038/nprot.2012.148.

52. Fedeles, B.I., Singh, V., Delaney, J.C., Li, D., and Essigmann, J.M. (2015). The AlkB Family of Fe(II)/alpha-Ketoglutarate-dependent Dioxygenases: Repairing Nucleic Acid Alkylation Damage and Beyond. The Journal of biological chemistry 290, 20734-20742, 10.1074/jbc.R115.656462.

53. Zheng, G., Dahl, J.A., Niu, Y., Fedorcsak, P., Huang, C.M., Li, C.J., Vagbo, C.B., Shi, Y., Wang, W.L., Song, S.H. et al. (2013). ALKBH5 is a mammalian RNA demethylase that impacts RNA metabolism and mouse fertility. Mol Cell 49, 18-29, 10.1016/j.molcel.2012.10.015.

54. Xiang, Y., Laurent, B., Hsu, C.H., Nachtergaele, S., Lu, Z., Sheng, W., Xu, C., Chen, H., Ouyang, J., Wang, S. et al. (2017). RNA m(6)A methylation regulates the ultraviolet-induced DNA damage response. Nature 543, 573-576, 10.1038/nature21671.

55. Tsao, N., Brickner, J.R., Rodell, R., Ganguly, A., Wood, M., Oyeniran, C., Ahmad, T., Sun, H., Bacolla, A., Zhang, L. et al. (2021). Aberrant RNA methylation triggers recruitment of an alkylation repair complex. Mol Cell 81, 4228-4242 e4228, 10.1016/j.molcel.2021.09.024.

56. Zhang, C., Chen, L., Peng, D., Jiang, A., He, Y., Zeng, Y., Xie, C., Zhou, H., Luo, X., Liu, H. et al. (2020). METTL3 and N6-Methyladenosine Promote Homologous Recombination-Mediated Repair of DSBs by Modulating DNA-RNA Hybrid Accumulation. Mol Cell 79, 425-442 e427, 10.1016/j.molcel.2020.06.017.

57. Abakir, A., Giles, T.C., Cristini, A., Foster, J.M., Dai, N., Starczak, M., Rubio-Roldan, A., Li, M., Eleftheriou, M., Crutchley, J. et al. (2020). N(6)-methyladenosine regulates the stability of RNA:DNA hybrids in human cells. Nature genetics 52, 48-55, 10.1038/s41588-019-0549-x.

58. Mohan, M., Akula, D., Dhillon, A., Goyal, A., and Anindya, R. (2019). Human RAD51 paralogue RAD51C fosters repair of alkylated DNA by interacting with the ALKBH3 demethylase. Nucleic acids research 47, 11729-11745, 10.1093/nar/gkz938.

59. Zhang, Q., Riddle, R.C., Yang, Q., Rosen, C.R., Guttridge, D.C., Dirckx, N., Faugere, M.C., Farber, C.R., and Clemens, T.L. (2019). The RNA demethylase FTO is required for maintenance of bone mass and functions to protect osteoblasts from genotoxic damage. Proceedings of the National Academy of Sciences of the United States of America 116, 17980-17989, 10.1073/pnas.1905489116.

60. Lan, N., Lu, Y., Zhang, Y., Pu, S., Xi, H., Nie, X., Liu, J., and Yuan, W. (2020). FTO - A Common Genetic Basis for Obesity and Cancer. Front Genet 11, 559138, 10.3389/fgene.2020.559138.

61. Kaklamani, V., Yi, N., Sadim, M., Siziopikou, K., Zhang, K., Xu, Y., Tofilon, S., Agarwal, S., Pasche, B., and Mantzoros, C. (2011). The role of the fat mass and obesity associated gene (FTO) in breast cancer risk. BMC medical genetics 12, 52, 10.1186/1471-2350-12-52.

62. Iles, M.M., Law, M.H., Stacey, S.N., Han, J., Fang, S., Pfeiffer, R., Harland, M., Macgregor, S., Taylor, J.C., Aben, K.K. et al. (2013). A variant in FTO shows association with melanoma risk not due to BMI. Nature genetics 45, 428-432, 432e421, 10.1038/ng.2571.

63. Montazeri, F., Hatami, H., Fathi, S., Hasanpour Ardekanizadeh, N., Bourbour, F., Rastgoo, S., Shafiee, F., Akbari, M.E., Gholamalizadeh, M., Mosavi Jarrahi, S.A. et al. (2022). FTO genotype was associated with breast cancer in HER2 negative patients. Clin Nutr ESPEN 49, 495-498, 10.1016/j.clnesp.2022.02.122.

64. Yang, S., Wei, J., Cui, Y.H., Park, G., Shah, P., Deng, Y., Aplin, A.E., Lu, Z., Hwang, S., He, C. et al. (2019). m(6)A mRNA demethylase FTO regulates melanoma tumorigenicity and response to anti-PD-1 blockade. Nat Commun 10, 2782, 10.1038/s41467-019-10669-0.

65. Lesbirel, S., and Wilson, S.A. (2019). The m(6)A-methylase complex and mRNA export. Biochim Biophys Acta Gene Regul Mech 1862, 319-328, 10.1016/j.bbagrm.2018.09.008.

66. Lesbirel, S., Viphakone, N., Parker, M., Parker, J., Heath, C., Sudbery, I., and Wilson, S.A. (2018). The m(6)A-methylase complex recruits TREX and regulates mRNA export. Sci Rep 8, 13827, 10.1038/s41598-018-32310-8.

67. Roundtree, I.A., Luo, G.Z., Zhang, Z., Wang, X., Zhou, T., Cui, Y., Sha, J., Huang, X., Guerrero, L., Xie, P. et al. (2017). YTHDC1 mediates nuclear export of N(6)-methyladenosine methylated mRNAs. Elife 6, 10.7554/eLife.31311.

68. Li, Q., Li, X., Tang, H., Jiang, B., Dou, Y., Gorospe, M., and Wang, W. (2017). NSUN2-Mediated m5C Methylation and METTL3/METTL14-Mediated m6A Methylation Cooperatively Enhance p21 Translation. J Cell Biochem 118, 2587-2598, 10.1002/jcb.25957.

69. Boo, S.H., Ha, H., and Kim, Y.K. (2022). m(1)A and m(6)A modifications function cooperatively to facilitate rapid mRNA degradation. Cell Rep 40, 111317, 10.1016/j.celrep.2022.111317.

70. Franken, N.A., Rodermond, H.M., Stap, J., Haveman, J., and van Bree, C. (2006). Clonogenic assay of cells in vitro. Nature protocols 1, 2315-2319, 10.1038/nprot.2006.339.

Contributions

TG, KK, and SH designed the study and analyzed the data. TG provided supervision to KK and SH and wrote the manuscript along with KK. TG, KK, SH, KR, SR, DG, and BJ performed experiments and analyzed the data. AV generated and verified knockout cell lines for ALKBH3 and FTO. ES contributed expertise on metaphase spread analysis. SS designed and supervised the study, analyzed the data, wrote the manuscript, and provided the laboratory environment for the study.

Acknowledgement

We are grateful to Professors C. Lukas and J. Lukas for reagents and helpful discussions; Decode Genetics for help with DNA sequencing; P.H. Petersen for technical advice on RNA Scope and J. Benada for critically reading the manuscript. This work was supported by the Icelandic Research Fund (IRF) (185242-051 & 228323-051) and the University of Iceland Research Fund.

Author information

These authors contributed equally: Þorkell Guðjónsson and Karen Kristjánsdóttir.

Correspondence and request for materials should be addressed to SS.

Competing interest

The authors declare that they have no competing interests.

Corresponding author

Stefan Sigurdsson (stefsi@hi.is)
University of Iceland
Department of Biochemistry and Molecular Biology
Biomedical Center, Sturlugata 8
101 Reykjavik, Iceland
Phone: +354–525-4839

Figures

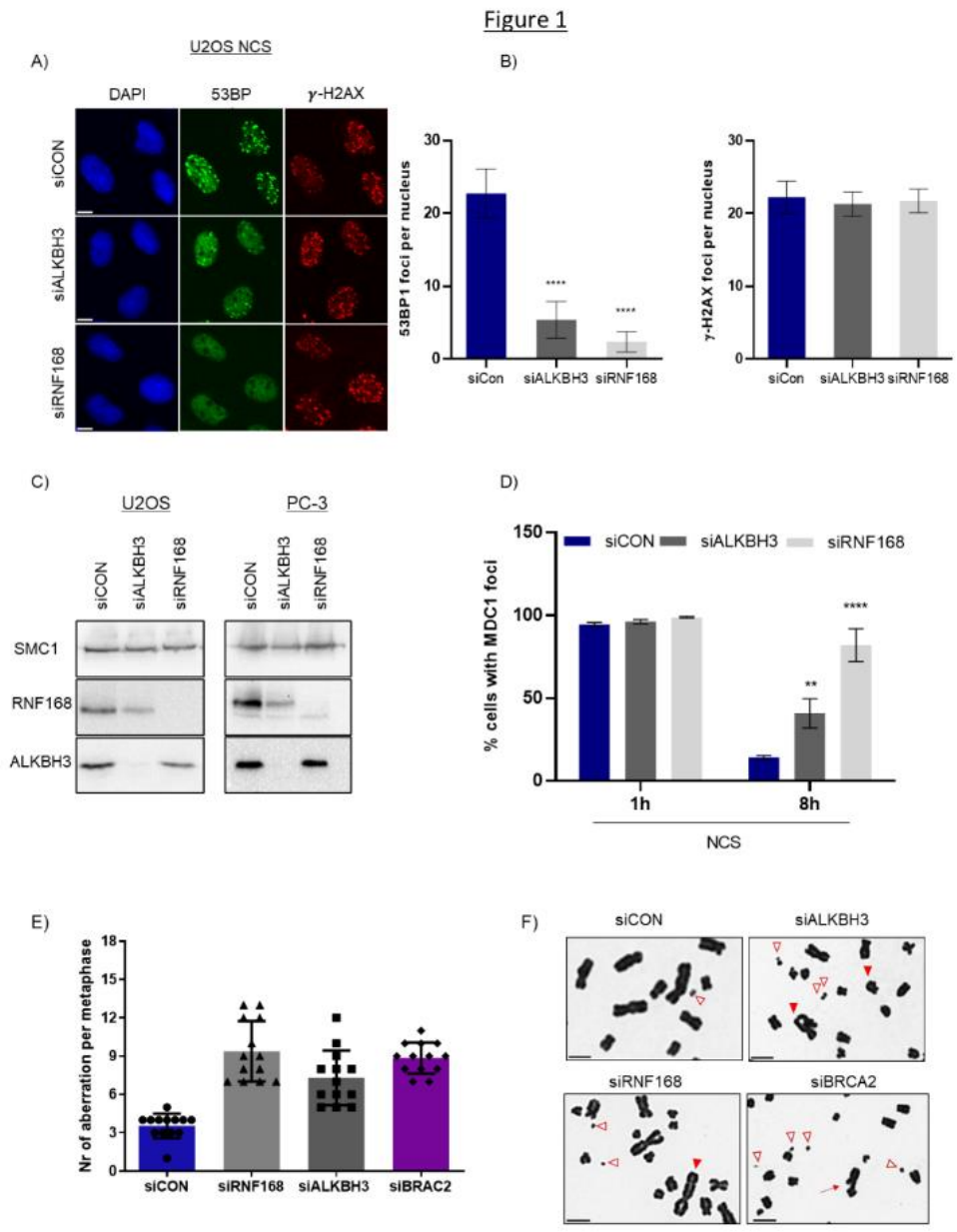

Figure 1. ALKBH3 promotes efficient expression of RNF168.

(**a-b**) Representative images (a) and quantification (b) of U2OS cells transfected with the indicated siRNAs, 48h post transfection cells were exposed to 50 ng/mL NCS for 15 min and fixed 1h later. Cells were immunostained with 53BP1 (green) and γH2AX (red) antibodies. Nuclear DNA was visualized by DAPI (blue). Graphs demonstrate the mean number of 53BP1 and γH2AX foci per nucleus from five biological replicates, at least 1000 cells were scored for each condition. Mean±SD (n=5) Scale bars: 10 μm. (**c**)

RNF168 and ALKBH3 protein expression analyzed by Western blotting in U2OS and PC-3 cells 48h post transfection with the indicated siRNA. SMC1 was used as a loading control. (**d**) Quantification of U2OS cells treated with the indicated siRNAs for 48h followed by a 15 min of 50 ng/mL NCS exposure. 1h and 8h post NCS treatment, cells were fixed and immunostained with MDC1 and 53BP1 antibodies, nuclear DNA was stained by DAPI. The graph is a summary of three experiments and shows percentage of cells with NCS induced MDC1 foci 1 and 8h following NCS treatment. At least 500 cells were analyzed per condition. Data are presented as mean±SD (n=3). **(e)** Quantification of the number of metaphase aberrations in U2OS cells treated with the indicated siRNA for 48h. The graph shows the number of number of aberrations in each sample, thirteen aberration were analyzed for each sample (n=2). **(f)** Representative images showing metaphase aberrations described in (**e**). DNA double strand breaks are shown with red arrows, DNA fragments with white triangles outlined in red and end fusion reprinted with red triangles. Scale bars: 10 µm.
Statistical significance was determined by One-Way ANOVA. * $P < 0.05$, ** $p < 0.01$, *** $p < 0.001$, **** $p<0.0001$.

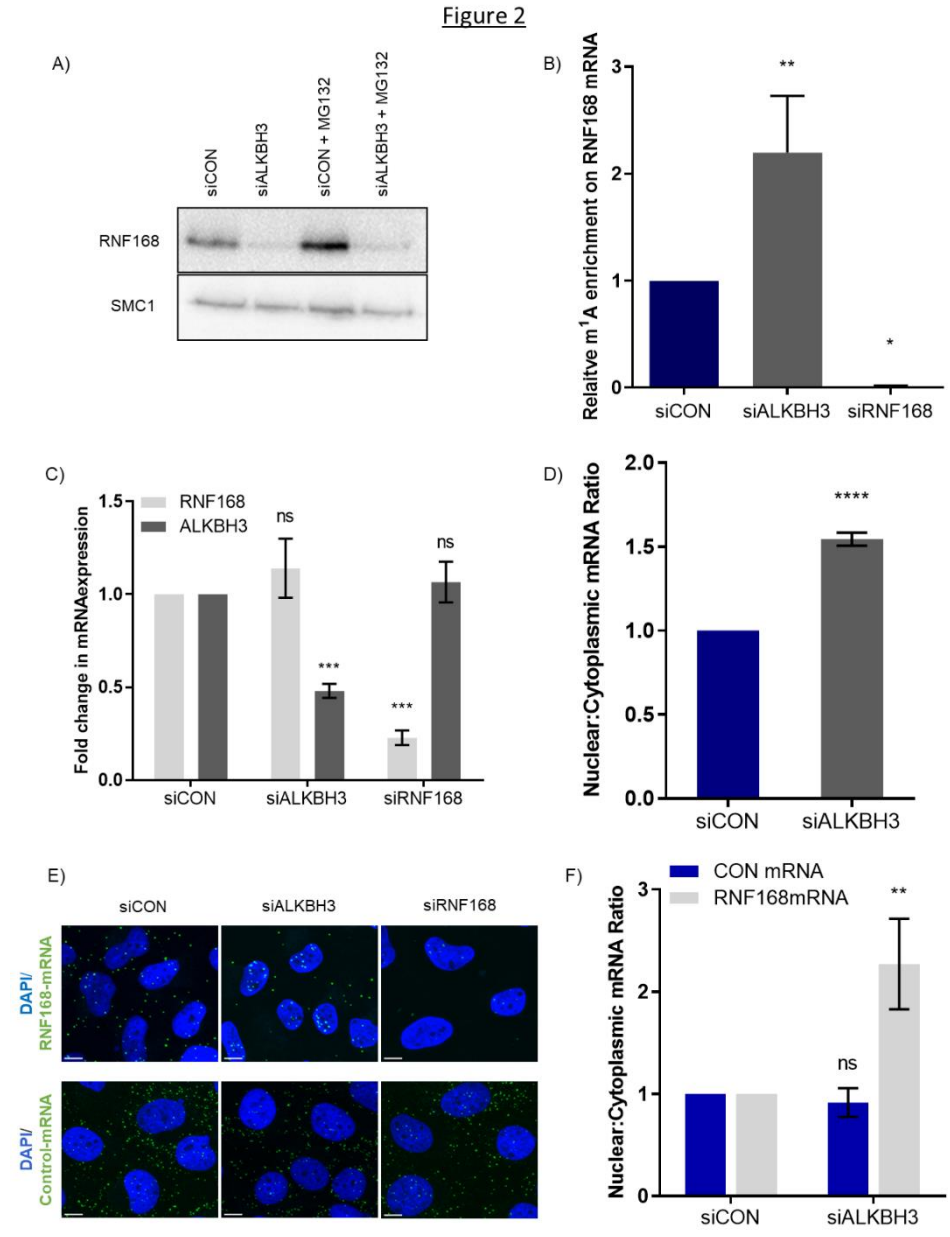

Figure 2. ALKBH3 promotes nuclear export of RNF168 mRNA.

(a) Western blot showing the protein levels of RNF168 in U2OS cells treated with control and ALKBH3 targeting siRNAs for 48h, in the presence or absence of the proteasome inhibitor MG-132 (3h). SMC1 was used as a loading control. **(b)** Relative quantification of RNF168 mRNA levels in m^{1}A pull-downs by MeRIP-qPCR analysis. U2OS cells were treated with indicated siRNAs for 48h, followed by RNA isolation and immunoprecipitation using m^{1}A antibody. RNF168 levels in the pulled-down RNA

samples were analyzed using quantitative real time PCR (q-PCR) and normalized to GAPDH housekeeping gene. Data are presented as mean±SD (n=3). **(c)** Total RNF168 and ALKBH3 mRNA levels in U2OS cells treated with control, ALKBH3 and RNF168 targeting siRNAs for 48h, analyzed with qPCR. The graph shows a summary of three experiments. In all samples, RNF168 expression was normalized to the GAPDH housekeeping gene. Data are presented as mean±SD (n=3). **(d)** The ratio between nuclear and cytoplasmic RNF168 mRNA levels in U2OS cells treated with indicated siRNAs for 48h analyzed using qPCR and normalized to internal control genes (beta actin and HPRT). Ratio >1 indicates more mRNA expression in nucleus. Ratio <1 indicates more mRNA expression in cytoplasm. Data are presented as mean±SD (n=3). **(e)** Representative images from the RNA Scope assay performed in U2OS cells treated with indicated siRNAs for 48h, followed by incubation with RNF168 specific and control mRNA probes (green) and nuclear DNA stained with DAPI. Images were acquired on a confocal microscope as Z-stacks and are displayed as maximum-intensity projections. PPIB probes were used as control-mRNA probes. Scale bars: 10 μm. (**f**) Quantification of the experiment described in (e). The graph shows nucleus:cytoplasmic ratio of RNF168 mRNA in each sample, normalized to control sample. Ratio>1 indicates increased mRNA expression in nucleus. Ratio<1 indicates increased mRNA expression in cytoplasm. The graph shows a summary of three independent experiments, mean±SD.

Statistical significance was determined by two-tailed unpaired t-test (D, F) or One-Way ANOVA (B-C). * $P < 0.05$, ** $p < 0.01$, *** $p < 0.001$, **** $p<0.0001$

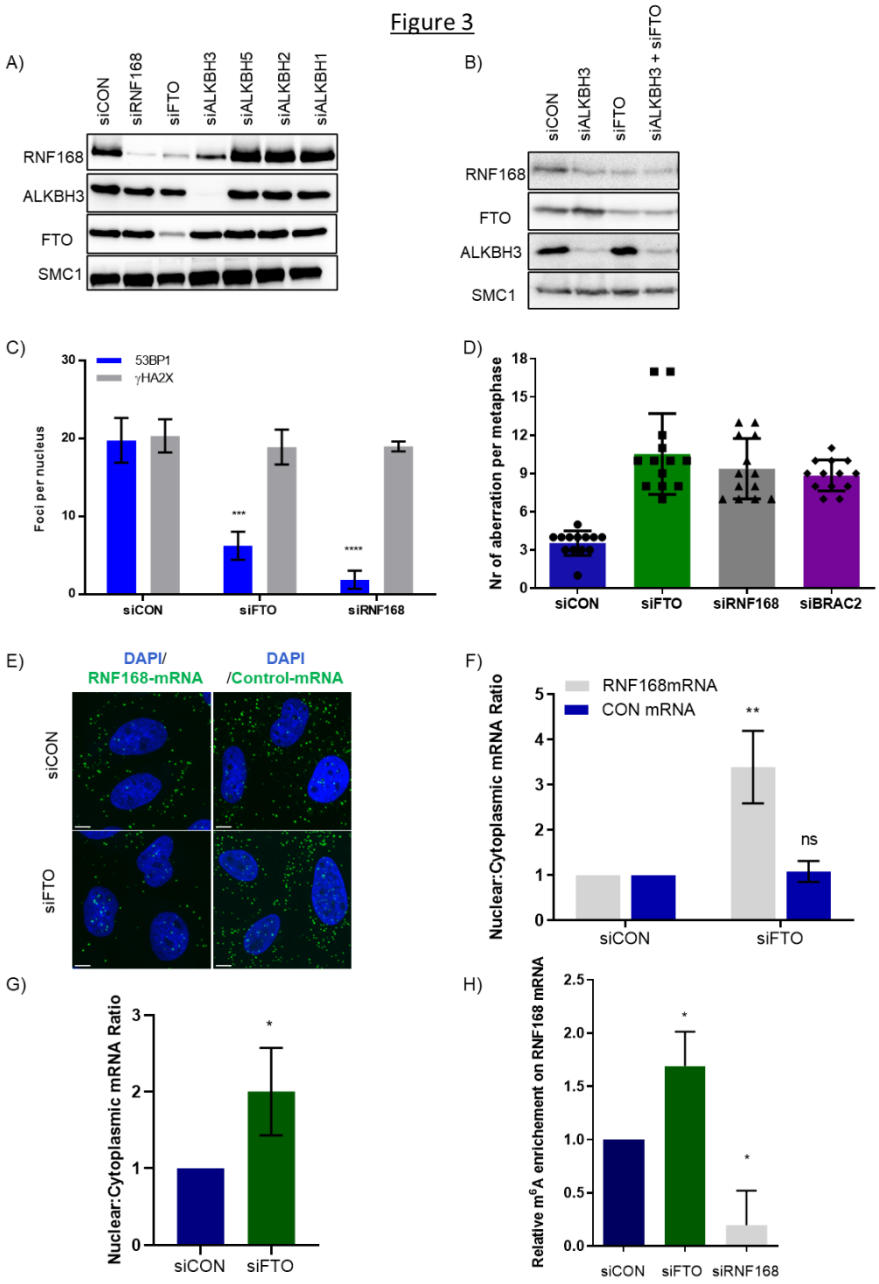

Figure 3. The potential role of additional AlkB family members in RNF168 regulation.

(**a-b**) U2OS cells were treated with the indicated siRNAs for 48h followed by Western blotting to analyze RNF168, ALKBH3 and FTO protein expression. SMC1 was used as a loading control. **(c)** U2OS cells were treated with siRNA for 48h as indicated and exposed to 50ng/mL NCS for 15 min, 1h later cells were immunostained with 53BP1 and γH2AX antibodies. Nuclear DNA was stained by DAPI. The graph is a summary of

three independent experiments showing the average number of foci per nucleus, mean±SD. **(d)** Quantification of the number of metaphase aberrations in U2OS cells treated with the indicated siRNA for 48h. The graph shows the relative change in number of aberrations compared to control siRNA treated cells. Data are presented as mean±SD (n=3). **(e)** Representative images from the RNA Scope assay performed in U2OS cells treated with FTO and control siRNAs for 48h, followed by incubation with RNF168 specific and control mRNA probes (green) and nuclear DNA stained with DAPI. Images were acquired on a confocal microscope as Z-stacks and are displayed as maximum-intensity projections. PPIB probes were used as control-mRNA probes. Scale bars: 10 µm. (**f**)Quantification of the experiment described in (e). The graph shows nucleus:cytoplasmic ratio of RNF168 mRNA in each sample, normalized to control sample. Ratio<1 indicates increased mRNA expression in cytoplasm. The graph shows a summary of three independent experiments, mean±SD. (**g**) The ratio between nuclear and cytoplasmic RNF168 mRNA levels in U2OS cells treated with indicated siRNAs for 48h analyzed using qPCR and normalized to internal control genes (beta actin and HPRT). Ratio >1 indicates more mRNA expression in nucleus. Ratio <1 indicates more mRNA expression in cytoplasm. Data are presented as mean±SD (n=3). **(h)** Relative quantification of RNF168 mRNA levels in m^{6}A pull-downs. U2OS cells were treated with indicated siRNAs for 48h, followed by RNA isolation and immunoprecipitation using m^{6}A antibody. RNF168 levels in the pulled-down RNA samples were analyzed using quantitative real time PCR (q-PCR) and normalized to GAPDH housekeeping gene. Data are presented as mean±SD (n=3).

Statistical significance was determined by two-tailed unpaired t-test (f-g) or One-Way ANOVA (C, H). * $P < 0.05$, ** $p < 0.01$, *** $p < 0.001$, **** $p<0.0001$

Figure 4

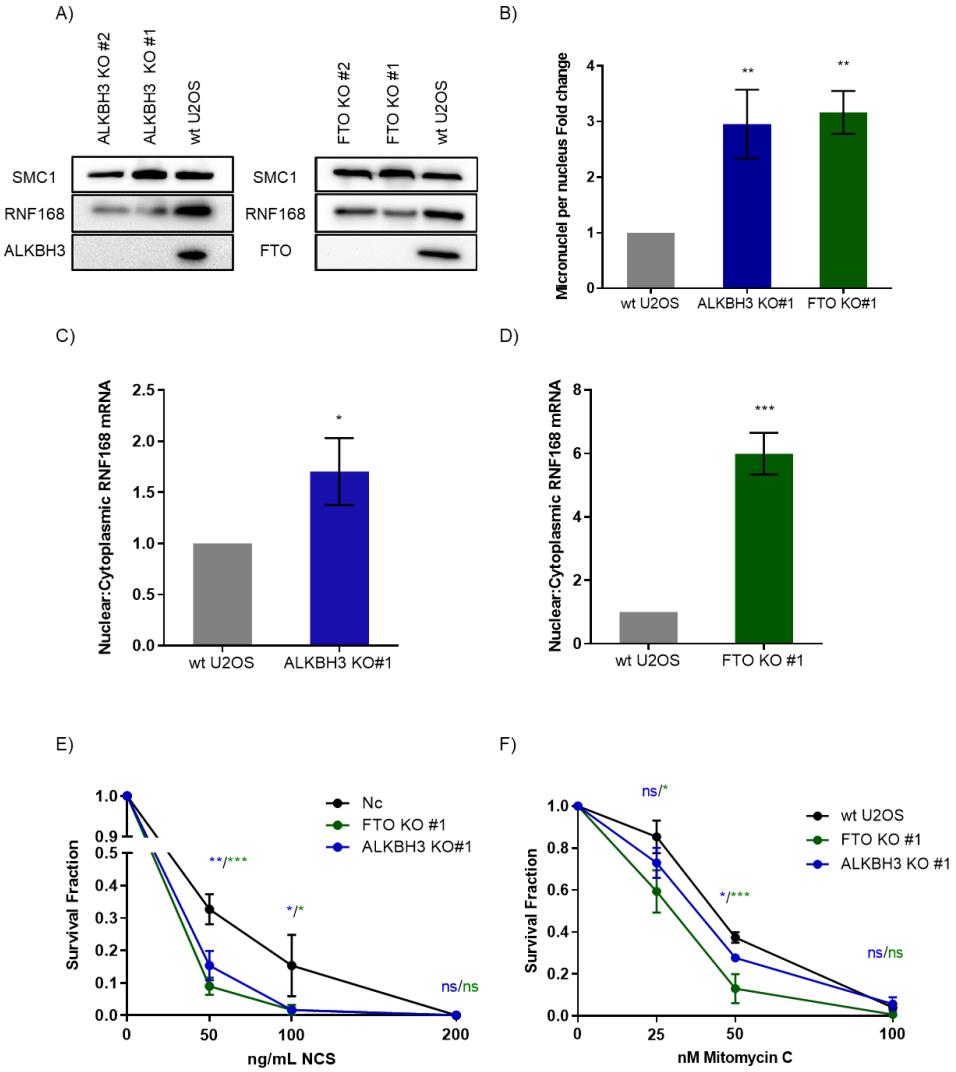

Figure 4. Genomic instability and increased sensitivity to genotoxic drugs in ALKBH3 and FTO knockout cell lines.

(a) RNF168, ALKBH3 and FTO protein expression in ALKBH3 and FTO CRISPR-Cas9 KO U2OS cells analyzed by Western blotting. SMC1 was used as a loading control. **(b)** Quantification of the number of micronuclei in ALKBH3 and FTO CRISP-Cas9 KO U2OS cells. DAPI staining was used to visualize the nucleus. Bar graph represents the relative number of micronuclei per nucleus compared to control sample mean±SD (n=3). **(c-d)**

The ratio between nuclear and cytoplasmic RNF168 mRNA levels in ALKBH3 (c) and FTO (d) CRISPR-Cas9 KO U2OS cells analyzed using qPCR and normalized to internal control genes (beta actin and HPRT). Ratio >1 indicates more mRNA expression in nucleus. Ratio <1 indicates more mRNA expression in cytoplasm. Data are presented as mean±SD (n=3). **(e-f)** Survival curves derived from colony formation assay in wild type and ALKBH3 and FTO CRISPR-Cas9 KO U2OS cells, exposed to the indicated concentration of NCS (e)and MMC (f), mean±SD (n=3).

Statistical significance was determined by two-tailed unpaired t-test (c-d) or One-Way ANOVA (b, e-f). * P < 0.05, ** p < 0.01, *** p < 0.001, **** p<0.0001

Supplementary material

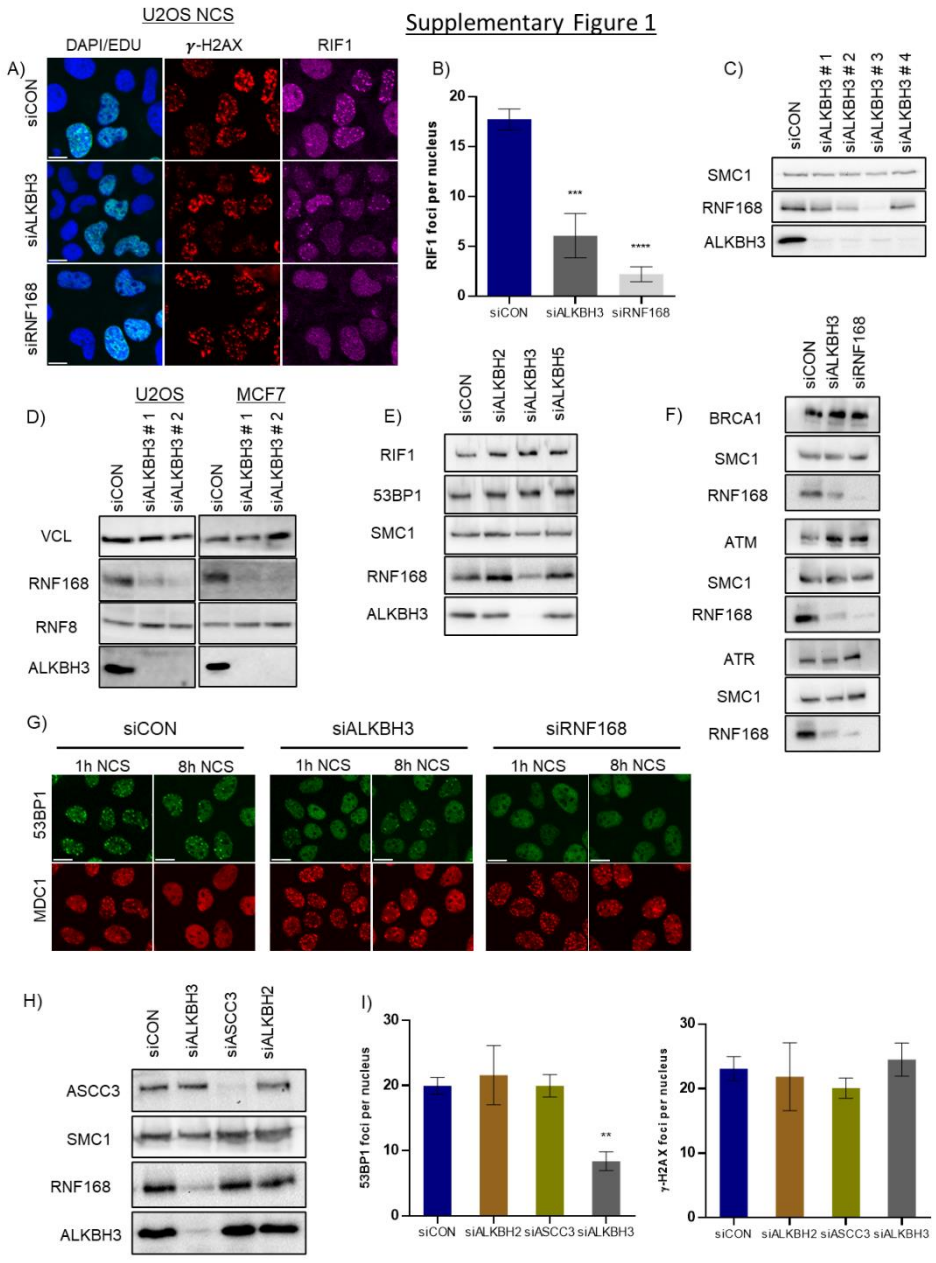

Supplementary Figure 1. ALKBH3 regulates RNF168 expression and DNA DSB induced signaling. the. Related to Figure 1.

(a) U2OS cells were treated with the indicated siRNAs for 48h and exposed to 50 ng/mL NCS for 15 min, 1h later cells were immunostained with RIF1 and γH2AX antibodies. Representative images showing DAPI (blue), RIF1 (magenta) and γH2AX

(red). Scale bars: 10 µm. **(b)** Quantifications of the average number of foci per nucleus from the experiment in (a), mean±SD (n=3).v**(c)** U2OS cells treated with four independent ALKBH3 siRNAs for 48h, followed by Western blotting to analyze RNF168 and ALKBH3 expression. SMC1 was used as a loading control. **(d)** MCF7 and U2OS cells were treated with two independent ALKBH3 siRNAs for 48h, followed by Western blotting to analyze RNF168, RNF8 and ALKBH3 protein expression. Vinculin (VCL) was used as a loading control. **(e-f)** U2OS cells were treated with indicated siRNAs for 48h followed by Western blotting to analyze the expression of indicated proteins. **(g)** Representative images. U2OS cells were treated with indicated siRNA for 48h followed by 50ng/mL NCS exposure for 15 min. 1h and 8h later cells were fixed and stained with MDC1 (red) and 53BP1 (green) antibodies. Scale bar: Scale bars: 10 µm. **(h)** Western blot in U2OS cells treated with indicated siRNA for 48h, using antibodies targeting ASCC3, RNF168 and ALKBH3. SMC1 was used as a loading control. **(i)** U2OS cells were treated with the indicated siRNA for 48h followed by 50 ng/mL NCS exposure for 15 min. 1h later cells were fixed and immunostained with antibodies targeting 53BP1 and γH2AX. The graph is a summary from three independent experiments, showing quantification of 53BP1 and γH2AX foci per nucleus, mean± SD.

Statistical significance was determined by One-Way ANOVA. * $P < 0.05$, ** $p < 0.01$, *** $p < 0.001$, **** $p<0.0001$

Supplementary Figure 2

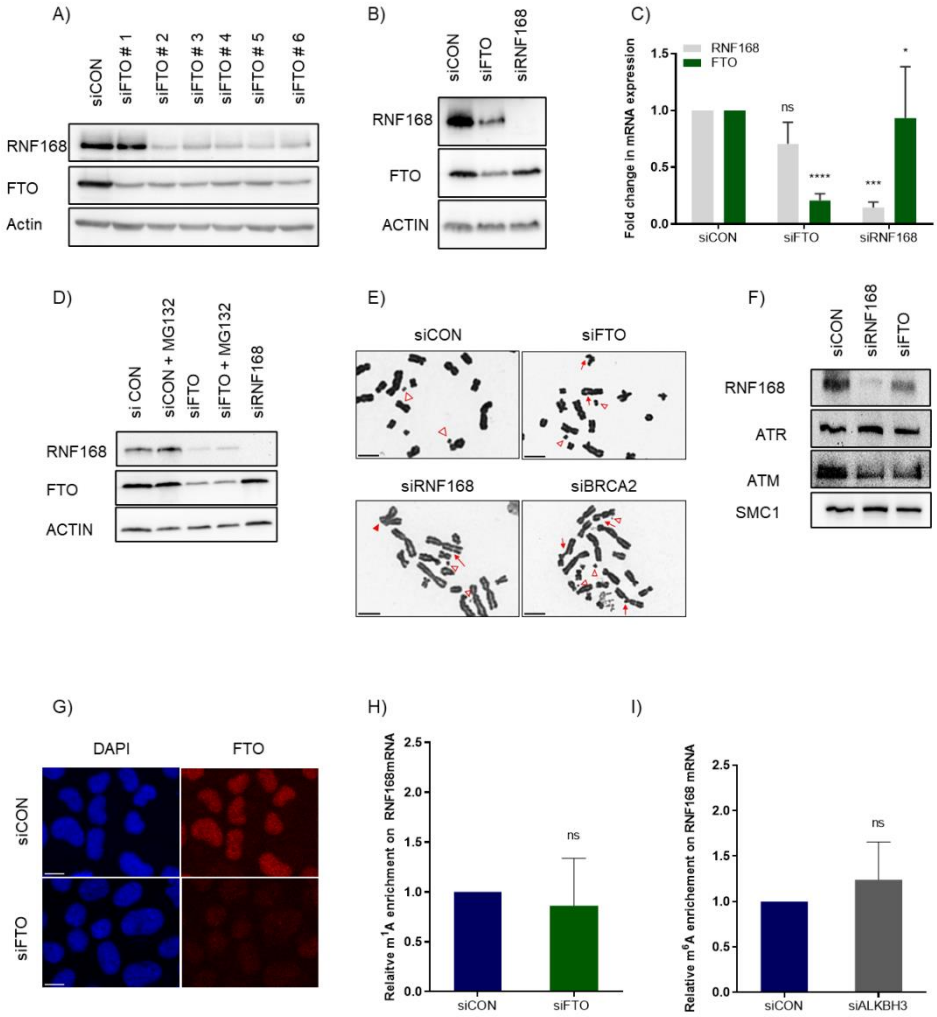

Supplementary Figure 2. FTO promotes genome stability and efficient RNF168 expression.

Related to Figure 3.

(a) U2OS cells were treated with five independent FTO siRNAs for 48h followed by Western blotting to analyze RNF168 and FTO protein expression. SMC1 was used as a loading control. **(b)** Western blot in PC-3 cells showing RNF168 and FTO protein levels in U2OS cells 48h post treatment with the indicated siRNAs. Actin was used as loading

control. **(c)** Total RNF168 and FTO mRNA levels in U2OS cells treated with indicated siRNAs for 48h analyzed with qPCR. mRNA expression values were normalized to housekeeping gene (GAPDH), mean±SD (n=3). **(d)** Western blot showing RNF168 and FTO protein levels in U2OS cells 48h post treatment with the indicated siRNAs, in the presence or absence of the proteasome inhibitor MG-132 (3h). Actin was used as loading control. **(e)** Representative images showing metaphase aberrations in cells treated with the indicated siRNAs. (Figure 3d). DNA double strand breaks are shown with red arrows, DNA fragments with white triangles outlined in red and end fusion reprinted with red triangles. Data are presented as mean±SD (n=3). Scale bar 10 μm. **(f)** U2OS cells were treated with indicated siRNAs for 48h, followed by Western blotting to analyze the expression of the indicated proteins. SMC1 was used as a loading control. **(g)** U2OS cells transfected with the indicated siRNAs, 48h post transfection cells were fixed and immunostained with a FTO specific antibody (red). Nuclear DNA was visualized by DAPI (blue). Scale bars: 10 μm. **(h-i)** Relative quantification of RNF168 mRNA levels in m^1A (g) and m^6A pull-downs (h). U2OS cells treated with indicated siRNAs for 48h, followed by RNA isolation and immunoprecipitation using m^1A or m^6A antibody. RNF168 levels in the pulled-down RNA samples were analyzed using quantitative real time PCR (q-PCR) and normalized to GAPDH housekeeping gene, mean±SD (n=3).

Statistical significance was determined by One-Way ANOVA. * $P < 0.05$, ** $p < 0.01$, *** $p < 0.001$, **** $p<0.0001$

Supplementary Figure 3

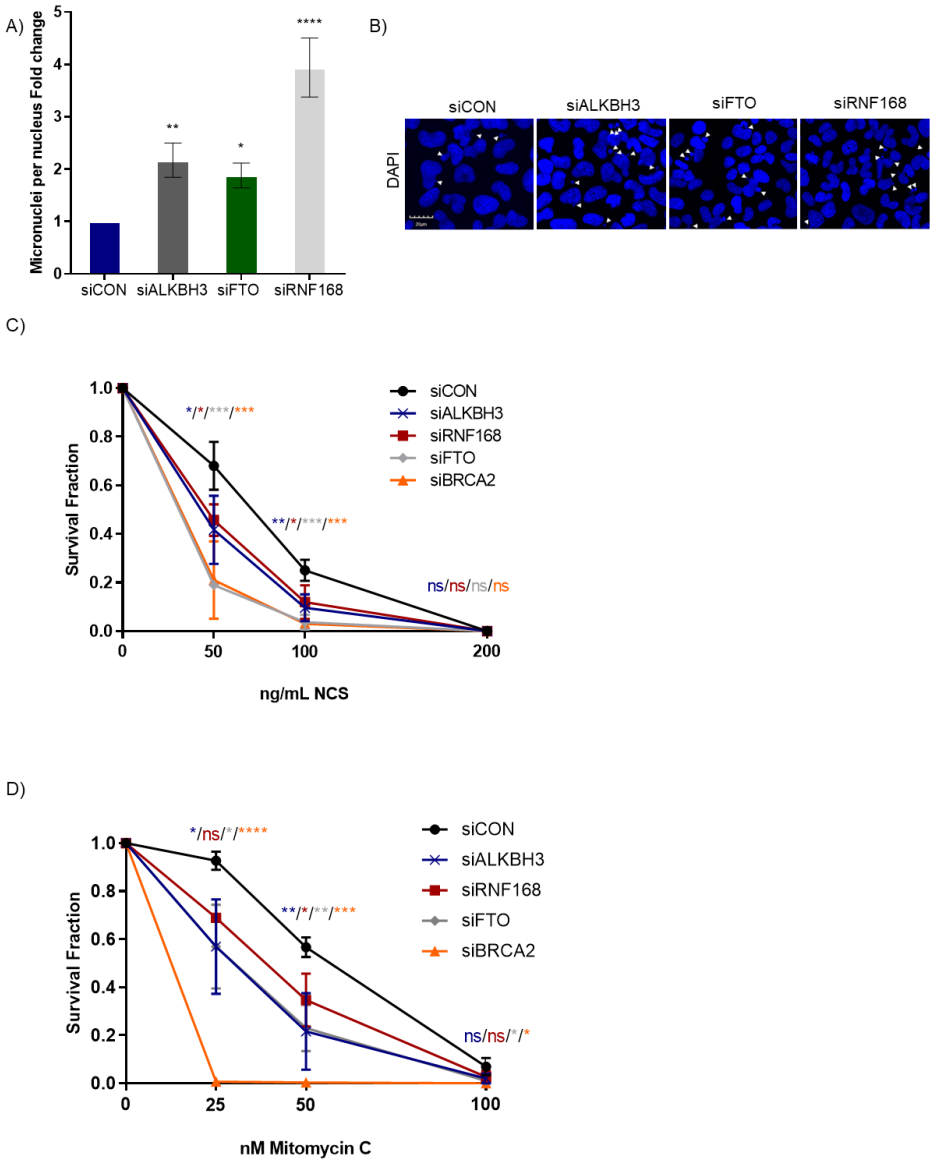

Supplementary Figure 3. ALKBH3 and FTO promote survival in response to genotoxic stress.

Related to Figure 4.

(a) Quantification of the number of micronucleated cells in U2OS cells treated with the indicated siRNA for 48h. The graph shows the relative change in number of micronuclei s compared to control siRNA treated cells. Data are presented as mean±SD (n=3). **(b)** Representative images of micronuclei cells described in (a). Micronuclei are

indicated with white arrows. Nuclear DNA was stained by DAPI (blue). Scale bar 20μm. **(c-d)** Survival curves derived from cells treated with the indicated siRNAs and exposed to the indicated concentration of NCS (c) and MMC (d). Data are presented as mean±SD (n=3).

Statistical significance was determined by One-Way ANOVA. * P < 0.05, ** p < 0.01, *** p < 0.001, **** p<0.0001

Supplementary table 1 – Antibodies used in this study.

Antibody	Source	Identifier	WB dilution	IF dilution	RNA-IP
53BP1	Santa Cruz Biotechnology	sc-22760	1:2000	1:100	-
Actin	AMD Millipore	MAB1501R	1:10000	-	-
Alexa Fluor 488 Anti-mouse IgG1	Life Technologies	A21121	-	1:1000	-
Alexa Fluor 555 IgG Anti rabbit	Life Technologies	A21434	-	1:1000	-
ALKBH3	Millipore	09-882	1:500	1:250	-
ASCC3	Bethyl	A304-014A-M	1:1000	1:1000	-
ATM	Santa Cruz	sc-23921	1:500	-	-
ATR	Santa Cruz	sc-1887	1:500	-	-
BRCA1	Calbiochem	OP92	1:1000	-	-
FLAG	Cell Signaling	# 14793	1:1000	1:1000	-
Flag M2	Sigma Aldrich	F1804	1:1000	1:1000	-
FTO	Abcam	ab126605	-	1:1000	-
gamma-H2AX	Cell Signaling	9718S	1:1000	1:500	-
gamma-H2AX	Abcam	ab22551	1:1000	1:1000	-
HRP Secondary Anti mouse	Santa Cruz Biotechnology	sc-2096	1:10000	-	-
HRP Secondary Anti rabbit	Santa Cruz Biotechnology		1:10000	-	-
MDC1	Abcam	ab11171	-	1:2000	-
N1-methyladenosine	Medical and Biological Laboratories (MBL)	D345-3		-	5µg
N6-methyladenosine	NEB	E1610S	-	-	5µg
N6-methyladenosine	Merk Millipore	ABE572	-	-	5µg
RIF1	Bethyl	A300-569A	1:500	1:500	-
RNF168	Millipore	ABE367	1:500	1:250	-
RNF8	Santa Cruz Biotechnology	sc-133971	-	1:500	-
SMC1	Abcam	ab9262	1:1000	-	-
Vinculin	Santa Cruz Biotechnology	sc-5573	1:1000	-	-

Supplementary table 2 – Primer used in qPCR analysis.

Primer	Sequence (5'-'3)
RNF168_forward 2	TCCAGTTACACCCAAGTCTGAA
RNF168_Reverse2	GAGGCTGACCCAAACTGAGA
Beta actine Forward	AGGCACCAGGGCGTGAT
Beta actine Reverse	GCCCACATAGGAATCCTTCTGAC
GADPH forward	GGCCTCCAAGGAGTAAGACC
GADPH reverse	AGGGGTCTACATGGCAACTG
ALKBH3 forward primer	AGCCACCAGTGATTGACAGAG
ALKBH3 reverse primer	ACAAACAGACCCTAGATACACCT
FTO forward primer	TGTTTTGGCCGGTTCACAAC
FTO reverse primer	ACATTCTGCAGAGCCAACTG
HPRT1 qPCR #3 Revers	CTTCGTGGGGTCCTTTTCACC
HPRT1 qPCR #3 Forward	ACCAGTCAACAGGGGACATAA

Supplementary table 3 – siRNA sequence information.

Oligonucleotide	Sequence (sense) 5'-'3	Identifier	Source
siControl	-	4390843	Thermo Fisher Scientific
siALKBH3 #1	GGACCUUGUUAAUCAUGGAtt	s47967	Thermo Fisher Scientific
siALKBH3 #2	CAUGGGACCUUGUUAAUCAtt	s47968	Thermo Fisher Scientific
siALKBH3 #3	GCAACUCAUFUUGGUAAUAtt	122027	Thermo Fisher Scientific
siALKBH3 #4	UAGUGAGGGUUCAUCAUCACUGUGC	10620318	Thermo Fisher Scientific
siFTO #1	CCAAGGAGACUGCUAUUUCtt	278910	Thermo Fisher Scientific
siFTO #2	CAUUACCUGCUGAUCAGAAtt	s35511	Thermo Fisher Scientific
siFTO #3	GAGAAGAAAUUCAUAAUGAtt	s35512	Thermo Fisher Scientific
siFTO #4	GCCUAACCUACUUUCCUCUtt	272126	Thermo Fisher Scientific
siFTO #5	GGCACCAGUCCUAAGGUGAtt	272127	Thermo Fisher Scientific
siFTO #6	CAUCCUCAUUGGUAAUCCAtt	278910	Thermo Fisher Scientific
siALKBH2	GAATCTGACTTTTCGTAAA	s42494	Thermo Fisher Scientific
siALKBH5	GGCUCAUCCUUACGUAGUUtt	s29688	Thermo Fisher Scientific
siRNF168	GGCGAAGAGCGAUGGAAGAtt	126171	Thermo Fisher Scientific
siBRCA2	GGAUUAUACAUAUUUCGCAtt	s2085	Thermo Fisher Scientific
siASCC3	CAAGCAAGAUAAUUAUAAUtt	s21605	Thermo Fisher Scientific

Supplementary table 4 – gRNA sequences

sgRNAs	Sequence (sense) 5′-′3	Identifier	Source
ALKBH3-1	CCCAGGGUCUGUUUGUAUCC	NA	Synthego
ALKBH3-2	CAGAGGACUGGCAUCAGAGA	NA	Synthego
ALKBH3-3	UACUAGGAAACAUUCCAGAG	NA	Synthego
FTO1	GCUUCUCGGAGAAUUAGUUU	NA	Synthego
FTO2	UGGCUGCUUAUUUCGGGACC	NA	Synthego
FTO3	CCGGUAUCUCGCAUCCUCAU	NA	Synthego
Positive Control1	CUCUCAGCUGGUACACGGCA	NA	Synthego
Positive Control2	GAGAAUCAAAAUCGGUGAAU	NA	Synthego
Positive Control3	ACAAAACUGUGCUAGACAUG	NA	Synthego

Appendix A

pCMV3 vector

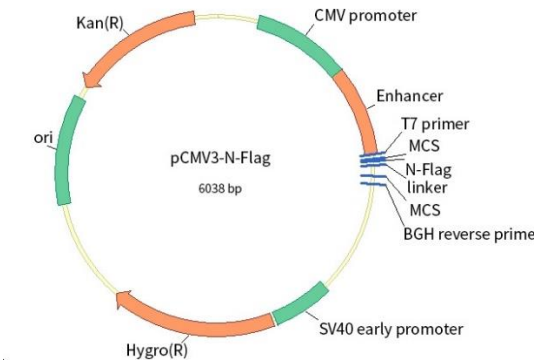

Supplementary Figure 1 – pCMV3 N-tagged FLAG mammalian expression vector.

pCMV3-N-FLAG vector utilized in co-immunoprecipitation experiments. Two vectors (HG15639-NF and HG12125-NF) from Nordic BioSite were used containing cDNA insert sequences encoding for either ALKBH3 and FTO to generate ALKBH3-FLAG and FTO-FLAG plasmids. Vector contains human enhanced cytomegalovirus immediate-early (CMV) promoter for high-level expression in a wider range of mammalian cells, hygromycin resistance gene for section of mammalian cell lines and a Kozak consensus sequence to enhance mammalian expression.

ALKBH3 cDNA insert

Green : FLAG tag

Yellow : Linker

ATGGATTACAAGGATGACGACGATAAGGGTGGAGGCGGTAGCGAGGAAAAAAGA
CGGCGAGCCCGAGTTCAGGGAGCCTGGGCTGCCCCTGTTAAAAGCCAGGCCATT
GCTCAGCCAGCTACCACTGCTAAGAGCCATCTCCACCAGAAGCCTGGCCAGACCT
GGAAGAACAAAGAGCATCATCTCTCTGACAGAGAGTTTGTGTTCAAAGAACCTCAGC
AGGTAGTACGTAGAGCTCCTGAGCCACGAGTGATTGACAGAGAGGGTGTGTATGAA

ATCAGCCTGTCACCCACAGGTGTATCTAGGGTCTGTTTGTATCCTGGCTTTGTTGACGT
GAAAGAAGCTGACTGGATATTGGAACAGCTTTGTCAAGATGTTCCCTGGAAACAGA
GGACCGGCATCAGAGAGGATATAACTTATCAGCAACCAAGACTTACAGCATGGTAT
GGAGAACTTCCTTACACTTATTCAAGAATCACTATGGAACCAAATCCTCACTGGCACC
CTGTGCTGCGCACACTAAAGAACCGCATTGAAGAGAACACTGGCCACACCTTCAAC
TCCTTACTCTGCAATCTTTATCGCAATGAGAAGGACAGCGTGGACTGGCACAGTGAT
GATGAACCCTCACTAGGGAGGTGCCCCATTATTGCTTCACTAAGTTTTGGTGCCACAC
GCACATTTGAGATGAGAAAGAAGCCACCACCAGAAGAGAATGGAGAGTACACATA
TGTGGAAAGAGTGAAGATACCCTTGGATCATGGGACCTTGTTAATCATGGAAGGAG
CGACACAAGCTGACTGGCAGCATCGAGTGCCCAAAGAATACCACTCTAGAGAACC
GAGAGTGAACCTGACCTTTCGGACAGTCTATCCAGACCCTCGAGGGGCACCCTGGT
GA

FTO cDNA insert

Yellow：linker

Green：FLAG tag

ATGGATTACAAGGATGACGACGATAAGGGTGGAGGCGGTAGCAAGCGCACCCCG
ACTGCCGAGGAACGAGAGCGCGAAGCTAAGAAACTGAGGCTTCTTGAAGAGCTTG
AAGACACTTGGCTCCCTTATCTGACCCCCAAAGATGATGAATTCTATCAGCAGTGGC
AGCTGAAATATCCTAAACTAATTCTCCGAGAAGCCAGCAGTGTATCTGAGGAGCTCC
ATAAAGAGGTTCAAGAAGCCTTTCTCACACTGCACAAGCATGGCTGCTTATTTCGGG
ACCTGGTTAGGATCCAAGGCAAAGATCTGCTCACTCCGGTATCTCGCATCCTCATTG
GTAATCCAGGCTGCACCTACAAGTACCTGAACACCAGGCTCTTTACGGTCCCCTGG
CCAGTGAAAGGGTCTAATATAAAACACACCGAGGCTGAAATAGCCGCTGCTTGTGA
GACCTTCCTCAAGCTCAATGACTACCTGCAGATAGAAACCATCCAGGCTTTGGAAGA
ACTTGCTGCCAAAGAGAAGGCTAATGAGGATGCTGTGCCATTGTGTATGTCTGCAGA
TTTCCCCAGGGTTGGGATGGGTTCATCCTACAACGGACAAGATGAAGTGGACATTAA
GAGCAGAGCAGCATACAACGTAACTTTGCTGAATTTCATGGATCCTCAGAAAATGCC
ATACCTGAAAGAGGAACCTTATTTTGGCATGGGGAAAATGGCAGTGAGCTGGCATC
ATGATGAAAATCTGGTGGACAGGTCAGCGGTGGCAGTGTACAGTTATAGCTGTGAA
GGCCCTGAAGAGGAAAGTGAGGATGACTCTCATCTCGAAGGCAGGGATCCTGATA
TTTGGCATGTTGGTTTTAAGATCTCATGGGACATAGAGACACCTGGTTTGGCGATACC
CCTTCACCAAGGAGACTGCTATTTCATGCTTGATGATCTCAATGCCACCCACCAACAC
TGTGTTTTGGCCGGTTCACAACCTCGGTTTAGTTCCACCCACCGAGTGGCAGAGTGC
TCAACAGGAACCTTGGATTATATTTTACAACGCTGTCAGTTGGCTCTGCAGAATGTCTG
TGACGATGTGGACAATGATGATGTCTCTTTGAAATCCTTTGAGCCTGCAGTTTTGAAAC
AAGGAGAAGAAATTCATAATGAGGTCGAGTTTGAGTGGCTGAGGCAGTTTTGGTTTC
AAGGCAATCGATACAGAAAGTGCACTGACTGGTGGTGTCAACCCATGGCTCAACTG

GAAGCACTGTGGAAGAAGATGGAGGGTGTGACAAATGCTGTGCTTCATGAAGTTAA
AAGAGAGGGGCTCCCCGTGGAACAAAGGAATGAAATCTTGACTGCCATCCTTGCCT
CGCTCACTGCACGCCAGAACCTGAGGAGAGAATGGCATGCCAGGTGCCAGTCAC
GAATTGCCCGAACATTACCTGCTGATCAGAAGCCAGAATGTCGGCCATACTGGGAA
AAGGATGATGCTTCGATGCCTCTGCCGTTTGACCTCACAGACATCGTTTCAGAACTCA
GAGGTCAGCTTCTGGAAGCAAAACCCTAA

Empty FLAG vector

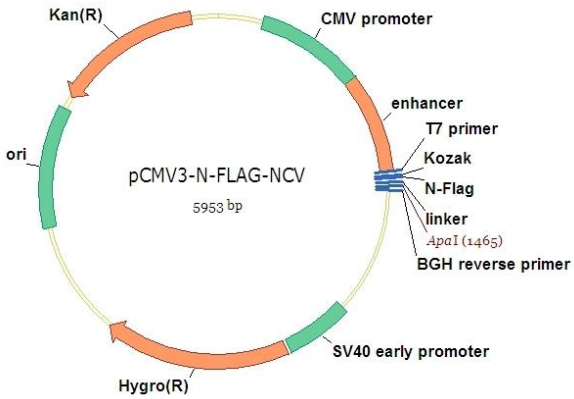

Supplementary Figure 2 – Negative control pCMV3 N-tagged FLAG mammalian expression vector.

ALKBH3 and FTO FLAG Catalytic dead plasmids

On order to make the ALKBH3-FLAG and FTO-FLAG plasmids catalytically dead the following two amino acids changes were made on the wild type ALKBH3 pCMV3 N-tagged FLAG mammalian expression vector.

Supplementary Figure 3 – Mutations introduced into ALKBH3-FLAG plasmid

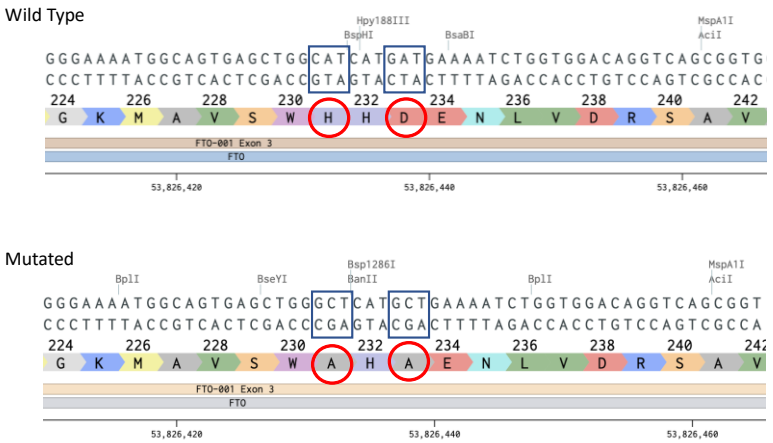

Supplementary Figure 4 - Mutations introduced into FTO-FLAG plasmid

Appendix B

DR-GFP reporter Plasmid: homologous recombination repair.

Supplementary Figure 5 – Homologous recombination reporer system.

HR reporter system contains a GFP gene cassette with I-Sce1 restriction site located within the gene cassette. Once the I-Sce1 endonuclease makes a cut, HR repair can generate two products. Firstly, by non-crossover gene conversion where iGPF is used as a donor sequence to fill in the gag, generating a GFP signal. Secondly in an event that does not restore the GFP signal. A homology mediated deletion product (not shown) which results from a long track gene conversation, conservative recombination with associated cross over or non-conservative SSA with degradation of the sequence between the GFP repeats (Bennardo et al., 2008).

EJ5GFP: Classic non-homologous end-joining repair.

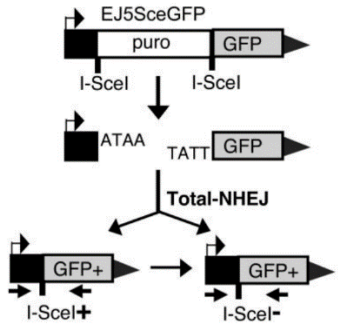

Supplementary Figure 6 – c-NHEJ reporter system.

A puromycin resistance gene separates the GFP gene cassette from its promoter and is flanked by two restriction sites. These restriction sites are recognized by the I-Sce1 restriction endonuclease. If the two restriction sites are cut by the I-Sce1 restriction enzyme and the brake is repaired by c-NHEJ, the puromycin gene is removed and the GFP gene cassette joined to its prompter thereby restoring the GFP gene (Bennardo et al., 2008).

hprtSAGFP reporter plasmid: Single strand annealing repair.

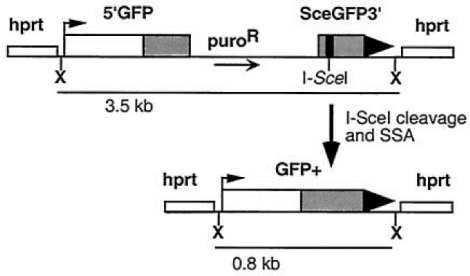

Supplementary Figure 7 – Single Stand annaling reporter system

The SSA repair reporter system is made up of hypoxanthine phosphoribosyl transferase (hprt) locus and contains the selectable puromycin resistance gene (puroR). The system contains two tandem GFP gene fragments (5'GFP and SceGFP3') one of which (SceGFP3') is interrupted by an I-Sce1 restriction site located within the GFP gene cassette. If the DSB generated by the I-Sce1 nuclease is repaired using SSA the SceGFP3' is annealed to the complementary strand of 5'GFP, followed by the appropriate DNA processing steps which results in a functional GFP gene. The SSA homologous sequence in the GFP gene fragments produces a 2.7kb deletion in the chromosome. The DSB generated by the I-Sce1 endonuclease can also be repaired by HR (not shown), however this does not result in a functional GFP gene (Stark et al., 2004).

Appendix C

Preliminary results regarding m^1A and m^6A methyltransferases (writers) and their influence on RNF168 protein expression along with methylation recognition proteins (readers) and their influence on *RNF168* mRNA nuclear retention.

In order to gain a better understanding of the significance of m^1A and m^6A methylations for normal RNF168 protein expression, key components of the m^6A methyltransferase complex (METTL3 and METTL14) were silenced, along with three m^1A methyltransferases known to methylate mRNA (TRMT6, TRMT61A and TRMT10c), using siRNA in U2OS cells. In addition, a double KD was performed where FTO along with two main units of the m^6A methyltransferase complex (METTL14 and METTL3) were knocked down and ALKBH3 along with the three above mentioned m^1A methyltransferases. Subsequently, RNF168 expression was examined (Supplementary Figure 8). The rationale behind this experiment is that if the methyltransferases fail to place the methylation on the *RNF168* transcript, there would be no substrate for ALKBH3 and FTO to remove, potentially allowing mRNA export to proceed uninterrupted if the sole purpose of the methylation were to act as a hindrance to mRNA export.

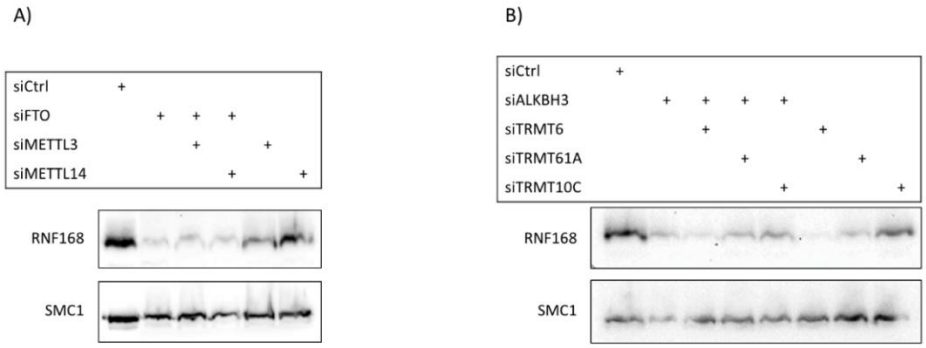

Supplementary Figure 8. RNF168 protein expression after KD of m^6A/m^1A methylation writers and erasers

U2OS cells were treated with the indicated siRNAs 48h and RNF168 expression was analyzed using western blot. SMC1 was used as loading control. A) m^6A methylation associated proteins. B) m^1A methylation associated proteins.

Co-depleting U2OS cells of methylation erasers and writers for either the m^6A or the m^1A modification did not appear to induce significant changes in the protein levels of RNF168 in either direction. These results suggest that co-depletion did not rescue the RNF168 phenotype or exacerbate it. Notably, depleting cells of the m^1A methyltransferases TRMT6 and TRMT61A resulted in a significant reduction in RNF168 protein expression compared to the control sample. TRM10C did not seem to affect

RNF168 protein expression significantly, aligning with the literature, which associates TRM10C more with m^1A removal of mitochondrial mRNA. The m^6A methyltransferase proteins, METTL3 and METTL14, did not appear to influence RNF168 protein expression as profoundly as the m^1A methyltransferases. Although METTL3 did affect RNF168 more than METTL14, inhibiting expression of either m^6A methyltransferase resulted in RNF168 downregulation compared to the control sample.

These results are preliminary as they have only been performed once and suffer from uneven loading controls (Supplementary Figure 8 B) and should therefore warrant cautious interpretation. However, these preliminary results provide some indication that the m^1A and m^6A modifications do not solely act as hindrances to mRNA export for RNF168 and could play a more significant role in the maturation of *RNF168* mRNA. Depleting cells of the methyltransferase proteins did not rescue RNF168 protein expression. This hints towards the importance of placing these methylations on the *RNF168* transcript for efficient mRNA export, similar to the crucial role played by FTO and ALKBH3 in removing them. However, in order to support these ideas further research is needed including repeating western blots and evaluating the nucleus/cytoplasmic ratio of *RNF168* mRNA after KD of the m^1A and m^6A reader proteins.

To evaluate the decrease in RNF168 protein expression following the KD of SRSF7, YTDHC1, and NXF1 (Figure 41), potentially attributed to increased nuclear retention of *RNF168* mRNA, we performed an RNA cellular fractionation assay. This assay was conducted in U2OS cells depleted of SRSF7, YTDHC1, and NXF1, and the results were compared to those obtained from ALKBH3, FTO, and YTHDF1 (NC) KD (Supplementary Figure 9). Despite affecting RNF168 protein expression, YTHDF3 was omitted from the RNA fractionation analysis due to its well-established role primarily influencing m^6A-mRNA stability and translation rather than export. Additionally, given its classification as a cytoplasmic m^6A reader, we reasoned that it would exert minimal influence on the mRNA export of RNF168.

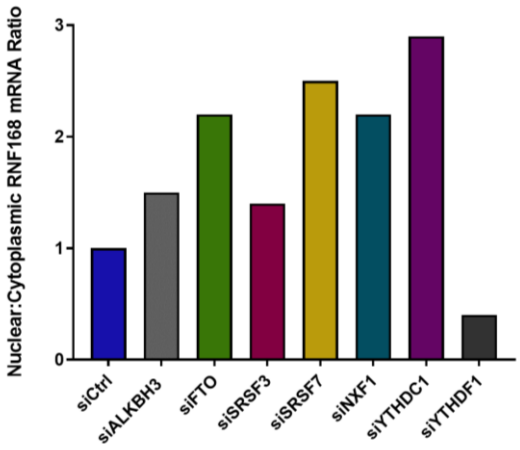

Supplementary Figure 9. Methylation reader and export factors influence on the nuclear: cytoplasmic expression of RNF168.

RNA fractionation assay. Ratio between nuclear and cytoplasmic *RNF168* mRNA expression in U2OS cells treated above siRNAs for 48h followed by qPCR, expression normalized to housekeeping gene HPRT. Ratio>1 indicates more mRNA expression in nucleus, ratio<1 demonstrates more mRNA expression in cytoplasm. Data are presented as n=1.

The RNA fractionation assay revealed intensified nuclear retention of *RNF168* mRNA following the KD of SRSF1 and SRSF7, NXF1, and YTHDC1. Interestingly, SRSF7 and YTHDC1 appeared to induce greater nuclear retention compared to both ALKBH3 and FTO KD. YTHDF1 KD did not result in nuclear retention of *RNF168* mRNA but led to more *RNF168* mRNA being expressed in the cytoplasm. YTHDF1 is not known to influence mRNA export but has instead proven capable of regulating target gene expression by promoting translation and regulating mRNA stability (Chen et al., 2021). These results should be interpreted with caution as they represent only one biological replicate, and to further confirm these findings, the experiment would need additional replication. Nevertheless, both western blot (Supplementary Figure 8) and RNA fractionation assays (Supplementary Figure 9) suggest that SRSF7, YTHDC1, and possibly to a lesser extent, SRSF3, could be playing a role in the mRNA export of RNF168.

Appendix D

Full list of protein-protein interactions identified in co-immunoprecipitation mass spectrometry assay.

Wild type ALKBH3 plasmid interactome.

Protein ID	Peptide count	Unique peptides	Description
Q96Q83	98	98	Alpha-ketoglutarate-dependent dioxygenase AlkB homolog 3(**ALKBH3**)
P11142	92	71	Heat shock cognate 71 kDa protein (HSP8)
P34932	56	51	Heat shock 70 kDa protein 4 (HSPA4)
P11021	41	37	Endoplasmic reticulum chaperone (HSPA5)
P38646	30	29	Stress-70 protein_ mitochondrial (HSPA9)
P0DMV9	39	22	Heat shock 70 kDa protein 1B (HSPA1B)
P07355	20	20	Annexin A2 (ANXA2)
P19338	19	19	Nucleolin (NCL)
Q92598	19	16	Heat shock protein 105 kDa (HSPH1)
Q6S8J3	17	13	POTE ankyrin domain family member (POTEE)
Q9C0B1	13	13	Alpha-ketoglutarate-dependent dioxygenase 9(**FTO)**
P35908	20	12	Keratin_ type II cytoskeletal 2 epidermal (KRT2)
P04264	16	12	Keratin_ type II cytoskeletal 1 (KRT1)
P13645	15	12	Keratin_ type I cytoskeletal 10 (KRT10)
P02768	12	12	Albumin (ALB)
P31948	12	12	Stress-induced-phosphoprotein 1 (STIP1)
O95816	11	11	BAG family molecular chaperone regulator 2 (BAG2)
P08670	11	10	Vimentin (VIM)
P04406	10	10	Glyceraldehyde-3-phosphate dehydrogenase (GAPDH)
P35527	11	9	Keratin_ type I cytoskeletal 9 (KRT9)
Q06830	9	8	Peroxiredoxin-1 (**PRDX1**)
P62633	8	8	CCHC-type zinc finger nucleic acid binding protein (CNBP)
P68104;	8	8	Elongation factor 1-alpha 1 (EEF1A1)
Q9UBW7	8	8	Zinc finger MYM-type protein 2 (ZMYM2)
O14744	8	7	Protein arginine N-methyltransferase 5 (**PRMT5**)
B2RC85	7	7	Radial spoke head 10 homolog B2 (RSPH10B2)
P07437	7	7	Tubulin beta chain (TUBB)
Q71U36	7	7	Tubulin alpha-1A chain (TUBA1A)
Q14103	7	7	Heterogeneous nuclear ribonucleoprotein D0 (**HNRNPD)**
P08238	10	6	Heat shock protein HSP 90-beta (HSP90AB1)
P63104	10	6	14-3-3 protein zeta/delta (YWHAZ)
P52597	8	6	Heterogeneous nuclear ribonucleoprotein F

			(**HNRNPF**)
P13639	6	6	Elongation factor 2 (EEF2)
P23588	6	6	Eukaryotic translation initiation factor 4B (EIF4B)
P60174	6	6	Triosephosphate isomerase (TPI1)
P62805	6	6	Histone H4 (H4-16)
Q7Z6K1	6	6	THAP domain-containing protein 5 (THAP5)
Q9BQA1	6	6	Methylosome protein 50 (WDR77)
P22626	6	5	Heterogeneous nuclear ribonucleoproteins A2/B1 (**HNRNPA2B1)**
P23528	6	5	Cofilin-1 (CFL1)
P25398	5	5	40S ribosomal protein S12 (RPS12)
P05387	6	4	60S acidic ribosomal protein P2 (RPLP2)
P06733	6	4	Alpha-enolase (ENO1)
P0CG47	5	4	Polyubiquitin-B (UBB)
P09651	5	4	Heterogeneous nuclear ribonucleoprotein A1 (**HNRNPA1**)
P62937	5	4	Peptidyl-prolyl cis-trans isomerase A (PPIA)
Q8TDI0	5	4	Chromodomain-helicase-DNA-binding protein 5 (CHD5)
A0A0B4J2E5	4	4	Utp12 domain-containing protein (LOC102724159)
P07195	4	4	L-lactate dehydrogenase B chain (LDHB)
P09382	4	4	Galectin-1 (LGALS1)
P10809	4	4	60 kDa heat shock protein_ mitochondrial (HSPD1)
P14618	4	4	Pyruvate kinase PKM (PKM)
P19474	4	4	E3 ubiquitin-protein ligase (TRIM21)
Q6P6C2	4	4	RNA demethylase ALKBH5 (**ALKBH5**)
Q8ND76	4	4	Cyclin-Y (CCNY)
P63261	10	3	Actin_ cytoplasmic 2 (ACTG1)
P61981	7	3	14-3-3 protein gamma (YWHAG)
P62258	7	3	14-3-3 protein epsilon (YWHAE)
P19012	6	3	Keratin_ type I cytoskeletal 15 (KRT15)
P23284	4	3	Peptidyl-prolyl cis-trans isomerase B (PPIB)
P31943	4	3	Heterogeneous nuclear ribonucleoprotein H (**HNRNPH1)**
Q9Y281	4	3	Cofilin-2 (CFL2)
Q12873	4	3	Chromodomain-helicase-DNA-binding protein 3 (CHD3)
P0C0S8	3	3	Histone H2A type 1 (H2AC17)
P04792	3	3	Heat shock protein beta-1 (HSPB1)
P07910	3	3	Heterogeneous nuclear ribonucleoproteins C1/C2 (**HNRNPC**)
P08758	3	3	Annexin A5 (ANXA5)
P25713	3	3	Metallothionein-3 (MT3)
P46776	3	3	60S ribosomal protein L27a (RPL27A)

P60510	**3**	**3**	**Serine/threonine-protein phosphatase 4 catalytic subunit (PPP4C)**
P61604	3	3	10 kDa heat shock protein_ mitochondrial (HSPE1)
P62851	3	3	40S ribosomal protein S25 (RPS25)
P62873	3	3	Guanine nucleotide-binding protein G(I)/G(S)/G(T) subunit beta-1 (GNB1)
Q8WVE0	3	3	EEF1A lysine methyltransferase 1 (EEF1AKMT1)
Q9HAV7	3	3	GrpE protein homolog 1_ mitochondrial (GRPEL1)
Q9UPP2	3	3	IQ motif and SEC7 domain-containing protein 3 (IQSEC3)
P54652	22	2	Heat shock-related 70 kDa protein 2 (HSPA2)
P07900	6	2	Heat shock protein HSP 90-alpha (HSP90AA1)
P31946	6	2	14-3-3 protein beta/alpha (YWHAB)
O95757	5	2	Heat shock 70 kDa protein 4L (HSPA4L)
P08779	5	2	Keratin_ type I cytoskeletal 16 (KRT16)
P05386	4	2	60S acidic ribosomal protein P1 (RPLP1)
P13929	4	2	Beta-enolase (ENO3)
Q7Z794	4	2	Keratin_ type II cytoskeletal 1b (KRT77)
Q9BYX7	4	2	Putative beta-actin-like protein 3 (POTEKP)
O76013	3	2	Keratin_ type I cuticular Ha6 (KRT36)
P14136	3	2	Glial fibrillary acidic protein (GFAP)
P30050	3	2	60S ribosomal protein L12 (RPL12)
Q12931	3	2	Heat shock protein 75 kDa_ mitochondrial (TRAP1)
A1L190	2	2	Synaptonemal complex central element protein 3 (SYCE3)
O75688	2	2	Protein phosphatase 1B (PPM1B)
P01614	2	2	Immunoglobulin kappa variable 2D-40 (IGKV2D-40)
P02787	2	2	Serotransferrin (TF)
P02788	2	2	Lactotransferrin (LTF)
P07737	2	2	Profilin-1 (PFN1)
P13984	2	2	General transcription factor IIF subunit 2 (GTF2F2)
P15531	2	2	Nucleoside diphosphate kinase A (NME1)
P15882	2	2	N-chimaerin (CHN1)
P24534	2	2	Elongation factor 1-beta (EEF1B2)
P43487	2	2	Ran-specific GTPase-activating protein (RANBP1)
P53367	2	2	Arfaptin-1 ARFIP1
P60660	2	2	Myosin light polypeptide 6 (MYL6)
P62249	2	2	40S ribosomal protein S16 (RPS16)
P62899	2	2	60S ribosomal protein L31 (RPL31)
Q5U5X0	2	2	Complex III assembly factor LYRM7 (LYRM7)
Q7L273	2	2	BTB/POZ domain-containing protein (KCTD9)
Q8N1T3	2	2	Unconventional myosin-Ih (MYO1H)
P34931	15	1	Heat shock 70 kDa protein 1-like (HSPA1L)
P04259	7	1	Keratin_ type II cytoskeletal 6B (KRT6B)

P19013	5	1	Keratin_ type II cytoskeletal 4 (KRT4)
P27348	5	1	14-3-3 protein theta (YWHAQ)
Q562R1	5	1	Beta-actin-like protein 2 (ACTBL2)
Q04917	5	1	14-3-3 protein eta (YWHAH)
P12035	4	1	Keratin_ type II cytoskeletal 3 (KRT3)
Q2M2I5	4	1	Keratin_ type I cytoskeletal 24 (KRT24)
P00338	2	1	L-lactate dehydrogenase A chain (LDHA)
P02765	2	1	Alpha-2-HS-glycoprotein (AHSG)
P32119	2	1	Peroxiredoxin-2 (PRDX2)
Q7RTS7	2	1	Keratin_ type II cytoskeletal 74 (KRT74)
Q9NSB2	2	1	Keratin_ type II cuticular Hb4 (KRT84)
Q58FG0	2	1	Putative heat shock protein HSP 90-alpha A5 (HSP90AA5P)
A0A075B6N3	1	1	T cell receptor beta variable 24-1 (TRBV24-1)
A0A075B6Z2	1	1	T cell receptor alpha joining 56 (Fragment) (TRAJ56)
O75391	1	1	Sperm-associated antigen 7 (SPAG7)
O94955	1	1	Rho-related BTB domain-containing protein 3 (RHOBTB3)
P08865	1	1	40S ribosomal protein SA (RPSA)
P11940	1	1	Polyadenylate-binding protein 1 (PABPC1)
P62081	1	1	40S ribosomal protein S7 (RPS7)
P62857	1	1	40S ribosomal protein S28 OS (RPS28)
Q6ISS4	1	1	Leukocyte-associated immunoglobulin-like receptor 2 (LAIR2)
Q96LB3	1	1	Intraflagellar transport protein 74 (IFT74)
P17066	15	0	Heat shock 70 kDa protein 6 (HSPA)
P31947	5	0	14-3-3 protein sigma SFN
Q5XKE5	5	0	Keratin_ type II cytoskeletal 79 (KRT79)
P05787	3	0	Keratin_ type II cytoskeletal 8 (KRT8)
P08729	3	0	Keratin_ type II cytoskeletal 7(KRT7)
P10599	1	0	Thioredoxin (TXN)

Catalytically dead ALKBH3 plasmid interactome.

Protein ID	Peptide count	Unique peptides	Description
P23588	58	57	Eukaryotic translation initiation factor 4B (EIF4B)
O14744	50	49	Protein arginine N-methyltransferase 5 (**PRMT5**)
Q9C0B1	33	32	Alpha-ketoglutarate-dependent dioxygenase 9 (**FTO**)
Q96Q83	28	26	Alpha-ketoglutarate-dependent dioxygenase AlkB homolog 3 (**ALKBH3**)
P04264	24	20	Keratin_ type II cytoskeletal 1 (KRT1)
P11144	28	19	Heat shock cognate 71 kDa protein (HSPA8)
P55072	20	19	Transitional endoplasmic reticulum ATPase (VCP)
Q9BQA1	19	18	Methylosome protein 50 (WDR77)
P34932	18	17	Heat shock 70 kDa protein 4 (HSPA4)
P19338	17	17	Nucleolin (NCL)
P07355	16	16	Annexin A2 (ANXA2)
Q06830	17	15	Peroxiredoxin-1 (**PRDX1**)
Q14766	16	14	Latent-transforming growth factor beta-binding protein 1 (LTBP1)
P35527	16	13	Keratin_ type I cytoskeletal 9 (KRT9)
P02768	14	13	Albumin (ALB)
Q15393	13	13	Splicing factor 3B subunit 3 (SF3B3)
P13645	16	12	Keratin_ type I cytoskeletal 10 (KRT10)
P08670	14	12	Vimentin (VIM)
P11021	13	11	Endoplasmic reticulum chaperone BiP (HSPA5)
P35908	18	10	Keratin_ type II cytoskeletal 2 epidermal (KRT2)
P22626	12	10	Heterogeneous nuclear ribonucleoproteins A2/B1 (HNRNPA2B1)
Q9Y2I7	10	9	1-phosphatidylinositol 3-phosphate 5-kinase (PIKFYVE)
P09382	10	9	Galectin-1 (LGALS1)
P07237	10	9	Protein disulfide-isomerase (P4HB)
Q96T23	10	9	Remodeling and spacing factor 1 (RSF1)
P68104	9	9	Elongation factor 1-alpha 1 (EEF1A1)
Q8N7X1	9	9	RNA-binding motif protein_ X-linked-like-3 (RBMXL3)

P50990	9	9	T-complex protein 1 subunit theta (CCT8)
P07437	9	9	Tubulin beta chain (TUBB)
P10809	8	8	60 kDa heat shock protein_ mitochondrial (HSPD1)
P62633	8	8	CCHC-type zinc finger nucleic acid binding protein (CNBP)
Q86VS8	8	8	Protein Hook homolog 3 (HOOK3)
Q9UBW7	8	8	Zinc finger MYM-type protein 2 (ZMYM2)
Q6S8J3	12	7	POTE ankyrin domain family member E (POTEE)
P04406	8	7	Glyceraldehyde-3-phosphate dehydrogenase (GAPDH)
Q96I25	8	7	Splicing factor 45 (RBM17)
P61978	7	7	Heterogeneous nuclear ribonucleoprotein K (**HNRNPK**)
P0CG47	7	7	Polyubiquitin-B (UBB)
P38159	7	7	RNA-binding motif protein_ X chromosome (**RBMX**)
Q14103	9	6	Heterogeneous nuclear ribonucleoprotein D0 (**HNRNPD**)
O95816	7	6	BAG family molecular chaperone regulator 2 (BAG2)
P23528	7	6	Cofilin-1 (CFL1)
P0DP24	6	6	Calmodulin-2 (CALM2)
P04792	6	6	Heat shock protein beta-1 (HSPB1)
P06748	6	6	Nucleophosmin (NPM1)
P62318	6	6	Small nuclear ribonucleoprotein Sm-D3 (SNRPD3)
P17987	6	6	T-complex protein 1 subunit alpha (TCP1)
P49368	6	6	T-complex protein 1 subunit gamma (CCT3)
P11940	17	5	Polyadenylate-binding protein 1 (PABPC1)
P63104	11	5	14-3-3 protein zeta/delta (YWHAZ)
P62258	10	5	14-3-3 protein epsilon (YWHAE)
P05387	6	5	60S acidic ribosomal protein P2 (RPLP2)
P01614	6	5	Immunoglobulin kappa variable 2D-40 (IGKV2D-40)
P02788	6	5	Lactotransferrin (LTF)
P07737	6	5	Profilin-1 (PFN1)
P38646	6	5	Stress-70 protein_ mitochondrial (HSPA9)
P60174	6	5	Triosephosphate isomerase (TPI1)
P08758	5	5	Annexin A5 (ANXA5)

O43852	5	5	Calumenin (CALU)
Q9NQ92	5	5	Coordinator of PRMT5 and differentiation stimulator (COPRS)
Q14669	5	5	E3 ubiquitin-protein ligase TRIP12 (**TRIP12**)
P62805	5	5	Histone H4 (H4-16)
P07195	5	5	L-lactate dehydrogenase B chain (LDHB)
P60660	5	5	Myosin light polypeptide 6 (MYL6)
P30041	5	5	Peroxiredoxin-6 (PRDX6)
Q7RTV0	5	5	PHD finger-like domain-containing protein 5A (PHF5A)
P43487	5	5	Ran-specific GTPase-activating protein (RANBP1)
Q07955	5	5	Serine/arginine-rich splicing factor 1 (**SRSF1**)
P50991	5	5	T-complex protein 1 subunit delta (CCT4)
Q99832	5	5	T-complex protein 1 subunit eta (CCT7)
Q5XKE5	11	4	Keratin_ type II cytoskeletal 79 (KRT79)
P19012	7	4	Keratin_ type I cytoskeletal 15 (KRT15)
P08238	6	4	Heat shock protein HSP 90-beta (HSP90AB1)
P52597	6	4	Heterogeneous nuclear ribonucleoprotein F (**HNRNPF**)
O43390	6	4	Heterogeneous nuclear ribonucleoprotein R (**HNRNPR**)
P02787	6	4	Serotransferrin (TF)
Q2V2M9	5	4	FH1/FH2 domain-containing protein 3 (FHOD3)
P62937	5	4	Peptidyl-prolyl cis-trans isomerase A (PPIA)
A0A075B6R9	5	4	Probable non-functional immunoglobulin kappa variable 2D-24 (IGKV2D-24)
Q92804	5	4	TATA-binding protein-associated factor 2N (TAF15)
P40227	5	4	T-complex protein 1 subunit zeta (CCT6A)
P25398	4	4	40S ribosomal protein S12 (RPS12)
P02765	4	4	Alpha-2-HS-glycoprotein (AHSG)
P06733	4	4	Alpha-enolase (ENO1)
Q8WXX5	4	4	DnaJ homolog subfamily C member 9 (DNAJC9)
Q14192	4	4	Four and a half LIM domains protein 2 (FHL2)
P04075	4	4	Fructose-bisphosphate aldolase A (ALDOA)
P09211	4	4	Glutathione S-transferase P (GSTP1)
P16402	4	4	Histone H1.3 (H1-3)
P00338	4	4	L-lactate dehydrogenase A chain (LDHA)

P54105	4	4	Methylosome subunit pICln (CLNS1A)
P55209	4	4	Nucleosome assembly protein 1-like 1 (NAP1L1)
P00558	4	4	Phosphoglycerate kinase 1 (PGK1)
Q8TAA3	4	4	Proteasome subunit alpha-type 8 (PSMA8)
P98175	4	4	RNA-binding protein 10 (**RBM10**)
P78371	4	4	T-complex protein 1 subunit beta (CCT2)
Q7Z6K1	4	4	THAP domain-containing protein 5 (THAP5)
P0DMV9	11	3	Heat shock 70 kDa protein 1B (HSPA1B)
P61981	9	3	14-3-3 protein gamma (YWHAG)
P31946	8	3	14-3-3 protein beta/alpha (YWHAB)
P67809	7	3	Y-box-binding protein 1 (YBX1)
P42262	6	3	Glutamate receptor 2 (GRIA2)
P07910	6	3	Heterogeneous nuclear ribonucleoproteins C1/C2 (**HNRNPC**)
O60506	5	3	Heterogeneous nuclear ribonucleoprotein Q (SYNCRIP)
Q9Y657	5	3	Spindlin-1 (SPIN1)
P62995	5	3	Transformer-2 protein homolog beta (TRA2B)
P62249	4	3	40S ribosomal protein S16 (RPS16)
P24534	4	3	Elongation factor 1-beta (EEF1B2)
P69891	4	3	Hemoglobin subunit gamma-1 (HBG1)
Q9BS92	4	3	Protein NipSnap homolog 3B (NIPSNAP3B)
Q01130	4	3	Serine/arginine-rich splicing factor 2 (SRSF2)
P62241	3	3	40S ribosomal protein S8 (RPS8)
P62857	3	3	40S ribosomal protein S28 (RPS28)
P36578	3	3	60S ribosomal protein L4 (RPL4)
Q07020	3	3	60S ribosomal protein L18 (RPL18)
P62888	3	3	60S ribosomal protein L30 (RPL30)
P62899	3	3	60S ribosomal protein L31 (RPL31)
Q96PX6	3	3	Coiled-coil domain-containing protein 85A (CCDC85A)
Q99965	3	3	Disintegrin and metalloproteinase domain-containing protein 2 (ADAM2)
P19474	3	3	E3 ubiquitin-protein ligase TRIM21 (TRIM21)
P84090	3	3	Enhancer of rudimentary homolog (ERH)
Q9H6D7	3	3	HAUS augmin-like complex subunit 4 (HAUS4)
Q9UPP2	3	3	IQ motif and SEC7 domain-containing protein 3 (IQSEC3)
P15531	3	3	Nucleoside diphosphate kinase A (NME1)

P25789	3	3	Proteasome subunit alpha type-4 (PSMA4)
P30101	3	3	Protein disulfide-isomerase A3 (PDIA3)
Q49A26	3	3	Putative oxidoreductase GLYR1 (GLYR1)
Q9P270	3	3	SLAIN motif-containing protein 2 (SLAIN2)
Q9BUA3	3	3	Spindlin interactor and repressor of chromatin-binding protein (SPINDOC)
P31948	3	3	Stress-induced-phosphoprotein 1 (STIP1)
P60709	12	2	Actin_ cytoplasmic 1 (ACTB)
A0A2R8Y4L2	11	2	Heterogeneous nuclear ribonucleoprotein A1-like 3 (**HNRNPA1L3**)
P08727	7	2	Keratin_ type I cytoskeletal 19 (KRT19)
Q12873	6	2	Chromodomain-helicase-DNA-binding protein 3 (CHD3)
Q7Z794	6	2	Keratin_ type II cytoskeletal 1b (KRT77)
Q5T7W0	6	2	Zinc finger protein 618 (ZNF618)
Q8TDI0	5	2	Chromodomain-helicase-DNA-binding protein 5 (CHD5)
P13646	5	2	Keratin_ type I cytoskeletal 13 (KRT13)
P08779	5	2	Keratin_ type I cytoskeletal 16 (KRT16)
P24539	4	2	ATP synthase F(0) complex subunit B1_ mitochondrial (ATP5PB)
A0A0G2JNQ3	4	2	Heterogeneous nuclear ribonucleoprotein C-like 2 (**HNRNPCL2**)
Q2M2I5	4	2	Keratin_ type I cytoskeletal 24 (KRT24)
Q7Z3Y7	4	2	Keratin_ type I cytoskeletal 28 (KRT28)
Q5JQF8	4	2	Polyadenylate-binding protein 1-like 2 (PABPC1L2B)
P07951	4	2	Tropomyosin beta chain (TPM2)
P61604	3	2	10 kDa heat shock protein_ mitochondrial (HSPE1)
P55036	3	2	26S proteasome non-ATPase regulatory subunit 4 (PSMD4)
P05386	3	2	60S acidic ribosomal protein P1 (RPLP1)
P29692	3	2	Elongation factor 1-delta (EEF1D)
P15311	3	2	Ezrin (EZR)
A6NFK2	3	2	Glutaredoxin domain-containing cysteine-rich protein 2 (GRXCR2)
Q9Y5Z7	3	2	Host cell factor 2 (HCFC2)
Q14532	3	2	Keratin_ type I cuticular Ha2 (KRT32)
Q14CN4	3	2	Keratin_ type II cytoskeletal 72 (KRT72)
Q14515	3	2	SPARC-like protein 1 (SPARCL1)

P30050	2	2	60S ribosomal protein L12 (RPL12)
P35268	2	2	60S ribosomal protein L22 (RPL22)
P61254	2	2	60S ribosomal protein L26 (RPL26)
P61353	2	2	60S ribosomal protein L27 (RPL27)
Q9BQD7	2	2	Adenine nucleotide translocase lysine N-methyltransferase (ANTKMT)
P42127	2	2	Agouti-signaling protein (ASIP)
Q07021	2	2	Complement component 1 Q subcomponent-binding protein_ mitochondrial (C1QBP)
Q9H336	2	2	Cysteine-rich secretory protein LCCL domain-containing 1 (CRISPLD1)
Q8WVE0	2	2	EEF1A lysine methyltransferase 1 (EEF1AKMT1)
P04908	2	2	Histone H2A type 1-B/E (H2AC8)
Q8N339	2	2	Metallothionein-1M (MT1M)
O14950	2	2	Myosin regulatory light chain 12B (MYL12B)
Q9H1E3	2	2	Nuclear ubiquitous casein and cyclin-dependent kinase substrate 1 (NUCKS1)
P23284	2	2	Peptidyl-prolyl cis-trans isomerase B (PPIB)
Q99873	2	2	Protein arginine N-methyltransferase 1 (PRMT1)
A6NEQ2	2	2	Protein FAM181B (FAM181B)
O75688	2	2	Protein phosphatase 1B (PPM1B)
P14618	2	2	Pyruvate kinase (PKM)
Q6P6C2	2	2	AlkB Homolog 5, RNA Demethylase (**ALKBH5**)
Q9Y5S9	2	2	RNA-binding protein 8A (RBM8A)
P62314	2	2	Small nuclear ribonucleoprotein Sm D1 (SNRPD1)
P62316	2	2	Small nuclear ribonucleoprotein Sm D2 (SNRPD2)
P14678	2	2	Small nuclear ribonucleoprotein-associated proteins B (SNRPB)
Q15427	2	2	Splicing factor 3B subunit 4 (SF3B4)
O14798	2	2	Tumor necrosis factor receptor superfamily member 10C (TNFRSF10C)
P63267	10	1	Actin_ gamma-enteric smooth muscle (ACTG2)
P04259	9	1	Keratin_ type II cytoskeletal 6B (KRT6B)
Q9H361	9	1	Polyadenylate-binding protein 3 (PABPC3)
Q32P51	8	1	Heterogeneous nuclear ribonucleoprotein A1-like 2 (**HNRNPA1L2**)
Q01546	8	1	Keratin_ type II cytoskeletal 2 oral (KRT76)

P12035	8	1	Keratin_ type II cytoskeletal 3 (KRT3)
P31943	7	1	Heterogeneous nuclear ribonucleoprotein H (HNRNPH1)
Q13310	7	1	Polyadenylate-binding protein 4 (PABPC4)
P55795	6	1	Heterogeneous nuclear ribonucleoprotein H2 (**HNRNPH2**)
P68363	6	1	Tubulin alpha-1B chain (TUBA1B)
P16989	5	1	Y-box-binding protein 3 (YBX3)
O14979	4	1	Heterogeneous nuclear ribonucleoprotein D-like (HNRNPDL)
Q9NY65	4	1	Tubulin alpha-8 chain (TUBA8)
P17661	3	1	Desmin (DES)
Q9NZM3	3	1	Intersectin-2 (ITSN2)
P19013	3	1	Keratin_ type II cytoskeletal 4 (KRT4)
P09493	3	1	Tropomyosin alpha-1 chain (TPM1)
Q9Y3D3	2	1	28S ribosomal protein S16_ mitochondrial (MRPS16)
O14647	2	1	Chromodomain-helicase-DNA-binding protein 2 (CHD2)
Q9Y281	2	1	Cofilin-2 (CFL2)
Q2NKX8	2	1	DNA excision repair protein ERCC-6-like (ERCC6L)
Q99729	2	1	Heterogeneous nuclear ribonucleoprotein A/B (**HNRNPAB**)
Q00839	2	1	Heterogeneous nuclear ribonucleoprotein U (**HNRNPU**)
Q9H1H9	2	1	Kinesin-like protein KIF13A (KIF13A)
A0A075B759	2	1	Peptidyl-prolyl cis-trans isomerase A-like 4E (PPIAL4E)
P0DJH9	2	1	Protein RD3-like (RD3L)
P0DME0	2	1	Protein SETSIP (SETSIP)
Q58FG0	2	1	Putative heat shock protein HSP 90-alpha A5 (HSP90AA5P)
O75526	2	1	RNA-binding motif protein_ X-linked-like-2 (**RBMXL2**)
Q9BRL6	2	1	Serine/arginine-rich splicing factor 8 (SRSF8)
P06753	2	1	Tropomyosin alpha-3 chain (TPM3)
Q8WVF2	2	1	Unique cartilage matrix-associated protein (UCMA)
Q9H6S1	1	1	5-azacytidine-induced protein 2 (AZI2)
P62913	1	1	60S ribosomal protein L11 (RPL11)
P50914	1	1	60S ribosomal protein L14 (RPL14)

P15813	1	1	Antigen-presenting glycoprotein (CD1D)
Q96CT7	1	1	Coiled-coil domain-containing protein 124 (CCDC124)
P06493	1	1	Cyclin-dependent kinase 1 (CDK1)
P61803	1	1	Dolichyl-diphosphooligosaccharide–protein glycosyltransferase subunit (DAD1)
P61576	1	1	Endogenous retrovirus group K member 104 Rec protein (HERV-K104)
P62861	1	1	FAU ubiquitin-like and ribosomal protein S30
P68431	1	1	Histone H3.1 (H3C12)
Q6UWN0	1	1	Ly6/PLAUR domain-containing protein 4 (LYPD4)
P40926	1	1	Malate dehydrogenase_ mitochondrial (MDH2)
P25713	1	1	Metallothionein-3 (MT3)
Q14978	1	1	Nucleolar and coiled-body phosphoprotein 1 (NOLC1)
Q86UD1	1	1	Out at first protein homolog (OAF)
Q8N819	1	1	Probable protein phosphatase 1N (PPM1N)
P12273	1	1	Prolactin-inducible protein (PIP)
Q719I0	1	1	Putative activator of 90 kDa heat shock protein ATPase homolog 2 (AHSA2P)
Q6ZP68	1	1	Putative protein ATP11AUN (ATP11AUN)
A6NCQ9	1	1	RING finger protein 222 (RNF222)
P84103	1	1	Serine/arginine-rich splicing factor 3 (SRSF3)
Q99865	1	1	Spindlin-2A (SPIN2A)
A0A075B6Z2	1	1	T cell receptor alpha joining 56 (TRAJ56)
A0A1W2PQ09	1	1	TATA-box-binding protein-associated factor 11-like 11 (TAF11L11)
P48643	1	1	T-complex protein 1 subunit epsilon (CCT5)
P10599	1	1	Thioredoxin (TXN)
Q14469	1	1	Transcription factor HES-1 (HES1)
P37802	1	1	Transgelin-2 (TAGLN2)
Q3YBM2	1	1	Transmembrane protein 176B (TMEM176B)
P09651	10	0	Heterogeneous nuclear ribonucleoprotein A1 (HNRNPA1)
P17066	8	0	Heat shock 70 kDa protein 6 (HSPA6)
P02538	8	0	Keratin_ type II cytoskeletal 6A (KRT6A)
P42261	6	0	Glutamate receptor 1 (GRIA1)
Q71U36	6	0	Tubulin alpha-1A chain (TUBA1A)
P34931	5	0	Heat shock 70 kDa protein 1-like (HSPA1L)

P0DPH7	5	0	Tubulin alpha-3C chain (TUBA3C)
Q562R1	4	0	Beta-actin-like protein 2 (ACTBL2)
A0A075B6S2	2	0	Immunoglobulin kappa variable 2D-29 (IGKV2D-29)
Q96G46	1	0	tRNA-dihydrouridine(47) synthase [NAD(P)(+)]-like (DUS3L)
Q15942	1	0	Zyxin (ZYX)

Wild type FTO plasmid interactome.

Protein ID	Peptide count	Unique peptides	Description
Q9C0B1	164	164	Alpha-ketoglutarate-dependent dioxygenase 9 (**FTO**)
P04264	11	11	Keratin_ type II cytoskeletal 1 (KRT1)
P07355	7	7	Annexin A2 (ANXA2)
P11142	5	5	Heat shock cognate 71 kDa protein (HSPA8)
Q06830	4	4	Peroxiredoxin-1 (**PRDX1**)
P07437	4	4	Tubulin beta chain (TUBB)
Q9H116	3	3	GDNF-inducible zinc finger protein 1 (GZF1)
P04406	3	3	Glyceraldehyde-3-phosphate dehydrogenase (GAPDH)
O43766	3	3	Lipoyl synthase_ mitochondrial (LIAS)
Q96HP4	3	3	Oxidoreductase NAD-binding domain-containing protein 1 (OXNAD1)
Q96NH3	3	2	Protein broad-minded (TBC1D32)
P62937	2	2	Peptidyl-prolyl cis-trans isomerase A (PPIA)
P0CG47	3	1	Polyubiquitin-B (UBB)
P62979	3	1	Ubiquitin-40S ribosomal protein S27a (RPS27A)
P01614	2	1	Immunoglobulin kappa variable 2D-40 (IGKV2D-40)
P04908	1	1	Histone H2A type 1-B/E (H2AC8)
Q96IS3	1	1	Retina and anterior neural fold homeobox protein 2 (RAX2)
P10599	1	1	Thioredoxin (TXN)
A0A075B6S2	2	0	Immunoglobulin kappa variable 2D-29 (IGKV2D-29)
A0A075B6R9	2	0	Probable non-functional immunoglobulin kappa variable 2D-24 (IGKV2D-24)

Catalytically dead FTO plasmid interactome.

Protein ID	Peptide count	Unique peptides	Description
Q9C0B1	150	150	Alpha-ketoglutarate-dependent dioxygenase 9 (**FTO**)
O14647	11	10	Chromodomain-helicase-DNA-binding protein 2 (CHD2)
P04264	8	8	Keratin_ type II cytoskeletal 1 (KRT1)
Q9Y2W1	8	8	Thyroid hormone receptor-associated protein 3 (THRAP3)
Q9HCM1	9	7	Retroelement silencing factor 1 (RESF1)
Q8N7X1	8	7	RNA-binding motif protein_ X-linked-like-3 (RBMXL3)
Q86W56	7	6	Poly(ADP-ribose) glycohydrolase (PARG)
Q70EL1	6	6	Inactive ubiquitin carboxyl-terminal hydrolase 54 (USP54)
Q6S8J3	8	5	POTE ankyrin domain family member E (POTEE)
P78332	6	5	RNA-binding protein 6 (**RBM6**)
Q5TCY1	6	5	Tau-tubulin kinase 1 (TTBK1)
P04406	5	5	Glyceraldehyde-3-phosphate dehydrogenase (GAPDH)
O75781	5	5	Paralemmin-1 (PALM)
Q06830	5	5	Peroxiredoxin-1 (**PRDX1**)
O00220	5	5	Tumor necrosis factor receptor superfamily member 10A (TNFRSF10A)
A3KMH1	5	4	von Willebrand factor A domain-containing protein 8 (VWA8)
P07355	4	4	Annexin A2 (ANXA2)
Q969Q1	4	4	E3 ubiquitin-protein ligase TRIM63 (TRIM63)
P11142	4	4	Heat shock cognate 71 kDa protein (HSPA8)
P07195	4	4	L-lactate dehydrogenase B chain (LDHB)
P19338	4	4	Nucleolin (NCL)
P06748	4	4	Nucleophosmin (NPM1)
P38159	4	4	RNA-binding motif protein_ X chromosome (RBMX)
P68363	4	4	Tubulin alpha-1B chain (TUBA1B)
Q9P2S6	4	3	Ankyrin repeat and MYND domain-containing protein 1 (ANKMY1)
Q08211	4	3	ATP-dependent RNA helicase A (**DHX9**)
Q9H078	4	3	Caseinolytic peptidase B protein homolog (CLPB)
Q5BKZ1	4	3	DBIRD complex subunit ZNF326 (ZNF326)
O94822	4	3	E3 ubiquitin-protein ligase listerin (LTN1)
Q96RT6	3	3	cTAGE family member 2 (CTAGE1)

P25713	3	3	Metallothionein-3 (MT3)
P04350	3	3	Tubulin beta-4A chain (TUBB4A)
P60709	5	2	Actin_ cytoplasmic 1 (ACTB)
P62258	4	2	14-3-3 protein epsilon (YWHAE)
P63104	4	2	14-3-3 protein zeta/delta (YWHAZ)
P54802	3	2	Alpha-N-acetyl glucosaminidase (NAGLU)
P35663	3	2	Cylicin-1 (CYLC1)
Q6Y7W6	3	2	GRB10-interacting GYF protein 2 (GIGYF2)
P28702	3	2	Retinoic acid receptor RXR-beta (RXRB)
Q9Y6N7	3	2	Roundabout homolog 1 (ROBO1)
Q96Q83	2	2	Alpha-ketoglutarate-dependent dioxygenase AlkB homolog 3 (**ALKBH3**)
P23528	2	2	Cofilin-1 (CFL1)
P04733	2	2	Metallothionein-1F (MT1F)
Q9BVV7	2	2	Mitochondrial import inner membrane translocase subunit Tim21 (TIMM21)
P0CG47	2	2	Polyubiquitin-B (UBB)
P10599	2	2	Thioredoxin (TXN)
Q9P287	2	1	BRCA2 and CDKN1A-interacting protein (BCCIP)
P09341	2	1	Growth-regulated alpha protein (CXCL1)
A0A087WW87	2	1	Immunoglobulin kappa variable 2-40 (IGKV2-40)
Q9HCE5	2	1	N6-adenosine-methyltransferase non-catalytic subunit (METTL14)
A0A075B6R9	2	1	Probable non-functional immunoglobulin kappa variable 2D-24 (IGKV2D-24)
Q9Y399	1	1	28S ribosomal protein S2_ mitochondrial (MRPS2)
P15880	1	1	40S ribosomal protein S2 (RPS2)
P62857	1	1	40S ribosomal protein S28 (RPS28)
P05386	1	1	60S acidic ribosomal protein P1 (RPLP1)
P05387	1	1	60S acidic ribosomal protein P2 (RPLP2)
Q9H257	1	1	Caspase recruitment domain-containing protein 9 (CARD9)
Q96S94	1	1	Cyclin-L2 (CCNL2)
Q01814	1	1	Plasma membrane calcium-transporting ATPase 2 (ATP2B2)
O75629	1	1	Protein CREG1 (CREG1)
Q12870	1	1	Transcription factor 15 (TCF15)
O15195	1	1	Villin-like protein (VILL)
Q9BTP6	1	1	Zinc finger BED domain-containing protein 2 (ZBED2)
A0A075B6S2	2	0	Immunoglobulin kappa variable 2D-29 (IGKV2D-29)